



Università degli Studi di Napoli *Federico II*

DOTTORATO DI RICERCA IN FISICA

Ciclo XXXIV

Coordinatore: prof. Salvatore Capozziello

Testing gravity around Sgr A*

Settore Scientifico Disciplinare FIS/05

Dottorando
Anna D'Addio

Tutor
Prof. [Mariafelicia De Laurentis](#)

Anni 2018/2021

*Qualcuno deve gridare che costruiremo le piramidi, non importa se poi non le
costruiremo.*
*Bisogna alimentare il desiderio, dobbiamo tirare l'anima da tutte le parti come se
fosse un lenzuolo dilatabile all'infinito.*
Se volete che il mondo vada avanti, dobbiamo tenerci per mano.
Andrej Arsen'evič Tarkovskij

CONTENTS

Symbols and Abbreviations	vii
List of Figures	xiii
List of Tables	xv
Acknowledgements	xvii
Preface	xix
1 Introduction	1
1.1 The most mysterious interaction	2
1.2 Brief history of gravity	2
1.3 Viability of gravitation theories	5
1.4 Creatures of gravity: black holes	6
1.4.1 Theoretical foundation	7
1.4.2 Black holes in the Universe	8
1.5 Concluding remarks	10
I Theoretical background	11
2 General Relativity	13
2.1 From gravity to geometry	14
2.2 Foundations of the theory	16
2.2.1 The structure of space-time	16
2.2.2 Einstein's equations of motion	19
2.3 Spherically symmetric solution	21
2.3.1 The Schwarzschild metric	21
2.3.2 Schwarzschild geodesics	24
2.4 Rotating black holes	27
2.4.1 Kerr metric	27
2.5 Post-Newtonian expansion	29
2.5.1 General features	29
2.6 General metrics	32
2.6.1 The General Static Isotropic gravitational field	33
2.6.2 Eddington-Robertson expansion	35
2.6.3 Precession of Perihelia	35
2.7 Concluding remarks	38

3	Extending General Relativity	39
3.1	Motivations	40
3.1.1	The cosmological problem	41
3.1.2	UV scales: the Quantum Gravity problem	43
3.1.3	IR scales: Dark Energy and Dark Matter	45
3.2	Beyond Einstein's theory	46
3.2.1	Lovelock theorem	46
3.2.2	A general class of Extended Theories of Gravity	48
3.3	$f(R)$ -gravity	50
3.3.1	Field equations	50
3.3.2	Weak field limit of $f(R)$ -gravity theory	52
3.3.3	Geodesic motion	54
3.3.4	Precession	56
3.4	Bootstrapped Newtonian Gravity	57
3.4.1	Potential in the vacuum	58
3.4.2	Harmonic and areal coordinates	60
3.4.3	Effective space-time metric	61
3.4.4	Precession	64
3.5	Concluding remarks	65
II	Applications	67
4	The Galactic Center	69
4.1	Toward the center of the Milky Way	70
4.2	The nuclear star cluster	72
4.2.1	The S -star cluster	73
4.3	Is Sgr A* a supermassive black hole?	75
4.3.1	Evidence for a central compact object	75
4.3.2	Constraints from stellar orbits	76
4.3.3	Alternatives to the black hole paradigm	77
4.4	A laboratory to test General Relativity	79
4.4.1	Monitoring stellar orbits	81
4.4.2	Pulsars timing	82
4.4.3	EHT observations	84
4.5	Concluding remarks	85
5	Test I: Stellar orbits at the Galactic Center	87
5.1	Data	88
5.1.1	The chosen stars	88
5.1.2	Description of the dataset	89
5.2	Simulation of the orbits	90
5.2.1	Formulation of the motion problem	90

5.2.2	Numerical integration	91
5.3	Fitting Procedure	94
5.4	Results	97
5.4.1	Test I.a: $f(R)$ -gravity	97
5.4.2	Test I.b: Bootstrapped Newtonian gravity	103
5.5	Concluding remarks	104
6	Test II: Precession of the Perihelia	111
6.1	Precession	112
6.1.1	Bootstrapped Newtonian gravity	112
6.1.2	$f(R)$ -gravity	112
6.2	Astronomical tests	113
6.2.1	Test II.a: Bootstrapped Newtonian gravity	113
6.2.2	Test II.b: $f(R)$ -gravity	116
6.3	Concluding remarks	117
7	Conclusions	121
7.1	Summary	121
7.2	Future prospects	122
	Bibliography	144

SYMBOLS AND ABBREVIATIONS

Symbols

a	Semi-major axis
c	Speed of light
ds^2	Space-time interval
$d\Omega^2$	Volume element
e	Eccentricity
$g_{\mu\nu}$	Metric tensor
g	Determinant of the metric
G_N	Newtonian constant of gravitation
$G_{\mu\nu}$	Einstein tensor
J	Black hole angular momentum
ℓ	Semilatus rectum
M_\odot	Solar mass
P	Pressure of the fluid
Q	Black hole quadrupole moment
R_S	Schwarzschild radius
\mathcal{R}	Kretschman invariant
R	Ricci scalar
$R_{\mu\nu}$	Ricci tensor
$R^\alpha_{\beta\mu\nu}$	Riemann tensor
S	Action of a gravity theory
\mathcal{L}	Lagrangian density
$T_{\mu\nu}$	Energy-Momentum tensor
u_μ	Four-velocity of the fluid particles
α, β, γ	PPN Parameters
δ	Universal constant
$\Gamma^\alpha_{\mu\nu}$	Christoffel symbol of first kind
$\eta_{\mu\nu}$	Minkowski metric
λ	Yukawa scale length
Λ	Cosmological constant
Ξ	Bootstrapped free parameter

Abbreviations

AGB	Asymptotic Giant Branch
AGN	Active Galactic Nucleus
AO	Adaptive Optics
BH	Black Hole
BOOMERANG	Balloon Observations Of Millimetric Extragalactic Radiation and Geophysics
CMB	Cosmic Microwave Background
CND	Circum-Nuclear Disk
DE	Dark Energy
Dec	Declination
DM	Dark Matter
EHT	Event Horizon Telescope
ESO	European Southern Observatory
ETG	Extended Theories of Gravity
GC	Galactic Center
GR	General Relativity
HST	Hubble Space Telescope
IR	Infrared
JWST	James Webb Space Telescope
LIGO	Laser Interferometer Gravitational-Wave Observatory
MACHO	MAssive Compact Halo Object
MAXIMA	Millimeter Anisotropy eXperiment IMaging Array
MPE	Planck Institute for Extraterrestrial Physics
NACO	Naos-Conica
NIR	Near Infrared
NRAO	National Radio Astronomy Observatory
NTT	New Technology Telescope
PK	Post-Keplerian
PN	Post-Newtonian
PPN	Parametrized Post Newtonian
PPTA	Parkes Pulsar Timing Arra
QED	Quantum Electrodynamics
RA	Right Ascension
SEP	Strong Equivalence Principle
Sgr A*	Sagittarius A*
SKA	Square-Kilometre-Arrai
SMBH	Supermassive Nlack Hole
UCLA	University of California
UT	Unit Telescope
UV	Ultraviolet

VLBI	Very Long Baseline Interferometry
VLA	Very Large Array
VLT	Very Large Telescope
WEP	Weak Equivalence Principle
WIMP	weakly Interacting Massive Particles
WMAP	Wilkinson Microwave Anisotropy Probe
WR	Wolf-Reyet
ZAMS	Zero Age Main Sequence
Λ CDM	Λ Cold Dark Matter

LIST OF FIGURES

2.1	Path built on the surface of a sphere with three arcs delimiting an octant.	18
2.2	Effective potential for the fixed value $l = 2.2$ as a function of $z = R_S/r$. Horizontal lines represent different types of motion depending on the value of the energy.	26
2.3	Elements of an ellipse referred to in the calculation of the precession of planetary orbits.	36
3.1	Diagram representing the ways in which the Lovelock's theorem can be violated giving rise to different classes of ETG.	48
3.2	Relative difference of the two gravitational fields $(\psi(r) - \Phi(r))/\Phi(r)$ as a function of the strength δ and r	55
3.3	Bootstrapped Newtonian potential V_0 compared to its expansion from Eq. (3.107) and to the Newtonian potential V_N (for $q = 1$).	61
4.1	Schematic image of the structures in the Galactic Center. The mini-spiral of ionized gas connects the central cluster region with the circumnuclear disk. The size of the central cluster (~ 0.7 pc) is indicated by a circle. The position of the compact radio source Sgr A * is indicated with a star.	70
4.2	Image at 2 cm of Sgr A West and Sgr A* (the bright central object in this image) [162].	71
4.3	Image at 1.6 μm as seen by NICMOS on the Hubble Space Telescope of the inner $19'' \times 19''$ region at the GC [162].	72
4.4	Best-fitting orbits from the multi-star fit (solid lines) with the corresponding radial velocity data [110].	77
4.5	The parameter space for gravitational fields of a wide range of astrophysical and cosmological systems (left) and their experimental counterpart (right).	80
4.6	Angular diameters and distances for a sample of supermassive black holes. Data are taken from [119].	81
4.7	Eight stations of the EHT 2017 campaign over six geographic locations as viewed from the equatorial plane (see Papers [86, 87, 88]).	85
4.8	The rim of the shadow corresponds to photons coming from infinity and reaching the observer after rotating many times around the black hole.	85
4.9	Shadow of the supermassive black hole at the center of <i>M87</i> galaxy [86].	86
5.1	Illustration of the true anomaly ϕ and the eccentric anomaly Φ on the equatorial plane of Sgr A*	91
5.2	Phase space diagram of orbits in the Yukawa potential for <i>S2</i> , <i>S38</i> and <i>S55</i>	95

5.3	Illustration of the classical orbital parameters i , Ω , and ω . The z -axis corresponds to the line of sight for a distant observer.	96
5.4	Comparison between the NTT/VLT astrometric observations (black circles) and the orbit of $S2$ predicted in $f(R)$ -gravity using the best-fit parameter reported in Table 5.3.	98
5.5	Comparison between the NTT/VLT astrometric observations (black circles) and the orbit of $S38$ predicted in $f(R)$ -gravity using the best fit parameter reported in Table 5.3.	99
5.6	Comparison between the NTT/VLT astrometric observations (black circles) and the orbit of $S55$ predicted in $f(R)$ -gravity using the best fit parameter reported in Table 5.3.	100
5.7	Comparison between observed and fitted coordinates (top), and the corresponding residuals (bottom) for $S2$, $S38$, and $S55$ for the $f(R)$ -gravity.	101
5.8	Best relativistic multi-star orbit fit of $S2$, $S38$, and $S55$ for the $f(R)$ -gravity.	102
5.9	Marginalized likelihood function $\mathcal{L}(\lambda)$, from which we infer a lower bound on λ	103
5.10	Comparison between the NTT/VLT astrometric observations (black circles) and the orbit of $S2$ predicted in Bootstrapped gravity using the best fit parameter reported in Table 5.4.	105
5.11	Comparison between the NTT/VLT astrometric observations (black circles) and the orbit of $S38$ predicted in Bootstrapped gravity using the best fit parameter reported in Table 5.4.	106
5.12	Comparison between the NTT/VLT astrometric observations (black circles) and the orbit of $S55$ predicted in Bootstrapped gravity using the best fit parameter reported in Table 5.4.	107
5.13	Top panels show the comparison between the observed and fitted coordinates, and bottom panels the corresponding residuals for $S2$, $S38$ and $S55$ for the Bootstrapped gravity.	108
5.14	Best relativistic multi-star orbit fit of $S2$, $S38$ and $S55$ for the Bootstrapped gravity.	109
5.15	Likelihood function $\mathcal{L}(\Xi)$	109
6.1	Bootstrapped orbital precession as a function of the parameter Ξ . Black lines give the theoretical prediction from Eq. (6.3), blue dashed lines represent the measurements adapted from [178] and red lines depict the GR values as in Eq. (2.167). Confidence regions for Ξ are shaded in grey.	114
6.2	Bootstrapped orbital precession as a function of the parameter Ξ for the star $S2$	116

6.3	$f(R)$ -gravity orbital precession as a function of the parameter δ . Black lines give the theoretical prediction, blue dashed lines represent the measurements adapted from [178] and red lines depict the GR values. Confidence regions for δ are shaded in grey.	118
6.4	$f(R)$ -gravity theory precession as a function of the parameter δ for the star $S2$	119



LIST OF TABLES

4.1	Keplerian parameters of the 40 S -stars whose orbit has been determined in Ref. [110]	78
5.1	Orbital parameters of $S2$, $S38$, and $S55$	92
5.2	Parameters of the central BH.	92
5.3	Best-fit values for δ and lower limit for λ	100
5.4	Best-fit values for Ξ	104
6.1	Values of semi-major axis (a), orbital period (P), tilt angle (i), eccentricity (e), observed orbital precession ($\Delta\phi_{\text{obs}}$), orbital precession as predicted by GR ($\Delta\phi_{\text{S}}$) and constraints on Ξ for Solar System's planets.	113
6.2	Orbital parameters from the Nasa Fact Sheet, the GR prediction for the precession in the sixth column and the values predicted by the bounds on the parameter Ξ of the Bootstrapped theory deduced for Venus (see Table 6.1).	115
6.3	Precession for Mars and Jupiter as predicted by confidence values for Ξ inferred from Mercury, Venus, Earth, and Saturn.	115
6.4	For the star $S2$, orbital parameters [116], observed orbital precession ($\Delta\phi_{\text{obs}}$), orbital precession as predicted by GR ($\Delta\phi_{\text{S}}$) and constraints on Ξ	116
6.5	Precession for $S2$ as predicted by confidence regions for Ξ inferred from Mercury, Venus, Earth and Saturn.	117
6.6	Values of semi-major axis (a), orbital period (P), tilt angle (i), eccentricity (e), observed orbital precession ($\Delta\phi_{\text{obs}}$), orbital precession as predicted by GR ($\Delta\phi_{\text{S}}$) and constraints on δ for Solar System's planets.	117
6.7	Orbital parameters from Nasa Fact Sheet, the GR prediction for the precession in the sixth column and the values predicted by the bounds on the parameter δ of the $f(R)$ -gravity theory deduced for Venus (see Table 6.6).	119
6.8	Precession for Mars and Jupiter as predicted by confidence values for δ inferred from Mercury, Venus, Earth, and Saturn.	119
6.9	For the star $S2$, orbital parameters [116], observed orbital precession ($\Delta\phi_{\text{obs}}$), orbital precession as predicted by GR ($\Delta\phi_{\text{S}}$), and constraints on δ	119
6.10	Precession for Mars, Jupiter, and $S2$ as predicted by confidence regions for δ inferred from Mercury, Venus, Earth, and Saturn.	120

ACKNOWLEDGEMENTS

Before proceeding with the discussion, I would like to dedicate a few lines to all those who contributed to the realization of this work.

First of all, I would like to express my gratitude to my PhD advisor, professor Mariafelicia De Laurentis, for having contributed to a precious enrichment of my scientific and human formation. During the journey undertaken together, she gave me the opportunity to work on one of the most fascinating topics in science, believing in me and transmitting not only the necessary scientific tools but also a working method that I will treasure.

I would like to thank the PhD coordinator, professor Salvatore Capozziello, for introducing me to the world of extended theories of gravity since the days of his inspiring Cosmology lessons.

Then, I would like to thank Dr. Ivan De Martino, for the fundamental role he had in completing my thesis, assisting me with professionalism and patience in the work of numerical simulations.

I would like to thank professors Roberto Casadio and Andrea Giusti for giving me the opportunity to work together and for their infinite availability and promptness in providing me with valuable advices useful for drafting the paper.

Furthermore, I would like to dedicate a few words to the remaining people who accompanied me on this journey.

I would like to thank Tommaso D., who taught me the relationship between the colors of reality and my behaviors, which was indispensable in my moments of distrust in myself.

I would like to sincerely thank Stefania Gravina. Our paths divided at the beginning of the PhD course, but this strengthened our friendship even more, made us grow, and did not prevent us from walking side by side sharing our anxiety but above all many pleasant moments.

Thanks to my whole family because every time we are all together it's a little bit of Christmas.

Thanks to my mom and my father, who, despite the physical and emotional quarantines, have stayed with me, taking care of me with selfless love and in the best way they could.

Thanks to my sister Jane, for the lightness we feel when we are together. I started this journey in a difficult historical era, and she was the light in the darkest moments.

A heartfelt thanks to Loris, my endless spring, for hugging me whole, for always supporting me, for the flowers in the storm.

Thanks to the books, the white nights, and Stellina.

Thanks to myself, for when on the Stellaburgis Hafniens I decided not to leave in my eyes “solo i sogni che non fanno svegliare”.



PREFACE

The currently accepted theory of gravity is the *General Relativity*, published by Albert Einstein (1879 – 1955) in 1916. General Relativity, built on an elegant mathematical structure, introduced a revolutionary treatment of the gravitational field and deeply changed the understanding of space and time. The idea behind it is simple: while most of the forces of nature are represented by fields defined on space-time, gravity is intimately bound to the structure of space-time itself. Einstein imagined the Universe as a four-dimensional variety whose curvature is determined by the distribution of matter and energy associated with celestial bodies. What we experience as the “force of gravity” is a manifestation of the curvature itself. Einstein’s theory correctly evaluated phenomena such as the precession of Mercury’s orbit and the gravitational deflection of light from the Sun, as measured in 1919 during a total solar eclipse by Sir Arthur Eddington (1882 – 1944). Furthermore, it predicted new gravitational effects, such as gravitational waves, gravitational lensing, and the time delay of the light travel confirmed experimentally.

Although General Relativity has proved valid at the Solar System scale, shortcomings came out undermining its validity at ultraviolet and infrared regimes. The first question is strictly related to one of the most important problems in modern physics: the difficulty of developing a unified theory that is capable of embracing all the laws of nature in a single, all-embracing theoretical framework. The central obstacle to the realization of a unified theory is the fundamental conflict between the two pillars of twentieth-century physics: General Relativity and Quantum Mechanics. Each of these theories has proved successful in its own arena of physical phenomena: General Relativity in the classical description of gravitating systems at large scales, and Quantum Mechanics at very small scales where the classic description fails. In other words, a complete Quantum Gravity Theory has not been found yet and General Relativity cannot describe adequately the Universe at extreme conditions. The second issue comes from Cosmology and Astrophysics: General Relativity cannot explain the current accelerated expansion of the Universe without resorting to two exotic, and still unobserved, components in matter-energy fluid, that is Dark Energy and Dark Matter. An approach to solve these problems relies on modifying the geometrical description of space-time, leaving the material interpretation unchanged. Correcting and expanding Einsteinian theory constitutes the approach of the so-called Extended Theories of Gravity, which have become a sort of paradigm in the study of gravitational interaction.

The study of possible modifications of Einstein’s theory has a long history that began around 1920. Extended Theories of Gravity are divided into two fundamental classes: *Higher-Order Theories* involve the addition of higher-order invariants of the curvature tensor and *Scalar-Tensor Theories* modify the gravitational Lagrangian introducing scalar fields that are minimally or not minimally coupled to the geometry.

In this thesis, we turn our attention to two theories: $f(R)$ -gravity theory and Bootstrapped Newtonian gravity theory. $f(R)$ -gravity generalizes the Einstein-Hilbert Lagrangian to an arbitrary function $f(R)$ of the Ricci scalar. The emerging gravita-

tional potential in the weak-field limit is characterized by a Yukawa-like term acting as a scale length of the system. This new scale length furnishes us with an automatic screening mechanism such that the Solar System constraints are recovered, and at the same time allows the explanation of galactic rotation curves in a self-consistent way. Moreover, we can develop geometrically an inflationary model by means of higher-order corrections. These reasons made such a theory a focus point in Cosmology. On the other hand, the Bootstrapped Newtonian gravity, inspired by Deser's conjecture, consists of a non-linear version of Newton's law which includes pressure effects and the gravitational self-interaction terms. It is an attempt to describe compact objects and coherent quantum states.

At the end of the formulation of a new physical theory, it must be tested on experimental data to certify its validity or rule it out. The purpose of this thesis is to give astronomical constraints to the aforementioned theories using a general method through which we could produce a broader classification of the large family of theories of gravity. In particular, we considered the Galactic Center to constrain the theory under consideration by studying S -star dynamics. Then, we reported a phenomenological investigation aiming at placing bounds on the free parameters from the observed precession of planets in the Solar System.

S -stars constitute a cluster of young stars revolving in the innermost arcsecond of the Galactic Center. Their motion points out the existence of a compact source of ~ 4 million solar masses and located at about 8 kpc: Sagittarius A* (Sgr A*). Such a source of gravitational field is most probably a supermassive black hole. S -star cluster has been monitored since 1992 by Speckle Imaging at European Southern Observatory's (ESO) New Technology Telescope (NTT) in La Silla, since 1995 at the Keck telescope, and since 2017, with the four-telescope interferometric beam combiner instrument GRAVITY. Among S -stars, we focused on $S2$, $S38$, and $S55$ because they are the brightest ones and they have the shortest period. Definitely, S -stars are a precious tool to study interactions between a massive compact object and its environment. It is crucial to probe gravity in the vicinity of very massive bodies since the environment around these objects is drastically different from that typical of the Solar System, where General Relativity has been extensively tested. Therefore, Sgr A* has become the primary target to solve the most debated topics of modern research; the main goal of scientists is to consolidate the black hole paradigm and shed light on the underlying theory of gravity. It's worth noticing that the Yukawa-like modifications to the standard potential have already been investigated by studying S -star motion around Sgr A*. Anyway, in literature, the extended potential has been analyzed by integrating the classical Newtonian equations of motion. In this work we used a new method, that is we adopted a fully relativistic approach implementing the modified Yukawa potential in the exact geodesic equations instead of just using the classical ones. This choice is motivated by the fact that S -star orbits could deviate from the Keplerian case due to relativistic effects as pointed out by recent results of GRAVITY Collaboration, which robustly detected the combined gravitational redshift and transverse Doppler shift and

then the Schwarzschild prograde orbital precession.

This thesis consists of two parts: the first part is theoretical and is aimed at illustrating the particular theories that we have chosen to study, while the second, fundamental part, sees the application of theoretical results to astronomical systems. The work is divided into seven chapters.

- In Chapter 1, we briefly retraced the history of gravitational theories until the advent of General Relativity. Motivated by the progress of science, which is periodically prompted to ask whether a given theory needs to be extended, we listed the criteria that must be satisfied by a given theory of gravity in order to be considered valid.
- In Chapter 2, we summarized the principles of General Relativity. In view of astronomical applications, we focused on the analysis of the black hole solutions.
- In Chapter 3, we exposed the reasons that led to the need of extending General Relativity. Subsequently, attention was paid to the detailed analysis of two extended theories: the $f(R)$ -gravity theory and the Bootstrapped Newtonian gravity theory.
- In Chapter 4, we initially described the properties of the area centered on the most mysterious object in the Galaxy: Sgr A*. Next, we exposed the observative results that consolidated the black hole paradigm, the most likely configuration among the alternatives scenario proposed in literature. Finally we summed up the main experiments that are currently undergoing to probe Sgr A* across the full electromagnetic spectrum.
- In Chapter 5, we presented the first astronomical test, consisting in constraining the parameters of the theories by analyzing stellar orbits at the Galactic Center using a fully relativistic approach.
- In Chapter 6, we exposed the second astronomical test, based on the comparison between the measured orbital precession of the Solar System planets and the theoretical predictions.
- Chapter 7 is devoted to conclusions.

The thesis was developed on the lines of research followed by professor Mariafelicia De Laurentis focused on the theories of gravitation in their theoretical and phenomenological aspects.

INTRODUCTION

Quando guardai il mio demonio, lo trovai serio, pesante, profondo, solenne: era lo spirito della gravità, — per cagion del quale cade ogni cosa.

– F. Nietzsche

1.1	The most mysterious interaction	2
1.2	Brief history of gravity	2
1.3	Viability of gravitation theories	5
1.4	Creatures of gravity: black holes	6
1.4.1	Theoretical foundation	7
1.4.2	Black holes in the Universe	8
1.5	Concluding remarks	10

Gravity pervades our daily world and gives the rhythm to the cosmic dance that millions and millions of bodies, from asteroids to galaxies, perform without rest. For the immediacy of perception of its effects, it was the first to be described mathematically since ancient times.

This introductory chapter will take us into the flow of the history of gravitational theories (Sec. 1.2), a history that began before Christ and is not yet finished. In this context, it is natural to ask what are the criteria that must be satisfied by a theory of gravitation in order to be considered valid (Sec. 1.3). Finally, we will be introduced to the physics of black holes, amazing objects predicted by the General Theory of Relativity (Sec. 1.4).

1.1 The most mysterious interaction

Gravity is probably the most mysterious of the four fundamental interactions in nature. It has the following “special” properties that distinguish it from other interactions, making it the only one suitable to understand astrophysical phenomena to which we are interested in this thesis.

Gravity is the *weakest* fundamental interaction in nature. Consider a system of two protons at a distance comparable to their size; their electromagnetic interaction is at least $1/137$ weaker than their nuclear (strong) interaction, their weak interaction is about 10^{-5} of the strong one and their gravitational attraction is 10^{-38} weaker. Despite this weakness gravity plays a key role for astrophysical objects, as its action is amplified at astronomical scales.

Secondly, weak and strong interactions are mediated by fields having not zero mass m connected to the characteristic Compton length $l_C = \hbar/mc$. It follows that the corresponding forces are important at short ranges and decay exponentially at distances $> l_C$; that is why the aforementioned interactions determine the structure of matter. Instead, gravity (like electromagnetism) is mediated by the massless *graviton* (photon), and the corresponding force has an *infinite effective range* falling as $\sim 1/r^2$. This is one reason why gravity dominates over astronomical distances.

The third remarkable property that differentiates gravity from electromagnetism is its *attractive* character. While there are two types of electrical charges, positive and negative, gravitational charges have the same sign, and always attract each other. It follows a mechanism of self-amplification consisting of the growth of the ability of a massive body to attract mass as a result of the increase in the mass itself. Gravitational forces, which are too weak for a single elementary particle, increase enormously when these particles form a macroscopic system, and totally determine its evolution.

Finally, gravity is *universal*, there are no neutral particles with respect to this interaction. The total energy of a system plays the role of gravitational charge. Everything in nature has energy and hence interacts gravitationally.

1.2 Brief history of gravity

The beginning of the history of attempts to describe gravitational interaction can be placed in the 4th century BC, when Aristotle hypothesized that objects fall at a speed determined by their own mass. He did not think that motion was induced by forces such as those we know are exerted between celestial bodies due to gravitation, but rather he believed that consistent with our intuitive thinking, heavy bodies fall towards their “natural place” guided by their own internal *gravitas* (heaviness).

Aristotle’s philosophy dominated until the time of Galileo Galilei (1564 – 1642). He discovered that bodies fall at a rate independent of their mass, using an inclined plane to slow the fall and a water clock to measure its duration.

The first to recognize that the terrestrial effects produced by gravity are analogous to the celestial ones was Sir Isaac Newton (1642 – 1727). At the end of the *Principia*, he described gravitation as a cause operating on the Sun and planets “*according to the quantity of solid matter which they contain and propagates on all sides to immense distances, decreasing always as the inverse square of the distances*” [175]. Given the space and time as two absolute entities, the new law of gravity described the gravitational interaction between two bodies of masses m_G and M with the well-known expression

$$\mathbf{F} = G_N \frac{m_G M}{r^3} \mathbf{r}, \quad (1.1)$$

where G_N is the gravitational constant. Newton knew that the “inertial mass” m_I entering in his second law

$$\mathbf{F} = m_I \mathbf{a} \quad (1.2)$$

was in principle conceptually different from the “gravitational mass” m_G appearing in the law of gravitation

$$\mathbf{F} = m_G \mathbf{g}, \quad (1.3)$$

where \mathbf{g} is a field depending on position and other masses. If so, the acceleration at a given point would be

$$\mathbf{a} = \left(\frac{m_G}{m_I} \right) \mathbf{g}, \quad (1.4)$$

and would depend on the values of the ratio m_G/m_I . This possibility was tested by Newton himself and later, in 1989, by Roland von Eötvös (1848 – 1919): the ratio m_G/m_I did not differ from one substance to another by more than one part in 10^9 [69, 206]. The observed equality opened the route towards the Principle of Equivalence which, as we will see, is the cornerstone of Einstein’s theory. The successes of Newton’s theory in explaining the motion of the Moon and planets culminated beautifully in the discovery of Neptune following its prediction, in 1846, independently by John Couch Adams (1819 – 1892) and Urbain Jean Joseph Le Verrier (1811 – 1877) [145], who were based on some irregularities in the orbit of Uranus. In the same period, Newton’s theory had to tackle the first observational problem. Le Verrier had calculated that the observed precession of Mercury was $35''$ /century in excess, and in 1882 Simon Newcomb (1835 – 1909) confirmed this discrepancy giving a value of $43''$. Le Verrier attributed such a discrepancy to a small planet between Mercury and the Sun, but it was never found.

Due attention should be paid to the conceptual basis of Newtonian theory, which expressed the belief shared since ancient times that matter represented the “substance” while space and time represented the “form”: space was thought of as a three-dimensional container in which God placed the material universe. In his words [175]:

“Absolute space, in its own nature and with regard to anything external, always remains similar and unmovable”.

This conception, therefore, conceived space as existing beyond and outside the spatial relations between objects. In other words, the description of every physical phenomenon (“event”) required an absolute definition of space, reduced to an infinite set of triples of distances from a point O (origin) along a given direction, and of time, reduced to a set of time intervals determined by a reference event.

The first constructive attack to the idea of absolute space was due to Ernst Mach (1838 – 1916) [68]. Going in contradiction with the Newtonian vision that inertia was always relative to an absolute frame of reference, he stated that “inertia originates in a kind of interaction (unspecified) between bodies”. In establishing his General Theory of Relativity, Einstein was very impressed by ideas of Mach and summarized them in the term “Mach’s principle”:

- space and time do not have an independent existence, since space is the separation between bodies and time expresses the succession of events;

- the inertia of a body would lose its meaning in the absence of masses. It isn’t related to the absolute space but is determined by all the matter in the Universe.

This delicate question was not resolved until 1905, the year in which Albert Einstein (1879 – 1955) completed his Special Theory of Relativity postulating that the speed of light in vacuum is constant and it does not depend on the motion of its source. Einstein’s new theory appeared to be incompatible with the Newtonian gravitation; in fact, according to the latter, the gravitational force exerted by one body on another depends only on the masses and the distance that separates them, implying that if anything changed in masses or in distance, bodies would instantly feel a change in gravitational force. The other postulate of Special Relativity is that laws of nature are the same in all inertial reference frames. The latter therefore are given a privilege; this preference must be considered as an independent property of the space-time continuum seen as an absolute entity, that is, “having a physical effect, but not influenced by physical conditions”. However, two objections could be made to this point of view. In the first place, it assumes the existence of an entity that acts but on which one cannot act. Secondly, no justification has yet been given for the equality between inertial mass and gravitational mass.

The final breakthrough in the understanding of gravity was due to Einstein’s theory of General Relativity (GR), which broke into the *Annalen der Physik* in 1916 [81]. It involved not only a generalization of Special Relativity that included gravity and non-inertial frames, but it also was the bearer of a deep revolution in the way of understanding the concepts of space and time. The greatest implication of this enlargement was that the space is curved, and its curvature is determined by the distribution of mass in it (as will be clear in Chapter 2).

This short chronological summary is useful to comprehend the current status of GR. As it will be evident from the next sections, the experimental successes and the elegant perfection of its mathematical apparatus do not hold off questions completely analogous to those that Newton's theory had to face, namely how to explain the increasingly accurate observational data of the modern epoch and how to be compatible with other sophisticated and consolidated theories.

1.3 Viability of gravitation theories

When a new physical theory is introduced, the suitable questions to be posed are the following. How large is the portion of the physical world adequately described by such a theory? And is this theory the only one for the description of relevant phenomena? These issues have made it necessary to consider extensions also of the current gravitational theory, that is GR. In the perspective to consider possible extensions, it is appropriate to underline the fundamental requirements that any gravitational theory should satisfy to be considered viable [32, 236].

- It must be *complete*, that is, he must be able to analyze from “first principles” the result of any experiment of interest. Equipped with a set of electrodynamic and quantum-mechanical laws, the theory must be able to determine the evolution of a body in a gravitational field.
- It must be *self-consistent*, that is, its prediction for the outcome of each experiment must be unique; two different, although equivalent, calculation methods must lead to the same results.
- It must be *relativistic*, that is, to the extent that gravity is “turned off”, non-gravitational laws of physics must reduce to those of Special Relativity.
- It must have the correct *Newtonian limit*, that is, for weak field and low velocities Newton laws must be reproduced. Besides, It should pass the classical Solar System tests and explain the Galactic dynamics given the observed baryonic matter and radiation.
- It must face the problem of *large-scale structure* and the question of *cosmological dynamics*, that is, cosmological parameters (as the expansion rate of the Universe, the Hubble constant, and so on) should be reproduced in a self-consistent way.

The simplest theory that satisfies the above requirements is the General Theory of Relativity, built on the idea that gravitational field, space-time, and matter-energy distribution are intertwined and governed by field equations [81]. It is based on three assumptions:

1. **Principle of Relativity.** All reference systems are equivalent with respect to the formulation of the fundamental laws of physics [170]. Physical equations must be invariant under *general* coordinate transformations.
2. **Principle of Equivalence.** This principle was stated by Einstein, who was impressed by the equality of the “inertial mass” m_I of a body, that is the property of that body that regulates its response to an applied force, and the “gravitational mass” m_G , that is the property that determines its response to gravitation:

$$m_I = m_G. \tag{1.5}$$

It implies as Einstein pointed out, that in a freely falling frame no external static homogeneous gravitational field could be detected. The Principle of Equivalence in its final form states that: “at every space-time point in an arbitrary gravitational field, it is possible to choose a locally inertial frame such that, in a region small enough to neglect inhomogeneities of the gravitational field, the laws of nature take the form as in unaccelerated Cartesian frame in the absence of gravitation”. This Principle thus formulated is known as the Weak Equivalence Principle (WEP). WEP can be extended to the Strong Equivalence Principle (SEP) if we replace “laws of nature” by “laws of motion of freely falling particles”. Thus, SEP generalizes WEP including effects of gravitation on all physical systems.

3. **Principle of General Covariance.** It deals with the mathematical representation of the Principle of Equivalence; it expresses Einstein’s postulate about the equality between all reference systems (and therefore of coordinates) for the description of the laws of physics. The Principle of General Covariance states that a physical equation holds in a gravitational field if the following conditions are satisfied: the equation recovers the Special Relativity in absence of gravitation, and the equation is generally covariant, that is, it is invariant under a general coordinate transformation.

The **Principle of Causality** crowns the above principles: every point of space-time must admit a notion of past, present, and future that is the same for all physical observers.

1.4 Creatures of gravity: black holes

Our journey among gravitational theories ended with GR, whose most fascinating prediction is the existence of black holes. As we will see, the properties of these objects are so weird and intriguing that most astronomers could hardly accept their existence. Now, after the theoretical and experimental advances that revolutionized astronomy, our vision changed: black holes are believed to be everywhere. We can classify them according to their main parameter, the mass M :

- stellar-mass black holes with $M \sim (3 - 30) M_{\odot}$;
- intermediate-mass black holes with $M \sim 10^3 M_{\odot}$;
- supermassive black holes with $M \sim (10^5 - 10^9) M_{\odot}$;
- primordial black holes with mass up to M_{\odot} ;
- micro-black holes.

As we will see soon, observations confirm the existence of stellar and supermassive black holes.

1.4.1 Theoretical foundation

Black holes' simplest configuration is described by the spherically symmetric vacuum solution found out by Karl Schwarzschild (1873 – 1916) in 1916 (see Section 2.3) [211]. A *black hole* can be defined as a space-time region where the gravitational field is so strong that even light cannot escape. A black hole is the result of the collapse of a body of mass M down to a dimension smaller than its *Schwarzschild radius*

$$R_S = \frac{2 G_N M}{c^2}, \quad (1.6)$$

where G_N is the Newton gravitational constant, M is its mass and c is the speed of light. It is surprising to observe that formula (1.6) was already presented by Pierre-Simon Laplace (1749 – 1827) in 1799 using purely Newtonian mechanics. Laplace speculated the existence of *dark objects*, which are hypothetical high-density objects with an escape velocity larger than the speed of light. The result can be obtained by setting the total energy of a test particle of mass m equal to zero

$$\frac{1}{2} m v^2 - G_N \frac{M m}{r} = 0. \quad (1.7)$$

From (1.7) follows that a particle cannot escape to infinity if the radius is smaller than $\frac{2 G_N M}{c^2}$. Returning to the Schwarzschild solution, it is afflicted by a singularity at the center ($r = 0$) and one at the radius $r = R_S$. For years it was not possible to deeply understand the significance of these features. Then, researchers realized that $r = 0$ corresponds to a true singularity, while in 1924 Arthur Eddington (1882 – 1944) determined that the space-time is regular at the surface R_S , and the singularity could be removed with a suitable choice of coordinates. Only in 1958 David Finkelstein (1929 – 2016) fully understood the nature of the surface at R_S [91] as a one-way surface: it is what we now call the *event horizon*. If something crosses it, it cannot influence the exterior region anymore.

In 1918 the Reissner-Nordström solution, describing a non-rotating black hole with a non-vanishing electrical charge was found [177].

A more realistic black hole model that takes into account the non-zero angular momentum of astrophysical systems became available in 1963 when Roy Kerr discovered a stationary and axisymmetric solution to Einstein’s equations. This solution also has a real singularity, but it is surrounded by an event horizon if the angular momentum is $J \leq J_* = G_N M^2/c$. A new effect is induced by rotation, the *dragging-into-rotation effect*; it involves the co-rotation of matter with the black hole in a region located outside the horizon called *ergosphere*. Due to the complexity of the Kerr metric, it was not possible to study the motion of particles and the field propagation until Carter discovered a new type of integrals connected to hidden symmetries [40].

The picture of black holes was completed at the end of the 1960s when a global geometrical approach was applied to the theory and many results were proved [241, 167, 125, 223, 95]. In particular, the no-hair theorem expresses the result that, under some assumptions, black holes are characterized by a small number of parameters (hair), namely the black hole mass, the black hole spin angular momentum, and the black hole electric charge. In 1965 the British theorist Roger Penrose, who awarded the Nobel Prize in 2020 “*for the discovery that black hole formation is a robust prediction of the general theory of relativity*”, published an article that became a milestone in GR [187]. Introducing new mathematical concepts, he demonstrated that black holes formation is a stable process and he described their properties. Penrose was based on the concept of *trapped surface*, which is a closed two-dimensional surface such that all orthogonal light rays converge when traced toward the future. This idea led him to demonstrate that once a trapped surface is formed, the collapse towards a singularity is unavoidable in GR [187].

The remarkable properties of these objects were summarized in the term black hole itself, which was coined in 1968 by J.A. Wheeler (1911 – 2008) as an excellent description of the alternative word “frozen star”, the dominant phrase in the literature until then [167].

This period was fertile both for the aforementioned theoretical advancement and for the technical innovations that produced the evidence of black holes and other compact objects.

1.4.2 Black holes in the Universe

For many years, black holes have been thought to be very exotic objects; Einstein himself found it difficult to believe the existence of a body with a size comparable to its gravitational radius.

A renewed interest in compact astrophysical objects grew when in the 1930s Chan-

drasekhar worked on white dwarfs [50], and Oppenheimer and Volkoff demonstrated the possibility of the existence of neutron stars [181], stars having a radius slightly higher than the gravitational radius. In the same years, the production of black holes at the end of the gravitational collapse of a massive star was described [180].

Guisenov and Zeldovich [121] showed that an X-ray source could be produced when collapsed stars in binaries pull gas from their companion liberating energy in a shock with temperatures of millions of degrees. Such a source can be identified as a neutron star if pulsations are discovered in their X-rays (thus the first neutron star was discovered), or a black hole. However, the identification of a black hole with an X-ray source requires not only the absence of pulsations but also the measurement of the mass through observations of the velocity changes of the companion. The evidence of stellar black holes dates back to the mass determination of the mass of X-ray binary Cygnus X-1's compact object [232, 21], which exceeded the maximum mass for a neutron star.

The discovery of black holes of much greater mass (up to $10^6 - 10^9 M_\odot$) was not expected by the theory. The picture changed in 1963 when distant luminous quasars were discovered [207]. These active galaxies are characterized by non-thermal emission from a small-size central region, called active galactic nucleus (AGN). Their small size and enormous luminosities (AGN generally produce 10^{39} W, more than two orders of magnitude larger than the luminosity of all stars in a galaxy!) indicated that the central engine must be associated with a large and compact mass; Salpeter and Zeldovich [205, 240] were the first to propose that the energy generation mechanism involved could be explained by the emission of radiation from the accretion of matter onto black holes. An accurate description of the phenomenon was presented by Lynden-Bell [157], who suggested explaining the spectra of quasars through the accretion disk formed by the gas around a massive object. Lynden-Bell also suggested that such supermassive black holes are hosted by many galaxies, including our Milky Way, living as a quiet remnant of a past active phase.

More recently, other aspects of black holes physics became very important for astrophysical applications. As predicted by GR, the collision of a black hole with a neutron star or coalescence of a pair of black holes is a strong source of gravitational radiation. The produced gravitational waves can be strong enough to reach the Earth; in 2016, the LIGO/Virgo collaboration announced the first direct detection occurred on 14 September 2015 from the coalescence of two black holes, each of them of $\sim 30 M_\odot$ [1].

Furthermore, the first direct image of the supermassive black hole in the center of the giant elliptical galaxy *M87* was published on 10 April 2019 by the Event Horizon Telescope (EHT) Collaboration [86].

Finally, we can probe black holes by analyzing stars orbiting around them. As will be evident in the second part of this thesis, they represent a formidable tool for the

direct deduction of the parameters of the gravitational field in which they revolve, such as the mass and the distance of the compact object, and to test gravitational theories in a not yet fully explored gravitational regime.

1.5 Concluding remarks

In this chapter, we outlined the history of attempts to explain the most enigmatic interaction: gravitation. Starting from the first scientific speculations dating back to before Christ, we arrived at the formulation of the GR, Einstein's elegant theory that weaves space and time into a single dynamic entity. We then introduced the basic concepts that characterize the most puzzling prediction of GR: black holes. We summarized the theoretical development that led to the current picture of these objects.

Paraphrasing S. Chandrasekhar, *“the black holes of nature are the most perfect macroscopic objects there are in the Universe: the only elements in their construction are our concepts of space and time. And since the general theory of relativity provides only a unique family of solutions for their description, they are the simplest objects as well”* [49].

Part I

Theoretical background

GENERAL RELATIVITY

Space-time tells matter how to move; matter tells space-time how to curve.

– J. A. Wheeler

2.1	From gravity to geometry	14
2.2	Foundations of the theory	16
2.2.1	The structure of space-time	16
2.2.2	Einstein's equations of motion	19
2.3	Spherically symmetric solution	21
2.3.1	The Schwarzschild metric	21
2.3.2	Schwarzschild geodesics	24
2.4	Rotating black holes	27
2.4.1	Kerr metric	27
2.5	Post-Newtonian expansion	29
2.5.1	General features	29
2.6	General metrics	32
2.6.1	The General Static Isotropic gravitational field	33
2.6.2	Eddington-Robertson expansion	35
2.6.3	Precession of Perihelia	35
2.7	Concluding remarks	38

In this chapter, we will dwell on the foundations of Einstein's theory and its most salient applications.

After summarizing the field equations derivation (Sec.2.2), we will focus on the Schwarzschild (Sec. 2.3) and Kerr (Sec. 2.4) solutions for their importance in astronomical applications. Then, we will explain how to find out an approximate solution of the

field equations by means of the post-Newtonian expansion (Sec. 2.5). Finally, we will expose the parameterized post-Newtonian formalism that will act as a bridge between GR and its extensions (Sec. 2.6). In this context we will discuss one of the crucial verifications of GR, which is the precession of the perihelia.

The importance of this summary of GR lies in keeping in mind that, in regimes in which it is solidly verified, it must be recovered from Extended Theories of Gravity.

2.1 From gravity to geometry

The Principle of Equivalence is the fulcrum from which springs the chain of deductions that led Einstein to abandon the preference of inertial systems over all other coordinate systems [82].

The Principle of Equivalence implies that gravity is indistinguishable from accelerated motion, and it requires that non-inertial systems can be used in the Galilean regions¹. On the other hand, to get rid of the problem of objective reasons why certain coordinate systems are preferred over others, we must be able to use coordinate systems in arbitrary motion. A mathematical description of such a generic system clashes with the physical interpretation of space and time shared by Special Relativity, as we can see from this simple example. Let us consider an inertial system K with axis z , and a system K' rotating at constant angular around its axis z' which coincides with z . Consider a large number of standard rules, of which U are arranged along the circumference and D along the diameter of a circle drawn in the $x'y'$ plane around the origin of K' . If K' does not rotate with respect to K , we will have

$$\frac{U}{D} = \pi. \tag{2.1}$$

Now suppose that K' rotates and we want to determine at a given instant t of K the position of the edges of all the samples. Since, with respect to K , the samples arranged on the circumference undergo the Lorentz contraction we will have

$$\frac{U}{D} > \pi. \tag{2.2}$$

With this exercise, we realize that, with respect to a rotating reference system, the configuration laws of rigid bodies are not in agreement with those formulated in terms of Euclidean geometry. In general, space and time cannot be defined with respect to K' as they were defined with respect to an inertial reference frame. On the other hand, according to the Equivalence Principle, K' can be considered as a system at rest on which a gravitational field acts. We thus arrive at this result: the gravitational field influences and even determines metric laws of the space-time continuum. *In the presence of a gravitational field, the geometry is not Euclidean.*

¹We call “Galilean regions” those regions where, with respect to an appropriately chosen reference frame, particles move without acceleration. In these regions laws of Special Relativity are valid.

The aforementioned case is similar to the one that occurs in the two-dimensional study of surfaces; the profound analogy between the laws of gravitation and the formulas of the Riemannian geometry is due to the metric properties on which the concepts of both theories are based. In the case of the theory of surfaces, Gauss's reasoning is the following [82, 233]. Plane geometry is based on the concept of distance ds between two infinitely close points, expressed by the formula $ds^2 = dx_1^2 + dx_2^2$. This notion of distance, from which the concepts of geodesic, interval, circle, and angle arise, can also be defined on a curved surface when it is observed that an infinitely small portion of this surface can be considered flat, less than an infinitesimal quantity. On this sufficiently small portion of a curved surface, it would be possible to find a locally Euclidean coordinate system so that the distance between two points (X_1, X_2) and $(X_1 + dX_1, X_2 + dX_2)$ satisfies the law of Pythagoras

$$ds^2 = dX_1^2 + dX_2^2. \quad (2.3)$$

In particular, the inner properties of such a surface can be described in terms of derivatives $\partial X^\alpha / \partial x^\mu$ of the function $X^\alpha(x)$ defining the transformation $x \rightarrow X$ from some general frame x to the locally Cartesian system X . The fundamental function of these derivatives is the quantity $g_{\mu\nu}$, which defines the distance between two points (x_1, x_2) and $(x_1 + dx_1, x_2 + dx_2)$:

$$ds^2 = g_{11}(x_1, x_2) dx_1^2 + 2g_{12}(x_1, x_2) dx_1 dx_2 + g_{22}(x_1, x_2) dx_2^2. \quad (2.4)$$

Here g_{11} , g_{12} , and g_{22} depend on the nature of the surface and the coordinate choice:

$$g_{11} = \left(\frac{\partial X_1}{\partial x_1} \right)^2 + \left(\frac{\partial X_2}{\partial x_1} \right)^2 \quad (2.5)$$

$$g_{12} = \left(\frac{\partial X_1}{\partial x_1} \right) \left(\frac{\partial X_1}{\partial x_2} \right) + \left(\frac{\partial X_2}{\partial x_1} \right) \left(\frac{\partial X_2}{\partial x_2} \right) \quad (2.6)$$

$$g_{22} = \left(\frac{\partial X_1}{\partial x_2} \right)^2 + \left(\frac{\partial X_2}{\partial x_2} \right)^2. \quad (2.7)$$

Similarly, an infinitely small region of the space-time continuum can be considered Galilean and there will always exist an inertial system $\{X_\alpha\}$ where the Special Relativity laws are valid. Generally, for space-time regions of finite extension that are not Galilean, no choice of coordinates will validate Special Relativity, but for two nearby events it will always exist the invariant ds expressible in arbitrary coordinates; it can be written in the form

$$ds^2 = g_{\mu\nu} dx^\mu dx^\nu. \quad (2.8)$$

The object $g_{\mu\nu}$ encodes the metric relations of the space-time continuum and the gravitational field.

2.2 Foundations of the theory

We arrived at this result: the heart of GR lies in the Principle of Equivalence, which tells us how a physical system responds to a gravitational field. We shall first see how to implement it mathematically, and then we will summarize the derivation of the differential equations that determine the gravitational field evolution.

2.2.1 The structure of space-time

The metric tensor

According to the Principle of Equivalence, we can always find a local inertial frame in a given gravitational field. Consider a particle in free fall in such a system; its motion is a straight line in space-time and it is described by the equation [36]:

$$\frac{d^2 \xi^\alpha}{ds^2} = 0, \quad (2.9)$$

where

$$ds^2 = \eta_{\alpha\beta} d\xi^\alpha d\xi^\beta \quad (2.10)$$

is the line element, and $\eta = \text{diag}(1, -1, -1, -1)$ is the Minkowski metric. Now suppose to apply coordinates transformations to Eq. (2.9) to switch to any other coordinate system x^μ

$$\xi^\alpha = \xi^\alpha(x^\beta); \quad (2.11)$$

Eq. (2.9) becomes

$$\begin{aligned} \frac{d^2 \xi^\alpha}{ds^2} &= \frac{d}{ds} \left(\frac{d\xi^\alpha}{ds} \right) = \frac{d}{ds} \left(\frac{\partial \xi^\alpha}{\partial x^\mu} \frac{dx^\mu}{ds} \right) \\ &= \frac{\partial \xi^\alpha}{\partial x^\mu} \frac{d^2 x^\mu}{ds^2} + \frac{\partial^2 \xi^\alpha}{\partial x^\mu \partial x^\nu} \frac{dx^\mu}{ds} \frac{dx^\nu}{ds} = 0. \end{aligned} \quad (2.12)$$

After multiplying by $\partial x^\lambda / \partial \xi^\alpha$ and using the relation

$$\frac{\partial \xi^\alpha}{\partial x^\mu} \frac{\partial x^\lambda}{\partial \xi^\alpha} = \delta_\mu^\lambda, \quad (2.13)$$

we get the equation of motion

$$\frac{d^2 x^\lambda}{ds^2} + \Gamma_{\mu\nu}^\lambda \frac{dx^\mu}{ds} \frac{dx^\nu}{ds} = 0, \quad (2.14)$$

where the quantities $\Gamma_{\mu\nu}^\lambda$

$$\Gamma_{\mu\nu}^\lambda = \Gamma_{\nu\mu}^\lambda = \frac{\partial^2 \xi^\alpha}{\partial x^\mu \partial x^\nu} \frac{\partial x^\lambda}{\partial \xi^\alpha} \quad (2.15)$$

represent the field determining the gravitational force and are called *affine connections*.

Now let us relate affine connections with the metric. Transformations (2.11) can be used to express the metric line element in an arbitrary reference frame:

$$ds^2 = \eta_{\alpha\beta} d\xi^\alpha d\xi^\beta = \eta_{\alpha\beta} \frac{\partial \xi^\alpha}{\partial x^\mu} dx^\mu \frac{\partial \xi^\beta}{\partial x^\nu} dx^\nu = g_{\mu\nu} dx^\mu dx^\nu. \quad (2.16)$$

Here, $g_{\mu\nu}$ is the *metric tensor* defined by

$$g_{\mu\nu} = g_{\nu\mu} = \eta_{\alpha\beta} \frac{\partial \xi^\alpha}{\partial x^\mu} \frac{\partial \xi^\beta}{\partial x^\nu}. \quad (2.17)$$

It can be easily proved [233] that starting from relation (2.17), the explicit expression for affinities in function of the metric can be obtained:

$$\Gamma_{\mu\nu}^\alpha = g^{\alpha\lambda} \frac{1}{2} (g_{\lambda\mu,\nu} + g_{\nu\lambda,\mu} - g_{\mu\nu,\lambda}). \quad (2.18)$$

We have shown that $g_{\mu\nu}$ plays the role of gravitational potential, being the field $\Gamma_{\mu\nu}^\lambda$ determined by its derivatives. We are facing a metric theory of space-time, in the sense that we are using 10 gravitational potentials ($g_{\mu\nu}$) instead of one, as in the case of the Newtonian gravitation.

A formulation of the law of freely falling particles as a variational principle allows a geometrical interpretation of equation (2.14): *a particle in free fall through a curved space-time (called gravitational field) will move on the shortest (or longest) possible path between two points, the proper time measuring the length, that is on extremal paths called geodesics* [233].

The curvature

Affine connections and their derivatives are at the basis of the Riemann tensor definition, the entity representing the heart of GR: the *curvature* of the space-time.

We can define the Riemann tensor starting from the notion of parallel transport [147]. By parallel transport we mean the transport of a vector carried out while keeping constant the angle it forms with the local geodesic. It is immediate to realize that in Euclidean space the parallel transport of a vector on a closed path brings the vector back on itself, but the same does not happen on a curved surface (see Figure 2.1).

A definition of “curvature” of space makes use of this property; a space is said to be flat if it is possible to uniquely define a vector for parallel transport on a closed line, otherwise it is said to be curved. This definition translates mathematically into the equivalence between the relation that expresses the return of a vector on itself after the parallel transport on a curved line and the cancellation of a defined algebraic quantity,

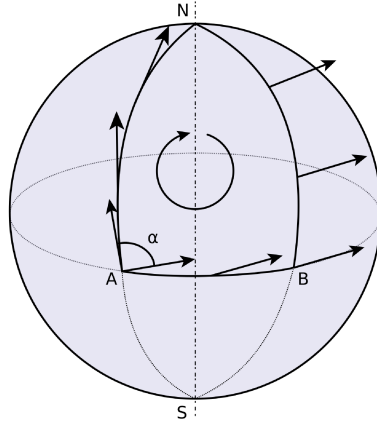


Figure 2.1: Path built on the surface of a sphere with three arcs delimiting an octant.

to be identified with the Riemann tensor $R_{\beta\mu\nu}^{\alpha}$. Indeed, from the definition of parallel transport of a vector B_{β} [36] it follows that

$$DB_{\beta} = dB_{\beta} - \delta B_{\beta} = B_{\beta;\mu} dx^{\mu} = 0. \quad (2.19)$$

The vector comes back on itself, after the transport on a closed line, if the spurious variation on this path vanishes

$$\oint \delta B_{\beta} = \oint \Gamma_{\beta\mu}^{\alpha} B_{\alpha} dx^{\mu} = 0. \quad (2.20)$$

By developing this relation, we find that imposing (2.20) is equivalent to require that

$$B_{\alpha} R_{\beta\mu\nu}^{\alpha} = 0, \quad (2.21)$$

where we introduced the quantity

$$R_{\beta\mu\nu}^{\alpha} = \Gamma_{\beta\nu,\mu}^{\alpha} - \Gamma_{\beta\mu,\nu}^{\alpha} + \Gamma_{\beta\nu}^{\sigma} \Gamma_{\sigma\mu}^{\alpha} - \Gamma_{\beta\mu}^{\sigma} \Gamma_{\sigma\nu}^{\alpha}. \quad (2.22)$$

The object $R_{\beta\mu\nu}^{\alpha}$ defines the Riemann tensor. Finally, we can claim that the necessary and sufficient condition for a space to be flat is that the Riemann tensor vanishes.

By contracting the first and the third indexes of the Riemann tensor we define the *Ricci tensor*

$$\begin{aligned} R_{\alpha\beta} &= R_{\alpha\mu\beta}^{\mu} = \frac{\partial}{\partial x^{\mu}} \Gamma_{\alpha\beta}^{\mu} - \frac{\partial}{\partial x^{\beta}} \Gamma_{\alpha\mu}^{\mu} + \Gamma_{\alpha\beta}^{\tau} \Gamma_{\tau\mu}^{\mu} - \Gamma_{\alpha\tau}^{\sigma} \Gamma_{\beta\sigma}^{\tau} \\ &= \frac{\partial}{\partial x^{\mu}} \Gamma_{\alpha\beta}^{\mu} - \frac{\partial^2}{\partial x^{\alpha} \partial x^{\beta}} \ln \sqrt{-g} + \Gamma_{\alpha\beta}^{\tau} \frac{\partial}{\partial x^{\tau}} \ln \sqrt{-g} - \Gamma_{\alpha\tau}^{\sigma} \Gamma_{\beta\sigma}^{\tau}. \end{aligned} \quad (2.23)$$

The *Ricci scalar* is defined as

$$R \equiv R_{\mu}^{\mu} = g^{\mu\nu} R_{\mu\nu}. \quad (2.24)$$

We now have the necessary mathematical tools to derive the equations of gravitational field.

2.2.2 Einstein's equations of motion

Einstein, according to the ideas of Riemann [83], postulated that the space-time curvature is locally determined by the distribution of the celestial sources. Acceptable differential equations that regulate the gravitational field dynamic evolution must obey some physical criteria imposed by the basic concepts discussed so far, and that here are summarized.

1. According to the Principle of Covariance, the laws of physics must be covariant under a general coordinate transformation.
2. When a gravitational field is present, space-time is curved and endowed with a metric of the form

$$ds^2 = g_{\mu\nu} dx^\mu dx^\nu, \quad (2.25)$$

where the metric tensor $g_{\mu\nu}$ binds geometry and gravitation. It consists of 10 functions of the space-time variables, of which 6 are independent.

3. The space-time curvature is determined by the masses distributed in it.
4. In the weak field limit, the Newtonian gravitational theory is valid.

The first result imposes that field equations must be written in tensor form; the second one implies that the laws must contain at least six quantities related to $g_{\mu\nu}$; the third suggests that the curvature must be related to a tensor representing the space-time matter-energy content; the fourth tells us that the gravitational equations, which must be of the second order, must provide the Newtonian solution for weak fields.

Initially, Einstein focused on finding vacuum field equations and, guided by the aforementioned criteria, he suggested

$$R_{\beta\mu\nu}^\alpha = 0. \quad (2.26)$$

But Eq. (2.26) does not contemplate solutions other than flat space-time; they are too restrictive to be accepted. To have equations that admit the existence of a gravitational field, we can consider some combinations of components of the Riemann tensor, such as the Ricci tensor $R_{\mu\nu}$; then, the right equations should be

$$R_{\mu\nu} = 0. \quad (2.27)$$

To connect equations in vacuum with those in presence of matter, Einstein relied on the postulate of the matter as the generator of the curvature, and he suggested

$$R_{\mu\nu} = \chi T_{\mu\nu}^{(m)}, \quad (2.28)$$

where χ is a dimensional constant. The rank-2 tensor $T_{\mu\nu}^{(m)}$, called energy-momentum tensor, is the covariant representation of a perfect fluid, that is a fluid composed of particles that have negligible interactions. It can be expressed as

$$T_{\mu\nu}^{(m)} = (P + \rho) u_\mu u_\nu + P g_{\mu\nu}, \quad (2.29)$$

where u_μ is the four-velocity of the fluid particles and P and ρ are the pressure and energy density of the fluid, respectively. Energy-momentum conservation implies that $T_{\mu\nu}^{(m)}$ satisfies the continuity equation, that is

$$\nabla^\mu T_{\mu\nu}^{(m)} = 0. \quad (2.30)$$

Equations (2.28) are not consistent from a physical point of view; in fact, according to the (2.30), left-hand side of the field equations should be represented by a divergence-free tensor, and this is not the case for $R_{\mu\nu}$. However, starting from the Ricci tensor we can build a divergence-free tensor as

$$G_{\mu\nu} = R_{\mu\nu} - \frac{1}{2} g_{\mu\nu} R. \quad (2.31)$$

The quantity $G_{\mu\nu}$ is the so-called Einstein tensor, and always obeys $\nabla^\mu G_{\mu\nu} = 0$. The suitable field equations can be therefore written as

$$G_{\mu\nu} = \chi T_{\mu\nu}^{(m)}. \quad (2.32)$$

The precise value of χ can be determined when the Newtonian limit is realized; Einstein's equations are consistent with Newton's theory provided that $\chi = 8\pi G_N/c^4$.

Furthermore, field equations must be mathematically consistent, i.e. they must descend from a variational principle. The starting point is to obtain the Hilbert-Einstein action. We start from the general action of a local gravity theory

$$S = \int \mathcal{L} d^4x, \quad (2.33)$$

where

$$\mathcal{L} = \mathcal{L}(g, \dots) \quad (2.34)$$

is a local Lagrangian density depending on the metric and its derivatives. In order to satisfy the principle of covariance, the action S must be a scalar, hence

$$\mathcal{L} = \sqrt{-g} L(g, \dots), \quad (2.35)$$

where L is a local scalar and $\sqrt{-g} d^4x$ is the invariant volume element. To obtain equations of the second order the Lagrangian must contain at least the squares of the first derivatives of the metric, which contain the Christoffel symbols that are not invariant. This suggests choosing expressions containing the metric, its first derivatives, and its second derivatives entering linearly:

$$\mathcal{L} = \sqrt{-g} L(g, \partial g, \partial^2 g). \quad (2.36)$$

The simplest choice is the scalar of curvature R , which contains the second derivatives of the metric linearly. The Hilbert-Einstein action can be finally written as [36]:

$$S_{\text{EH}} = \frac{1}{2k^2} \int d^4x \sqrt{-g} R, \quad (2.37)$$

where k^2 is a dimensional constant, necessary for S to have the correct physical dimensions. Hilbert's choice was arbitrary, but it was the simplest to generate the field equations already found by Einstein. Field equations in presence of matter can be obtained by adding the matter action S_{m} :

$$S_{\text{m}} = \int d^4x \sqrt{-g} \mathcal{L}_{\text{m}}, \quad (2.38)$$

where \mathcal{L}_{m} is the matter Lagrangian density whose variational derivative is

$$T_{\mu\nu}^{(\text{m})} = -\frac{2}{\sqrt{-g}} \frac{\delta(\sqrt{-g} \mathcal{L}_{\text{m}})}{\delta g_{\mu\nu}}. \quad (2.39)$$

The behaviour of the Hilbert-Einstein action with respect to small variations of the metric is therefore studied. It can be proven that its stationary points coincide with the Einstein equations, which can be written in one of the two equivalent forms:

$$G_{\mu\nu} = R_{\mu\nu} - \frac{1}{2} g_{\mu\nu} R = \frac{8\pi G_{\text{N}}}{c^4} T_{\mu\nu}^{(\text{m})}, \quad (2.40)$$

$$R_{\mu\nu} = \frac{8\pi G_{\text{N}}}{c^4} \left(T_{\mu\nu}^{(\text{m})} - \frac{1}{2} g_{\mu\nu} T^{(\text{m})} \right). \quad (2.41)$$

As John Wheeler summarized, *matter tells space how to curve, and space tells matter how to move* [234].

2.3 Spherically symmetric solution

The first exact solution to the field equations was found, in 1916, by Karl Schwarzschild in the special case of a spherically symmetric space-time. Although it is an approximation (astronomical objects rotate!), it is the basis of numerous applications.

2.3.1 The Schwarzschild metric

The most general spherically symmetric metric is [36, 51]

$$ds^2 = A(r, t) c^2 dt^2 - B(r, t) dr^2 - 2C(r, t) dr dt - D(r, t)(d\theta^2 + \sin^2 \theta d\phi^2), \quad (2.42)$$

where A, B, C and D are arbitrary function of space and time. It is possible to find a new coordinate system where, making the transformations

$$r' = F(r, t), \quad t' = G(r, t), \quad (2.43)$$

we have

$$C' = 0, \quad D' = r^2. \quad (2.44)$$

We can choose for A' and B' any function of r and t without changing the spherical symmetry; to simplify the calculations we choose an exponential form and the line element can be recast in the form

$$ds^2 = e^{\nu(r,t)} c^2 dt^2 - e^{\lambda(r,t)} dr^2 - r^2 d\Omega^2, \quad d\Omega^2 \equiv d\theta^2 + \sin^2 \theta d\varphi^2. \quad (2.45)$$

With these expressions for the coefficients of the metric

$$g_{tt} = e^{\nu(r,t)}, \quad g_{rr} = -e^{\lambda(r,t)}, \quad g_{\theta\theta} = -r^2, \quad g_{\varphi\varphi} = -r^2 \sin^2 \theta, \quad (2.46)$$

and its inverse

$$g^{tt} = e^{-\nu(r,t)}, \quad g^{rr} = -e^{-\lambda(r,t)}, \quad g^{\theta\theta} = -r^{-2}, \quad g^{\varphi\varphi} = -r^{-2} \sin^{-2} \theta, \quad (2.47)$$

it's easy to compute the Christoffel symbols from the expression

$$\Gamma_{\mu\nu}^{\alpha} = g^{\alpha\lambda} \frac{1}{2} (g_{\lambda\mu,\nu} + g_{\nu\lambda,\mu} - g_{\mu\nu,\lambda}). \quad (2.48)$$

After some calculations, we find that the nonvanishing symbols are:

$$\Gamma_{tt}^t = \frac{\nu_t}{2c}, \quad \Gamma_{tr}^t = \Gamma_{rt}^t = \frac{\nu_r}{2}, \quad \Gamma_{rr}^t = \frac{\lambda_t}{2c} e^{\lambda-\nu}, \quad \Gamma_{tt}^r = \frac{\nu_r}{2} e^{\nu-\lambda}, \quad (2.49)$$

$$\Gamma_{rr}^r = \frac{\lambda_r}{2}, \quad \Gamma_{tr}^r = \Gamma_{rt}^r = \frac{\lambda_t}{2c}, \quad \Gamma_{\theta\theta}^r = -r e^{-\lambda}, \quad \Gamma_{\varphi\varphi}^r = -r \sin^2 \theta e^{-\lambda}, \quad (2.50)$$

$$\Gamma_{r\theta}^{\theta} = \Gamma_{\theta r}^{\theta} = \frac{1}{r}, \quad \Gamma_{\varphi\varphi}^{\theta} = -\sin \theta \cos \theta, \quad \Gamma_{r\varphi}^{\varphi} = \Gamma_{\varphi r}^{\varphi} = \frac{1}{r}, \quad (2.51)$$

$$\Gamma_{\theta\varphi}^{\varphi} = \Gamma_{\varphi\theta}^{\varphi} = \cot \theta. \quad (2.52)$$

Einstein's equations in vacuum are obtained by setting to zero the components of $R_{\mu\nu}$. The first important result is obtained for $\mu = t$ and $\nu = r$:

$$R_{tr} = \frac{1}{c r} \lambda_t = 0, \quad (2.53)$$

from which it is deduced that λ does not depend on time. The remaining non-zero components of the Ricci tensor are

$$R_{tt} = \frac{1}{2} e^{\nu-\lambda} \left(\nu'' + \frac{1}{2} \nu'^2 - \frac{1}{2} \nu' \lambda' + 2 \frac{\nu'}{r} \right) = 0, \quad (2.54)$$

$$R_{rr} = \frac{1}{2} \left(\nu'' + \frac{1}{2} \nu'^2 - \frac{1}{2} \nu' \lambda' - 2 \frac{\lambda'}{r} \right) = 0, \quad (2.55)$$

where a $'$ indicates derivative with respect the time. From (2.54) and (2.55) we get

$$\nu' + \lambda' = 0 \rightarrow \nu' = -\lambda'. \quad (2.56)$$

Furthermore, asymptotic flatness, which requires a flat metric ($e^\nu \rightarrow 1$ and $e^\lambda \rightarrow 1$) for $r \rightarrow \infty$, implies a zero integration constant

$$\lambda + \nu = 0. \quad (2.57)$$

It can be proven that after integrating Eq. (2.54), where we used the result (2.56), we get:

$$e^\nu = A + \frac{B}{r}, \quad (2.58)$$

where A and B are integration constants. For

$$r \rightarrow \infty, \quad e^\nu = 1 \quad (2.59)$$

so we get the value for the constant A :

$$A = 1. \quad (2.60)$$

The value of B can be determined by requiring that Newton's law holds at large distances:

$$e^\nu = g_{00} = 1 - \frac{2U}{c^2} = 1 - \frac{2G_N M}{r c^2}. \quad (2.61)$$

The quantity R_S is defined as the *Schwarzschild radius*:

$$R_S \equiv \frac{2G_N M}{c^2}. \quad (2.62)$$

R_S has the dimensions of a length and it can be associated with all the bodies having mass M . Finally, the solution of the metric is:

$$ds^2 = \left(1 - \frac{R_S}{r}\right) c^2 dt^2 - \left(1 - \frac{R_S}{r}\right)^{-1} dr^2 - r^2 d\Omega^2. \quad (2.63)$$

The Schwarzschild metric describes gravitational field outside a spherical distribution of matter, which may be either static or have radial motion. In fact, from the above solution, it can be seen that by assuming the only hypothesis of a spherically symmetrical system the resulting metric is static. This important result is known as Birkhoff's theorem: *the empty space-time outside a spherically symmetric distribution of matter is describable by a static metric.*

The metric (2.63) describes the space-time outside a spherically symmetric black hole and R_S locates its *event horizon*. At $r = R_S$ the Schwarzschild solution contains an apparent singularity, indeed the metric coefficients of solution (2.63) become singular:

$$g_{00} = (g_{11}^{-1}) = 0. \quad (2.64)$$

But the surface $r = R_S$ is a regular surface of the space-time manifold, as we can see by calculating the curvature invariants; for example, the Kretschman invariant

$$\mathcal{R}^2 \equiv R_{\mu\nu\lambda\rho} R^{\mu\nu\lambda\rho} = \frac{12 R_S^2}{r^6} \quad (2.65)$$

is finite at $r = R_S$. The mentioned singularity is a “coordinate singularity”, while the physical singularity of the metric is at $r = 0$ (“curvature singularity”). At $r = 0$ the curvature becomes infinite and the tidal forces grow.

The Schwarzschild solution is expressed in the “standard” form in Eq. (2.63), but it can be equivalently expressed in the “isotropic” form by introducing the new radius variable ρ as

$$\rho \equiv \frac{1}{2} \left[r - \frac{R_S}{2} + (r^2 - R_S r)^{1/2} \right] \quad (2.66)$$

or

$$r = \rho \left(1 + \frac{R_S}{4\rho} \right)^2. \quad (2.67)$$

After substitutions, Eq. (2.63) becomes

$$ds^2 = \frac{\left(1 - \frac{R_S}{4\rho} \right)^2}{\left(1 + \frac{R_S}{4\rho} \right)^2} dt^2 - \left(1 + \frac{R_S}{4\rho} \right)^4 (d\rho^2 + \rho^2 d\theta^2 + \rho^2 \sin^2 \varphi^2). \quad (2.68)$$

2.3.2 Schwarzschild geodesics

Equations of motion of particles in a space-time described by the metric $g_{\mu\nu}$ can be derived from the associated Lagrangian $2\mathcal{L} = g_{\mu\nu} \frac{dx^\mu}{d\tau} \frac{dx^\nu}{d\tau}$, where τ is some affine parameter along the geodesic [94]. The Lagrangian corresponding to the Schwarzschild solution is

$$\mathcal{L} = \frac{1}{2} \left[\left(1 - \frac{R_S}{r} \right) \dot{t}^2 - \left(1 - \frac{R_S}{r} \right)^{-1} \dot{r}^2 - r^2 \dot{\theta}^2 - (r^2 \sin^2 \theta) \dot{\varphi}^2 \right] \quad (2.69)$$

where $\dot{\cdot} = \frac{d}{d\tau}$, and the associated canonical momenta are

$$\begin{aligned} p_t &= \frac{\partial \mathcal{L}}{\partial \dot{t}} = \left(1 - \frac{R_S}{r} \right) \dot{t}, & p_\varphi &= -\frac{\partial \mathcal{L}}{\partial \dot{\varphi}} = (r^2 \sin^2 \theta) \dot{\varphi}, \\ p_r &= -\frac{\partial \mathcal{L}}{\partial \dot{r}} = \left(1 - \frac{R_S}{r} \right)^{-1} \dot{r}, & \text{and } p_\theta &= -\frac{\partial \mathcal{L}}{\partial \dot{\theta}} = r^2 \dot{\theta}. \end{aligned} \quad (2.70)$$

To find the integrals of motion of the problem consider the Euler-Lagrange equations

$$\frac{dp_t}{d\tau} = \frac{d}{d\tau} \frac{\partial \mathcal{L}}{\partial \dot{t}} = \frac{\partial \mathcal{L}}{\partial t} = 0, \quad (2.71)$$

$$\frac{dp_\varphi}{d\tau} = -\frac{d}{d\tau} \frac{\partial \mathcal{L}}{\partial \dot{\varphi}} = -\frac{\partial \mathcal{L}}{\partial \varphi} = 0, \quad (2.72)$$

from which it follows that

$$p_t = \left(1 - \frac{R_S}{r}\right) \frac{dt}{d\tau} = \text{constant} = E, \quad (2.73)$$

$$p_\varphi = r^2 \sin^2 \theta \frac{d\varphi}{d\tau} = \text{constant} = L. \quad (2.74)$$

If we consider the equation of motion for θ

$$\frac{dp_\theta}{d\tau} = \frac{d}{d\tau}(r^2 \dot{\theta}) = -\frac{\partial \mathcal{L}}{\partial \theta} = (r^2 \sin \theta \cos \theta) \left(\frac{d\varphi}{d\tau}\right)^2 \quad (2.75)$$

it's easy to see that if put $\theta = \pi/2$ when $\dot{\theta} = 0$, then we also have $\ddot{\theta} = 0$ and the motion will lie in an invariant plane. By rescaling the affine parameter τ , and with \dot{t} and $\dot{\varphi}$ expressed in terms of E and L , the Lagrangian for time-like geodesics becomes

$$\frac{E^2}{1 - \frac{R_S}{r}} - \frac{\dot{r}^2}{1 - \frac{R_S}{r}} - \frac{L^2}{r^2} = 2\mathcal{L} = 1. \quad (2.76)$$

We can rewrite Eqns (2.74) and (2.76) as

$$\left(\frac{dr}{d\tau}\right)^2 + \left(1 - \frac{R_S}{r}\right) \left(1 + \frac{L^2}{r^2}\right) = E^2 \quad (2.77)$$

and

$$\frac{d\varphi}{d\tau} = \frac{L}{r^2}. \quad (2.78)$$

To get information about the types of trajectories, we can rewrite Eq. (2.77) highlighting the effective potential U as

$$\left(\frac{dr}{d\tau}\right)^2 = E^2 - U. \quad (2.79)$$

The effective potential is given by

$$U = (1 - z)(1 + l^2 z^2), \quad (2.80)$$

where we introduced the new variables $z = R_S/r$ ($z = 0$ is the spatial infinity and $z = 1$ is the black hole horizon) and $l = L/R_S$. The equation giving extrema of the potential for a fixed l is

$$U_{,z} = -1 - 3l^2 z^2 + 2l^2 z = 0, \quad (2.81)$$

whose solution is

$$z_{\pm}(l) = \frac{1 \pm \sqrt{1 - 3l^{-2}}}{3}. \quad (2.82)$$

Studying the second derivative of U with respect to z

$$U_{,zz} = 2l^2 (1 - 3z), \quad (2.83)$$

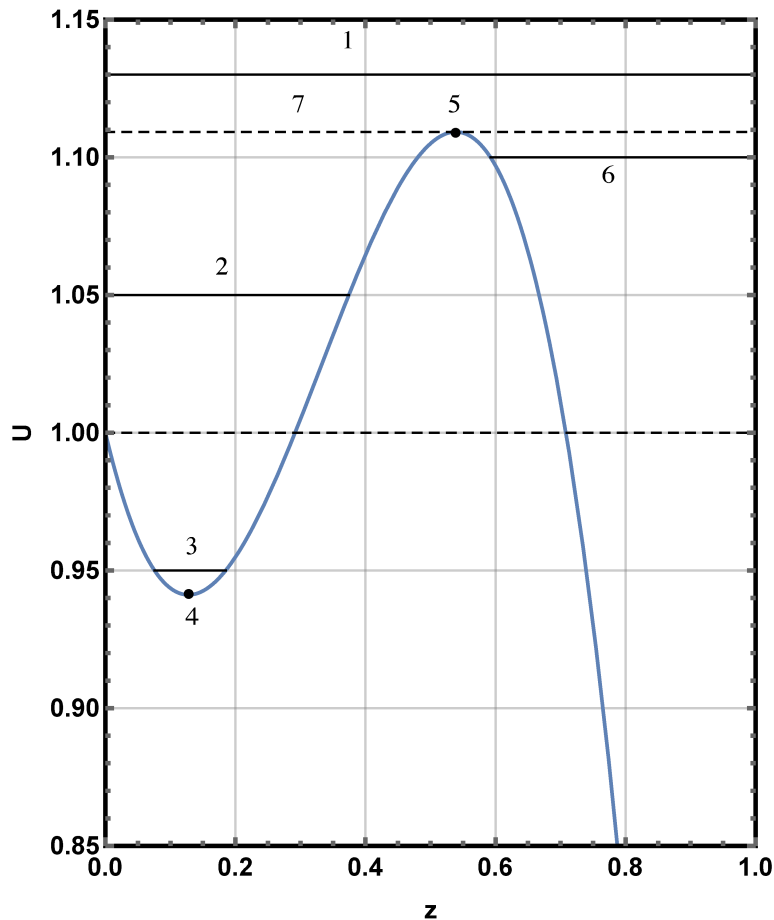


Figure 2.2: Effective potential for the fixed value $l = 2.2$ as a function of $z = R_S/r$. Horizontal lines represent different types of motion depending on the value of the energy.

we can see that at $z = z_-$ ($z = z_+$) the potential has the minimum U_- (the maximum U_+):

$$U_{\pm} = \frac{2[l(l^2 + 9) \pm (l^2 - 3)^{3/2}]}{27l}. \quad (2.84)$$

For $0 < l < \sqrt{3}$, U monotonically decreases from 1 at infinity to 0 at the horizon; we don't have any bounded motion. The bounded motion becomes possible for $l > \sqrt{3}$, where we have a minimum and a maximum. For $l > 2$ the maximum is greater than 1. In Fig. 2.2 an example of the potential for $l > 2$ is depicted. In that case, the following types of motion are possible:

1. gravitational capture, $E^2 > U_+$;
2. hyperbolic motion, $E^2 \in (1, U_+)$ and $z < z_+$;
3. bounded orbits, $E^2 \in (U_-, \min(U_+, 1))$ and $z < z_+$;
4. stable circular orbits, $E^2 = U_-$ and $z = z_-$;

5. unstable circular orbits, $E^2 = U_+$ and $z = z_+$;
6. near horizon trapped motion, $E^2 < U_-$ and $z > z_+$;
7. marginal outer ($z < z_+$) and inner ($z > z_+$) orbits, $E^2 = U_+$.

To obtain the geometry of the geodesics in the invariant plane, consider the function $r(\varphi)$ and let $u = r^{-1}$; the final equation is

$$\left(\frac{du}{d\varphi}\right)^2 = R_S u^3 - u^2 + \frac{R_S}{L^2} u - \frac{1 - E^2}{L^2}. \quad (2.85)$$

The solution, once obtained $u(\varphi)$, can be completed by integrating the equations

$$\frac{d\tau}{d\varphi} = \frac{1}{L u^2}, \quad \frac{dt}{d\varphi} = \frac{E}{L u^2 (1 - R_S u)}. \quad (2.86)$$

2.4 Rotating black holes

The Schwarzschild solution describes a black hole in the simplest approximation: a nonrotating black hole. However, a more realistic representation should include rotation: astrophysical objects (stars, planets, and galaxies) do rotate! Generally, the progenitor of a black hole (as a collapsing rotating star) has an angular momentum value other than zero. Even if this angular momentum got lost during the formation and the newly born black hole has only a small value, the surrounding accreting matter will give it mass and angular momentum.

An exact solution of Einstein's equations outside a black hole with mass M and angular momentum J exists, and it was found in 1963 by Roy P. Kerr [167, 94].

2.4.1 Kerr metric

The explicit form of the Kerr metric in the Boyer-Lindquist coordinates is the following:

$$ds^2 = -\left(1 - \frac{2Mr}{\Sigma}\right) dt^2 - \frac{4Mra \sin^2\theta}{\Sigma} dt d\phi + \frac{A \sin^2\theta}{\Sigma} d\phi^2 + \frac{\Sigma}{\Delta} dr^2 + \Sigma d\theta^2, \quad (2.87)$$

where

$$\Sigma = r^2 + a^2 \cos^2\theta, \quad (2.88)$$

$$\Delta = r^2 - 2Mr + a^2, \quad (2.89)$$

$$A = (r^2 + a^2)^2 - \Delta a^2 \sin^2\theta. \quad (2.90)$$

Observing the line element (2.87), we can deduce the main properties of the Kerr metric:

- It does not depend explicitly on ϕ , that is, it is axisymmetric. This should be expected because the rotation occurs around an axis which breaks the spherical symmetry.
- It does not depend explicitly on t , that is, it is stationary. However, differently from the non-rotating case, the reflection of time $t \rightarrow -t$ changes the direction of rotation: it is not static. On the other hand, the metric is invariant under a joint transformation $(t, \phi) \rightarrow (-t, -\phi)$.
- The Kerr metric is asymptotically flat: it reduces to Minkowski space-time for $r \rightarrow \infty$.
- The Kerr metric reduces to Schwarzschild metric in the limit $a \rightarrow 0$ ($M \neq 0$).

The Kerr metric depends on two parameters, the black hole mass M and its spin parameter (angular momentum per unit mass) $a \equiv J/M$. For values of the spin

$$|a| \leq M, \quad (2.91)$$

the object exhibits an event horizon at the radius ($\Delta = 0$)

$$r_+^L = M + \sqrt{M^2 - a^2}. \quad (2.92)$$

The *infinite redshift surface* Γ_+ , called also *ergosurface*, is defined by the equation $g_{tt} = 0$:

$$\Sigma - 2Mr = r^2 - 2Mr + a^2 \cos^2 \theta = 0, \quad (2.93)$$

or

$$r = r_0 \equiv M + \sqrt{M^2 - a^2 \cos^2 \theta}. \quad (2.94)$$

The surface Γ_+ is null in the Schwarzschild case and coincides with the event horizon. Instead, in the Kerr metric, the ergosurface cannot represent the event horizon since it is time-like. Considering a moving particle, it can be seen that outside Γ_+ ($g_{tt} < 0$), the observer can both corotate and counter-rotate with the black hole, while inside Γ_+ all of the observers are corotating with the black hole. The region between the ergosurface and the event horizon is called the *ergosphere*.

A set of important theorems proven by R.H. Price, B. Carter, W. Israel, D.C. Robinson, and S.W. Hawking, suggest that the external gravitational field of a black hole is determined uniquely by two parameters: the mass M and the intrinsic angular momentum J . In other words, during the formation and the accretion process, all the properties of the incoming material, apart from mass and spin, are radiated away by gravitational radiation (“*black holes have no hair*”, as John A. Wheeler summarized). Heuristically, we can understand the reason observing that these properties are associated with long-range fields exerting an influence at large distances. The cosmic

tensorship conjecture requires that the spin angular momentum J of the black hole satisfies

$$\chi \equiv \frac{c}{G_{\text{N}}} \frac{J}{M^2} \leq 1. \quad (2.95)$$

This theorem implies that all high multipole moments ($l \geq 2$) of the gravitational field of a non-charged black hole in GR can be expressed only in terms of M and J . In particular, the quadrupole moment Q , the lowest-order moment measurable, should satisfy the relation

$$q \equiv \frac{c^4}{G_{\text{N}}^2} \frac{Q}{M^3} = -\chi^2. \quad (2.96)$$

Eq. (2.96) represents a useful tool to test GR: the Kerr hypothesis can be verified by measuring the mass, spin, and quadrupole moment of an astrophysical black hole and see if they fulfill the relation.

2.5 Post-Newtonian expansion

The difficulty of solving Einstein's equations in the general case of a system that has no particular symmetries has led to the need to develop a systematic approximation method. One of these methods is the Post-Newtonian (PN) approximation, which applies to a system of slowly moving particles bound together by gravitational forces.

2.5.1 General features

The Post-Newtonian expansion is a procedure used in GR to find an approximate solution of the field equations. The approximations are expanded in a small parameter, assumed to be < 1 , expressing orders of deviations from Newton's law (first-order), which is the ratio v^2/c^2 of the velocity of the matter creating the gravitational field and the speed of light.

Consider a system of particles that, like the Sun and the planets, are bound by their mutual gravitational attraction [32]. Let \bar{M} , \bar{r} , and \bar{v} the typical values of the masses, separations, and velocities of these particles. From Newtonian mechanics we know that the typical kinetic energy $\frac{1}{2}\bar{M}\bar{v}^2$ is approximately of the same order of magnitude as the gravitational energy $\frac{G_{\text{N}}\bar{M}^2}{\bar{r}}$, so that

$$\bar{v}^2 \sim \frac{G_{\text{N}}\bar{M}}{\bar{r}}. \quad (2.97)$$

Typical values of the significant physical quantities in the Solar System are the following: the Newtonian gravitational potential U is $\leq 10^{-5}$, the planetary velocities \bar{v}^2 are $\leq U$, the matter pressure P inside the Sun and the planets is smaller than the

energy density ρU of the matter, and the specific energy density Π of the other forms of energy in the Solar System (stresses, radiation, etc.) are $\leq U$. It follows that these quantities give only second-order contributions, considered as functions of velocity

$$U \sim v^2 \sim \frac{P}{\rho} \sim \Pi \sim \mathcal{O}(2). \quad (2.98)$$

Since the velocity v contributes to order $\mathcal{O}(1)$, in this approximation we have

$$\frac{\partial}{\partial x^0} \sim v \cdot \nabla, \quad (2.99)$$

and

$$\frac{|\partial/\partial x^0|}{\nabla} \sim \mathcal{O}(1). \quad (2.100)$$

In the Newtonian approximation, based on the hypothesis of small velocities ($v \ll c$) and retaining only first-order terms in the deviations of $g_{\mu\nu}$ from the Minkowski metric $\eta_{\mu\nu}$, the particle equations of motion reduce to [233]

$$\frac{d^2 x^i}{d(x^0)^2} \simeq -\Gamma_{00}^i \simeq -\frac{1}{2} \frac{\partial g_{00}}{\partial x^i}, \quad (2.101)$$

where the relationship between affinities and derivatives of the metric has been taken into account. Since $g_{00} - 1$ is of order $G_N \bar{M}/\bar{r}$, the Newtonian approximation gives $d^2 x^i/dt^2$ to order $G_N \bar{M}/\bar{r}^2$ (that is, to order \bar{v}^2/\bar{r}). Therefore, the post-Newtonian approximation requires the calculation of $d^2 x^i/dt^2$ to the order \bar{v}^4/\bar{r} . The order up to which expanding the various components of affine connections can be deduced by making explicit the accelerations from expression (2.18):

$$\frac{d^2 x^i}{dt^2} = -\Gamma_{00}^i - 2\Gamma_{0j}^i \frac{dx^j}{dt} - \Gamma_{jk}^i \frac{dx^j}{dt} \frac{dx^k}{dt} + \left[\Gamma_{00}^0 + 2\Gamma_{0j}^0 \frac{dx^j}{dt} + \Gamma_{jk}^0 \frac{dx^j}{dt} \frac{dx^k}{dt} \right] \frac{dx^i}{dt}. \quad (2.102)$$

According to the local flatness of space-time, we expect that it is possible to find a coordinate system in which the metric tensor is nearly equal to the Minkowski tensor $\eta_{\mu\nu}$, the corrections being expandable in powers of $\bar{M} G_N/\bar{r} \sim \bar{v}^2$:

$$g_{00}(x^0, \mathbf{x}) = -1 + g_{00}^{(2)}(x^0, \mathbf{x}) + g_{00}^{(4)}(x^0, \mathbf{x}) + \mathcal{O}(6), \quad (2.103)$$

$$g_{0i}(x^0, \mathbf{x}) = g_{0i}^{(3)}(x^0, \mathbf{x}) + \mathcal{O}(5), \quad (2.104)$$

$$g_{ij}(x^0, \mathbf{x}) = \delta_{ij} + g_{ij}^{(2)}(x^0, \mathbf{x}) + \mathcal{O}(4). \quad (2.105)$$

The inverse metric is

$$g^{00}(x^0, \mathbf{x}) = -1 + g^{(2)00}(x^0, \mathbf{x}) + g^{(4)00}(x^0, \mathbf{x}) + \mathcal{O}(6), \quad (2.106)$$

$$g^{0i}(x^0, \mathbf{x}) = g^{(3)0i}(x^0, \mathbf{x}) + \mathcal{O}(5), \quad (2.107)$$

$$g^{ij}(x^0, \mathbf{x}) = \delta^{ij} + g^{(2)ij}(x^0, \mathbf{x}) + \mathcal{O}(4). \quad (2.108)$$

The symbol $g_{\mu\nu}^{(N)}$ denotes the term in $g_{\mu\nu}$ of order \bar{v}^N . From (2.102) and using the estimates (2.103)-(2.108), we find the following expansions for the components Γ_{00}^i , Γ_{jk}^i and Γ_{0i}^0

$$\Gamma_{\nu\lambda}^\mu = \Gamma_{\nu\lambda}^{(2)\mu} + \Gamma_{\nu\lambda}^{(3)\mu} + \dots \quad (2.109)$$

and for the components Γ_{0j}^i , Γ_{00}^0 and Γ_{ij}^0

$$\Gamma_{\nu\lambda}^\mu = \Gamma_{\nu\lambda}^{(3)\mu} + \Gamma_{\nu\lambda}^{(5)\mu} + \dots \quad (2.110)$$

Computation of the affine connections is based on the explicit formula (2.18), and on the fact that since the space and time scales are set respectively by \bar{r} and \bar{r}/\bar{v} , spatial and time derivatives are of the order

$$\frac{\partial}{\partial x^i} \sim \frac{1}{\bar{r}}, \quad \frac{\partial}{\partial x^0} \sim \frac{\bar{v}}{\bar{r}}. \quad (2.111)$$

Explicitly:

$$\Gamma_{00}^{(3)0} = \frac{1}{2} g_{00}^{(2),0}, \quad (2.112)$$

$$\Gamma_{00}^{(2)i} = \frac{1}{2} g_{00}^{(2),i}, \quad (2.113)$$

$$\Gamma_{jk}^{(2)i} = \frac{1}{2} \left(g_{jk}^{(2),i} - g_{j,k}^{(2)i} - g_{k,j}^{(2)i} \right), \quad (2.114)$$

$$\Gamma_{ij}^{(3)0} = \frac{1}{2} \left(g_{i,j}^{(3)0} - g_{j,i}^{(3)0} - g_{ij}^{(3),0} \right), \quad (2.115)$$

$$\Gamma_{0j}^{(3)i} = \frac{1}{2} \left(g_{0j}^{(3),i} - g_{0,j}^{(3)i} - g_{j,0}^{(2)i} \right), \quad (2.116)$$

$$\Gamma_{0i}^{(4)0} = \frac{1}{2} \left(g_{0,i}^{(4)0} + g^{(2)00} g_{00,i}^{(2)} \right), \quad (2.117)$$

$$\Gamma_{00}^{(4)i} = \frac{1}{2} \left(g_{00}^{(4),i} + g^{(2)im} g_{00,m}^{(2)} - 2g_{0,0}^{(3)i} \right), \quad (2.118)$$

$$\Gamma_{0i}^{(2)0} = \frac{1}{2} g_{0,i}^{(2)0}. \quad (2.119)$$

The corresponding components of the Ricci tensor are calculated using Eq. (2.2.1):

$$R_{00}^{(2)} = \frac{1}{2} \nabla^2 g_{00}^{(2)} \quad (2.120)$$

$$R_{00}^{(4)} = \frac{1}{2} \nabla^2 g_{00}^{(4)} - \frac{1}{2} g_{,m}^{(2)mn} g_{00,n}^{(2)} - \frac{1}{2} g^{(2)mn} g_{00,mn}^{(2)} + \frac{1}{2} g^{(2)m}{}_{m,00} - \frac{1}{4} g^{(2)0,m} g_{00,m}^{(2)} - \frac{1}{4} g_{m,n}^{(2)m,n} g_{00,n}^{(2)} - g_{0,m0}^{(3)m}, \quad (2.121)$$

$$R_{0i}^{(3)} = \frac{1}{2} \nabla^2 g_{0i}^{(3)} - \frac{1}{2} g_{i,m0}^{(2)m} - \frac{1}{2} g_{0,mi}^{(3)m} + \frac{1}{2} g_{m,0i}^{(2)m}, \quad (2.122)$$

$$R_{ij}^{(2)} = \frac{1}{2} \nabla^2 g_{ij}^{(2)} - \frac{1}{2} g_{i,mj}^{(2)m} - \frac{1}{2} g_{j,mi}^{(2)m} - \frac{1}{2} g_{0,ij}^{(2)0} + \frac{1}{2} g_{m,i}^{(2)m}. \quad (2.123)$$

These expressions can be simplified by choosing the harmonic gauge [233], that is a coordinate system x^μ so that it is satisfied the condition

$$g^{\mu\nu} \Gamma_{\mu\nu}^\lambda = 0. \quad (2.124)$$

It follows that, in this gauge, the Ricci tensor components are

$$R_{00}^{(2)} = \frac{1}{2} \nabla^2 g_{00}^{(2)}, \quad (2.125)$$

$$R_{00}^{(4)} = \frac{1}{2} \nabla^2 g_{00}^{(4)} - \frac{1}{2} g^{(2)mn} g_{00,mn}^{(2)} - \frac{1}{2} g^{(2)0}_{0,00} - \frac{1}{2} \left| \nabla \nabla_{\eta} g_{00}^{(2)} \right|^2, \quad (2.126)$$

$$R_{0,i}^{(3)} = \frac{1}{2} \nabla^2 g_{0i}^{(3)}, \quad (2.127)$$

$$R_{ij}^{(2)} = \frac{1}{2} \nabla^2 g_{ij}^{(2)}, \quad (2.128)$$

and the Ricci scalar is

$$R^{(2)} = R^{(2)0}_0 - R^{(2)m}_m = \frac{1}{2} \nabla^2 g^{(2)0}_0 - \frac{1}{2} \nabla^2 g^{(2)m}_m, \quad (2.129)$$

$$\begin{aligned} R^{(4)} &= R^{(4)0}_0 + g^{(2)00} R_{00}^{(2)} + g^{(2)mn} R_{mn}^{(2)} \\ &= \frac{1}{2} \nabla^2 g^{(4)0}_0 - \frac{1}{2} g^{(2)0,0}_{0,0} - \frac{1}{2} g^{(2)mn} \left(g^{(2)0}_{0,mn} - \nabla^2 g_{mn}^{(2)} \right) - \frac{1}{2} \left| \nabla g^{(2)0}_0 \right|^2 + \frac{1}{2} g^{(2)00} \nabla^2 g_{00}^{(2)}. \end{aligned} \quad (2.130)$$

Using the definition of the Lagrangian of a particle in the gravitational field, we get

$$\begin{aligned} L &= \left(g_{\rho\sigma} \frac{dx^\rho}{dx^0} \frac{dx^\sigma}{dx^0} \right)^{1/2} = (g_{00} + 2g_{0m}v^m + g_{mn}v^m v^n)^{1/2} \\ &= \left(1 + g_{00}^{(2)} + g_{00}^{(4)} + 2g_{0m}^{(3)}v^m - \mathbf{v}^2 + g_{mn}^{(2)}v^m v^n \right)^{1/2}, \end{aligned} \quad (2.131)$$

which reduces to the Newtonian Lagrangian $L_N = \left(1 + g_{00}^{(2)} - v^2 \right)$ to second order and includes higher order terms in the Post-Newtonian limit.

2.6 General metrics

In this section, we wonder what it is the general form of the metric produced by a spherically symmetrical static object (Sec. 2.6.1), which in first approximation represents an astrophysical object (such as the Sun, or a black hole). Under these assumptions, three tests to support GR were carried out [233]:

1. Gravitational redshift of spectral lines;
2. Deflection of light by the Sun;
3. Precession of the perihelia of the orbits of the inner planets.

In particular, we will focus on treating the precession of the perihelia in the context of the Parametrized Post Newtonian (PPN) formulation (Sec. 2.6.3), an approach that aims at finding deviations from the Schwarzschild solution in a model-independent way (Sec. 2.6.2).

2.6.1 The General Static Isotropic gravitational field

The most general metric tensor representing a static isotropic gravitational field, in the “standard” form, is [233]

$$d\tau^2 = B(r) dt^2 - A(r) dr^2 - r^2 (d\theta^2 + \sin^2 \theta d\varphi^2). \quad (2.132)$$

The metric tensor $g_{\mu\nu}$ is diagonal and its nonvanishing components are

$$g_{tt} = -B(r) \quad g_{rr} = A(r) \quad g_{\theta\theta} = r^2 \quad g_{\varphi\varphi} = r^2 \sin^2 \theta \quad . \quad (2.133)$$

Its inverse has the coefficients

$$g^{tt} = -B^{-1}(r) \quad g^{rr} = A^{-1}(r) \quad g^{\theta\theta} = r^{-2} \quad g^{\varphi\varphi} = r^{-2} \sin^{-2} \theta \quad . \quad (2.134)$$

The general functions $A(r)$ and $B(r)$ can be determined by solving the field equations. The nonvanishing Christoffel symbols, calculated from the usual formula (2.18), are

$$\begin{aligned} \Gamma_{rr}^r &= \frac{1}{2} \frac{dA(r)}{A(r) dr} \\ \Gamma_{\theta\theta}^r &= -\frac{r}{A(r)} \\ \Gamma_{\varphi\varphi}^r &= -\frac{r \sin^2 \theta}{A(r)} \\ \Gamma_{tt}^r &= \frac{1}{2} \frac{dB(r)}{A(r) dr} \\ \Gamma_{r\theta}^\theta &= \Gamma_{\theta r}^\theta = \frac{1}{r} \\ \Gamma_{\varphi\varphi}^\theta &= -\sin \theta \cos \theta \\ \Gamma_{\varphi r}^\varphi &= \Gamma_{r\varphi}^\varphi = \frac{1}{r} \\ \Gamma_{\varphi\theta}^\varphi &= \Gamma_{\theta\varphi}^\varphi = \cot \theta \\ \Gamma_{tr}^t &= \Gamma_{rt}^t = \frac{1}{2B(r)} \frac{dB(r)}{dr}. \end{aligned} \quad (2.135)$$

We now consider equations of motion of a freely falling particle in such a metric

$$\frac{d^2 x^\mu}{dp^2} + \Gamma_{\nu\lambda}^\mu \frac{dx^\nu}{dp} \frac{dx^\lambda}{dp} = 0, \quad (2.136)$$

where p is an affine parameter that can be normalized for a material particle so that $p = \tau$. Using expressions (2.135) for the affine connections, we define the following

system

$$0 = \frac{d^2 r}{dp^2} + \frac{A'(r)}{2A(r)} \left(\frac{dr}{dp} \right)^2 - \frac{r}{A(r)} \left(\frac{d\theta}{dp} \right)^2 - r \frac{\sin^2 \theta}{A(r)} \left(\frac{d\varphi}{dp} \right)^2 + \frac{B'(r)}{2A(r)} \left(\frac{dt}{dp} \right)^2 \quad (2.137)$$

$$0 = \frac{d^2 \theta}{dp^2} + \frac{2}{r} \frac{d\theta}{dp} \frac{dr}{dp} - \sin \theta \cos \theta \left(\frac{d\varphi}{dp} \right)^2 \quad (2.138)$$

$$0 = \frac{d^2 \varphi}{dp^2} + \frac{2}{r} \frac{d\varphi}{dp} \frac{dr}{dp} + 2 \cot \theta \frac{d\varphi}{dp} \frac{d\theta}{dp} \quad (2.139)$$

$$0 = \frac{d^2 t}{dp^2} + \frac{B'(r)}{B(r)} \frac{dt}{dp} \frac{dr}{dp}, \quad (2.140)$$

where $' = \frac{d}{dr}$. Isotropy allows us to assume that the orbit lies in the equatorial plane, that is to fix $\theta = \pi/2$. Two constants of motion can be found by dividing (2.139) and (2.140) by $d\varphi/dp$ and dt/dp respectively:

$$\frac{d}{dp} \left\{ \ln \frac{d\varphi}{dp} + \ln r^2 \right\} = 0 \quad (2.141)$$

$$\frac{d}{dp} \left\{ \ln \frac{dt}{dp} + \ln B \right\} = 0. \quad (2.142)$$

The solution of (2.142), after normalizing p , is

$$\frac{dt}{dp} = \frac{1}{B(r)}. \quad (2.143)$$

The other constant is obtained by solving (2.141), and represents the angular momentum per unit mass

$$r^2 \frac{d\varphi}{dp} = J. \quad (2.144)$$

Substituting (2.143) and (2.144) in (2.137), we get the remaining equation of motion

$$\frac{d}{dp} \left\{ A(r) \left(\frac{dr}{dp} \right)^2 + \frac{J^2}{r^2} - \frac{1}{B(r)} \right\} = 0, \quad (2.145)$$

which gives our last constant of motion

$$A(r) \left(\frac{dr}{dp} \right)^2 + \frac{J^2}{r^2} - \frac{1}{B(r)} = -E \quad (\text{constant}). \quad (2.146)$$

Since we are more interested in the shape of orbits, that is, in r as a function of φ , we can eliminate dp from (2.144) and (2.146)

$$\frac{A(r)}{r^4} \left(\frac{dr}{d\varphi} \right)^2 + \frac{1}{r^2} - \frac{1}{J^2 B(r)} = -\frac{E}{J^2}. \quad (2.147)$$

The solution can be determined by a quadrature:

$$\varphi = \pm \int \frac{A^{1/2}(r) dr}{r^2 \left(\frac{1}{J^2 B(r)} - \frac{E}{J^2} - \frac{1}{r^2} \right)^{1/2}}. \quad (2.148)$$

2.6.2 Eddington-Robertson expansion

Here we will expose a useful test of GR as formulated by Eddington and Robertson. We ask ourselves what is the general form in which to express the metric produced by a static spherically symmetrical body, which could be in principle different from that calculated from the Einstein equations. It is reasonable to expect that such a form should be isotropic and should have metric coefficients expressible in power series in the small parameter $\frac{M G_N}{r} = \frac{R_S}{2r}$:

$$d\tau^2 = \left(1 - \alpha \frac{R_S}{2\rho} + \beta \frac{R_S^2}{2\rho^2} + \dots\right) dt^2 - \left(1 + \gamma \frac{R_S}{\rho} + \dots\right) (d\rho^2 + \rho^2 d\theta^2 + \rho^2 \sin^2 \theta d\varphi^2) \quad (2.149)$$

where α , β and γ are unknown dimensionless parameters, whose value must be fixed by measurements. Comparison with the isotropic form of the Schwarzschild solution [233] shows that GR is recovered for

$$\alpha = \beta = \gamma = 1. \quad (2.150)$$

It's convenient to express the metric in its "standard" form by defining

$$r \equiv \rho \left(1 + \gamma \frac{R_S}{2\rho} + \dots\right) \quad (2.151)$$

or

$$\rho = r \left(1 - \gamma \frac{R_S}{2r} + \dots\right). \quad (2.152)$$

After substitution we obtain

$$d\tau^2 = \left(1 - \alpha \frac{R_S}{r} + (\beta - \alpha\gamma) \frac{R_S^2}{2r^2} + \dots\right) dt^2 - \left(1 + \gamma \frac{R_S}{r} + \dots\right) dr^2 - r^2 d\theta^2 - r^2 \sin^2 \theta d\varphi^2. \quad (2.153)$$

2.6.3 Precession of Perihelia

Consider a test particle in a bound orbit, for example around the Sun (see Figure 2.3) [233].

When r reaches its minimum and maximum values, that is respectively at perihelia r_- and aphelia r_+ , $dr/d\varphi$ vanishes, so (2.147) gives

$$\frac{1}{r_{\pm}^2} - \frac{1}{J^2 B(r_{\pm})} = -\frac{E}{J^2}. \quad (2.154)$$

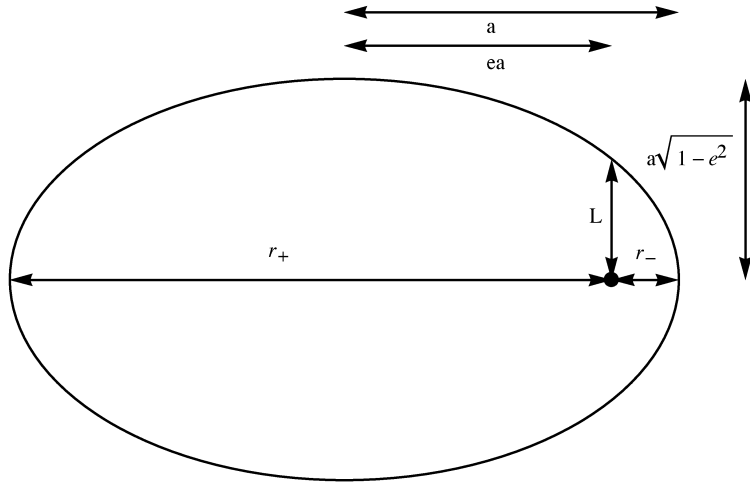


Figure 2.3: Elements of an ellipse referred to in the calculation of the precession of planetary orbits.

From these two equations two constants of motion can be inferred:

$$E = \frac{\frac{r_+^2}{B(r_+)} - \frac{r_-^2}{B(r_-)}}{r_+^2 - r_-^2} \quad (2.155)$$

$$J^2 = \frac{\frac{1}{B(r_+)} - \frac{1}{B(r_-)}}{\frac{1}{r_+^2} - \frac{1}{r_-^2}}. \quad (2.156)$$

When the position vector as r increases from r_- to a generic value r , it sweeps away an angle given by Eq. (2.148):

$$\varphi(r) = \varphi(r_-) + \int_{r_-}^r A^{1/2}(r) \left[\frac{1}{J^2 B(r)} - \frac{E}{J^2} - \frac{1}{r^2} \right]^{-1/2} \frac{dr}{r^2}. \quad (2.157)$$

Using (2.155) and (2.156), Eq. (2.157) becomes

$$\begin{aligned} \varphi(r) - \varphi(r_-) = \int_{r_-}^r \left[\frac{r_-^2(B^{-1}(r) - B^{-1}(r_-)) - r_+^2(B^{-1}(r) - B^{-1}(r_+))}{r_+^2 r_-^2 (B^{-1}(r_+) - B^{-1}(r_-))} - \frac{1}{r^2} \right]^{-1/2} \\ \times A^{1/2}(r) r^{-2} dr. \end{aligned} \quad (2.158)$$

The total change in φ per revolution is $2|\varphi(r_+) - \varphi(r_-)|$, and it would be equal to 2π if the orbit was a closed ellipse. In general the orbit precesses in each revolution by an angle

$$\Delta\varphi = 2|\varphi(r_+) - \varphi(r_-)| - 2\pi. \quad (2.159)$$

Let us use for $A(r)$ and $B(r)$ the Robertson expansions

$$A(r) = 1 + \gamma \frac{R_S}{r} + \dots \quad (2.160)$$

$$B(r) = 1 - \frac{R_S}{r} + \frac{(\beta - \gamma)R_S^2}{2r^2} + \dots \quad (2.161)$$

It's useful to realize that by using the expansion

$$B^{-1}(r) \simeq 1 + \frac{R_S}{r} + \frac{(2 - \beta + \gamma)R_S^2}{2r^2} \quad (2.162)$$

the argument of the first square root of (2.158) becomes a quadratic function of $1/r$; it vanishes at $r = r_{\pm}$, so

$$\begin{aligned} \frac{r_-^2(B^{-1}(r) - B^{-1}(r_-)) - r_+^2(B^{-1}(r) - B^{-1}(r_+))}{r_+^2 r_-^2 (B^{-1}(r_+) - B^{-1}(r_-))} - \frac{1}{r^2} &= \\ &= C \left(\frac{1}{r_-} - \frac{1}{r} \right) \left(\frac{1}{r} - \frac{1}{r_+} \right). \end{aligned} \quad (2.163)$$

We can determine C by putting $r \rightarrow \infty$:

$$C \simeq 1 - (2 - \beta + \gamma) \frac{R_S}{2} \left(\frac{1}{r_+} + \frac{1}{r_-} \right). \quad (2.164)$$

Substituting the above result in the integral (2.158), and defining the new variable ψ

$$\frac{1}{r} \equiv \frac{1}{2} \left(\frac{1}{r_+} - \frac{1}{r_-} \right) + \frac{1}{2} \left(\frac{1}{r_+} + \frac{1}{r_-} \right) \sin \psi \quad (2.165)$$

we finally find

$$\begin{aligned} \varphi(r) - \varphi(r_-) &= \left[1 + \frac{1}{4}(2 - \beta + 2\gamma) R_S \left(\frac{1}{r_+} + \frac{1}{r_-} \right) \right] \left[\psi + \frac{\pi}{2} \right] \\ &\quad - \frac{1}{4} \gamma R_S \left(\frac{1}{r_+} - \frac{1}{r_-} \right) \cos \psi. \end{aligned} \quad (2.166)$$

At aphelion $\psi = \pi/2$, so that the precession per revolution is

$$\Delta\varphi = \left(\frac{3\pi R_S}{\ell} \right) \left(\frac{2 - \beta + 2\gamma}{3} \right) \text{ (radians/revolution)} \quad (2.167)$$

where ℓ is called the *semilatus rectum*

$$\frac{1}{\ell} \equiv \frac{1}{2} \left(\frac{1}{r_+} + \frac{1}{r_-} \right). \quad (2.168)$$

The elements defining planetary orbits are the semi-major axis a and eccentricity e , defined as

$$r_{\pm} = (1 \pm e)a. \quad (2.169)$$

Hence the expression of ℓ in terms of a and e is

$$\ell = (1 - e^2)a. \quad (2.170)$$

Einstein's field equations yield $\beta = \gamma = 1$, so they predict a precession

$$\Delta\varphi = 3\pi \frac{R_S}{\ell} \text{ radians/revolution.} \quad (2.171)$$

This is positive, meaning that the whole orbit should precess in the same direction as the motion of the test particle.

For Mercury, GR predicts

$$\Delta\varphi_S = 42.9822'' \text{ per century } (\S). \quad (2.172)$$

According to observations $\Delta\varphi_{\text{obs}} = 43.1000 \pm 0.5000''$ per century (see Sec. 6.2.1).

These data served as the first important verification of GR. The result we are most interested in is Eq. (2.167): it represents a great tool to test other theories of gravitation, as we will see in Sec. 3.4.4.

2.7 Concluding remarks

In this chapter, we retraced the developments of GR, currently the most successful gravitational theory thanks to its formal elegance and experimental confirmations. When Einstein formulated GR he did not supplant Newton's laws, but he broadened their field of applicability. He explained what happened under conditions that could not be adequately described by the old theory, such as strong gravitational fields and motion close to the speed of light. In general, when introducing a new theory in physics, for it to be valid it must include successes of the one that preceded it, and at the same time, it must broaden the range of situations that the previous one did not describe with precision. The newborn paradigm must explain what has already been explained and should predict something that has not yet been conceived. In the next chapter, we will examine the signals that GR is at a point analogous to Newton's theory when it was "extended". Some inconsistencies have emerged from a large amount of new observational data and theoretical progress.

EXTENDING GENERAL RELATIVITY

Veritatem inquirenti, semel in vita de omnibus, quantum fieri potest, esse dubitandum.

– R. Descartes

3.1	Motivations	40
3.1.1	The cosmological problem	41
3.1.2	UV scales: the Quantum Gravity problem	43
3.1.3	IR scales: Dark Energy and Dark Matter	45
3.2	Beyond Einstein’s theory	46
3.2.1	Lovelock theorem	46
3.2.2	A general class of Extended Theories of Gravity	48
3.3	$f(R)$ -gravity	50
3.3.1	Field equations	50
3.3.2	Weak field limit of $f(R)$ -gravity theory	52
3.3.3	Geodesic motion	54
3.3.4	Precession	56
3.4	Bootstrapped Newtonian Gravity	57
3.4.1	Potential in the vacuum	58
3.4.2	Harmonic and areal coordinates	60
3.4.3	Effective space-time metric	61
3.4.4	Precession	64
3.5	Concluding remarks	65

In this chapter, we will introduce Extended Theories of Gravity (ETG). After analyzing the reasons that led many scientists to extend GR (Sec. 3.1), we will focus on two particular ETG: the $f(R)$ -gravity theory (Sec. 3.3), which helps us in the natural

solution of some problems at infrared scales, and the Bootstrapped Newtonian gravity theory (Sec. 3.4), born from the attempt to frame gravitational theory in a quantum context. On this background, we will define the system of geodesics equations to apply to the exact study of stellar orbits at the Galactic Center.

3.1 Motivations

Attempts to apply GR at extreme regimes, far from the Solar System where it proved to be successful, led to the question of whether it is the definitive theory to explain gravitational interaction. Such a question has both theoretical and experimental roots [35], which will be summarized in this section.

First of all, the Standard Model of Big-Bang cosmology, which refers to an adiabatically expanding radiation-dominated Universe described by a Robertson-Walker metric, is afflicted by the flatness problem and the horizon problem [122].

Remaining in the cosmological context, another delicate issue is that the observed accelerated expansion of the Universe requires mysterious and still undetected ingredients in the global matter-energy content: dark energy (DE) and dark matter (DM).

Then, since the Einsteinian scheme is classical, a unification of gravity with the other interactions based on a quantum description is not possible. A unifying scheme is desired for many reasons [28, 131], although the quantum gravity correction becomes essential at an experimentally inaccessible scale (that is the Planck scale $l_P \sim 10^{-33}$ cm). An example is given by the Big Bang scenario: in the Planck era, the Universe experiences dimensions smaller than l_P and this requires an adequate quantum treatment. Moreover, in GR space-time is a continuum and all scales are relevant, therefore the quantum question must be addressed for a definitive study of the intimate nature of space-time.

Other reasons to modify GR are dictated by the attempt to fully incorporate Mach's principle into the theory. This principle states that the inertial forces observed locally in an accelerated laboratory can be interpreted as gravitational effects originating from distant matter accelerated relative to the laboratory. These ideas found a limited expression in GR, where the geometry is influenced by the mass distribution but is not uniquely specified; here it is not possible to specify boundary conditions on the field equations that bring the theory in accordance with Mach's Principle.

These reasons led to propose several "alternative theories", within which GR and its successes should be replicated. One of the most productive approaches has been that of *Extended Theories of Gravitation* (ETG), defined as semiclassical theories in which the effective field Lagrangian is modified, with respect to the Hilbert-Einstein Lagrangian of gravitation, by higher-order terms in the invariants of curvature (as R^2 , $R^{\mu\nu}R_{\mu\nu}$, $R^{\mu\nu\alpha\beta}R_{\mu\nu\alpha\beta}$, $R\Box R$, $R\Box^k R$), or by terms with scalar fields not minimally coupled to

the geometry (as $\phi^2 R$) [32].

Below we will see why ETG could play a relevant role in the problems mentioned.

3.1.1 The cosmological problem

The Standard Model of Big-Bang cosmology is problematic for its puzzling assumptions on initial conditions [36, 122]. Let us briefly summarize its fundamental equations to see what generates the cosmological problem.

The Universe is described by the Robertson-Walker metric:

$$d\tau^2 = dt^2 - R^2(t) \left[\frac{dr^2}{1 - k r^2} + r^2 (d\theta^2 + \sin^2 \theta d\phi^2) \right], \quad (3.1)$$

where $k = \{1, -1, 0\}$ depending on whether the Universe is closed, open or flat. Einstein equations regulate the evolution of $R(t)$ ¹:

$$\ddot{R} = -\frac{4\pi}{3} G(\rho + 3p) R \quad (3.2)$$

$$H^2 + \frac{k}{R^2} = \frac{8\pi}{3} G \rho, \quad \text{with} \quad H = \frac{\dot{R}}{R}. \quad (3.3)$$

Conservation of energy translates into the equation

$$\frac{d}{dt}(\rho R^3) = -p \frac{d}{dt} R^3, \quad (3.4)$$

where p indicates the pressure. Another assumption at the basis of the Standard Model is the adiabatic expansion, that is

$$\frac{d}{dt}(s R^3) = 0, \quad (3.5)$$

where s is the entropy density and $S = s R^3$ is the total entropy. To complete the previous set of equations, we must write the equation of state of an ideal quantum gas of massless particles describing matter. Thermodynamic quantities can be expressed as

$$\rho = 3p = \frac{\pi^2}{30} \mathfrak{R}(T) T^4 \quad (3.6)$$

$$s = \frac{2\pi^2}{45} \mathfrak{R}(T) T^3 \quad (3.7)$$

$$n = \frac{\zeta(3)}{\pi^2} \mathfrak{R}'(T) T^3. \quad (3.8)$$

¹The dot represents the derivative with respect to t .

Here n is the particle number density, $\zeta(3) = 1.20206\dots$ is the Riemann zeta function,

$$\mathfrak{R}(T) = N_b(T) + \frac{7}{8} N_f(T) \quad (3.9)$$

$$\mathfrak{R}'(T) = N_b(T) + \frac{3}{4} N_f(T) \quad (3.10)$$

and $N_b(T)$ and $N_f(T)$ are the number of spin degrees of freedom for bosons and fermions at temperature T . Let us rewrite Eq. (3.3) in terms of T :

$$\left(\frac{\dot{T}}{T}\right)^2 + \epsilon(T) T^2 = \frac{4\pi^3}{45} G_N \mathfrak{R}(T) T^4 \quad \text{with} \quad \epsilon(T) = \frac{k}{R^2 T^2} = k \left[\frac{2\pi^2 \mathfrak{R}(T)}{45 S} \right]^{2/3}. \quad (3.11)$$

Today, observations point out that ρ is very close to the critical value, in the sense that $0.01 < \Omega_0 < 10$, where

$$\Omega \equiv \frac{\rho}{\rho_{\text{cr}}} = \frac{8\pi G \rho}{3 H^2}. \quad (3.12)$$

So, taking $\rho < 10 \rho_{\text{cr}}$, we have $|k/R^2| < 9H^2$. Next, assuming $k = \pm 1$ it follows that $R > \frac{1}{3} H^{-1} \sim 3 \times 10^9$ years. Assuming the photon temperature $T_\gamma = 2.7^\circ\text{K}$ and that there are three species of massless neutrinos (e , μ , and τ), we find that $S_\gamma > 3 \times 10^{85}$ and $S_\nu = 21/22 S_\gamma$. Then:

$$S > 10^{86} \quad (3.13)$$

and

$$|\epsilon| < 10^{-58} \mathfrak{R}^{2/3}. \quad (3.14)$$

Finally, taking $T = 10^{17}$ GeV and $\mathfrak{R} \sim 10^2$, one finds

$$\left| \frac{\rho - \rho_{\text{cr}}}{\rho} \right| = \frac{45}{4\pi^3} \frac{M_{\text{P}}^2}{\mathfrak{R} T^2} |\epsilon| < 10^{-55}. \quad (3.15)$$

This is the *flatness* problem. The heart of the problem lies in the smallness of this relationship; required initial conditions are very stringent. If the Universe initial density could have assumed any value, it seems extremely surprising to discover a value so close to ρ_{cr} . A small deviation of Ω_0 from unity in the early Universe would have amplified enormously during the following billions of years, leading to a current density value far from the critical one.

Deleting ϵT^2 from (3.117), we get $T^2 = M_{\text{P}}/(2\gamma t)$ ($\gamma^2 = (4\pi^3/45) \mathfrak{R}$). According to the conservation of entropy, we have $RT = \text{constant}$, so that $R \propto t^{1/2}$. Starting at $t = 0$, a light pulse will have traveled a physical horizon distance, after a time t , equal to

$$l(t) = R(t) \int_0^t dt' R^{-1}(t') = 2t. \quad (3.16)$$

The horizon distance must be compared with the radius $L(t)$ of the region at time t , which according to the conservation of entropy can be written as

$$L(t) = [s_{\text{p}}/s(t)]^{1/3} L_{\text{p}}, \quad (3.17)$$

where s_p is the present entropy density and $L_p \sim 10^{10}$ years is the radius of the currently observed Universe. Let us write the ratio of volumes:

$$\frac{l_0^3}{L_0^3} = 10^{-83}. \quad (3.18)$$

The initial Universe consists of at least $\sim 10^{83}$ separate regions which are causally disconnected, that is have not yet had time to communicate with each other. Instead, it is observed that the radiation of the Cosmic Microwave Background (CMB) is isotropic up to an accuracy of the order of $10^{-(4-5)}$. This indicates that all regions have been in contact with one another sometime in the past. This is the *horizon* problem.

Now assume that there has been a period of inflation: it is a process imagined in 1981 by A. Guth [122] during which the scale factor expands exponentially ($\ddot{a} > 0$)

$$a(t) \sim e^{Ht}, \quad H = \text{constant}. \quad (3.19)$$

Then, the problems of flatness and the horizon could be avoided.

The key point to solve the flatness problem is that entropy is no longer constant and the temperatures corresponding to t_{in} and t_{R} are nearly equal, where t_{R} denotes the *reheating* time (time of the end of the inflation). Then, entropy increases during inflation and ϵ decreases [36]; so, $(\rho - \rho_{\text{cr}})/\rho$ could be nearly 1 both at t_{in} and the present time.

During inflation, the future light cone increases exponentially, while the past light cone isn't influenced by $t \geq t_{\text{R}}$. If the duration of the inflation $\Delta t = t_{\text{R}} - t_{\text{in}}$ is large enough, $l_{\text{future}}^c(t_{\text{R}})$ will be greater than $l_{\text{past}}^c(t_{\text{R}})$.

In the context of GR, the occurrence of an inflationary phase requires the source of gravity to have negative pressure. This becomes possible with an approximately constant energy density, such as the vacuum energy provided by the potential of some scalar field, the inflaton. There are two main classes of inflationary models: models where gravity is essentially described by Einstein's equations and the scalar field (or scalar fields) acts as a source that produces inflation, and models where both gravity and the source of the field equations are changed. ETG are included in this second family.

3.1.2 UV scales: the Quantum Gravity problem

ETG play a fundamental role in the quantum gravity problem, consisting in the incapability of quantizing the gravity and treating it at a fundamental level. Such difficulty arises from the double role played by the gravitational field $g_{\mu\nu}$; it describes both the dynamical aspects of gravity and the background space-time structure. In other words, GR cannot be formulated as a quantum field theory on a Minkowski space-time as the other interactions, since there is not a priori a geometry for the space-time background.

Generally, when the concept of classical space-time metric is absent, a good definition of causality fails. Consider a semi-classical approximation in which the gravitational field is treated classically and the matter is represented by quantum fields; according to this description, Einstein's equations take the form

$$G_{\mu\nu} \equiv R_{\mu\nu} - \frac{1}{2} g_{\mu\nu} R = \langle T_{\mu\nu} \rangle, \quad (3.20)$$

where on the left there is the usual Einstein tensor $G_{\mu\nu}$ and on the right there is the expectation value of the quantum energy-momentum tensor. More precisely, if $|\Psi\rangle$ is a quantum state that describes the early Universe, then

$$\langle T_{\mu\nu} \rangle \equiv \langle \Psi | \hat{T}_{\mu\nu} | \Psi \rangle, \quad (3.21)$$

where $\hat{T}_{\mu\nu}$ is the quantum operator associated with the classical energy-momentum tensor. According to Eq. (3.20), the gravitational field should change in a discontinuous manner to keep into account the quantum behaviour of the matter. To overcome this difficulty the gravitational field should be quantized and in this respect two main approaches have been tried [36, 230]: the covariant and the canonical method.

The basic working hypothesis of the *covariant method* is that it is always possible to separate the metric $g_{\mu\nu}$ into a kinematic part $\eta_{\mu\nu}$, which represents the background space-time, and a dynamic part $h_{\mu\nu}$, which represents a small perturbation of the space time:

$$g_{\mu\nu} = \eta_{\mu\nu} + h_{\mu\nu}. \quad (3.22)$$

The background geometry is used to define notions of causality and time. The dynamic field, considered as a background perturbation, is the quantity to be quantized. Quanta are spin 2 particles, called *gravitons*, which propagate in flat space-time and are defined by $h_{\mu\nu}$. Thus, in principle, perturbative methods familiar to the Quantum Electrodynamics (QED) can be used to treat gravitation. Unfortunately, the resulting perturbation theory for $h_{\mu\nu}$ is renormalizable only at the one-loop level. The fact that GR is not renormalizable to all orders simply means that its validity ceases at high energies (i.e. at small scales), while it describes well phenomena in the low energy domain (i.e. and at great distances). Ultimately, the correct theory of gravity must be invoked in the Planck era, while, well below this time, GR is sufficient. In this perspective, higher-order terms and non-minimal couplings are added to the Hilbert-Einstein action.

The second approach, applicable after the Hamiltonian formulation of the classical theory in question, is the *canonical method*. It is based on three steps: taking the states of the system to be described by the wave functions $\psi(q)$ of the configuration variables, replacing each momentum variable by differentiation with respect to the conjugate configuration variable, and determining the time evolution of ψ by means of the Schrödinger equation $i \hbar \partial\psi/\partial t = \hat{H} \psi$. The Hamiltonian formalism, first developed by Arnowitt, Deser, and Misner [237], is based on foliating the four-dimensional manifold;

the canonical variables are the three-metric on the obtained spatial submanifolds. The fundamental difficulty that emerges is how to physically interpret the solution wave function of the evolution equation of the three-metrics and their conjugate momenta, known as the *Wheeler-De Witt equation*. Starting from it we can define an inner product, which is still independent of the space-like surface belonging to a generic leaflet, but it is not defined as positive. This particularity prevents the adoption of a probabilistic interpretation; there is no longer a Hilbert space. A further difference is due to the fact that resulting equations involve products of operators defined at the same point in space-time and, moreover, involve the construction of physically unclear distributions.

Given the aforementioned difficulties in the attempt to “quantize” GR, it is natural to consider extensions to the Hilbert-Einstein action, in particular by adding terms of higher-order in the curvature.

3.1.3 IR scales: Dark Energy and Dark Matter

In recent years, a considerable amount of astrophysical data has been accumulated which has made it necessary to consider a new approach also in recent times: ETG would play a fundamental role in this context. The picture that emerges is that of a spatially flat universe that is currently undergoing a phase of accelerated expansion.

The first evidence of accelerated expansion comes from the study of high redshift deviations from Hubble’s linear law of type Ia supernovae [133, 188, 90, 224], which gives information about density parameters. In particular, these observations show that the value of Ω_Λ , that is the contribution to the cosmic fluid due to the cosmological constant, is greater than Ω_M , the matter density parameter; this entails an accelerated expansion. This evidence is strengthened by other observations.

First, the abundance of galaxy clusters and the fraction of gas in the clusters constrain the density parameter of matter to be $\Omega_M \sim 0.3$. Moreover, the measurement of the anisotropies in the spectrum of the cosmic background radiation, first obtained with BOOMERANG [58] and MAXIMA [220] and later with WMAP [128, 217, 218] satellite, provide the constraint $\Omega_k \simeq 0.0$, where Ω_k is the contribution of spatial curvature: the Universe is spatially flat. These facts strongly indicate that one must have $\Omega_\Lambda \simeq 0.7$ for the equation of the *cosmic triangle* to be satisfied

$$\Omega_k + \Omega_M + \Omega_\Lambda = 1. \quad (3.23)$$

The model just outlined is called the “*concordance model*” and is based on the aforementioned percentages of the different Ω_i (with $i = M, \Lambda, k$). The most difficult open problem is the value of Ω_Λ which is usually attributed to the cosmological constant; the cause of the accelerated expansion is identified with some form of “dark energy” having only a dynamic role in the cosmic fluid, to which it contributes about 70%. In this case the concordance model is called Λ CDM (Λ *Cold Dark Matter*), which interprets

the cosmic fluid as a mixture of cosmological constant [204], cold dark matter (given by not relativistic particles) and baryonic matter. The issue is that if we interpret Λ as vacuum energy, in analogy with inflation, we realize that the value according to the observations is 120 orders of magnitude smaller than that of the fundamental theories that should have operated in the primordial Universe; this leads us to suppose the existence of some dynamic entity that reduces the vacuum energy. As a possible solution, many authors have replaced the cosmological constant with a scalar field which, like the inflaton, slowly rolls into a self-interacting potential with a process that has allowed vacuum energy to become dominant only in recent times; these models are known as *quintessence* [53, 182]. This approach is afflicted by a fine-tuning problem, called “*coincidence problem*”, consisting in the incapability of explaining why precisely in the current cosmological era, the contributes of Ω_Λ and Ω_M have the same order of magnitude. Furthermore, the origin of this scalar field is mysterious, and the forms adopted in the literature for the potential for self-interaction, which seem to have no immediate physical explanations are difficult to justify.

The unknown nature of dark energy has prompted many authors to seek a different explanation for this accelerated phase; it is in fact possible that the observed cosmic acceleration is the sign of a failure, in the infrared limit, of the laws of gravitation as we know them.

In this conceptual framework, it is possible to develop alternative models that naturally provide a cosmological component with negative pressure originating in the geometry of the Universe.

3.2 Beyond Einstein’s theory

In the previous section, we realized the inevitability of extending GR at low and high energies. Suitable alternatives should be able to cure shortcomings at extremes regimes and be consistent with GR in the intermediate-energy regime. There are countless ways to modify GR, that is why we discuss the Lovelock theorem. It is useful to classify extensions of GR based on which of the underlying assumptions of the theorem they violate. Then, we will discuss a general class of ETG which, depending on the choice of specific parameters, give us all the cases of interest.

3.2.1 Lovelock theorem

ETG carry out modifications of GR and hence the abandonment of some of its fundamental assumptions. It follows that a principle governing the innumerable ways of extending GR is given by examining basic postulates of Einstein’s theory. Such a guide resides in Lovelock’s theorem [155, 156], which expresses GR as the only theory

emerging from a system of specific premises. It can be stated as follows:

Theorem. *In four space-time dimensions, the only divergence-free symmetric rank-2 tensor constructed solely from the metric $g_{\mu\nu}$ and its derivatives up to the second differential order, and preserving diffeomorphism invariance, is the Einstein tensor plus a cosmological term.*

By analyzing the theorem, we can see that each class of ETG can be traced back to the circumvention of one of its assumptions [15]; in particular, as summarized by Figure 3.1, there are four ways to bypass Lovelock's theorem.

1. **Additional fields** - The simplest way to evade Lovelock's theorem consists of adding extra degrees of freedom coupling the metric to extra fundamental fields (scalar, vector, tensor). Since any higher differential order theory can always be brought to second-order form plus a specific number of extra fields, the same possibilities can be obtained by lifting the assumption of second differential order. Finally, by dropping the implicit assumption that the matter stress-energy tensor $T_{\mu\nu}$ enters the field equations linearly, it is possible to construct theories where the Einstein's tensor is left unchanged and the right-hand side is a nonlinear combination of $T_{\mu\nu}$ preserving the vanishing of its covariant divergence [183]. Nonlinear couplings can solve some of the curvature singularities that emerge in fluid collapse and early-time cosmology in GR [4]. These theories are equivalent to GR in vacuum and satisfy the WEP.
2. **Violations of diffeomorphism invariance** - This assumption can be left in two ways. The first assumes that the *Lorentz invariance*, which has been tested in the Standard Model sector, is just an emergent symmetry that is broken at high energy in the gravitational sector. The resulting class of theories improves the UV behaviour of GR [129]. The second way to discard the diffeomorphism invariance is equivalent to abandon the hypothesis that gravity should be mediated by a *massless* spin-2 field. This generates the massive gravity theories [66], important for their role to solve the cosmological constant problem.
3. **Higher dimensions** - The class of theories emerging from postulating higher dimensions have many theoretical applications, in particular, they are used to formulate consistent string theories and they may solve the hierarchy problem. GR in higher dimensions naturally introduces additional scalar and gauge fields when a dimensional reduction from $D > 4$ to $D = 4$ is performed.
4. **WEP violations** - The requirement that the left-hand side of Einstein's equation is divergence-free is dictated by the WEP. Various classes of theories that circumvent Lovelock's theorem only by postulating a nonminimal coupling to the matter sector (and thus violating the weak equivalence principle) have been proposed [16, 32].

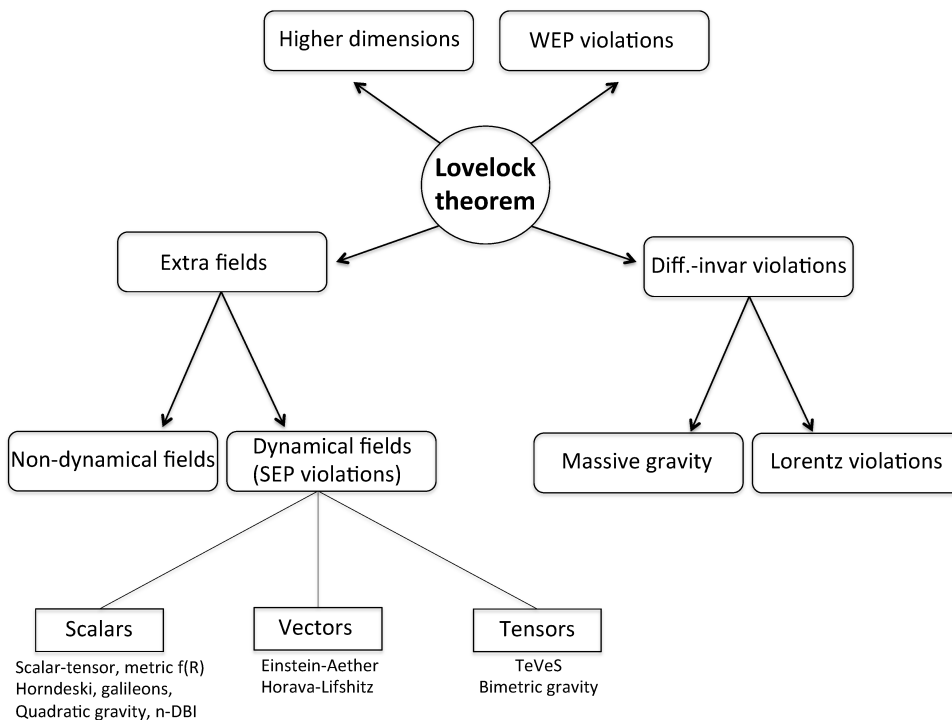


Figure 3.1: Diagram representing the ways in which the Lovelock's theorem can be violated giving rise to different classes of ETG.

In summary, GR corrections are always attributable to a violation of its postulates, so that the corresponding ETG will fall into one of the aforementioned classes.

3.2.2 A general class of Extended Theories of Gravity

ETG fall into two main classes: *scalar-tensor* theories of gravity where the geometry couple non-minimally to some scalar field and *higher-order* theories where derivatives of the metric of order > 2 may appear.

We can join these classes in an effective action describing a general class of higher-order-scalar-tensor theories in four dimensions

$$S = \int d^4x \sqrt{-g} \left[F(R, \square R, \square^2 R, \dots, \square^k R, \phi) - \frac{\epsilon}{2} g^{\mu\nu} \phi_{;\mu} \phi_{;\nu} + 2k \mathcal{L}_m \right], \quad (3.24)$$

where F is a not a priori specified function of curvature invariants and of a scalar field ϕ , \mathcal{L}_m is the minimally coupled matter contribution and ϵ is a constant. In particular, its values can be $\epsilon = \pm 1, 0$ fixing the nature of the scalar field which can be a standard scalar field, a phantom field, or a field without dynamics [33, 176, 202]. The field equations, which will be of order $2K + 4$, are obtained by varying the action (3.24)

with respect to $g_{\mu\nu}$:

$$\begin{aligned}
 G^{\mu\nu} = & \frac{1}{\mathcal{G}} \left[k T^{\mu\nu} + \frac{1}{2} g^{\mu\nu} (F - \mathcal{G} R) + (g^{\mu\lambda} g^{\nu\sigma} - g^{\mu\nu} g^{\lambda\sigma}) \mathcal{G}_{;\lambda\sigma} \right. \\
 & + \frac{1}{2} \sum_{i=1}^k \sum_{j=1}^i (g^{\mu\nu} g^{\lambda\sigma} - g^{\mu\lambda} g^{\nu\sigma}) (\square^{j-i})_{;\sigma} \left(\square^{i-j} \frac{\partial F}{\partial \square^i R} \right)_{;\lambda} \\
 & \left. - g^{\mu\nu} g^{\lambda\sigma} \left((\square^{j-1} R)_{;\sigma} \square^{i-j} \frac{\partial F}{\partial \square^i R} \right)_{;\lambda} \right], \tag{3.25}
 \end{aligned}$$

where $G^{\mu\nu}$ is the Einstein tensor and

$$\mathcal{G} \equiv \sum_{j=0}^n \square^j \left(\frac{\partial F}{\partial \square^j R} \right). \tag{3.26}$$

The stress-energy tensor is given by the contribution of the ordinary matter and of the kinetic part of the scalar field:

$$T_{\mu\nu} = T_{\mu\nu}^{(m)} + \frac{\epsilon}{2} \left[\phi_{;\mu} \phi_{;\nu} - \frac{1}{2} \phi^{;\alpha} \phi_{;\alpha} \right]. \tag{3.27}$$

The Klein-Gordon equation is obtained by varying the action with respect to ϕ :

$$\epsilon \square \phi = - \frac{\partial F}{\partial \phi}. \tag{3.28}$$

The simplest extension of GR is achieved by assuming

$$F = f(R), \quad \epsilon = 0. \tag{3.29}$$

It is the $f(R)$ -gravity theory and will be discussed in detail in the next section.

Another interesting case is obtained by putting

$$F = F(\phi) R - V(\phi), \quad \epsilon = -1, \tag{3.30}$$

where $V(\phi)$ and $F(\phi)$ are generic functions describing the potential and the coupling of a scalar field ϕ . The action becomes

$$S = \int V(\phi) \left[F(\phi) R + \frac{1}{2} g^{\mu\nu} \phi_{;\mu} \phi_{;\nu} - V(\phi) \right]. \tag{3.31}$$

The action (3.31) goes back to the Brans-Dicke theory of gravity for $V(\phi) = 0$. Originally, Brans-Dicke theory was born from the attempt to implement the principle of Mach in a relativistic theory of gravity [27].

3.3 $f(R)$ -gravity

$f(R)$ gravities have been proposed as the prototype of the infrared corrections to GR as an alternative to models based on DM and DE. The necessity of introducing DM arises from the evidence that studying astrophysical systems, the dynamically inferred mass is greater than that attributed to the luminous components. The ‘missing matter’ problem was first addressed by J. H. Oort in the 1930s [179]; when he calculated the mass of our Galaxy as the sum of its luminous components, it turned out that such a value was lower than the mass required by the dynamic estimation based on the Doppler red-shifts values of the stars. Moreover, in the 1960s, it was observed that far from the Galactic Center all the stars travel with a velocity independent from the distance from the Center. At larger scales, F. Zwicky found that the visible mass of the galaxies constituting the Coma cluster wasn’t large enough to avoid the cluster to come apart [242]. The ‘missing matter’ was initially attributed to invisible dark entities, such as MACHO’s or WIMPs. Since there is no proof that these objects exist, we try to address the problem by adopting the approach of the ETG, consisting in leaving unchanged the material sector of the field equations and intervening on the geometry. In particular, the $f(R)$ -gravity theory consists in replacing the Ricci curvature scalar R in the Hilbert-Einstein action by a generic function $f(R)$, whose true form could be “reconstructed” from the data.

3.3.1 Field equations

In the vacuum case, the $f(R)$ -gravity action reads as [36]

$$S = \int \sqrt{-g} f(R) d^4x. \quad (3.32)$$

$f(R)$ is a continuous and differentiable function of R and g is the determinant of the metric $g_{\mu\nu}$. Field equations can be obtained from a variational principle by varying Eq. (3.32) with respect to the metric in a local inertial frame:

$$\delta S = \delta \int \sqrt{-g} f(R) d^4x = 0. \quad (3.33)$$

We get ²

$$\begin{aligned} \delta \int \sqrt{-g} f(R) d^4x &= \int \left[\delta \sqrt{-g} f(R) + \sqrt{-g} \delta(f(R)) \right] d^4x = \\ &= \int \sqrt{-g} \left[f'(R) R_{\mu\nu} - \frac{1}{2} g_{\mu\nu} f(R) \right] \delta g^{\mu\nu} d^4x + \int \sqrt{-g} f'(R) g^{\mu\nu} \delta R_{\mu\nu} d^4x, \end{aligned} \quad (3.35)$$

²We used the well-known relationship $\delta g = g g^{\mu\nu} \delta g_{\mu\nu} = -g g_{\mu\nu} \delta g^{\mu\nu}$, from which it follows that

$$\delta \sqrt{-g} = -\frac{1}{2\sqrt{-g}} \delta g = -\frac{1}{2} \sqrt{-g} g_{\mu\nu} \delta g^{\mu\nu}. \quad (3.34)$$

where $' = \frac{d}{dR}$. The second integral of Eq. (3.35) can be written as

$$\int \sqrt{-g} f'(R) g^{\mu\nu} \delta R_{\mu\nu} d^4x = \int \sqrt{-g} f'(R) \partial_\sigma W^\sigma d^4x. \quad (3.36)$$

Here, the quantity

$$W^\sigma \equiv g^{\mu\nu} \delta \Gamma_{\mu\nu}^\sigma - g^{\mu\sigma} \delta \Gamma_{\mu\nu}^\nu \quad (3.37)$$

has been defined starting from the relation between the Ricci tensor and the connections Γ

$$g^{\mu\nu} \delta R_{\mu\nu} = g^{\mu\nu} \partial_\sigma (\delta \Gamma_{\mu\nu}^\sigma) - g^{\mu\sigma} \partial_\sigma (\delta \Gamma_{\mu\nu}^\nu) \equiv \partial_\sigma W^\sigma. \quad (3.38)$$

Integrating by parts Eq. (3.36), we get

$$\int \sqrt{-g} f'(R) g^{\mu\nu} \delta R_{\mu\nu} d^4x = \int \partial_\sigma [\sqrt{-g} f'(R) W^\sigma] d^4x - \int \partial_\sigma [\sqrt{-g} f'(R)] W^\sigma d^4x. \quad (3.39)$$

Assuming that there are no fields at infinity, for the divergence theorem the first of such integral vanishes. To write W^σ in terms of the metric, consider the definition of affine connection (2.18); we obtain

$$\begin{aligned} \delta \Gamma_{\mu\nu}^\sigma &= \delta \left[\frac{1}{2} g^{\sigma\alpha} (\partial_\mu g_{\alpha\nu} + \partial_\nu g_{\mu\alpha} - \partial_\alpha g_{\mu\nu}) \right] \\ &= \frac{1}{2} g^{\sigma\alpha} [\partial_\mu (\delta g_{\alpha\nu}) + \partial_\nu (\delta g_{\mu\alpha}) - \partial_\alpha (\delta g_{\mu\nu})], \end{aligned} \quad (3.40)$$

since in a locally inertial reference frame the relation $\nabla_\alpha g_{\mu\nu} = \partial_\alpha g_{\mu\nu} = 0$ holds. Similarly, we obtain the other relation

$$\delta \Gamma_{\mu\nu}^\nu = \frac{1}{2} g^{\nu\alpha} \partial_\mu (\delta g_{\nu\alpha}). \quad (3.41)$$

Contracting Eq. (3.40) and (3.41) with $g^{\mu\nu}$ and $g^{\mu\sigma}$, we get

$$\begin{aligned} g^{\mu\nu} \delta \Gamma_{\mu\nu}^\sigma &= g^{\mu\nu} \frac{1}{2} [-\partial_\mu (g_{\alpha\nu} \delta g^{\alpha\sigma}) - \partial_\nu (g_{\mu\alpha} \delta g^{\sigma\alpha}) - g^{\sigma\alpha} \partial_\alpha (\delta g_{\mu\nu})] = \\ &= \frac{1}{2} \partial^\sigma (g_{\mu\nu} \delta g^{\mu\nu}) - \partial^\mu (g_{\alpha\mu} \delta g^{\nu\alpha}), \end{aligned} \quad (3.42)$$

$$g^{\mu\sigma} \delta \Gamma_{\mu\nu}^\nu = -\frac{1}{2} \partial^\sigma (g_{\nu\alpha} \delta g^{\nu\alpha}). \quad (3.43)$$

Inserting these expressions in Eq. (3.37) and Eq. (3.39), we obtain

$$W^\sigma = \partial^\sigma (g_{\mu\nu} \delta g^{\mu\nu}) - \partial^\mu (g_{\mu\nu} \delta g^{\sigma\nu}). \quad (3.44)$$

and

$$\int \sqrt{-g} f'(R) g^{\mu\nu} \delta R_{\mu\nu} d^4x = \int \partial_\sigma [\sqrt{-g} f'(R)] [\partial^\mu (g_{\mu\nu} \delta g^{\sigma\nu}) - \partial^\sigma (g_{\mu\nu} \delta g^{\mu\nu})] d^4x. \quad (3.45)$$

Integrating by parts and eliminating the vanishing terms for the divergence theorem, we have

$$\begin{aligned} \int \sqrt{-g} f(R) d^4x &= \int \sqrt{-g} \left[f'(R) R_{\mu\nu} - \frac{1}{2} f(R) g_{\mu\nu} \right] \delta g^{\mu\nu} d^4x + \\ &+ \int \left[g_{\mu\nu} \partial^\sigma \partial_\sigma (\sqrt{-g} f'(R)) - g_{\sigma\nu} \partial^\sigma \partial_\mu (\sqrt{-g} f'(R)) \right] \delta g^{\mu\nu} d^4x. \end{aligned} \quad (3.46)$$

For this variation to vanish it must be

$$f'(R) R_{\mu\nu} - \frac{1}{2} f(R) g_{\mu\nu} = \nabla_\mu \nabla_\nu f'(R) - g_{\mu\nu} \square f'(R), \quad (3.47)$$

where $\square \equiv g^{\mu\nu} \nabla_\mu \nabla_\nu$. Their trace is

$$3 \square f'(R) + f'(R) R - 2 f(R) = 0. \quad (3.48)$$

Field equations (3.47) can be written in terms of the Einstein tensor. We can write

$$f'(R) R_{\mu\nu} - \frac{1}{2} f'(R) g_{\mu\nu} R + \frac{1}{2} f'(R) g_{\mu\nu} R - \frac{1}{2} f(R) g_{\mu\nu} = f'(R)_{;\mu;\nu} - g_{\mu\nu} \square f'(R), \quad (3.49)$$

from which

$$G_{\mu\nu} = \frac{1}{f'(R)} \left\{ \frac{1}{2} g_{\mu\nu} [f(R) - f'(R) R] + f'(R)_{;\mu;\nu} - g_{\mu\nu} \square f'(R) \right\}. \quad (3.50)$$

The higher-order terms of the right member in Eq. (3.50) can be considered as effective fields and read as a source term $T_{\mu\nu}^{(\text{curv})}$ contributing to the field equations

$$G_{\mu\nu} = T_{\mu\nu}^{(\text{curv})}. \quad (3.51)$$

3.3.2 Weak field limit of $f(R)$ -gravity theory

Here we develop the PN limit of an analytic $f(R)$ -gravity assuming a spherically symmetric metric following [34, 37, 38], showing that a gravitational potential with a Yukawa correction is obtained.³

The solution of field equations (3.47), inferred from action (3.32), can be obtained starting from a general spherically symmetric metric:

$$ds^2 = g_{\sigma\tau} dx^\sigma dx^\tau = g_{tt}(x^0, r) dx^{02} - g_{rr}(x^0, r) dr^2 - r^2 d\Omega^2, \quad (3.52)$$

where $x^0 = ct$ and $d\Omega^2$ is the solid angle. Let us assume that the metric can be developed around a Minkowskian background as $g_{\mu\nu} = \eta_{\mu\nu} + h_{\mu\nu}$ and for simplicity let

³In general, the number of Yukawa corrections appearing in the modified gravitational potential depends on the differential degree of the field equations [89].

us use $c = 1$ for the moment. We assume a general analytic function for the $f(R)$ term, expanding it in Taylor series around a certain value $R = R_0$:

$$f(R) = \sum_n \frac{f^n(R_0)}{n!} (R - R_0)^n \simeq f_0 + f'_0 R + f''_0 R^2 + f'''_0 R^3 + \dots \quad (3.53)$$

The weak field approximation consists in inserting the last expansions in the field equations (3.47) and expanding the system at orders $\mathcal{O}(0)$, $\mathcal{O}(2)$, and $\mathcal{O}(4)$. At the zeroth order the field equations give the condition $f_0 = 0$. At second order the equations are

$$f'_0 r R^{(2)} - 2 f'_0 g_{tt,r}^{(2)} + 8 f''_0 R_{,r}^{(2)} - f'_0 r g_{tt,rr}^{(2)} + 4 f''_0 r R^{(2)} = 0, \quad (3.54)$$

$$f'_0 r R^{(2)} - 2 f'_0 g_{rr,r}^{(2)} + 8 f''_0 R_{,r}^{(2)} - f'_0 r g_{tt,rr}^{(2)} = 0, \quad (3.55)$$

$$2 f'_0 g_{rr}^{(2)} - r \left[f'_0 r R^{(2)} - f'_0 g_{tt,r}^{(2)} - f'_0 g_{rr,r}^{(2)} + 4 f''_0 R_{,r}^{(2)} + 4 f''_0 r R_{,rr}^{(2)} \right] = 0, \quad (3.56)$$

$$f'_0 r R^{(2)} + 6 f''_0 \left[2 R_{,r}^{(2)} + r R_{,rr}^{(2)} \right] = 0, \quad (3.57)$$

$$2 g_{rr}^{(2)} + r \left[2 g_{tt,r}^{(2)} - r R^{(2)} + 2 g_{rr,r}^{(2)} + r g_{tt,rr}^{(2)} \right] = 0. \quad (3.58)$$

The general solution at $\mathcal{O}(2)$ -order can be obtained using the trace equation:

$$g_{tt}^{(2)} = \delta_0 - \frac{\delta_1}{f'_0 r} + \frac{\delta_2(t) \lambda^2 e^{-r/\lambda}}{3} + \frac{\delta_3(t) \lambda^3 e^{r/\lambda}}{6 r}, \quad (3.59)$$

$$g_{rr}^{(2)} = -\frac{\delta_1}{f'_0 r} - \frac{\delta_2(t) \lambda^2 (r/\lambda + 1) e^{-r/\lambda}}{3 r} + \frac{\delta_3(t) \lambda^3 (1 - r/\lambda) e^{r/\lambda}}{6 r}, \quad (3.60)$$

$$R^{(2)} = \frac{\delta_2(t) e^{-r/\lambda}}{r} + \frac{\delta_3(t) \lambda e^{r/\lambda}}{2 r}, \quad (3.61)$$

where $\lambda = \sqrt{-6f''_0/f'_0}$, the integration constant δ_0 can be neglected, δ_1 is an arbitrary integration constant, and $\delta_2(t)$ and $\delta_3(t)$ are two functions of time with dimensions of length⁻¹ and length⁻², which can be set to a constant since the system (3.59)-(3.61) contains only spatial derivatives. In particular, we can set $\delta_1 = G_N M$ if we notice that it recovers the standard weak field limit in the limit $f(R) \rightarrow R$ for a point-like mass M . A suitable black hole metric must be asymptotically flat, that is, Yukawa growing mode in the system (3.59)-(3.61) must be set to zero. The resulting solution is

$$g_{tt}(x^0, r) = 1 - \frac{R_S}{2 f'_0 r} + \frac{\delta_2(t) \lambda^2 e^{-r/\lambda}}{3}, \quad (3.62)$$

$$g_{rr}(x^0, r) = 1 + \frac{R_S}{2 f'_0 r} + \frac{\delta_2(t) \lambda^2 (1 + r/\lambda) e^{-r/\lambda}}{3 r}, \quad (3.63)$$

$$R = \frac{\delta_2(t) e^{-r/\lambda}}{r}. \quad (3.64)$$

It follows that the gravitational potential in $f(R)$ -gravity is:

$$\Phi(r) = -\frac{R_S}{2 f'_0 r} + \frac{\delta_2(t) \lambda^2 e^{-r/\lambda}}{6 r}. \quad (3.65)$$

From Eq. (3.65) it descends that the Newtonian potential is recovered only in the special case $f(R) = R$. By defining $1 + \delta = f'_0$ and assuming that δ_2 is quasi-constant and is related to δ by

$$\delta_2 = -\frac{3R_S}{\lambda^2} \frac{\delta}{1 + \delta}, \quad (3.66)$$

Eq. (3.65) can be recast as

$$\Phi(r) = -\frac{R_S}{2(1 + \delta)r} (1 + \delta e^{-r/\lambda}). \quad (3.67)$$

Eq. (3.67) is given by the sum of two terms: the first term is the Newtonian contribution generated by a point-like mass $\frac{M}{1 + \delta}$, and the second one is the Yukawa-like modification with a scale length λ , which naturally arises from the theory. The parameter δ is a universal constant quantifying the discrepancy with the Newtonian potential, which is recovered if $\delta = 0$. The parameter λ is a scale length acting as a screening mechanism, indeed it makes the Yukawa corrections negligible at small scales and relevant from galactic to cosmological scales, explaining galaxy rotation curves, cluster of galaxies and the accelerated expansion of the Universe in a more natural way than introducing Dark Matter and Dark Energy [62, 39, 60, 61, 173, 31].

The values of these corrections are unknown, and they must be considered as free parameters to be constrained by observations. In Part II we will test $f(R)$ -gravity at Galactic scale, proposing a completely general approach to classify other ETG at different scales.

3.3.3 Geodesic motion

In this section we will derive the geodesics equations associated to the metric determined by the coefficients (3.62) and (3.63), which can be recast as

$$ds^2 = [1 + \Phi(r)] dt^2 - [1 - \psi(r)] dr^2 - r^2 d\Omega^2, \quad (3.68)$$

where ⁴

$$\Phi(r) = -\frac{R_S (\delta e^{-r/\lambda} + 1)}{r (\delta + 1)}, \quad (3.69)$$

$$\Psi(r) = \frac{R_S}{r} \left[\frac{(\delta e^{-r/\lambda} + 1)}{(\delta + 1)} + \frac{\left(\frac{\delta r e^{-r/\lambda}}{\lambda} - 2 \right)}{(\delta + 1)} \right]. \quad (3.70)$$

The potential $\psi(r)$ can be written as

$$\psi(r) = \Phi(r) + \delta\Phi(r). \quad (3.71)$$

⁴The speed of light has been restored.

Figure 3.2: Relative difference of the two gravitational fields $(\psi(r) - \Phi(r))/\Phi(r)$ as a function of the strength δ and r .

It is possible to verify that for systems of our interest the extra term $\delta\Phi(r)$ can be neglected, as we can see from Fig. 3.2 where we show the density plot of the ratio $(\psi(r) - \Phi(r))/\Phi(r)$. We used the units $G_N = M = c = 1$, we fixed the scale length to the confidence value $\lambda = 5000$ AU [59] and we varied δ from -0.1 to 0.1 . As indicated by the color bar, the departure of $\psi(r)$ from $\Phi(r)$ is $\sim 20\%$ for $\delta = \pm 0.1$, and it decreases to 2% for $\delta \sim \pm 0.01$. Since we are interested in binary systems where we expect very small deviations from GR, we will assume $\psi(r) \sim \Phi(r)$, and the line element (3.68) becomes

$$ds^2 = [1 + \Phi(r)] c^2 dt^2 - [1 - \Phi(r)] dr^2 - r^2 d\Omega^2. \quad (3.72)$$

Using Euler-Lagrange equations

$$\frac{d}{ds} \frac{\partial \mathcal{L}}{\partial \dot{x}^\mu} - \frac{\partial \mathcal{L}}{\partial x^\mu} = 0, \quad (3.73)$$

geodesic equations are straightforwardly obtained from the metric:

$$\ddot{r} = \Delta_a^{-1} \left[\frac{R_S}{2} (\dot{r}^2 - c^2 \dot{t}^2) (\delta(\lambda + r) + \lambda e^{\frac{r}{\lambda}}) + \lambda(1 + \delta) e^{\frac{r}{\lambda}} r^3 (\dot{\theta}^2 + \dot{\phi}^2 \sin^2 \theta) \right], \quad (3.74)$$

$$\ddot{\theta} = \dot{\phi}^2 \cos \theta \sin \theta - \frac{2\dot{r}\dot{\theta}}{r}, \quad (3.75)$$

$$\ddot{\phi} = -\frac{2\dot{\phi}}{r} [\dot{r} + r\dot{\theta} \cot \theta], \quad (3.76)$$

$$\ddot{t} = \Delta_b^{-1} \left[R_S [\lambda (e^{\frac{r}{\lambda}} + \delta) + \delta r] \dot{r} \dot{t} \right], \quad (3.77)$$

where we have defined

$$\Delta_a \equiv \lambda r \left[R_S \delta + e^{\frac{r}{\lambda}} (R_S + (1 + \delta) r) \right], \quad (3.78)$$

$$\Delta_b \equiv \lambda r \left[R_S \delta + e^{\frac{r}{\lambda}} (R_S - (1 + \delta) r) \right]. \quad (3.79)$$

Here, a *dot* indicates the derivative with respect to the proper time, and we recall that $R_S = 2 G_N M / c^2$.

This system of parametric non-linear differential equations is the starting point for the definition of the theoretical model in our fitting procedure; it can be numerically integrated to obtain the orbital motion of a two-body system.

3.3.4 Precession

Following Ref. [59], let us report the basic steps to compute the periastron shift for the Yukawa-like potential. We must start from orbits equation $r = r(\phi)$ which, as shown in Ref. [59], assumes the form:

$$\left(\frac{dr}{d\phi} \right)^2 = \frac{E^2 - [\Phi(u) + 1] [L^2 u^2 + 1]}{L^2 u^4 [\Phi(u)^2 - 1]}, \quad (3.80)$$

where $u = 1/r$. Energy, E , and angular momentum, L , are two conserved quantities:

$$p_t \equiv \frac{\partial \mathcal{L}}{\partial \dot{t}} = [1 + \Phi(r)] \dot{t} \equiv E, \quad (3.81)$$

$$p_\phi \equiv \frac{\partial \mathcal{L}}{\partial \dot{\phi}} = r^2 \sin^2 \theta \dot{\phi} \equiv L. \quad (3.82)$$

Imposing $(du/d\phi)^2 = 0$ and after simple calculations, we get

$$\frac{\delta R_S u e^{-1/\lambda u}}{(\delta + 1) L^2} + \frac{R_S u}{(\delta + 1) L^2} + \frac{\delta R_S u^3 e^{-1/\lambda u}}{(\delta + 1)} + \frac{R_S u^3}{(\delta + 1)} + \frac{E^2}{L^2} - \frac{1}{L^2} - u^2 = 0. \quad (3.83)$$

The following step is to rewrite the previous equation in terms of two orbital parameters: the eccentricity e and the latus rectum ℓ . Let us use the ansatz

$$u = \frac{1 + e \cos \chi}{\ell}, \quad (3.84)$$

where χ is the relativistic anomaly. After substitution of Eq. (3.84) in Eq. $(du/d\phi)^2 = 0$, we get

$$\left(\frac{d\chi}{d\phi} \right)^2 = \left[1 - (e^2 + 3) \mu + 2 \mu (e \cos \chi + 1)^2 \right] \Upsilon + (e^2 - 1)(1 - 4\mu) \mu^2 - \mu^2 (e \cos \chi + 1)^2, \quad (3.85)$$

where $\mu \equiv M/\ell$ and we defined the variables

$$\Upsilon = \frac{2\mu^2(e \cos \chi + 1)}{\delta + 1}(\Upsilon_1 + 1), \quad (3.86)$$

$$\Upsilon_1 = \delta \left(\frac{1}{2\lambda^2\mu^2(e \cos \chi + 1)^2} - \frac{1}{\lambda\mu(e \cos \chi + 1)} + 1 \right). \quad (3.87)$$

It's worth noticing that since we want to study systems in which the semi-major axis of the orbit is lower than the Yukawa scale length, we expanded in Taylor series the term $e^{-1/\lambda u}$. Integrating Eq. (3.85), we get the relation for the periastron advance

$$\Delta\phi = \frac{3\pi R_S}{a(1-e^2)} \left(1 + \frac{\delta R_S^2}{6a^2(1-e^2)^2} - \frac{\pi\delta R_S^2}{2a(1-e^2)\lambda} - \frac{3\delta R_S}{2a(1-e^2)} - \frac{\delta R_S^2}{24(\delta+1)\lambda^2} + \frac{\delta R_S}{6\lambda} \right). \quad (3.88)$$

Eq. (3.88) reduces to the GR expression $\Delta\phi_{\text{GR}}$ for $\delta = 0$:

$$\Delta\phi_{\text{GR}} = \frac{3\pi R_S}{a(1-e^2)}. \quad (3.89)$$

3.4 Bootstrapped Newtonian Gravity

Bootstrapped Newtonian gravity [44, 42] is the second attempt we propose as an alternative to GR. It arises from the need to elaborate a consistent quantum theory to cure the various shortcomings afflicting the classical picture of black hole formation [9, 125]. This approach is inspired by Deser's idea [67] that, starting from the Fierz-Pauli action in Minkowski space-time and adding gravitational self-coupling terms (consistent with diffeomorphisms invariance), it should be possible to fully reconstruct Einstein's theory. Since we don't know *a priori* what the underlying theory of gravity is, the coupling constants for the additional terms are left free to vary allowing the possibility of alternative dynamics. This program furnishes a non-linear equation for the gravitational potential acting on test particles at rest, which includes pressure and gravitational self-interaction effects. Such an equation was used to study compact objects [43, 45, 46] and coherent quantum states [41, 48]. A full (effective) metric tensor can be derived from the Bootstrapped Newtonian potential [47], which allows exact analysis of the trajectories of test particles and photons around astrophysical compact objects. The Bootstrapped effective metric is given in terms of Eddington-Robertson Parametrized Post-Newtonian parameters [233], chosen to minimize deviations from Schwarzschild metric up to a certain order beyond which a free parameter appears.

In Sec. 3.4.1 we describe the derivation of the Bootstrapped potential and in Sec. 3.4.3 we illustrate how a full effective metric, compatible with a starting potential, can be reconstructed. The theoretical results will be tested in Part II, where we will bound the free parameter using the measured precession in Solar System and studying S -star orbits around the black hole in the center of the Galaxy.

3.4.1 Potential in the vacuum

It's worth remembering that if the space-time is static, it is always possible to choose the time coordinate x^0 such that the metric reads

$$g_{\mu\nu} = \eta_{\mu\nu} + \epsilon h_{\mu\nu}(x^i), \quad (3.90)$$

where the small parameter ϵ quantifies the deviations from flat space-time. Considering a massive particle initially at rest in this reference frame ($\dot{x}^i = 0$, which implies that $\dot{x}^0 \simeq 1$), as long as $|\dot{x}^i| \simeq \epsilon \ll 1$ (weak-field approximation), its geodesic equation (2.14) to the first order in ϵ becomes

$$\dot{x}^i \simeq \frac{1}{2} \epsilon h_{00,i}. \quad (3.91)$$

Eq. (3.91) yields Newton's second law for a particle in the potential V if we set

$$g_{00} = -1 + \epsilon h_{00} = -(1 + 2V). \quad (3.92)$$

Indeed, the linearized Einstein equations furnish the potential V since it reduces to the Poisson equation

$$r^{-2}(r^2 V')' \equiv \Delta V = 4\pi G_N \rho \quad (3.93)$$

in the *de Donder* gauge

$$\partial^\alpha h_{\alpha\mu} - \frac{1}{2} \partial_\mu h = 0, \quad (3.94)$$

where $h \equiv \eta^{\alpha\beta} h_{\alpha\beta}$. We must assume then that the coordinates x^μ in which the components of the metric take the form in Eq.(3.90) are *harmonic*, that is they must satisfy the equation

$$\square x^\mu = 0. \quad (3.95)$$

We can now start to derive heuristically the potential outside a static and spherically symmetric source by considering the Newtonian Lagrangian for a source of density $\rho = \rho(r)$

$$L_N[V] \simeq -4\pi \int_0^\infty r^2 dr \left[\frac{(V')^2}{8\pi G_N} + \rho V \right], \quad (3.96)$$

where $' = \frac{d}{dr}$. The corresponding equation is the Poisson equation. To describe mean-field deviations from GR induced by quantum physics, we will add interacting terms to this action. To do this it's worth noticing that the Hamiltonian

$$H_N[V] = -L_N[V] = 4\pi \int_0^\infty r^2 dr \left(-\frac{V \Delta V}{8\pi G_N} + \rho V \right), \quad (3.97)$$

computed on shells by means of Eq.(3.93), gives the Newtonian potential energy

$$U_N(r) = 2\pi \int_0^r \bar{r}^2 d\bar{r} \rho(\bar{r}) V(\bar{r}) \quad (3.98)$$

$$= \frac{1}{2G_N} \int_0^r \bar{r}^2 d\bar{r} V(\bar{r}) \Delta V(\bar{r}) \quad (3.99)$$

$$= -\frac{1}{2G_N} \int_0^r \bar{r}^2 d\bar{r} [V'(\bar{r})]^2, \quad (3.100)$$

where we assumed that boundary terms can be discarded. The above U_N is given by the interaction of the matter distribution enclosed in a sphere of radius r with the gravitational field; we can then associate it to a self-gravitational source J_V , that is

$$J_V(r) = \frac{4}{4\pi r^2} \frac{d}{dr} U_N(r) = -\frac{1}{2\pi G_N} [V'(r)]^2. \quad (3.101)$$

Next, we add the ‘‘loop correction’’ $J_\rho = -2V^2$ which couples with the matter source. Finally, since the pressure becomes relevant for large compactness, we also add the term

$$J_p \simeq -\frac{1}{4\pi r^2} \frac{dU_p}{dr}, \quad (3.102)$$

where U_p is the potential energy associated with the work done by the force responsible for the pressure. The total Lagrangian is

$$\begin{aligned} L[V] &= L_N[V] - 4\pi \int_0^\infty r^2 dr [q_V J_V V + 3q_p J_p V + q_\rho J_\rho (\rho + 3q_p p)] \\ &= -4\pi \int_0^\infty r^2 dr \left[\frac{(V')^2}{8\pi G_N} (1 - 4q_V V) + (\rho + 3q_p p) V (1 - 2q_\rho V) \right], \end{aligned} \quad (3.103)$$

where q_V , q_p and q_ρ are three coupling constants which quantify the different contributions. The Einstein-Hilbert action at next-to-leading order in ϵ in Eq.(3.90) is recovered for $q_V = q_p = q_\rho = 1$ [48]. The field equation for V is

$$\Delta V = 4\pi G_N \frac{1 - 4q_p V}{1 - 4q_V V} (\rho + 3q_p p) + \frac{2q_V (V')^2}{1 - 4q_V V}, \quad (3.104)$$

which is completed by the conservation equation $p' = -V'(p + \rho)$. In vacuum ($p = \rho = 0$), Eq. (3.104) reduces to

$$\Delta V = \frac{2q_V (V')^2}{1 - 4q_V V}. \quad (3.105)$$

The exact solution reads [44]

$$V_0 = \frac{1}{4q_V} \left[1 - \left(1 + \frac{6q_V G_N M}{r} \right)^{2/3} \right], \quad (3.106)$$

whose asymptotic expansion far from the source is

$$V_0 \simeq -\frac{G_N M}{r} + q_V \frac{G_N^2 M^2}{r^2} - q_V^2 \frac{8G_N^3 M^3}{3r^3}. \quad (3.107)$$

The post-Newtonian terms of the above expansion depend on the coupling constant q_V , whose exact value can be constrained by observations.

3.4.2 Harmonic and areal coordinates

Before reconstructing a metric compatible with (3.106), let us illustrate the relation between the radial coordinate r appearing in the potential and the areal coordinate \bar{r} used to write the general static spherically symmetric metric as

$$ds^2 = -\bar{B}(\bar{r}) d\bar{t}^2 + \bar{A}(\bar{r}) d\bar{r}^2 + \bar{r}^2 d\Omega^2. \quad (3.108)$$

Cartesian coordinates $x^i = (x, y, z)$ in flat space satisfy the condition (3.95) which can be extended to general space-times by defining harmonic coordinates $x^\mu = (t, x, y, z)$ such that

$$\square x^\mu = g^{\alpha\beta} \Gamma_{\alpha\beta}^\mu = 0. \quad (3.109)$$

Since we are interested in spherically symmetric space-times, we associate polar coordinates to the harmonic ones by

$$x = r(\bar{r}) \sin \theta \cos \phi, \quad y = r(\bar{r}) \sin \theta \sin \phi, \quad z = r(\bar{r}) \cos \theta, \quad (3.110)$$

where the “harmonic” r^5 is an invertible smooth function of the areal coordinate \bar{r} . Explication of Eq. (3.109) gives $r = r(\bar{r})$:

$$\frac{d}{d\bar{r}} \left(\bar{r}^2 \sqrt{\frac{\bar{B}}{\bar{A}}} \frac{dr}{d\bar{r}} \right) = 2\sqrt{\bar{A}\bar{B}}r. \quad (3.111)$$

The metric (3.108) can be expressed in terms of the rotationally invariant forms $d\mathbf{x}^2 = dr^2 + r^2 d\Omega^2$ and $(\mathbf{x} \cdot d\mathbf{x})^2 = r^2 dr^2$ as

$$ds^2 = -B dt^2 + \frac{\bar{r}^2}{r^2} d\mathbf{x}^2 + \left[A \left(\frac{d\bar{r}}{dr} \right)^2 - \frac{\bar{r}^2}{r^2} \right] \frac{(\mathbf{x} \cdot d\mathbf{x})^2}{r^2}, \quad (3.112)$$

where $dt = d\bar{t}$, $\bar{r} = \bar{r}(r)$, $A = \bar{A}(\bar{r}(r))$ and $B = \bar{B}(\bar{r}(r))$.

It’s useful recall that Schwarzschild solution is given by

$$\bar{B}_S = \frac{1}{\bar{A}_S} = 1 - \frac{R_S}{\bar{r}}, \quad (3.113)$$

where $R_S = 2 G_N M$. By solving (3.111) we find

$$r = \bar{r} - R_S, \quad (3.114)$$

which leads to the potential for the Schwarzschild metric in harmonic coordinates

$$V_S = \frac{1}{2} [B_S - 1] = -\frac{G_N M}{r} \left(1 + \frac{G_N M}{r} \right)^{-1}. \quad (3.115)$$

In Fig. (3.3) we can see the comparison between V_S and V_0 of Eq.(3.107); GR is recovered to the first order in q_V if $q_V = 1$. We now replace V_S with V_0 , that is

⁵We refer to r as the “harmonic” radial coordinate although polar coordinate do not satisfy condition (3.109).

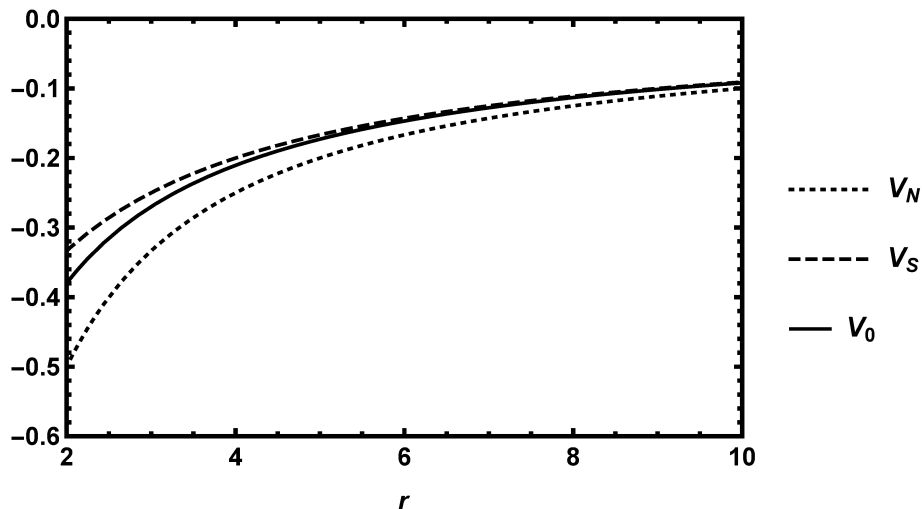


Figure 3.3: Bootstrapped Newtonian potential V_0 compared to its expansion from Eq. (3.107) and to the Newtonian potential V_N (for $q = 1$).

$$B = 1 + 2V_0. \quad (3.116)$$

We can notice that the metric coefficient \bar{B} is fully determined by the potential V_0 and the relation $r = r(\bar{r})$. Using $\bar{C} = \bar{A}\bar{B}$, it is convenient to rewrite Eq. (3.111) as

$$\bar{r} r'' + \left(2 - \frac{\bar{r} \bar{C}'}{2\bar{C}} + \bar{r} \frac{\bar{B}'}{\bar{B}}\right) r' = 2 \frac{\bar{C} r}{\bar{B} \bar{r}}, \quad (3.117)$$

where $' = \frac{d}{d\bar{r}}$. This equation determines the relation between \bar{A} and \bar{r} , but we need more than one equation to determine both $r = r(\bar{r})$ and $\bar{A} = \bar{A}(\bar{r})$ given $B = B(r)$.

3.4.3 Effective space-time metric

The starting point to derive the metric is to analyze the region far from the source by expanding in Taylor series the metric coefficients and $r = r(\bar{r})$ in powers of the dimensionless ratio $R_S/\bar{r} \sim M/\bar{r}$, that is

$$\bar{A} = 1 + \sum_{k=1} a_k \left(\frac{R_S}{\bar{r}}\right)^k, \quad (3.118)$$

$$\bar{B} = 1 + \sum_{k=1} b_k \left(\frac{R_S}{\bar{r}}\right)^k, \quad (3.119)$$

$$\frac{r}{\bar{r}} = 1 + \sum_{k=1} \sigma_k \left(\frac{R_S}{\bar{r}}\right)^k. \quad (3.120)$$

We introduce

$$\bar{C} = 1 + \sum_{k=1} \Xi_k \left(\frac{R_S}{\bar{r}}\right)^k; \quad (3.121)$$

the coefficients a_k 's are fully determined by the Ξ_k 's and b_k 's since $\bar{C} = \bar{A}\bar{B}$. To determine the metric up to the third order in R_S/\bar{r} , let us solve Eq. (3.117).

At the first and second order in R_S/\bar{r} we get

$$\sigma_1 = \frac{b_1}{2} - \frac{3}{4}\Xi_1 \quad (3.122)$$

$$\sigma_2 = \frac{\Xi_1}{4}(2\Xi_1 - b_1) - \frac{\Xi_2}{2}, \quad (3.123)$$

while the third-order equation gives

$$\Xi_3 = \frac{5}{2}\Xi_1\Xi_2 - \frac{1}{2}b_1^2\Xi_1 - b_1\Xi_2 + b_2\Xi_1 + \frac{5}{4}b_1\Xi_1^2 - 2b_3 - \frac{3}{2}\Xi_1^3. \quad (3.124)$$

To match the Eq. (3.116) we fix the b_k 's, that is

$$\bar{B} \simeq 1 - \frac{R_S}{r(\bar{r})} + \frac{q_V R_S^2}{2[r(\bar{r})]^2} - \frac{2q_V^2 R_S^3}{3[r(\bar{r})]^3}, \quad (3.125)$$

which gives $b_1 = -1$ and

$$b_2 = \frac{q_V}{2} - \frac{3}{4}\Xi_1 - \frac{1}{2} \quad (3.126)$$

$$b_3 = \frac{q_V}{4}(2 + 3\Xi_1) - \frac{2}{3}q_V^2 - \frac{\Xi_1}{16}(8 + \Xi_1) - \frac{\Xi_2}{2} - \frac{1}{4}. \quad (3.127)$$

After replacing these expressions in \bar{A} , we get

$$a_1 = 1 + \Xi_1 \quad (3.128)$$

$$a_2 = \frac{3}{2} - \frac{q_V}{2} + \frac{7}{4}\Xi_1 + \Xi_2 \quad (3.129)$$

$$a_3 = \frac{11}{4} + \left(2q_V - \frac{5}{2} - \frac{9}{4}\Xi_1\right)q_V + \frac{7}{2}(\Xi_1 + \Xi_2) + \frac{\Xi_1}{2}\left(5\Xi_2 - \frac{17}{8}\Xi_1 - 3\Xi_1^2\right). \quad (3.130)$$

To fix all the coefficients from physical considerations, we introduce the Eddington-Robertson Parametrized Post-Newtonian (PPN) formalism [233], in which the metric reads

$$ds^2 \simeq - \left[1 - \alpha \frac{R_S}{\bar{r}} + (\beta - \alpha\gamma) \frac{R_S^2}{2\bar{r}^2} + (\zeta - 1) \frac{R_S^3}{\bar{r}^3} \right] c^2 dt^2 + \left[1 + \gamma \frac{R_S}{\bar{r}} + \xi \frac{R_S^2}{\bar{r}^2} + \sigma \frac{R_S^3}{\bar{r}^3} \right] d\bar{r}^2 + \bar{r}^2 d\Omega^2, \quad (3.131)$$

where we can set $\alpha = 1$ by the definition of the gravitational radius. This is in agreement with $b_1 = -\alpha = -1$ and we can identify the first order PPN parameters

$$\Xi_1 = \gamma - 1 \quad \text{and} \quad q_V = \beta + \frac{\gamma - 1}{2}. \quad (3.132)$$

Finally, we obtain

$$\begin{aligned}\bar{B} \simeq & 1 - \frac{R_S}{\bar{r}} + (\beta - \gamma) \frac{R_S^2}{2\bar{r}^2} \\ & + [7 + 4\beta(5 + \gamma) - 32\beta^2 - \gamma(26 - 7\gamma) - 24\Xi_2] \frac{R_S^3}{48\bar{r}^3}\end{aligned}\quad (3.133)$$

and

$$\begin{aligned}\bar{A} \simeq & 1 + \gamma \frac{R_S}{\bar{r}} - (\beta - 3\gamma - 2\Xi_2) \frac{R_S^2}{2\bar{r}^2} \\ & + [5 + 32\beta^2 - 4\beta(9 + \gamma) + 3\gamma(6 + 15\gamma - 8\gamma^2) + 8\Xi_2(2 + 5\gamma)] \frac{R_S^3}{16\bar{r}^3}\end{aligned}\quad (3.134)$$

so that

$$\begin{aligned}\bar{C} \simeq & 1 + (\gamma - 1) \frac{R_S}{\bar{r}} + \Xi_2 \frac{R_S^2}{\bar{r}^2} \\ & + [11 + 32\beta^2 - 8\beta(4 - \gamma) - \gamma(22 - 59\gamma - 36\gamma^2) - 12\Xi_2(1 - 5\gamma)] \frac{R_S^3}{24\bar{r}^3}.\end{aligned}\quad (3.135)$$

The harmonic radius can be written as

$$r \simeq \bar{r} + \frac{1 - 3\gamma}{4} R_S + (1 - 3\gamma + 2\gamma^2 - 2\Xi_2) \frac{R_S^2}{4\bar{r}}.\quad (3.136)$$

Experimental data strongly constrain $|\gamma - 1| \simeq |\beta - 1| \ll 1$. Assuming $\beta = \gamma = 1$, that is $\Xi_1 = 0$ and $q_V = 1$, we find that the Bootstrapped metric which describes the minimum deviation from the Schwarzschild form is given by

$$\bar{B} \simeq 1 - \frac{R_S}{\bar{r}} - (5 + 6\Xi) \frac{R_S^3}{6\bar{r}^3}\quad (3.137)$$

$$\simeq B_S(\bar{r}) - (6\xi - 1) \frac{R_S^3}{6\bar{r}^3}\quad (3.138)$$

$$\bar{A} = 1 + \frac{R_S}{\bar{r}} + (1 + \Xi) \frac{R_S^2}{\bar{r}^2} + (9 + 14\Xi) \frac{R_S^3}{4\bar{r}^3}\quad (3.139)$$

$$\simeq A_S(\bar{r}) + (\xi - 1) \frac{R_S^2}{4\bar{r}^2} + (14\xi - 9) \frac{R_S^3}{4\bar{r}^3},\quad (3.140)$$

and

$$r \simeq \bar{r} - \frac{R_S}{2} - (\xi - 1) \frac{R_S^2}{2\bar{r}}.\quad (3.141)$$

From now on, we will put $\Xi_2 = \Xi$ for clarity. The second-order PPN parameters are both determined by the parameter Ξ as

$$\xi = 1 + \Xi, \quad \zeta = 1 - \frac{5 + 6\Xi}{12} = \frac{13 - 6\xi}{12},\quad (3.142)$$

so that the combination $\xi = \zeta = 1$ corresponding to the PPN expansion of the Schwarzschild metric is not allowed. We can see that the new contribution to \bar{A} at

the second order only vanishes for $\Xi = 0$, but higher-order corrections cannot be eliminated. Correspondingly, for $\beta = \gamma = 1$, we have

$$\bar{C} \simeq 1 + (\xi - 1) \frac{R_S^2}{r^2} + (12\xi - 7) \frac{R_S^3}{6r^3}. \quad (3.143)$$

The geodesic equations ⁶

$$\ddot{x}^\mu + \Gamma_{\alpha\beta}^\mu \dot{x}^\alpha \dot{x}^\beta = 0 \quad (3.144)$$

can be equivalently computed using the Euler-Lagrange equations

$$\frac{d}{ds} \frac{\partial \mathcal{L}}{\partial \dot{x}^\mu} - \frac{\partial \mathcal{L}}{\partial x^\mu} = 0, \quad (3.145)$$

with $\mathcal{L} = g_{\alpha\beta} \dot{x}^\alpha \dot{x}^\beta = -1$ for a massive object. From the metric in Eq. (3.131), one then finds

$$\begin{aligned} \ddot{r} = & \frac{R_S \left\{ 2(1 + \Xi) R_S r \dot{r}^2 + (R_S^2/4) \left[3(9 + 14\Xi) \dot{r}^2 - c^2(5 + 6\Xi) \dot{t}^2 \right] + r^2 (\dot{r}^2 - c^2 \dot{t}^2) \right\}}{2r \left[2(9 + 14\Xi) (R_S^3/8) + (1 + \Xi) R_S^2 r + R_S r^2 + r^3 \right]} \\ & + \frac{r^5 (\dot{\theta}^2 + \dot{\phi}^2 \sin^2 \theta)}{2r \left[2(9 + 14\Xi) (R_S^3/8) + (1 + \Xi) R_S^2 r + R_S r^2 + r^3 \right]} \end{aligned} \quad (3.146)$$

$$\ddot{\theta} = \dot{\phi}^2 \sin \theta \cos \theta - \frac{2\dot{r}\dot{\theta}}{r} \quad (3.147)$$

$$\ddot{\phi} = -\frac{2\dot{\phi}}{r} (\dot{r} + r\dot{\theta} \cot \theta) \quad (3.148)$$

$$\ddot{t} = \frac{6\dot{r}\dot{t} \left[(5 + 6\Xi) (R_S^3/8) + (R_S/2) r^2 \right]}{(5 + 6\Xi) (R_S^3/4) r + 3R_S r^3 - 3r^4}. \quad (3.149)$$

Spherical symmetry as usual implies that the orbital motion occurs on a plane which we can arbitrarily set at $\theta = 0 = \dot{\theta}$.

The third and fourth equations are the usual conservation equations for the angular momentum and energy conjugated to t , respectively. The above parametric system of non-linear differential equations can be integrated numerically in order to study the orbits.

3.4.4 Precession

As we saw in Sect. 2.6.3, the precession of Newtonian orbits of planets and stars with semilatus rectum ℓ and eccentricity e can be expressed in terms of the PPN parameters. At the first order in R_S/ℓ it reads

$$\Delta\varphi^{(1)} = \pi(2 - \beta + 2\gamma) \frac{R_S}{\ell}, \quad (3.150)$$

⁶A dot indicates the derivative with respect to the proper time.

and reproduces the GR result for $\beta = \gamma = 1$. The second order correction depends on both ξ and ζ and, for $\beta = \gamma = 1$, is given by

$$\begin{aligned}\Delta\phi^{(2)} &= \pi \left[(41 + 10\xi - 24\zeta) + (16\xi - 13) \frac{e^2}{2} \right] \frac{R_S^2}{4\ell^2} \\ &\simeq \pi \left[(37 + 22\Xi) + (3 + 16\Xi) \frac{e^2}{2} \right] \frac{R_S^2}{4\ell^2} \\ &\simeq \Delta\phi_S^{(2)} + 2\pi \left[11\xi - 7 + 4(\xi - 1)e^2 \right] \frac{R_S^2}{4\ell^2},\end{aligned}\tag{3.151}$$

where the GR result $\Delta\phi_S^{(2)}$ corresponds to $\xi = \zeta = 1$. From Eq. (3.142), it follows that we cannot have $\xi = \zeta = 1$ for any value of Ξ , and a deviation from GR remains.

3.5 Concluding remarks

In this chapter we focused on two ETG: $f(R)$ -gravity theory and Bootstrapped Newtonian gravity theory. Deviations between these theories and GR are encoded in specific parameters. After having ascertained the consistency of a certain theory, this must be selected or ruled out on the basis of experimental observations. To this aim, it must be constrained at all the observation scales. In the next part, we will see how to bound such parameters astronomically, studying the stellar orbits at the Galactic Center and the orbital precession of the Solar System planets.

Part II

Applications

THE GALACTIC CENTER

Dopo tanta nebbia a una a una si svelano le stelle.

– G. Ungaretti

4.1	Toward the center of the Milky Way	70
4.2	The nuclear star cluster	72
4.2.1	The <i>S</i> -star cluster	73
4.3	Is Sgr A* a supermassive black hole?	75
4.3.1	Evidence for a central compact object	75
4.3.2	Constraints from stellar orbits	76
4.3.3	Alternatives to the black hole paradigm	77
4.4	A laboratory to test General Relativity	79
4.4.1	Monitoring stellar orbits	81
4.4.2	Pulsars timing	82
4.4.3	EHT observations	84
4.5	Concluding remarks	85

Our home galaxy, the Milky Way, is an ordinary barred spiral galaxy, which hides in its central 100 pc a region of unique phenomena: the **Galactic Center** (GC). Here astronomers can study relevant physical processes common to extra-galactic centers of a similar type with unprecedented spatial resolution. Indeed, located at a distance of about 8 kpc (26000 light-years) away from the Earth, there lies the closest galactic nucleus (the GC is $\sim 10^5$ times nearer than the closest galaxies).

In this chapter, after presenting a schematic description of the central region, we will summarize the recent observational and theoretical progress on the innermost parsec. We will focus on the evidence that contributed to strengthen the black hole nature

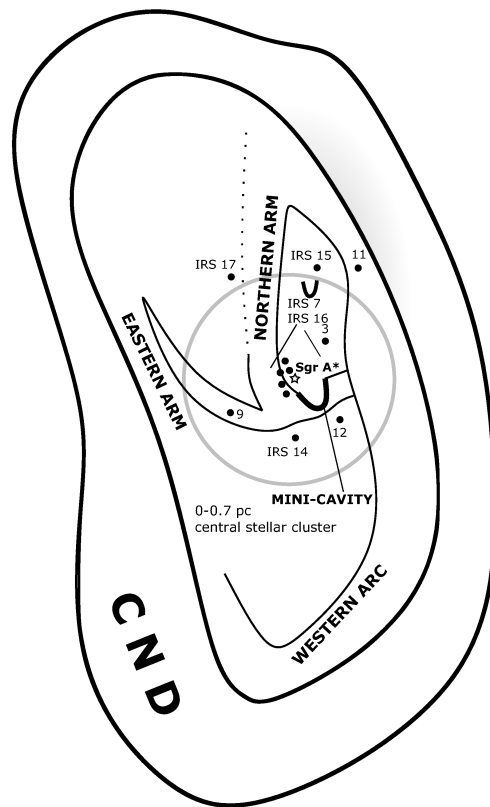


Figure 4.1: Schematic image of the structures in the Galactic Center. The mini-spiral of ionized gas connects the central cluster region with the circum-nuclear disk. The size of the central cluster (~ 0.7 pc) is indicated by a circle. The position of the compact radio source Sgr A* is indicated with a star.

hypothesis of the central compact object associated with the radio source **Sagittarius A*** (Sgr A*). The existence of such a gravitational source of about ~ 4 million solar masses is inferred mainly from the study of the dynamics of stars revolving around it, known as *S-stars*.

Thanks to its proximity, the GC represents a superb astrophysical laboratory where, in a gravitational regime almost unexplored, scientists can test the nature of the central compact object and the underlying theory of gravity. However, since the central region is obscured by dust, observations need to be performed at wavelengths other than the optical: infrared and microwave, or *X-rays* and γ -rays.

4.1 Toward the center of the Milky Way

A schematic representation of the different structures and objects that populate the GC is shown in Figure 4.1 [74]. The innermost region of the Milky Way is composed of

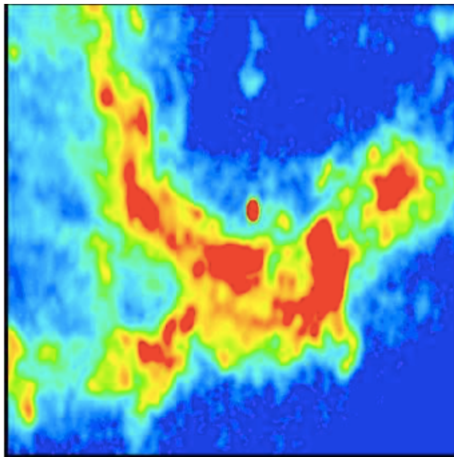


Figure 4.2: Image at 2 cm of Sgr A West and Sgr A* (the bright central object in this image) [162].

a dense star cluster and several components of extremely hot gas interacting mutually [97, 14, 100, 198, 99, 164].

Let us start from the center where is located a compact radio source no bigger than ~ 1 AU [140, 5, 150, 200, 141, 152]: Sgr A*. Sgr A* was discovered in 1974 by Bruce Balick and Robert Brown at Green Bank with the National Radio Astronomy Observatory (NRAO) interferometer [10, 153, 239]. This discovery was confirmed by Westerbork [84] and Very Large Baseline Interferometry (VLBI) observations [154]. From accurate observations by Very Large Array (VLA) [29], it was inferred that Sgr A* is located near the dynamical center of the gas streamers. Furthermore, at that time it was discovered its radio variability [30]. VLBI observations pointed out that its intrinsic size is about 3 – 10 light minutes [140, 200, 71, 140, 23, 214]. Therefore, from the very first observations, Sgr A* appeared as an unusual object and it became the ideal candidate for a supermassive black hole.

The central parsec is enveloped in the “three-arm” spiral structure of ionized gas and dust named Sgr A West [85, 151] (Fig. 4.2 shows a ~ 2 pc \times 2 pc region). Spectroscopic observations of the hot gas in this structure [213, 127, 199] highlight a rotation of ~ 150 km s $^{-1}$ around Sgr A* in a counter-clockwise direction. In Fig. 4.3 we can see the stellar distribution, centered on Sgr A*, at 1.5 μ m on the same spatial scale as Fig. 4.2. Between its northern and eastern arms, adjacent to Sgr A* and IRS16 (the blue stellar cluster to the east of Sgr A*), there is a hole in the distribution of the radio continuum emission with a diameter of 2'' indicated as “mini-cavity”. The complex Sgr A West is externally surrounded by a gaseous circumnuclear ring (or circumnuclear disk, CND) at $R \sim 3$ pc [13, 57, 144]. This central cavity is pervaded by ultraviolet radiation heating the dust and gas within the inner 8 pc of the galaxy. Outside the outer edge of the CND, there is a young supernova remnant (Sgr A East) and several dense molecular

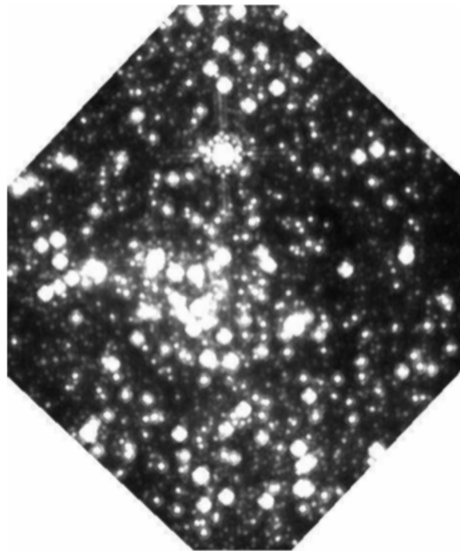


Figure 4.3: Image at $1.6 \mu\text{m}$ as seen by NICMOS on the Hubble Space Telescope of the inner $19'' \times 19''$ region at the GC [162].

clouds at $5 - 100 \text{ pc}$. In summary, the larger region of $\sim 50 \text{ pc} \times 50 \text{ pc}$ known as Sgr A complex, reveals a complicated morphology by radio continuum measurements. The brightest continuum features are Sgr A West and Sgr A East. Moreover, X-ray observations [193, 137, 215, 6] reveal emitting regions of high temperature and pressure, signalling the presence of unbound gas. On a larger scale of hundreds of parsecs, we can find many synchrotron-emitting filamentary structures perpendicularly to the Galactic plane. These features may be magnetic field lines lit up by relativistic electrons, e.g., in a reconnection zone between the Galactic field lines and those from molecular clouds.

The last decades have witnessed an incessant improvement of the techniques and instruments of observations, accelerating greatly the progress of knowledge of the GC in the whole electromagnetic spectrum.

4.2 The nuclear star cluster

Observations of the stars at the GC, whose spectra are approximately those of the black body, are conducted in the infrared, especially in the K-band.

It is observed that the stellar population at the GC is made up of a large number of bright stars. Infrared spectroscopy reveals that a part of these bright stars is what we expect to find in an old nuclear star cluster. Indeed, 98% of them are old ($> 1 \text{ Gyr}$); they are divided into late-type giants and helium-burning stars on the horizontal branch, which have masses $m \sim (0.5 - 4) M_{\odot}$ and temperatures of $\sim (3500 - 3700) \text{ }^{\circ}\text{K}$. Moreover, there are few bright and cool ($T \sim 2700 \text{ }^{\circ}\text{K}$) asymptotic giant branch stars

(AGB). Finally, in the central region, there are a few more massive red supergiants stars [19]. Observations show that their motion and distribution are random and isotropic [227]. This cluster is associated with a slow solid-body rotation in the sense of the rotation of the Galaxy, with an amplitude of $\sim (1.4 \text{ km s}^{-1})/\text{arcsec}$ [161, 104, 227, 208].

It was found that the other part of these stars are hot early-type ‘HeI-stars’ [138, 221, 20, 148, 104, 222, 184], such as post-main-sequence, blue supergiants and Wolf-Reyet (WR) stars with ages of 2 – 8 Myr and zero-age main-sequence (ZAMS) masses (30 – 100) M_{\odot} [172, 160]. Radial velocities and proper motions measurements revealed that most of such stars are arranged on a disk in a clockwise rotation around Sgr A* ($j_z > 0$)¹ [103]. On the other hand, it emerged that some stars exhibit a counter-clockwise motion, and it became clear that all the stars are arranged on two strongly inclined disks relative to each other [103]. In the central arcsecond is found a faint population of blue stars. This population constitutes the so-called *S*-star cluster.

The discovery of this remarkable concentration of young stars is surprising. According to the standard theories of stellar evolution, formation processes should be strongly inhibited in this region due to the intense tidal field of the central body. A still unanswered question is whether they formed in situ, or they were transported into the center from further out. The processes proposed to explain the presence of these stars constitute the *Paradox of Youth*.

4.2.1 The *S*-star cluster

S-star cluster consists of lighter stars that exhibit a distribution different from the planar structure. A robust accounting is made by Gillessen et al. [111], who derived the individual orbit for 28 of them. Of the stars with a semi-major axis $a \leq 1''$, 16 are *B*-stars and 3 are late-type stars.

A NIR spectroscopic study [123] throws light on parameters of *S*-stars within a distance of 0.04 pc from the black hole (*S1*, *S2*, *S4*, *S6*, *S7*, *S8*, *S9*, and *S12*). The effective temperature lies in the range (21000–28500) °K, characteristic of spectral type from *B0* to *B2.5*. Such stars have surface gravity within the range $\log(g) > 3.4 - 4.2$, classifying themselves as dwarfs on the main sequence stage, that is, below the turn due to central hydrogen exhaustion. Their projected rotational velocities fall in the range from 60 to 170 km s^{-1} , and their luminosities in the range $\log(L/L_{\odot}) \sim 3.6 - 4.3$. Their age is estimated to be less than 15 Myr (in particular, they derived for *S2* an age of $6.6_{-4.7}^{+3.4}$ Myr), compatible with the age of the young clockwise-rotating stellar disk. The brightest member of the *B*-star cusp is the star *S2/S02* [159]. According

¹We can define the projected, normalized specific angular momentum of the motion on the sky as $j_z = (xv_y - yv_x)/(\{x^2 + y^2\}\{v_x^2 + v_y^2\})^{1/2}$. If $j_z > 0$ the motion is clockwise, while if $j_z < 0$ it is counter-clockwise.

to its spectrum, *S2* can be classified as a main-sequence (dwarf) $B0 - 2.5 V$ star with a ZAMS mass of $m_{\text{ZAMS}} \sim 19.5 M_{\odot}$ and with a low rotation velocity typical of the solar neighbourhood BV stars. The high abundance of He/H ($0.25 - 0.5$), makes *S2* a member of the ‘He-rich’ class of B -stars.

Box 1: Observing S -stars

S -star motion has been monitored for the last three decades by two main observational teams, one led by Genzel at the Max Planck Institute for Extraterrestrial Physics (MPE), using telescopes in Chile at the European Southern Observatory (ESO), and the other led by Ghez at the University of California (UCLA), using the Keck Observatory in Hawaii. They were awarded by Nobel Prize in Physics 2020 for discovering a compact object at the center of our galaxy [98]. The two teams performed their observations in the K-band, centered at $\lambda = 2.2 \mu\text{m}$, to reduce the attenuation due to interstellar dust. Both teams initially used the technique of speckle imaging in the NIR, based on a series of short exposures (just above a tenth of a second) to compensate for the smearing of photons’ trajectories due to the Earth’s atmosphere. This technique allowed the measurements of the projected velocity of the stars, which was inferred from the shift in their position. These first data were obtained, for Genzel’s group, between 1992 and 2002 with the SHARP camera at the ESO’S 3.5 m NTT. Despite the power of such a technique to spatially resolve the stars, its limitation is to be found in its functioning: the short exposure times limited the observation to only the brightest stars. These shortcomings were overcome when adaptive optics was developed. Such a technique uses a bright reference object next to the observation target, while a deformable secondary mirror changes shape to compensate for aberrations to the known reference object with a feedback loop, thus enabling longer exposure time and high-resolution images. These data began to be taken at ESO from 2002 when the Naos-Conica (NACO) system was mounted at the telescope Yepun (8 m) of the VLT. From then on it was also possible to use a spectrograph to study the stars’ composition and measure their radial velocities. The decisive turning point in S -star observations is achieved with the development of GRAVITY, the cryogenic, interferometric beam combiner of the four UTs of the VLT, along with the AO systems for all four UTs [118]. GRAVITY is able to detect also faint stars with an angular resolution that exceeds that of adaptive-optics assisted imaging by a factor of ~ 20 . With GRAVITY it was possible to precisely detect the first-order GR-effects of the orbit of *S2*.

S -star cluster is the perfect tool to answer many astrophysical and physical questions. In particular, they provide direct constraints on the nature of Sgr A*, as we will see in the next sections.

4.3 Is Sgr A* a supermassive black hole?

In this section, we will summarize the steps that led to the following conclusion: **in the central parsec there is a combination of a dense nuclear star cluster and a central compact object associated with Sgr A***. The crucial question is: does the center of the Milky Way host a SMBH or some other type of compact object? We can obtain the definitive proof of the existence of a massive black hole in two ways:

- analyzing the gravitational potential to the scale of the event horizon;
- demonstrating that the gravitational potential of a galactic nucleus is dominated by a compact “dark” mass that can be only a black hole.

4.3.1 Evidence for a central compact object

The first evidence of a large central mass concentration came out at the end of the 1970s. At that time the group of Townes [238], based on the increase of the radial velocity of ionized gas (in the 12.8 μm line of the NeII) to a few hundred km/s towards the center, concluded that the total mass within a radius of 1 pc about the GC was estimated to be of the order of 2 – 4 million solar masses. The Berkley group advanced the hypothesis that this mass concentration could plausibly be a black hole associated with the radio source Sgr A* [143, 142]. However many scientists did not judge this conclusion convincing, first of all, because gas reacts to forces other than gravity (magnetic fields, friction, radiation pressure, etc.), then because in this method only line of sight velocities come into play, and finally because there wasn't detection of a luminous infrared or X-ray source associated to Sgr A* [197, 3, 136]. Since then, the focus has been mainly put on stars.

The first stellar velocity dispersion measurements, confirming the gas measurements, came from spectroscopy of 2 μm CO absorption bands in late-type giants and supergiants (from $p \sim 10''$ to $p \sim 3''$) [198, 161, 212, 124]. However, these data, sampling the mass at a large radius, were far to be conclusive. The evidence of a massive central object was reinforced by a virial analysis applied to the first blue supergiants detected in the central 10'' [93, 138].

An improved analysis of the mass distribution from 2.5'' to $\sim 1''$ is found in Ref. [104, 124], which was based on radial velocities of ~ 200 late-type stars and two dozen early-type stars available at that time. Genzel et al. deduced a combination of a $3.0 \times 10^6 M_\odot$ central mass and a $10^6 M_\odot$ star cluster with a core radius of $\sim 10''$. The corresponding average stellar density in the core was $\sim 10^6 M_\odot \text{pc}^{-3}$.

²Here p denotes the projected angular distance.

The turning point came with the determination of proper motions of the fast-moving (velocities up to $\sim 10^3$ km/s) S -stars within $\leq 1''$ of Sgr A*, thanks to the above mentioned speckle imaging [72, 73, 102, 105]. Both ESO NTT and Keck datasets were in agreement with the conclusion that velocity dispersion of the stars follows a Kepler-law around a compact mass ($\sigma(v) \sim R^{-1/2}$) to a scale of about 0.01 pc; the idea of the presence of a compact mass at the GC began to be considered satisfactory.

4.3.2 Constraints from stellar orbits

The breakthrough occurred with the determination of individual stellar orbits [96, 107, 203, 78]. The first orbit to be studied was that of the star $S2$ [209, 108]. Revolving with a period of 16.00 years, at the time of writing two full orbits are observed. Data from NTT/VLT and Keck telescopes agreed within the uncertainties, giving 4.1×10^6 [209] and $4.6 \times 10^6 M_\odot$ [108].

The most recent work on the S -stars orbits has strengthened this evidence thanks to the advent of many more and higher quality data coming from upgraded facilities, such as GRAVITY. Regarding Genzel’s team, after 25 years of uninterrupted monitoring of stellar orbits, they measured accelerations for 47 stars (see Fig. 4.4 for the graphic representation), and used 17 of them for a Keplerian multi-star orbit fit to determine parameters of the central mass, that is its mass M and its distance R , and orbital elements for the stellar orbits. Best-fit keplerian parameters for S -stars are reported in Table 2.1, while the best estimates for the potential’s parameter are given by:

$$M = (4.35 \pm 0.13) \times 10^6 M_\odot, \quad (4.1)$$

$$R_0 = 8.33 \pm 0.12 \text{ kpc}. \quad (4.2)$$

The most recent estimates obtained by the GRAVITY collaboration [116] include the superb 2017 – 2019 astrometry and the pericentre passage observation. They were the first to detect the GR Schwarzschild precession in $S2$ ’s orbit, that is $\Delta\phi_{\text{per orbit}} = f_{SP} \times 12.1' = (1.10 \pm 0.19) \times 12.1'$. They obtained for the mass and the distance of the black hole the following estimates:

$$M = (4.261 \pm 0.012) \times 10^6 M_\odot, \quad (4.3)$$

$$R_0 = 8246.7 \pm 9.3 \text{ pc}. \quad (4.4)$$

In summary, the dynamical study of S -stars demonstrates the existence of a highly concentrated mass of $\sim 4 \times 10^6 M_\odot$ within the pericenter of $S2$ (125 AU). This corresponds to a minimum density of $5 \times 10^{15} M_\odot \text{ pc}^{-3}$.

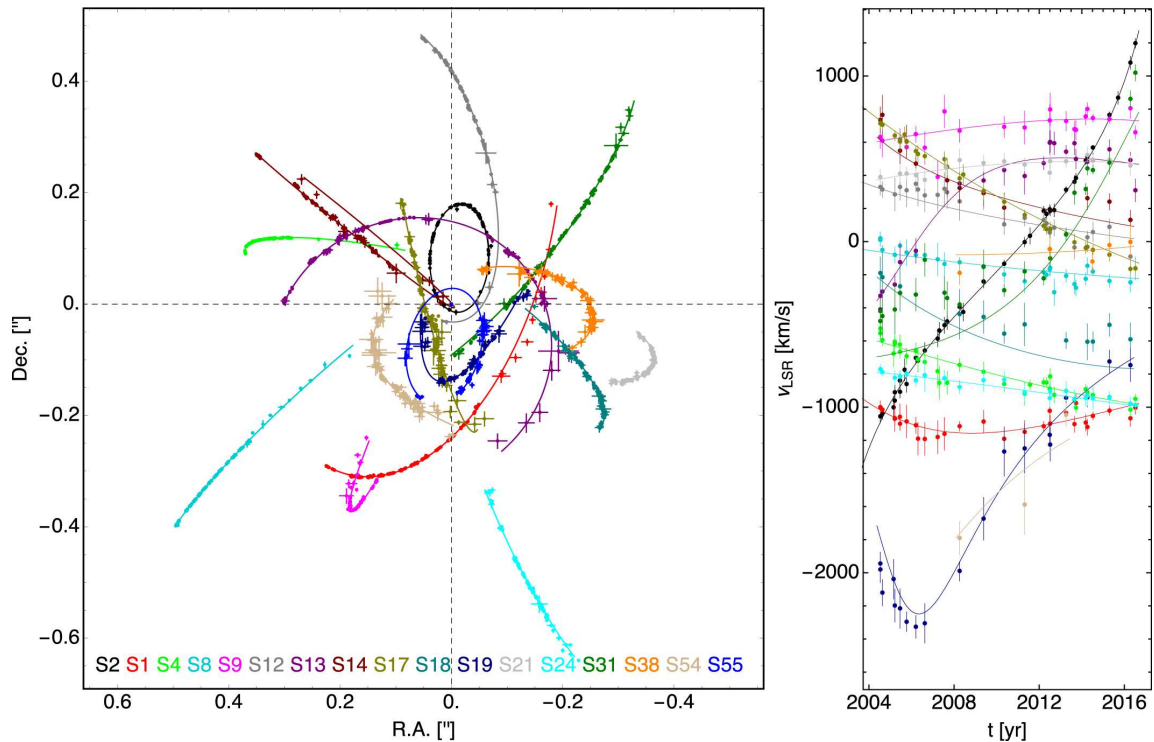


Figure 4.4: Best-fitting orbits from the multi-star fit (solid lines) with the corresponding radial velocity data [110].

4.3.3 Alternatives to the black hole paradigm

Although observations go in the direction of consolidating the black hole paradigm, the issue of the nature of the object at the center of the Milky Way is a hotly debated topic. Many scientists have wondered to what extent we are sure that Sgr A* is a black hole, and have proposed several alternative solutions to the black hole paradigm. To complete this discussion, let us briefly discuss the most important of these speculations and how they can reasonably be ruled out.

“Dark” cluster- In the last years, thanks to Hubble Space Telescope (HST) and to VLBI, astronomers inferred the presence of central high density “dark” mass in many galaxies [134, 120]. By “dark” (i.e., nonstellar) objects we mean objects that do not emit radiation and that are only discovered by their effects on the kinematics of nearby stars and gases; possible candidates include low-mass stars, brown dwarfs, planets, or compact stellar remnants (white dwarfs and neutron stars). On the other side, dynamic studies in the center of the Milky Way indicate that the central object has a minimum density of $10^{16} M_{\odot} \text{pc}^{-3}$. The enormous density deduced excludes that the central mass could be made up of a dark cluster because it should have a lifetime of less than a few 10^5 years, a very small fraction of the lifetime of the galaxy [158]. This stability argument strongly suggests that no sufficiently long-lived astrophysical object can be so massive and so small unless it is a single or binary black hole.

Table 4.1: Keplerian parameters of the 40 S -stars whose orbit has been determined in Ref. [110]

Star	a(°)	e	i(°)	Ω (°)	ω (°)	t_P (years)	T (years)	m_K
S1	0.595 ± 0.024	0.556 ± 0.018	119.14 ± 0.21	342.04 ± 0.32	122.3 ± 1.4	2001.80 ± 0.15	166.0 ± 5.8	14.7
S2	0.1255 ± 0.0009	0.8839 ± 0.0019	134.18 ± 0.40	226.94 ± 0.60	65.61 ± 0.57	2002.33 ± 0.01	16.00 ± 0.02	13.95
S4	0.3570 ± 0.0037	0.3905 ± 0.0059	80.33 ± 0.08	258.84 ± 0.07	290.8 ± 1.5	1957.4 ± 1.2	77.0 ± 1.0	14.4
S6	0.6574 ± 0.0006	0.8400 ± 0.0003	87.24 ± 0.06	85.07 ± 0.12	116.23 ± 0.07	2108.61 ± 0.03	192.0 ± 0.17	15.4
S8	0.4047 ± 0.0014	0.8041 ± 0.0075	74.37 ± 0.30	315.43 ± 0.19	346.70 ± 0.41	1983.64 ± 0.24	92.9 ± 0.41	14.5
S9	0.2724 ± 0.0041	0.644 ± 0.020	82.41 ± 0.24	156.60 ± 0.10	150.6 ± 1.0	1976.71 ± 0.92	51.3 ± 0.70	15.1
S12	0.2987 ± 0.0018	0.8883 ± 0.0017	33.56 ± 0.49	230.1 ± 1.8	317.9 ± 1.5	1995.59 ± 0.04	58.9 ± 0.22	15.5
S13	0.2641 ± 0.0016	0.4250 ± 0.0023	24.70 ± 0.48	74.5 ± 1.7	245.2 ± 2.4	2004.86 ± 0.04	49.00 ± 0.14	15.8
S14	0.2863 ± 0.0036	0.9761 ± 0.0037	100.59 ± 0.87	226.38 ± 0.64	334.59 ± 0.87	2000.12 ± 0.06	55.3 ± 0.48	15.7
S17	0.3559 ± 0.0096	0.397 ± 0.011	96.83 ± 0.11	191.62 ± 0.21	326.0 ± 1.9	1991.19 ± 0.41	76.6 ± 1.0	15.3
S18	0.2379 ± 0.0015	0.471 ± 0.012	110.67 ± 0.18	49.11 ± 0.18	349.46 ± 0.66	1993.86 ± 0.16	41.9 ± 0.18	16.7
S19	0.520 ± 0.094	0.750 ± 0.043	71.96 ± 0.35	344.60 ± 0.62	155.2 ± 2.3	2005.39 ± 0.16	135 ± 14	16.6
S21	0.2190 ± 0.0017	0.764 ± 0.014	58.8 ± 1.0	259.64 ± 0.62	166.4 ± 1.1	2027.40 ± 0.17	37.00 ± 0.28	16.9
S22	1.31 ± 0.28	0.449 ± 0.088	105.76 ± 0.95	291.7 ± 1.4	95 ± 20	1996.9 ± 10.2	540 ± 63	16.6
S23	0.253 ± 0.012	0.56 ± 0.14	48.0 ± 7.1	249 ± 13	39.0 ± 6.7	2024.7 ± 3.7	45.8 ± 1.6	17.8
S24	0.944 ± 0.048	0.8970 ± 0.0049	103.67 ± 0.42	7.93 ± 0.37	290 ± 15	2024.50 ± 0.03	331 ± 16	15.6
S29	0.428 ± 0.019	0.728 ± 0.052	105.8 ± 1.7	161.96 ± 0.80	346.5 ± 5.9	2025.96 ± 0.95	101.0 ± 2.0	16.7
S31	0.449 ± 0.010	0.5497 ± 0.0025	109.03 ± 0.27	137.16 ± 0.30	308.0 ± 3.0	2018.07 ± 0.14	108. ± 1.2	15.7
S33	0.657 ± 0.026	0.608 ± 0.064	60.5 ± 2.5	100.1 ± 5.5	303.7 ± 1.6	1928 ± 12	192.0 ± 5.2	16.
S38	0.1416 ± 0.0002	0.8201 ± 0.0007	171.1 ± 2.1	101.06 ± 0.24	17.99 ± 0.25	2003.19 ± 0.01	19.2 ± 0.02	17.
S39	0.370 ± 0.015	0.9236 ± 0.0021	89.36 ± 0.73	159.03 ± 0.10	23.3 ± 3.8	2000.06 ± 0.06	81.1 ± 1.5	16.8
S42	0.95 ± 0.18	0.567 ± 0.083	67.16 ± 0.66	196.14 ± 0.75	35.8 ± 3.2	2008.24 ± 0.75	335 ± 58	17.5
S54	1.20 ± 0.87	0.893 ± 0.078	62.2 ± 1.4	288.35 ± 0.70	140.8 ± 2.3	2004.46 ± 0.07	477 ± 199	17.5
S55	0.1078 ± 0.0010	0.7209 ± 0.0077	150.1 ± 2.2	325.5 ± 4.0	331.5 ± 3.9	2009.34 ± 0.04	12.80 ± 0.11	17.5
S60	0.3877 ± 0.0070	0.7179 ± 0.0051	126.87 ± 0.30	170.54 ± 0.85	29.37 ± 0.29	2023.89 ± 0.09	87.1 ± 1.4	16.3
S66	1.502 ± 0.095	0.128 ± 0.043	128.5 ± 1.6	92.3 ± 3.2	134 ± 17	1771 ± 38	664 ± 37	14.8
S67	1.126 ± 0.026	0.293 ± 0.057	136.0 ± 1.1	96.5 ± 6.4	213.5 ± 1.6	1705 ± 22	431 ± 10	12.1
S71	0.973 ± 0.040	0.899 ± 0.013	74.0 ± 1.3	35.16 ± 0.86	337.8 ± 4.9	1695 ± 21	346 ± 11	16.1
S83	1.49 ± 0.19	0.365 ± 0.075	127.2 ± 1.4	87.7 ± 1.2	203.6 ± 6.0	2046.8 ± 6.3	656 ± 69	13.6
S85	4.6 ± 3.30	0.78 ± 0.15	84.78 ± 0.29	107.36 ± 0.43	156.3 ± 6.8	1930.2 ± 9.8	3580 ± 2550	15.6
S87	2.74 ± 0.16	0.224 ± 0.027	119.54 ± 0.87	106.32 ± 0.99	336.1 ± 7.7	611 ± 154	1640 ± 105	13.6
S89	1081 ± 0.055	0.639 ± 0.038	87.61 ± 0.16	238.99 ± 0.18	126.4 ± 4.0	1783 ± 26	406 ± 27	15.3
S91	1917 ± 0.089	0.303 ± 0.034	114.49 ± 0.32	105.35 ± 0.74	356.4 ± 1.6	1108 ± 69	958 ± 50	12.2
S96	1499 ± 0.057	0.174 ± 0.022	126.36 ± 0.96	115.66 ± 0.59	233.6 ± 2.4	1646 ± 16	662 ± 29	10.
S97	2.32 ± 0.46	0.35 ± 0.11	113.0 ± 1.3	113.2 ± 1.4	28 ± 14	2132 ± 29	1270 ± 309	10.3
S111	-12.3 ± 8.4	1.092 ± 0.064	102.68 ± 0.40	52.34 ± 0.75	132.4 ± 3.3	1947.7 ± 4.5	N.A.	13.8
S145	1.12 ± 0.18	0.50 ± 0.25	83.7 ± 1.6	263.92 ± 0.94	185 ± 16	1808 ± 58	426 ± 71	17.5
S175	0.414 ± 0.039	0.9867 ± 0.0018	88.53 ± 0.60	326.83 ± 0.78	68.52 ± 0.40	2009.51 ± 0.01	96.2 ± 5.0	17.5
R34	1.81 ± 0.15	0.641 ± 0.098	136.0 ± 8.3	330 ± 19	57.0 ± 8.0	1522 ± 52	877 ± 83	14.
R44	3.9 ± 1.4	0.27 ± 0.27	131.0 ± 5.2	80.5 ± 7.1	217 ± 24	1963 ± 85	2730 ± 1350	14.

Fermion ball - An alternative model suggested by Viollier [228] and De Paolis [64] conjectured that “dark” compact objects could be *fermion balls* [80]. These are objects in which, thanks to the Pauli exclusion principle, the degeneracy pressure of the fermions is balanced by the self-gravity of the system. The maximum mass of such an object is given by the Oppenheimer-Volkoff limit M_{OV} ; given the fermion mass, all objects heavier than the corresponding M_{OV} must then be black holes [228]. A fermion ball would help to describe the low luminosity of Sgr A*, but several drawbacks can be highlighted. First, describing different SMBHs requires different typologies of the constituent fermions according to their mass. For example, M87 [231], with a mass of $\sim 6.3 \times 10^9 M_\odot$ implies a fermion mass around $17 \text{ keV}/c^2$. A fermion ball with such a mass would have a radius of ~ 10 light days, or at the distance of Sgr A*, about 8.3 mpc. In this case, some parts of the S2 orbit would be located inside the ball. Heavier objects would require even smaller fermion masses. Observational characteristics of S2 constrain instead the fermion mass to be $> 400 \text{ keV}/c^2$ [228, 17]. The impossibility of having a universal model of a fermion ball capable of describing all SMBHs is the first sign that we should exclude this hypothesis. Secondly, X-ray and NIR flares observations [171, 174, 12, 76, 192, 79, 109, 77, 101, 6, 7] indicate that emission comes from regions much smaller than the Schwarzschild radius of a fermion ball corresponding to a given mass. Ultimately, this scenario carries with it

the inevitable convergence to a black hole at some point. In fact, it does not explain what happens to the continuously in-falling matter, which accumulating in the potential well, will collapse into a black hole.

Boson star - Another model capable to explain massive compact objects is the *boson star*, proposed by Torres [225]. By their nature, such agglomerations of bosons are supported by the Heisenberg Uncertainty Principle. Depending on the mass of the constituent bosons and the particular self-interaction potential assumed, a large variety of masses of compact objects can be generated. The mass of the constituent bosons also determines the size of the hypothetical compact object; generally, it will not be larger than some Schwarzschild radius. This is the first reason that makes it difficult to distinguish between boson stars and black holes observationally [226, 166, 165]. But similar to what happens for fermion stars, it is unlikely that at some point in their life these objects will not collapse into black holes as a result of the accretion of baryonic matter. One way to discriminate between boson stars and black holes would be offered by the discovery of pulsars around Sgr A*, which would allow us to measure the quadrupole moment of the central object. Furthermore, to obtain supermassive objects one should *ad hoc* introduce a weak repulsive force between bosons [52]. We can reasonably exclude the bosonic scenario.

In summary, noting the fragility of the aforementioned alternative configurations, **the hypothesis that Sgr A* is a black hole, for now, remains the most likely one.**

4.4 A laboratory to test General Relativity

The most interesting application at the GC for the current research is to probe GR through tests involving the entire electromagnetic spectrum. Since Eddington's solar eclipse observation in 1919 [235], GR has been robustly verified by many experiments. However, most of the tests were conducted in weak gravitational regimes, where there is no way that large deviations from GR can be detected. On the other hand, the need to understand what the definitive theory of gravity is and whether there may be deviations from Einstein's theory involves extending the tests to stronger gravitational regimes, where the predictions of the two theories may be dramatically different. But how can we define a strong gravitational regime?

For this purpose, it's worth remembering that space-time is completely described by three tensors: the metric describing the curvature of space-time at one point, the Ricci tensor describing how much of the curvature is due to the local mass and the Riemann curvature tensor describing the total contributes to the curvature (local mass and gravitational fields due to distant masses). Starting from these tensors, we can define two parameters that intuitively allow us to characterize the entity of the gravitational regime on the basis of dimensional arguments: ϵ and ξ [194]. The parameter ϵ measures

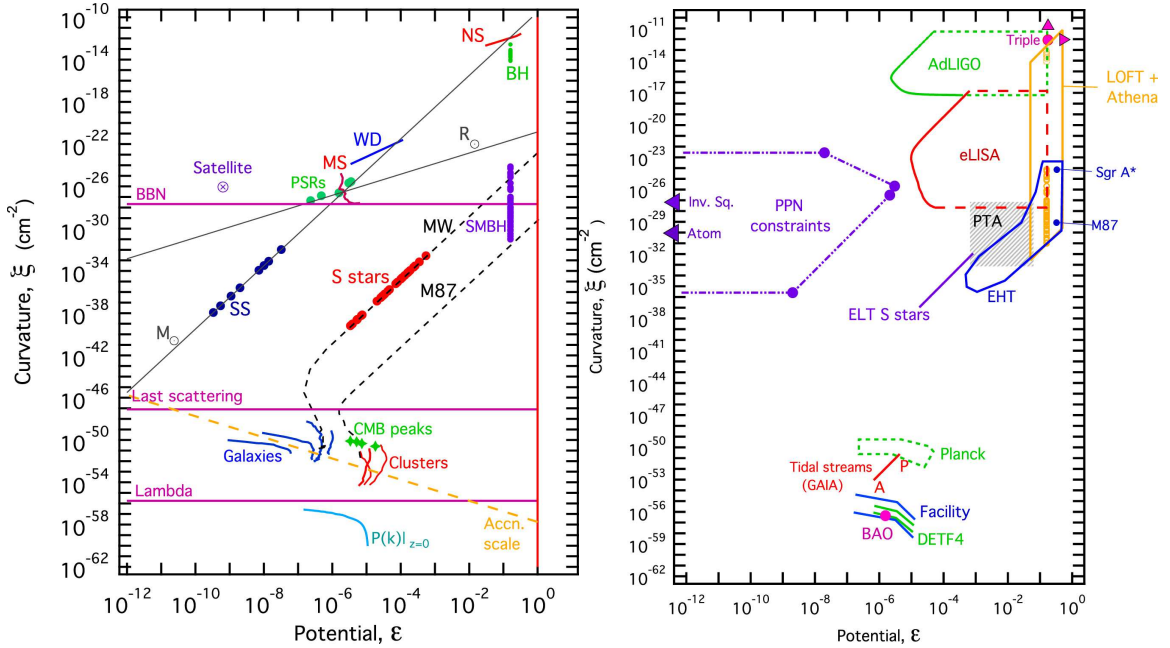


Figure 4.5: The parameter space for gravitational fields of a wide range of astrophysical and cosmological systems (left) and their experimental counterpart (right).

the strength of the gravitational field at a distance r from an object of mass M

$$\epsilon \equiv \frac{G_N M}{r c^2}. \quad (4.5)$$

In particular, infinitesimal gravitational fields correspond to $\epsilon \rightarrow 0$ (Minkowski space-time), weak gravitational fields correspond to $\epsilon \ll 1$ (Newtonian gravity), and strong fields are found for $\epsilon \rightarrow 1$ (at $\epsilon \simeq 1$ the event horizon is approached). Instead, the parameter ξ approximately measures the space-time curvature through the Kretschmann $(R^{\alpha\beta\gamma\delta} R_{\alpha\beta\gamma\delta})^{1/2} = \sqrt{48} \frac{G_N M}{r^3 c^2}$ and is defined as

$$\xi \equiv \frac{G_N M}{r^3 c^2}. \quad (4.6)$$

These parameters span a two-dimensional surface where we can put the gravitational fields probed by different objects and experiments. Figure 4.5 shows the (ϵ, ξ) -space for a wide range of situations.

In this work, we considered the following astrophysical gravitational system: stars orbiting close Sgr A*. Sgr A* is the perfect tool to test GR for many reasons. First of all, the environment of Sgr A* is made extreme by its strong gravitational field, one of the strongest in the Universe as we can see in Fig. 4.5 [8, 195]. Second, NIR observations of stars orbiting Sgr A* allowed us to accurately measure the values of its mass and its distance from us, equal respectively to $\sim 4 \times 10^6 M_\odot$ and ~ 8 kpc

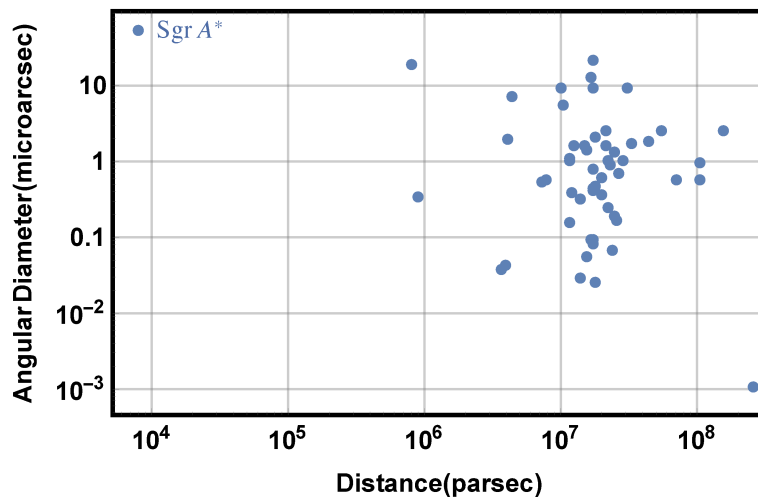


Figure 4.6: Angular diameters and distances for a sample of supermassive black holes. Data are taken from [119].

[106, 111, 112, 163]. Third, Sgr A* is the closest black hole and its shadow, having the largest opening angle in the sky, is resolvable with VLBI observations [132, 168]. In Fig. 4.6 we can see the angular diameter of a sample of supermassive black holes in the sky³.

There are three main kinds of ground-based experiments which are currently probing space-time around Sgr A*:

- NIR monitoring of stars close to Sgr A*;
- High-precision timing with pulsars;
- Very-Long Baseline Interferometric observations of the accretion flow with EHT.

Most of the stars and pulsars are at radii $r \gg R_S$ and the first two kind of observations probe Sgr A* in the weak field regime, while EHT probes space-time in the strong-field regime, i.e., at radii $r \sim R_S$.

4.4.1 Monitoring stellar orbits

Let us summarize how we can answer a wealth of fundamental questions by NIR observations of stars at the GC.

³For a Kerr black hole with mass M , the angular diameter θ_{ring} of the photon ring is given by the ratio of its diameter and distance

$$\theta_{ring} = \frac{L}{D}, \quad (4.7)$$

where $L \simeq 10.4 \frac{G_N M}{c^2}$. For Sgr A*, $\theta \simeq 52 \mu\text{as}$.

First of all, tracing individual orbits of stars around Sgr A* provides direct constraints on its main parameters (Sec. 4.3.2): the mass and the distance from us. Knowing the mass of the central object, M , is salient to place the Milky Way onto scaling relations [135]. Determining the distance to the GC, R , is equally important in astronomy since its value determines the size of the Milky Way. To date, many measurements of M and R are available, made more and more precise by the use of GRAVITY which has an astrometric accuracy of $\sim 10 \mu\text{as}$. The above measurements outline for Sgr A* a mass of $\sim 4 \times 10^6 M_\odot$ and a distance from us of $\sim 8 \text{ kpc}$.

Astrometric and spectroscopic observations of these stars allow the detection of distinct relativistic effects caused by the corrections to the Newtonian potential of Sgr A*. The Schwarzschild-type corrections lead to precession in the orbital plane of the star given by Eq. (2.171). Orbits having angular momenta not parallel to the black hole spin S exhibit a precession of the orbital angular momentum around S due to frame dragging (Lense-Thirring precession of the nodes). The ascending node, Υ , shows an advancement per orbit given by $\Delta\Upsilon = \Omega_{\text{LT}}P$, where $P = 2\pi\sqrt{a^3/G_N M}$ is the Newtonian period and

$$\Omega_{\text{LT}} \equiv \frac{8\pi^2}{(1-e^2)^{3/2}} \frac{G_N M}{c^3 P^2} \chi \quad (4.8)$$

is the Lense-Thirring frequency. Such effects are more evident in stars moving on very eccentric orbits and for large spin values [196]. So, observing stellar orbits may also provide a measure of the spin and the quadrupole moment of Sgr A*, allowing an elegant test of the no-hair theorem through the Eq. (2.96). In Ref. [196] it is estimated the precision with which the spin and the quadrupole moment of Sgr A* can be measured with GRAVITY observations.

Relativistic effects on the orbits of S -stars may also be reflected by gravitational lensing events. Such events depend mainly on the mass and distance of Sgr A* but could be also influenced by its spin and quadrupole moments thus giving the possibility to reveal deviations from GR [24, 25, 26, 65, 229].

4.4.2 Pulsars timing

Another tool to test GR is constituted by radio pulsars. These objects are characterized by the emission of steady beams of electromagnetic radiation, the periods of which are regular and can be measured precisely. In the case the pulsar is in a binary system (two pulsars or a pulsar and a companion), timing observations can be used to infer parameters of the system such as the mass of both objects. Discovering a pulsar sufficiently close to Sgr A* would allow us to deduce its mass, spin, and quadrupole moment, and thus would represent another way to test the no-hair theorem.

Binary systems are usually modeled by a set of Keplerian parameters such as the eccentricity e , the orbital period P_b , the semi-major axis, and a set of post-Keplerian

parameters [59, 189]. Let us describe the last ones considering a system where m_1 and m_2 are respectively the masses of a pulsar and Sgr A* and assuming GR. The mean rate of pericenter advance, $\langle \dot{\omega} \rangle$, can be used to determine the total mass of the system:

$$\langle \dot{\omega} \rangle = \frac{2\pi}{P_b} \left(\frac{2\pi G_N m}{c^3 P_b} \right)^{2/3} (1 - e^2)^{-1}, \quad (4.9)$$

where $m = m_1 + m_2$. The Einstein delay of the emitted radio pulse, γ_E , is a combination of the relativistic Doppler effect and the gravitational redshift:

$$\gamma_E = e \left(\frac{2\pi}{P_b} \right)^{-1} \left(\frac{2\pi G_N m}{c^3 P_b} \right)^{2/3} \frac{m_2}{m} \left(1 + \frac{m_2}{m} \right). \quad (4.10)$$

The orbital period derivative \dot{P}_b is

$$\dot{P}_b = -\frac{192\pi}{5} \left(\frac{2\pi \mathcal{M}}{P_b} \right)^{5/3} \left(1 + \frac{73}{24}e^2 + \frac{37}{96}e^4 \right) (1 - e^2)^{-7/2}, \quad (4.11)$$

where

$$\mathcal{M} \equiv \frac{G_N M_\odot}{c^3} \frac{(m_1 m_2)^{3/5}}{(m_1 + m_2)^{1/5}}. \quad (4.12)$$

Finally, the Shapiro delay experienced by the radio pulse represents the extra traveling time due to the curvature of space-time; it is

$$\Delta s \simeq \frac{2 G_N M_{\text{BH}}}{c^3} \ln \left(\frac{1 + e \cos \varphi}{1 - \sin i \sin(\omega + \varphi)} \right), \quad (4.13)$$

where $M_{\text{BH}} \equiv m_2 \gg m_1$, and ω and φ are the angular distance of the pericenter in the orbital plane and the orbital phase of the pulsar, and i is the inclination of the orbital plane with respect to the line of sight.

Instead, to deduce the spin of Sgr A*, we must consider the precession of the orbital plane. Precession rates of the angles Φ and Ψ (Φ is the equatorial longitude of the ascending node, and Ψ is the equatorial longitude of pericenter) can be written as

$$\dot{\Phi} = \Omega_{\text{LT}} \quad (4.14)$$

$$\dot{\Psi} = -3 \Omega_{\text{LT}} \cos \theta. \quad (4.15)$$

Then, we can expand in Taylor series ω and the projected semi-major axis x ,

$$\omega = \omega_0 + \dot{\omega}_0(t - t_0) + \frac{1}{2}\ddot{\omega}_0(t - t_0)^2 + \dots \quad (4.16)$$

$$x = x_0 + \dot{x}_0(t - t_0) + \frac{1}{2}\ddot{x}_0(t - t_0)^2 + \dots \quad (4.17)$$

where the coefficients (and so the spin magnitude and orientation) are inferred from a fit of the timing data. In Ref. [149, 196] the precision with which a test of the no-hair theorem can be performed is reported.

In addition to test GR through the no-hair theorem, we can test alternative theories by generalizing the Post-Keplerian (PK) parameters appropriately [59]. In this case, the two masses are not the only free parameters. For example, in $f(R)$ -gravity the parameters δ and λ , introduced previously, also come into play. These additional parameters turn out to be degenerate with masses. So, the only way to infer values of the masses is to calculate more PK parameters and break the degeneracy. In $f(R)$ -gravity, the periastron advance for a binary system can be generalized in the following manner as shown by De Laurentis in [59]

$$\begin{aligned} \dot{\omega} = \frac{\dot{\omega}_{\text{GR}}}{\delta + 1} & \left[1 + \frac{2\delta}{(1-e^2)^2} \left(\frac{2\pi}{P_b} \right)^{4/3} \frac{G_{\text{N}}^{4/3}}{c^4} (m_1 + m_2)^{4/3} \right. \\ & - \frac{2\delta}{(1-e^2)\lambda} \left(\frac{2\pi}{P_b} \right)^{2/3} \frac{G_{\text{N}}^{5/3}}{c^4} (m_1 + m_2)^{2/3} \\ & \left. - \frac{2\delta}{(1-e^2)} \left(\frac{2\pi}{P_b} \right)^{2/3} \frac{G_{\text{N}}^{2/3}}{c^2} (m_1 + m_2)^{2/3} - \frac{\delta}{2\lambda^2} \frac{G_{\text{N}}^2}{c^4} (m_1 + m_2)^2 + \frac{\delta}{\lambda} \frac{G_{\text{N}}}{c^2} (m_1 + m_2) \right] \end{aligned} \quad (4.18)$$

where

$$\dot{\omega}_{\text{GR}} = \left(\frac{2\pi}{P_b} \right)^{5/3} \frac{G_{\text{N}}^{2/3}}{c^2} \frac{(m_1 + m_2)^{2/3}}{(1-e^2)}. \quad (4.19)$$

Definitely, we could test $f(R)$ -gravity via the previous equation and by means of observations from the Parkes Pulsar Timing Array (PPTA) and from the next-generation instruments such as the Square-Kilometre-Array (SKA) [139, 54, 219].

4.4.3 EHT observations

We expect to have undeniable evidence that Sgr A* is a supermassive black hole by means of upcoming sub-millimeter VLBI images from EHT Collaboration [70]. The EHT [92, 86] is a global collaboration based on the technique of linking radio dishes across the Earth to create an Earth-sized interferometer (See Fig. 4.7).

The way in which we expect to determine if Sgr A* is a Kerr black hole or an alternative theory black hole is by means of its *shadow*.

To understand what is the shadow, consider a source of light behind a rotating black hole, or more concretely photons emitted from the accreting disk and those propagating close to the black hole: a distant observer will see the apparent image of the black hole in the form of a dark spot [94]. The contour of this shadow corresponds to photons revolving the black hole many times before they reach the distant observer (see Fig. 4.8).

The shadow of a black hole is circular for a Schwarzschild space-time, while its shape depends on the mass, spin, and inclination for a Kerr metric. However, shadows

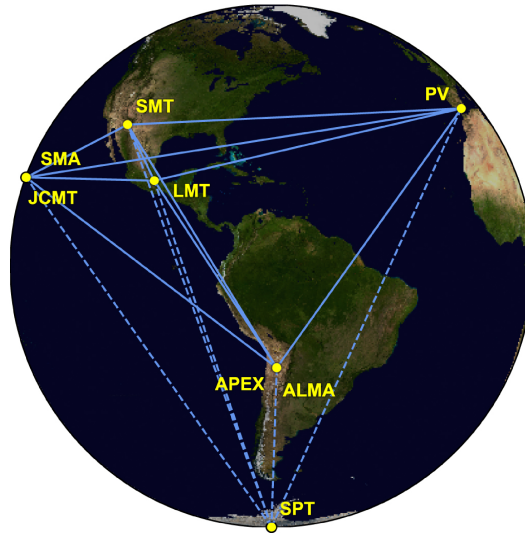


Figure 4.7: Eight stations of the EHT 2017 campaign over six geographic locations as viewed from the equatorial plane (see Papers [86, 87, 88]).

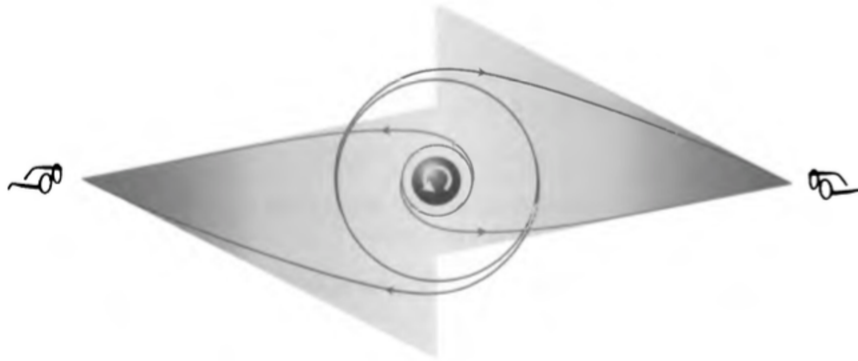


Figure 4.8: The rim of the shadow corresponds to photons coming from infinity and reaching the observer after rotating many times around the black hole.

geometry can change dramatically if the no-hair theorem is violated. Alternative theories of gravity predict a slightly different shadow geometry. That is why establishing the shape of the shadow would be an observational test of the underlying gravity in the strong gravitational regime. EHT collaboration presented in 2019 the first event-horizon scale images of *M87* [86] from the campaign conducted in 2017 (see Figure 4.9).

4.5 Concluding remarks

In this chapter, we summarized the recent progress on the innermost parsec of the Milky Way, focusing on the evidence that helped to consolidate the black hole paradigm. A black hole is a philosophically interesting object since its existence can only be proved by indirect observations. The issue of whether we face a situation of underdetermi-

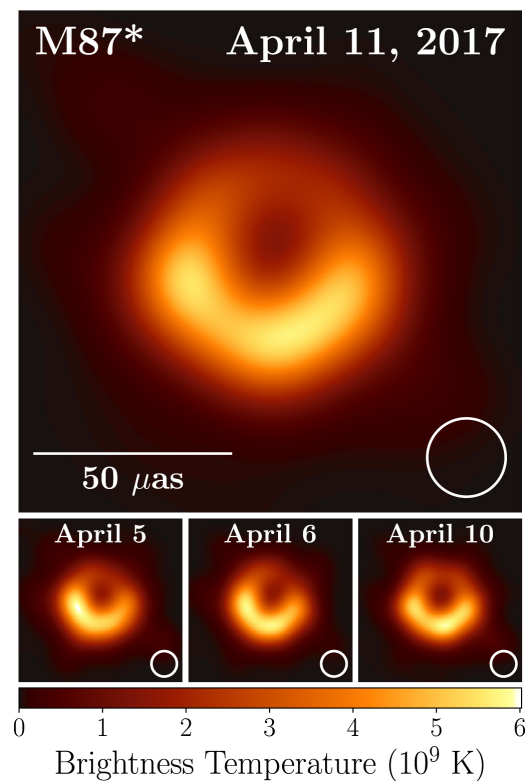


Figure 4.9: Shadow of the supermassive black hole at the center of *M87* galaxy [86].

nation in the search for SMBHs led many scientists to propose alternative theories describing massive compact objects in terms of “exotic” matter. However, such delicate alternative configurations can be excluded with a certain degree of confidence, on the basis of observations and theoretical reasonings. In the current research, GC is therefore configured as a superb laboratory where scientists can probe the gravitational field in a little-explored regime and answer fundamental questions such as *do black holes exist? What is the theory of gravity underlying nature?* In the following chapter, we will present a method to test theoretical results reported in the first part through the study of stellar orbits at the GC.

TEST I: STELLAR ORBITS AT THE GALACTIC CENTER

I vari sforzi [compiuti] dai tempi di Euclide, per il corso di duemila anni, mi spinsero a sospettare nei concetti stessi [della geometria] non si racchiuda ancora quella verità che si voleva dimostrare, e che può essere controllata, in modo simile alle altre leggi fisiche, soltanto da esperienze, quali, ad esempio, le osservazioni astronomiche.

– N. I. Lobačevskij

5.1	Data	88
5.1.1	The chosen stars	88
5.1.2	Description of the dataset	89
5.2	Simulation of the orbits	90
5.2.1	Formulation of the motion problem	90
5.2.2	Numerical integration	91
5.3	Fitting Procedure	94
5.4	Results	97
5.4.1	Test I.a: $f(R)$ -gravity	97
5.4.2	Test I.b: Bootstrapped Newtonian gravity	103
5.5	Concluding remarks	104

In this chapter, which is based on the articles [55, 56], we will use S -stars orbits to search departures from GR at the inner parsec of our Galaxy. Their proximity to Sgr A* and their high speed that reaches thousands of km/s, make the S -stars perfect objects to probe the gravitational potential in which they move. Their peculiar dynamics helped astronomers to establish the nature of the central object: a supermassive black

hole of $\simeq 4 \times 10^6 M_\odot$. However, their most profound application in the present research is the possibility to test the underlying theory of gravity. Indeed, *S*-stars probe gravity regimes of up to $\epsilon \sim 10^{-4}$, that are two orders of magnitude stronger than the Solar System regime ($\epsilon \sim 10^{-6}$) where GR has turned out to be successful.

Our approach to test theories of gravity consists of three fundamental steps: simulation of the orbits in a given theory through a fully relativistic procedure (Sec. 5.2.2), comparison between mock orbits and the data (Sec. 5.1), determination of allowed regions for the parameters characterizing the theory in question (Sec. 5.3).

5.1 Data

The data used in this work are taken from Ref. [110], where the result of 25 years of monitoring stellar orbits around Sgr A* is presented. The authors measured the accelerations of 47 stars, and they determined the orbit for 40 of them. We focused our calculations on three of these stars: *S2*, *S38* and *S55*.

5.1.1 The chosen stars

Our choice falls on the stars *S2*, *S38*, and *S55* for two main reasons: their short periods, less than twenty years, and their high brightness. Stars with short periods are desirable for two reasons: first of all, they allow us to sample a larger portion of the orbit during an observational period, and then they simplify the detection of relativistic effects, most of which are cumulative and grow with increasing phase coverage. On the other hand, we look for highly bright sources since they are less prone to be confused with other members of the cluster.

- *S2*: The star *S2*, also known as *S0–2*, has a period of 16 years and is the brightest member of the cluster, having a near-infrared K_s -band magnitude equal to $m_K = 14.2$. Observing *S2*'s motion helped to strengthen the evidence for the existence of a compact object at the center of the Milky Way of about 4 million solar masses [98]. *S2* reached the closest approach to Sgr A* in 2018 with a velocity of 7650 km/s. During this event, the relativistic effects predicted by Einstein, as the combined transverse Doppler and gravitational redshift, were more evident and for the first time have been measured by the GRAVITY collaboration with an unseen accuracy [115]. Moreover, they robustly detected an orbital precession of $\simeq 12'$ /orbit, in agreement with General Relativity [117]. The NTT and VLT set of *S2*'s observations contains 145 astrometric observations, ranging from 1992.224 to 2016.53.
- *S38*: The star *S38*, or *S0–38*, has a period of 19.2 years and a K_s -band magnitude of $m_K = 17$. Since its orbit is located in a much less crowded zone, the west of Sgr

A*, it is more distinguishable. We have a set of 114 observations, from 2004.24 to 2016.287.

- S55: The star *S55*, or *S0 – 102*, has a period of 12.80 years, the shortest known so far, and a K_s -magnitude of $m_k = 17.5$. The dataset covered the period from 2004.511 to 2013.617 with 44 astrometric observations.

5.1.2 Description of the dataset

In this section, we briefly describe the dataset presented in Ref. [110]. The measurements were performed in the near-infrared (NIR) since interstellar extinction reduces from ~ 30 magnitudes of the optical to ~ 3 magnitudes. They were obtained with different instruments, undergoing an improvement in accuracy as the observational techniques advanced. Specifically:

- SHARP - The SHARP camera, built by Max-Planck-Institut scientists, was used between 1992 and 2002 at the ESO's 3.5 m NTT in Chile [75]. The first high-resolution data of the inner parsec of the Galaxy were taken in speckle mode with exposures time of 0.3 s, 0.5 s, and 1.0 s, and revealed high proper motion around the central compact object. The data are described in detail in Ref. [210].
- NACO - The Naos-Conica (NACO) system, mounted at the telescope Yepun (8.0 m) of the VLT [146, 201], introduced us the technique of adaptive optics (AO) imaging in 2002. The quality of the data increased due to the larger telescope aperture and the higher Strehl ratios ($\sim 40\%$).
- GEMINI - These observations were produced in 2000 by the 8 m telescope Gemini North (Mauna Kea, Hawaii) using AO system in combination with the NIR camera Quirc. The Gemini team made publicly available these data after processing.

The detailed astrometric calibration description of the above data is fully explained in Ref. [113]. We could summarize it in these steps: extracting pixel positions from maps of the *S*-stars and transforming them to a common astrometric coordinate system. In particular, the astrometric reference frame is implemented relating the *S*-stars positions to a set of selected reference stars, which are in turn related to a set of SiO maser stars with known positions from Sgr A*.

For a complete implementation of such a reference frame, the drift of the central mass cannot be neglected. This motion could be added up to the coordinates of the fitting ellipse or removed from the data points. We used the precise determination of position and proper motion of Sgr A* by Plewa et al. [191], who concluded that the

average motion in units of mas is:

$$\Delta x(t) \sim (-0.16 \pm 0.17) + (-0.04 \pm 0.08)(t - 2009.02), \quad (5.1)$$

$$\Delta y(t) \sim (+0.08 \pm 0.17) + (-0.01 \pm 0.07)(t - 2009.02). \quad (5.2)$$

5.2 Simulation of the orbits

In general, the analytical resolution of the field equations is complicated by their non-linearity, and becomes possible only for systems that are assumed to have particular symmetries. To tackle the problem of motion in the most general case, that is, in the case of a generic metric representing a nonstandard space-time, it is necessary to solve the equations of geodesics directly with numerical methods. In this section, we will explain how to construct mock stellar orbits starting from the symbolic expression of an extended metric (Sec. 5.2.1) and integrating the corresponding geodesics by means of the Runge-Kutta method (Sec. 5.2.2). The whole code was implemented in Mathematica.

5.2.1 Formulation of the motion problem

The first part of the code to produce mock orbits is symbolic. Given a generic metric $g_{\mu\nu}(\vec{p})$, the starting point is to make explicit the corresponding Lagrangian $\mathcal{L}(\vec{p}) = g_{\alpha\beta}(\vec{p}) \dot{x}^\alpha \dot{x}^\beta$. Here, $\{\vec{p}\}$ denotes the overall set of parameters characterizing the theory. In particular, we examined two Extended Theories of Gravity: the $f(R)$ -gravity and the Bootstrapped Newtonian gravity. The corresponding parameters are, respectively, $\{\vec{p}\} = \{\delta, \lambda\}$ and $\{\vec{p}\} = \{\Xi\}$.

Given $\mathcal{L}(\vec{p})$, the corresponding geodesic equations can be straightforwardly computed using the Euler-Lagrange equations (Eq. (3.73)). The resulting four equations (system (3.74)-(3.77) for the $f(R)$ -gravity, and (3.146)-(3.149) for the Bootstrapped Newtonian gravity) constitute a second-order nonlinear differential system for the four-dimensional coordinates $\{r, \theta, \phi, t\}$, with the proper time τ as an independent parameter. To be well-posed, this Cauchy system must be equipped with initial conditions for the unknown functions and their derivatives with respect to the proper time: $\{r(0), \dot{r}(0), \theta(0), \dot{\theta}(0), \phi(0), \dot{\phi}(0), t(0), \dot{t}(0)\}$. Spherical symmetry implies that the orbit lies on a fixed plane, hence we assume that initially, the star is in the equatorial plane, $\theta(0) = 0$, and its velocity is parallel to such a plane, $\dot{\theta}(0) = 0$. It follows that the condition $\ddot{\theta} = 0$ is satisfied identically. Values for r and ϕ at a given time are retrieved from the expressions of the Cartesian coordinates in the orbital plane $(x_{\text{orb}}, y_{\text{orb}})$ (see Fig. 5.1)

$$(x_{\text{orb}}, y_{\text{orb}}) = \left(a (\cos \Phi - e), a \sqrt{1 - e^2} \sin \Phi \right), \quad (5.3)$$

where a is the semi-major axis, e is the eccentricity and Φ is the eccentric anomaly. The Cartesian components of the velocity in the same plane are

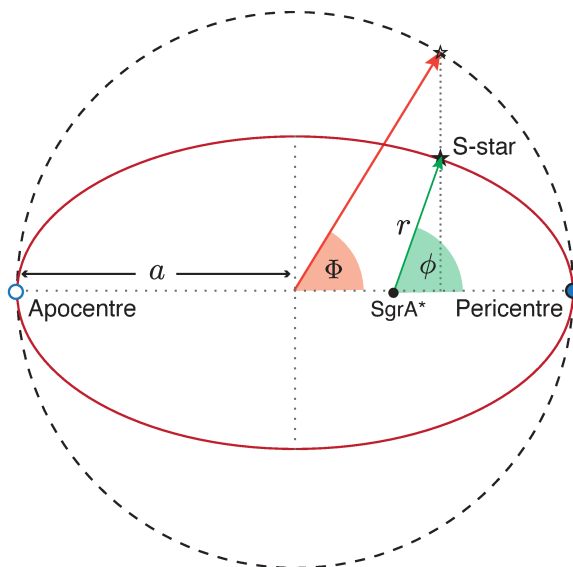


Figure 5.1: Illustration of the true anomaly ϕ and the eccentric anomaly Φ on the equatorial plane of Sgr A*.

$$(v_{x,\text{orb}}, v_{y,\text{orb}}) = \left(-K \sin \Phi, K \sqrt{1 - e^2} \cos \Phi \right), \quad (5.4)$$

where $K \equiv \frac{2\pi a^2}{T r}$. In particular, we assume the initial time coinciding with the time of passage at apocentre $t_a = t_p - T/2$, where t_p is the time of the pericentre passage and T is the orbital period. Here, $\dot{r} = 0$ and $\phi = \Phi = \pi$, so that initial conditions simplify as

$$(x_{\text{orb}}, y_{\text{orb}}) = (-a(1 + e), 0), \quad (5.5)$$

$$(v_{x,\text{orb}}, v_{y,\text{orb}}) = \left(0, K \sqrt{1 - e^2} \right). \quad (5.6)$$

Finally, the initial condition for \dot{t} is deduced from the normalization of the quadrivelocities in the case of time-like geodesics:

$$u^2 = g_{\alpha\beta} u^\alpha u^\beta = -c^2. \quad (5.7)$$

We set the values of the Keplerian parameters and the central mass parameters to those reported in Tables 5.1 and 5.2.

In particular, we used the values deduced by the Gravity Collaboration [117] to study *S2*, and those obtained by Gillessen et al. [110] to analyze *S38* and *S55*.

5.2.2 Numerical integration

Now that the values of the physical constants are fixed, and the Cauchy problem is well-posed, we can numerically integrate the geodesics equations.

Parameter	S2	S38	S55
a (mas)	125.058 ± 0.041	141.6 ± 0.2	107.8 ± 1.0
Ω ($^\circ$)	228.171 ± 0.031	101.06 ± 0.24	325.5 ± 4.0
e	0.884649 ± 0.000066	0.8201 ± 0.0007	0.7209 ± 0.0077
i ($^\circ$)	134.567 ± 0.033	171.1 ± 2.1	150.1 ± 2.2
ω ($^\circ$)	66.263 ± 0.031	17.99 ± 0.25	331.5 ± 3.9
t_p (yr)	2018.37900 ± 0.00016	2003.19 ± 0.01	2009.34 ± 0.04
T (yr)	16.0455 ± 0.0013	19.2 ± 0.02	12.80 ± 0.11
m_K	13.95	17.	17.5
Ref.	[117]	[110]	[110]

Table 5.1: Orbital parameters of $S2$, $S38$, and $S55$.

Star	$M(M_\odot)$	$R(kpc)$	Ref.
S2	$(4.261 \pm 0.012) \times 10^6$	8.2467 ± 0.0093	GRAVITY [117]
S38	$(4.35 \pm 0.13) \times 10^6$	8.33 ± 0.12	Gillessen [110]
S55	$(4.35 \pm 0.13) \times 10^6$	8.33 ± 0.12	Gillessen [110]

Table 5.2: Parameters of the central BH.

In order to constrain a given set of parameters through observations, we have introduced a Do loop that makes them vary over a range of values $[p_{i,\min}, p_{i,\max}]$ with an appropriate step Δp_i , where $p_i = \{\delta, \lambda, \Xi\}$. In particular, for the $f(R)$ -gravity we defined a double cycle for δ and λ : δ in the range $[-0.9, 2]$ with an increment of $\Delta\delta = 0.05$ and λ in the range $[1000 \text{ AU}, 60000 \text{ AU}]$ with a step of $\Delta\lambda = 100 \text{ AU}$. The choice of $\delta > -1$ ensures that we are avoiding the singularity in the gravitational potential, while the range of variation for λ has a lower extreme comparable with the semi-major axis of the selected S -stars and extends for about an order of magnitude. Instead, to test the Bootstrapped Newtonian theory we let Ξ vary in the range $[-350000, 350000]$ with an increment $\Delta\Xi = 100$.

We have grafted a numerical differential equations solver in the Do loop, so as to find, for each value of the parameters space, a numerical solution for our differential system with independent variable τ from τ_{\min} to τ_{\max} . Specifically, we used NDSolve, the numerical solver in Mathematica. NDSolve is a very sophisticated tool; it allows users to choose among a lot of explicit Runge-Kutta methods (see **Box 2**), the most efficient class of methods for many nonstiff systems. Moreover, it's able to do automatic stiffness detection by default. Another nice characteristic is that it includes interpolation for all kinds of solutions to make them continuous.

Box 2: Runge-Kutta methods

To understand the idea on which the Runge-Kutta method is based ^a, consider the set of N first-order coupled differential equations having the general form

$$\frac{dy_i(x)}{dx} = f_i(x, y_1, \dots, y_N), \quad i = 1, \dots, N, \quad (5.8)$$

where the functions f_i are known and all y_i are specified at some initial value. The idea behind any routine that can solve such an initial value problem is to rewrite dy and dx in terms of finite quantities Δy and Δx , and multiply the equations by Δx to obtain algebraic formulas for the variation of the functions following the increment of the independent variable x by a quantity Δx . The literal implementation of this procedure results in Euler's method, the simplest and least accurate, based on the formula

$$y_{n+1} = y_n + h f(x_n, y_n), \quad (5.9)$$

which advances the solution from x_n to $x_{n+1} \equiv x_n + h$. Accuracy is given by the degree of matching of high terms with the Taylor expansion of the solution. In Euler's method, errors start at powers of h^2 (first-order accuracy). Moreover, this formula is not symmetric: it advances the solution through an interval h , but uses the information of the derivative only at the beginning of that interval. Hence the idea of considering this formula as an intermediate "test" step to obtain higher-order methods. In general, denote the Runge-Kutta method for the approximate solution to an initial value problem at $t_{n+1} = t_n + h$ by

$$g_i = y_n + h \sum_{j=1}^s a_{ij} k_j, \quad (5.10)$$

$$k_i = f(t_n + c_i h, g_i), \quad i = 1, 2, \dots, s, \quad (5.11)$$

$$y_{n+1} = y_n + h \sum_{i=1}^s b_i k_i \quad (5.12)$$

where s is the number of stages. It is assumed that the row-sum conditions are satisfied:

$$c_i = \sum_{j=1}^s a_{ij}, \quad i = 1, \dots, s. \quad (5.13)$$

Such conditions determine the points at which the function is sampled. Explicit Runge-Kutta methods include the special case where the matrix A is lower triangular.

^aWolfram Documentation

We, therefore, integrated the two differential equations systems with the Runge-Kutta method, starting from the above initial conditions. In particular, we performed

both backward and forward integration starting from the apocentre passage for $S2$, while for $S38$ and $S55$ forward integration was enough. Indeed, astrometric data for $S38$ and $S55$ have been collected after their last apocentre passage (which occurred on 1993.59 and 2002.94, respectively), while data for $S2$ span the period 1992.224 to 2016.53 including the apocentre time (2010.35).

To summarize, the schematic code constituting the heart of the numerical part is the following:

$$\text{Do} [\text{NDSolve}[\text{equations}, \{r, \theta, \phi, t\}, \{\tau, \tau_{\min}, \tau_{\max}\}], \{p_i, p_{i,\min}, p_{i,\max}, \Delta p_i\}]. \quad (5.14)$$

The numerical integration produces a four-dimensional parametric array $\{t(\tau), r(\tau), \theta(\tau), \phi(\tau)\}$ for each star and for each point in the grid of parameters, from which we calculate the vector $(x_{\text{orb}}(\tau), y_{\text{orb}}(\tau))$ representing the mock orbit on the orbital plane:

$$x_{\text{orb}}(\tau) = r(\tau) \sin \theta(\tau) \cos \phi(\tau), \quad (5.15)$$

$$y_{\text{orb}}(\tau) = r(\tau) \sin \theta(\tau) \sin \phi(\tau). \quad (5.16)$$

We illustrate in Fig. 5.2 the phase portrait of $\dot{r}(\tau)$ versus $r(\tau)$ for the GR solution.

Our aim of comparing theoretical orbits with the ones observed from the Earth requires the projection of mock coordinates in the orbital plane onto apparent coordinates in the observer's plane. Such a transformation from the true positions, $(x_{\text{orb}}(\tau), y_{\text{orb}}(\tau))$, into the apparent position, $(x^{\text{th}}(\tau), y^{\text{th}}(\tau))$, is performed by means of three Keplerian elements (see Fig. 5.3): the angle of the line of node Ω , the angle from ascending node to pericentre ω , and the inclination i . These parameters are reported in Table 5.1. From the theory of binary stars [2, 216], the following Thiele-Innes formulas are known

$$x^{\text{th}}(\tau) = l_1 x_{\text{orb}}(\tau) + l_2 y_{\text{orb}}(\tau), \quad (5.17)$$

$$y^{\text{th}}(\tau) = m_1 x_{\text{orb}}(\tau) + m_2 y_{\text{orb}}(\tau). \quad (5.18)$$

Expressions for the Thiele-Innes elements l_1 , l_2 , m_1 and m_2 are related to the Keplerian parameters by

$$l_1 = \cos \Omega \cos \omega - \sin \Omega \sin \omega \cos i, \quad (5.19)$$

$$m_1 = \sin \Omega \cos \omega + \cos \Omega \sin \omega \cos i, \quad (5.20)$$

$$l_2 = -\cos \Omega \sin \omega - \sin \Omega \cos \omega \cos i, \quad (5.21)$$

$$m_2 = -\sin \Omega \sin \omega + \cos \Omega \cos \omega \cos i. \quad (5.22)$$

5.3 Fitting Procedure

To summarize, for each point in the space of the parameters $\{\vec{p}\}$, we integrated numerically the geodesics equations (Eqns (3.74)-(3.77) for the $f(R)$ -gravity, and (3.146)-(3.149) for the Bootstrapped gravity) to find true positions $(x_{\text{orb}}(\tau), y_{\text{orb}}(\tau))$ of the stars

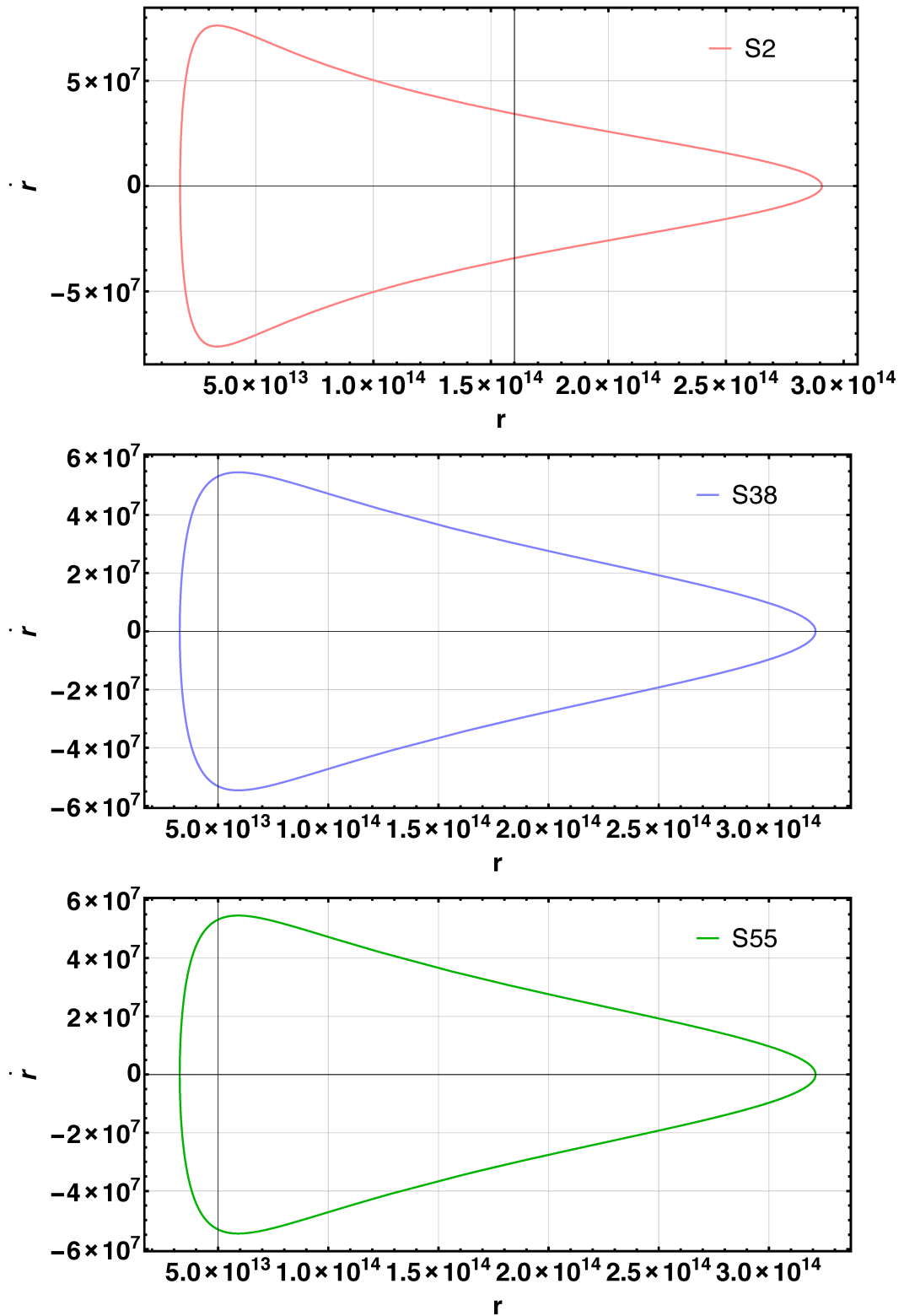


Figure 5.2: Phase space diagram of orbits in the Yukawa potential for $S2$, $S38$ and $S55$.

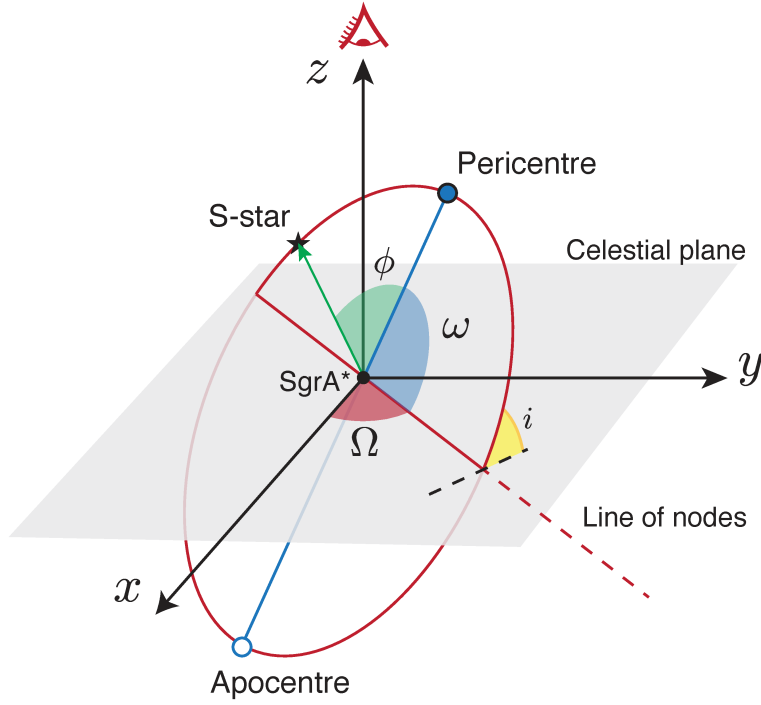


Figure 5.3: Illustration of the classical orbital parameters i , Ω , and ω . The z -axis corresponds to the line of sight for a distant observer.

(Sec. 5.2.2). True positions are translated into the apparent positions $(x^{\text{th}}(\tau), y^{\text{th}}(\tau))$ by means of Thiele-Innes formulas (5.17)-(5.18).

On the other hand, for each star, we have a dataset of N observations of the type

$$\{t_i, x_i^{\text{obs}}, \sigma_{x_i}^{\text{obs}}, y_i^{\text{obs}}, \sigma_{y_i}^{\text{obs}}\}, \quad i = 1, \dots, N, \quad (5.23)$$

where t_i are the observation epochs, $(x_i^{\text{obs}}, y_i^{\text{obs}})$ are the observed coordinates in mas and $(\sigma_{x_i}^{\text{obs}}, \sigma_{y_i}^{\text{obs}})$ are the corresponding uncertainties. So, to compare $(x^{\text{th}}(\tau), y^{\text{th}}(\tau))$ with observations we must calculate them in the observed epochs, that is, we must find

$$\tau \quad | \quad t = t_i, \quad i = 1, \dots, N \quad (5.24)$$

and get the array of theoretical positions $(x_i^{\text{th}}, y_i^{\text{th}})$.

We can finally compute the reduced χ^2 -distribution as

$$\chi_{\text{red}}^2 = \frac{1}{2N - D} \sum_i^N \left[\left(\frac{x_i^{\text{obs}} - x_i^{\text{th}}}{\sigma_{x_i}^{\text{obs}}} \right)^2 + \left(\frac{y_i^{\text{obs}} - y_i^{\text{th}}}{\sigma_{y_i}^{\text{obs}}} \right)^2 \right], \quad (5.25)$$

where D is the number of free parameters of the theory ($D = 2$ for the $f(R)$ -gravity and $D = 1$ for the Bootstrapped gravity). Then, we derive the likelihood probability distribution, $-2 \log \mathcal{L} = \chi_{\text{red}}^2(\vec{p})$. In the case of the $f(R)$ -gravity, for each parameter

p_i , we marginalized the likelihood distribution over the other parameter to obtain the one dimensional likelihood:

$$\mathcal{L}(p_i) = \frac{\int d^{N_j} p_j \mathcal{L}(p_i, p_j)}{\int d^{N_j} p_j}, \quad (5.26)$$

where $i = (\delta, \lambda)$, $i \neq j$ and N_j is the dimension of the j -th parameter's space. In the case of the Bootstrapped gravity, it is sufficient to calculate the one-dimensional likelihood function.

To calculate the best fit value for δ , we considered the point that maximizes the marginalized likelihood distribution. The confidence interval at 68%, $[\hat{\delta} - \sigma_-, \hat{\delta} + \sigma_+]$, is determined by the Neyman interval, which takes into account the asymmetry of the distribution [11]:

$$\int_{-0.9}^{\sigma_-} P(\delta') d\delta' = 0.16 = \int_{\sigma_+}^2 P(\delta') d\delta', \quad (5.27)$$

where $P(\delta')$ is the probability distribution obtained by normalizing the likelihood distribution, and $[-0.9, 2]$ are the extremes of the variation range for δ . We repeated the same procedure for Ξ . On the contrary, we can set only a lower limit on λ at 1σ level.

5.4 Results

In this section our results are reported.

5.4.1 Test I.a: $f(R)$ -gravity

The outcome of our analysis is summarized in Table 5.3 and illustrated from the Figures 5.4 to 5.9.

Figures 5.4, 5.5, and 5.6 depict mock orbits corresponding to the best fit parameters of the selected stars as listed in Table 5.3. We report the data with their own error bars to visually check the effectiveness of our procedure in fitting observations. More in detail, the first, the second, and the third plots are particularized respectively for $S2$, $S38$ and $S55$.

Figure 5.7 illustrates the comparisons between the observed and mock coordinates with the corresponding residuals. In the left column (right column) the results for the right ascension (RA) (declination (Dec)) are depicted. In both coordinates, and in all stars, residuals are larger at the beginning of the observing interval time, and decrease as astrometric accuracy improves.

Finally, to visually show the effectiveness of our multi-star approach, Figure 5.8 depicts the orbits of the analyzed S -stars corresponding to the best estimates of the parameters in the multi-star run, as reported in the fourth row of Table 5.3.

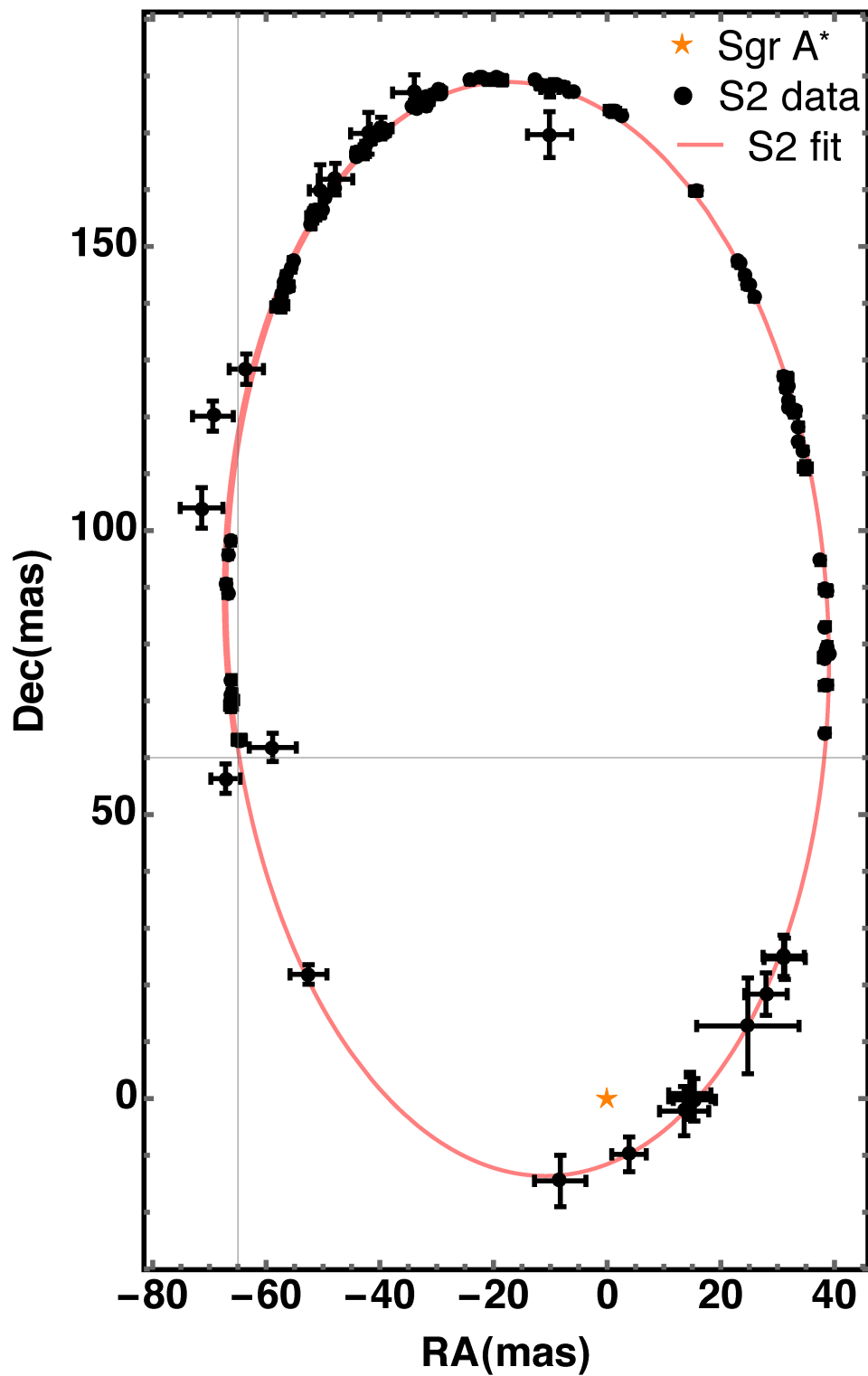


Figure 5.4: Comparison between the NTT/VLT astrometric observations (black circles) and the orbit of *S2* predicted in $f(R)$ -gravity using the best-fit parameter reported in Table 5.3.

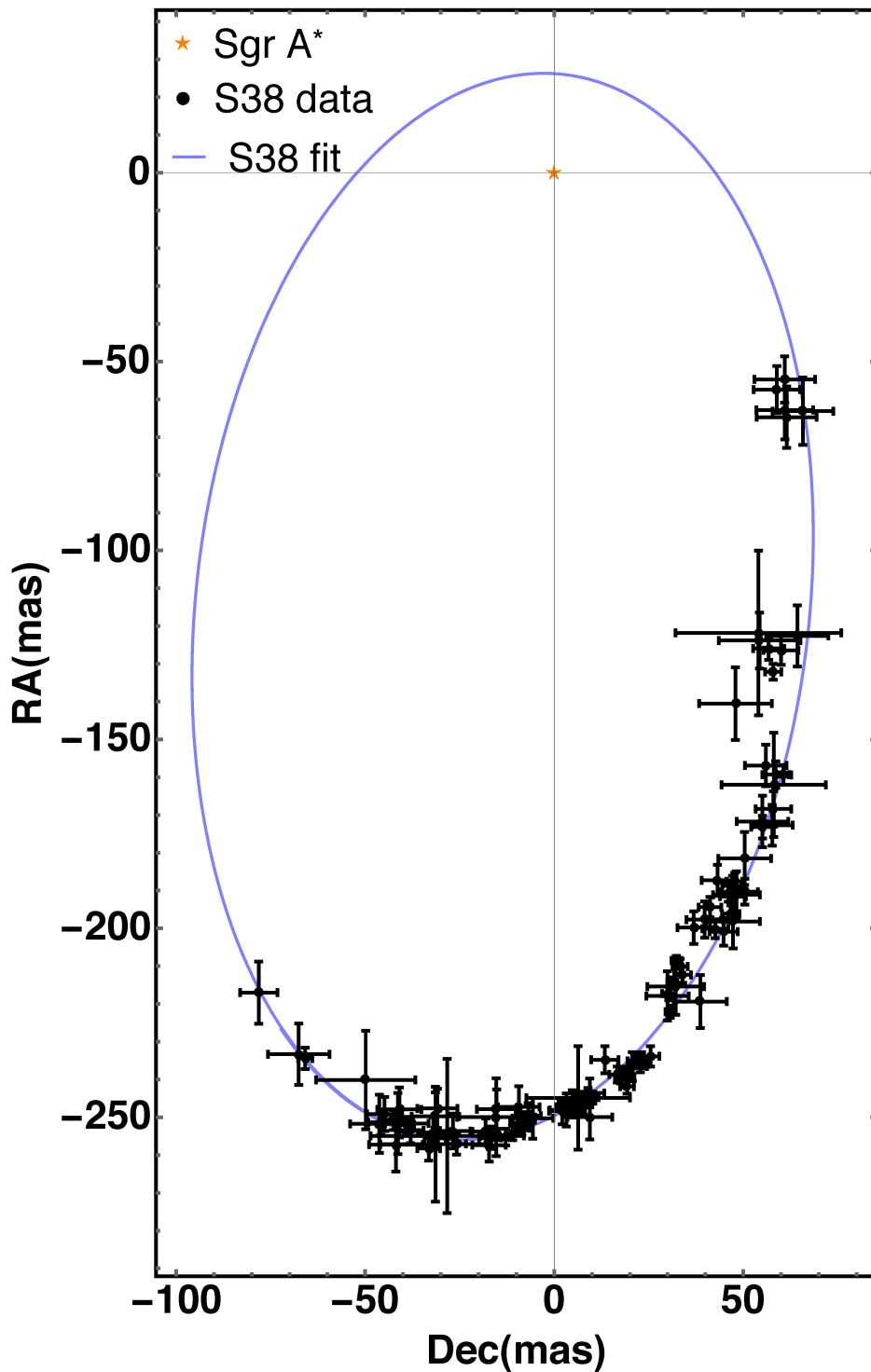
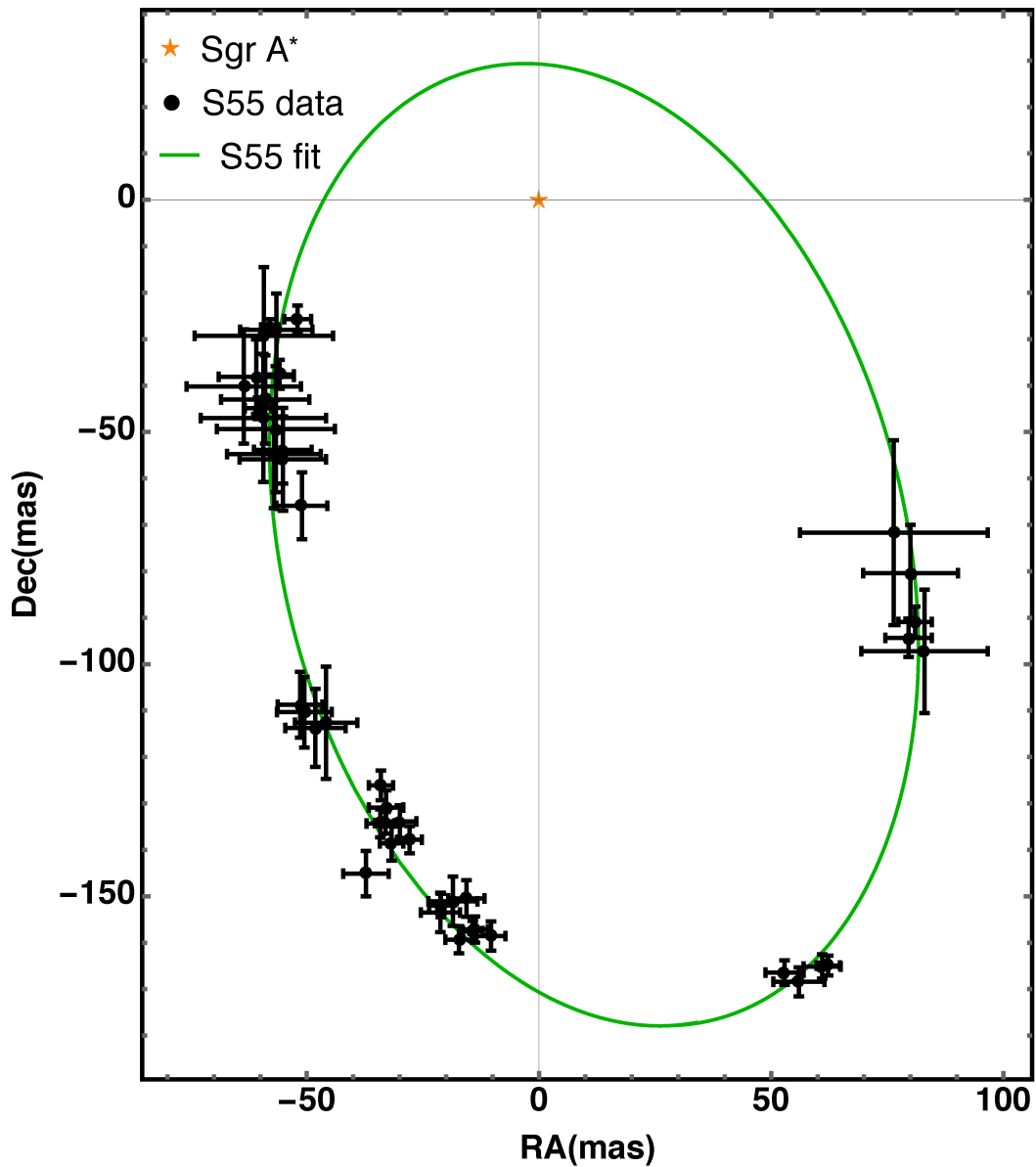


Figure 5.5: Comparison between the NTT/VLT astrometric observations (black circles) and the orbit of *S38* predicted in $f(R)$ -gravity using the best fit parameter reported in Table 5.3.

Star	δ	$\lambda(\text{AU})$
<i>S2</i>	$0.00^{+1.53}_{-0.36}$	≥ 7059.29
<i>S38</i>	$0.00^{+1.54}_{-0.34}$	≥ 5731.30
<i>S55</i>	$-0.10^{+1.62}_{-0.33}$	≥ 3511.95
Multi-Star	$0.00^{+1.69}_{-0.52}$	≥ 6336.23

Table 5.3: Best-fit values for δ and lower limit for λ .Figure 5.6: Comparison between the NTT/VLT astrometric observations (black circles) and the orbit of *S55* predicted in $f(R)$ -gravity using the best fit parameter reported in Table 5.3.

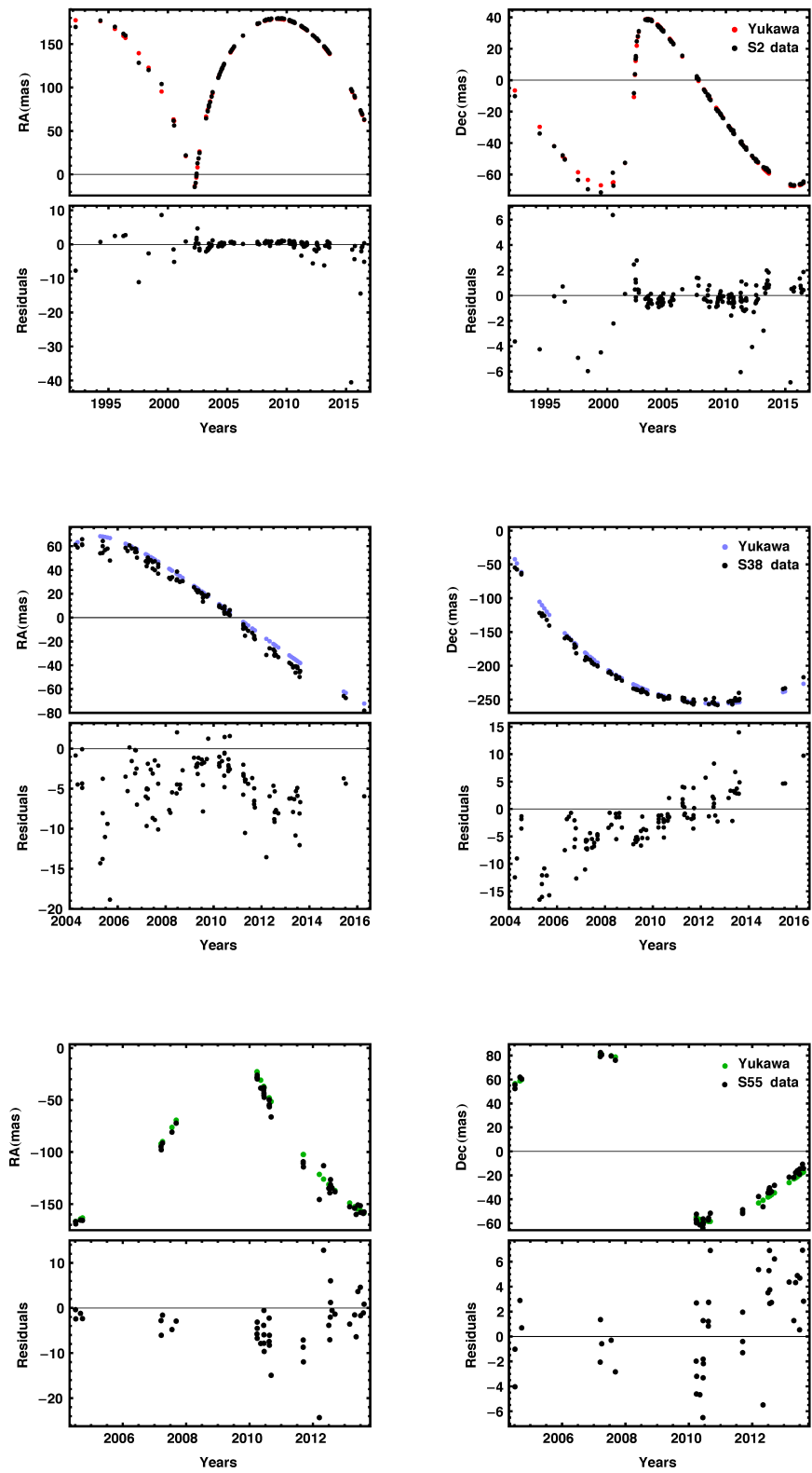


Figure 5.7: Comparison between observed and fitted coordinates (top), and the corresponding residuals (bottom) for $S2$, $S38$, and $S55$ for the $f(R)$ -gravity.

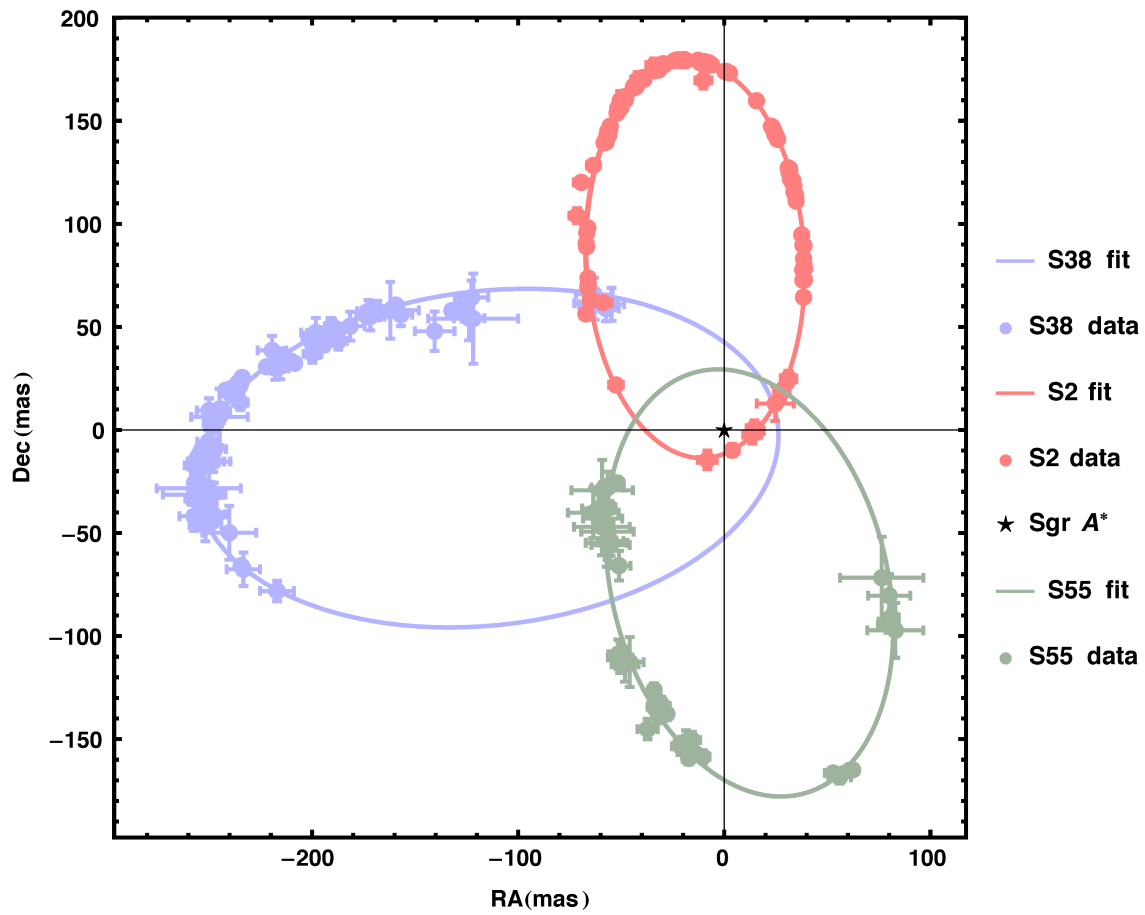


Figure 5.8: Best relativistic multi-star orbit fit of $S2$, $S38$, and $S55$ for the $f(R)$ -gravity.

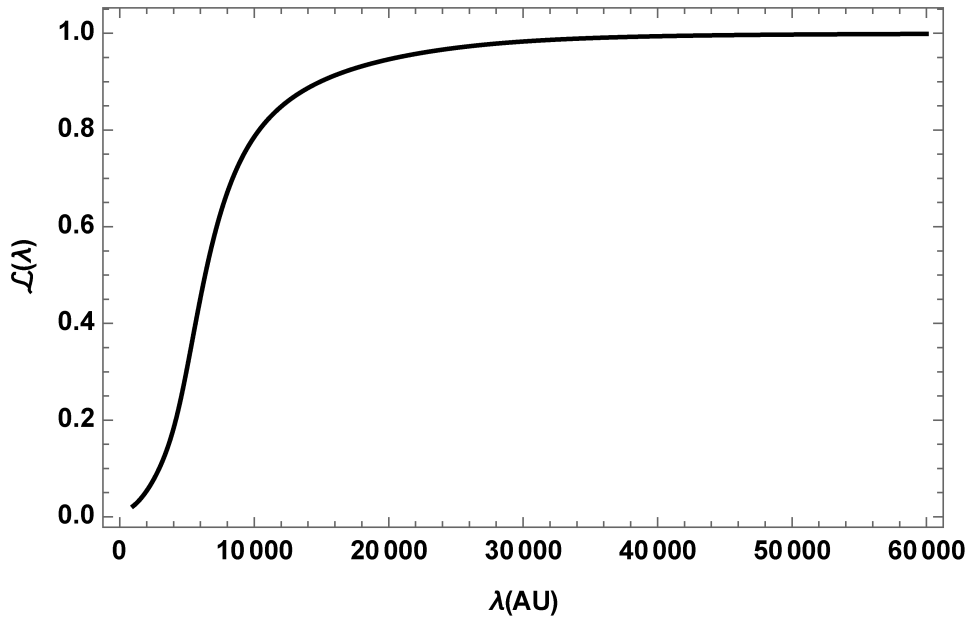


Figure 5.9: Marginalized likelihood function $\mathcal{L}(\lambda)$, from which we infer a lower bound on λ .

As expected, the strength parameter (δ) in the Yukawa-like potential is compatible with zero at 68% of confidence level not showing any departure from GR. Our analysis leads to $\delta = 0.00_{-0.52}^{+1.69}$ using all selected S -stars. Although our approach is based on the integration of geodesics, our results are similar to Hees et al. [126], who studied the motion of $S2$ and $S38$ integrating the Newtonian equation of motion with a Yukawa potential arising in the context of the fifth force.

Additionally, we can only set lower bounds on λ as reported in the third column of Table 5.3, due to the degeneracy with δ . Using the three S -stars, we exclude the regions $\lambda < 6336.23$ AU, as we can see from the marginalized likelihood function depicted in Fig. 5.9. Our constraint on the Yukawa length scale, λ , agrees with the results obtained by Borka et al. [22], who integrated Newton’s law instead of geodesics and fixed one of the free parameters to some fiducial value, and with Hees et. al. [126], who found a 90% confidence limit of $\lambda > 5000$ AU.

Finally, we found that allowed values of λ are larger than the typical size of the stellar orbits at the GC (semi-major axis of the selected S -stars are of about 1000 AU) as also predicted for other modified theories of gravity [130, 169].

5.4.2 Test I.b: Bootstrapped Newtonian gravity

Our results are summarized in Table 5.4, and represented from Figure 5.10 to 5.15.

Figures 5.10, 5.11, and 5.12 depict the comparison between best fit and observed

Star	Ξ
<i>S2</i>	$-5900^{+39358.8}_{-44964.9}$
<i>S38</i>	$25500^{+22607.1}_{-23312.88}$
<i>S55</i>	$60400^{+81386}_{-87446.9}$
Multi-Star	$17400^{+30555.6}_{-32244.3}$

Table 5.4: Best-fit values for Ξ .

orbits respectively of *S2*, *S38*, and *S55*.

Figure 5.13 depicts the comparisons between the observed and simulated coordinates with the corresponding residuals; the left and the right column are particularized respectively for the right ascension (RA) and the declination (Dec).

Finally, we show in Figure 5.14 the orbits of the studied *S*-stars corresponding to the best multi-star fit for $\Xi = 7400^{+30555.6}_{-32244.3}$ (last row of Table 5.4), the point maximizing the likelihood distribution shown in Fig. 5.15.

5.5 Concluding remarks

We investigated the orbital motion of *S*-stars in the framework of $f(R)$ -gravity and Bootstrapped Newtonian-gravity theories. In order to constrain the parameters $\{\delta, \lambda, \Xi\}$, we varied them freely in an appropriate range. We solved the geodesic equations numerically setting initial conditions at the apocenter. Then, we applied the Thiele-Innes formulas to convert the mock positions to the reference frame of a distant observer. The numerical integration is carried out on the basis of a two-body approach, i.e. perturbations due to other members of the *S*-stars cluster, as well as other possible existing extended structures of matter, have been neglected. Finally, we performed χ^2 -statistics to compute the best fit values of the parameters, and their uncertainties.

We do not detect any departure from GR, even using more stars simultaneously. This result was rather expected since *S*-stars are, on average, at a distance $r > 1000 R_S$ (for Sgr A*, $R_S \sim 0.08$ AU) from the source. Therefore, any strong-field effect is negligible.

The proposed approach is completely general and could be useful in the task of classifying other gravitational theories on the basis of dynamical tests at the GC.

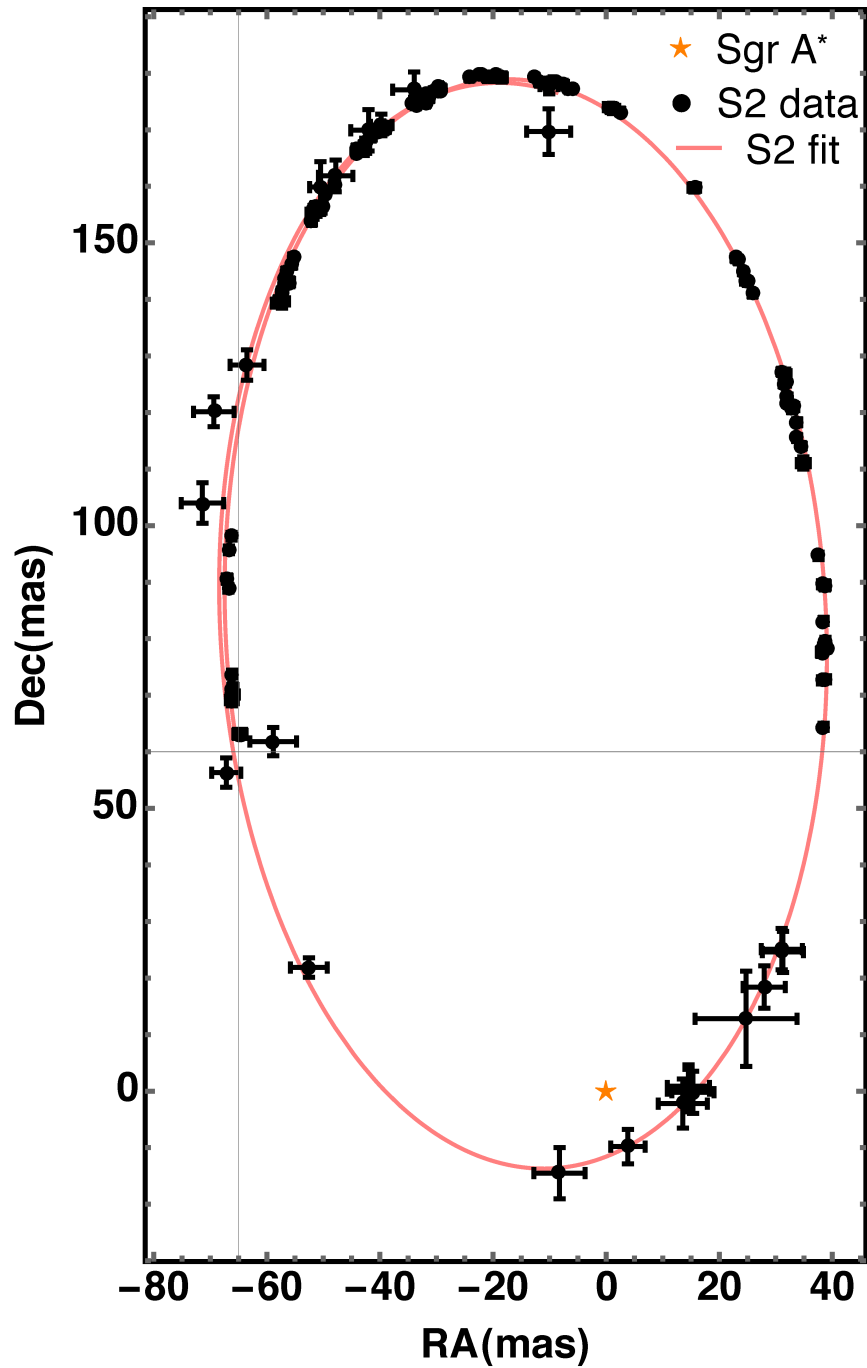


Figure 5.10: Comparison between the NTT/VLT astrometric observations (black circles) and the orbit of *S2* predicted in Bootstrapped gravity using the best fit parameter reported in Table 5.4.

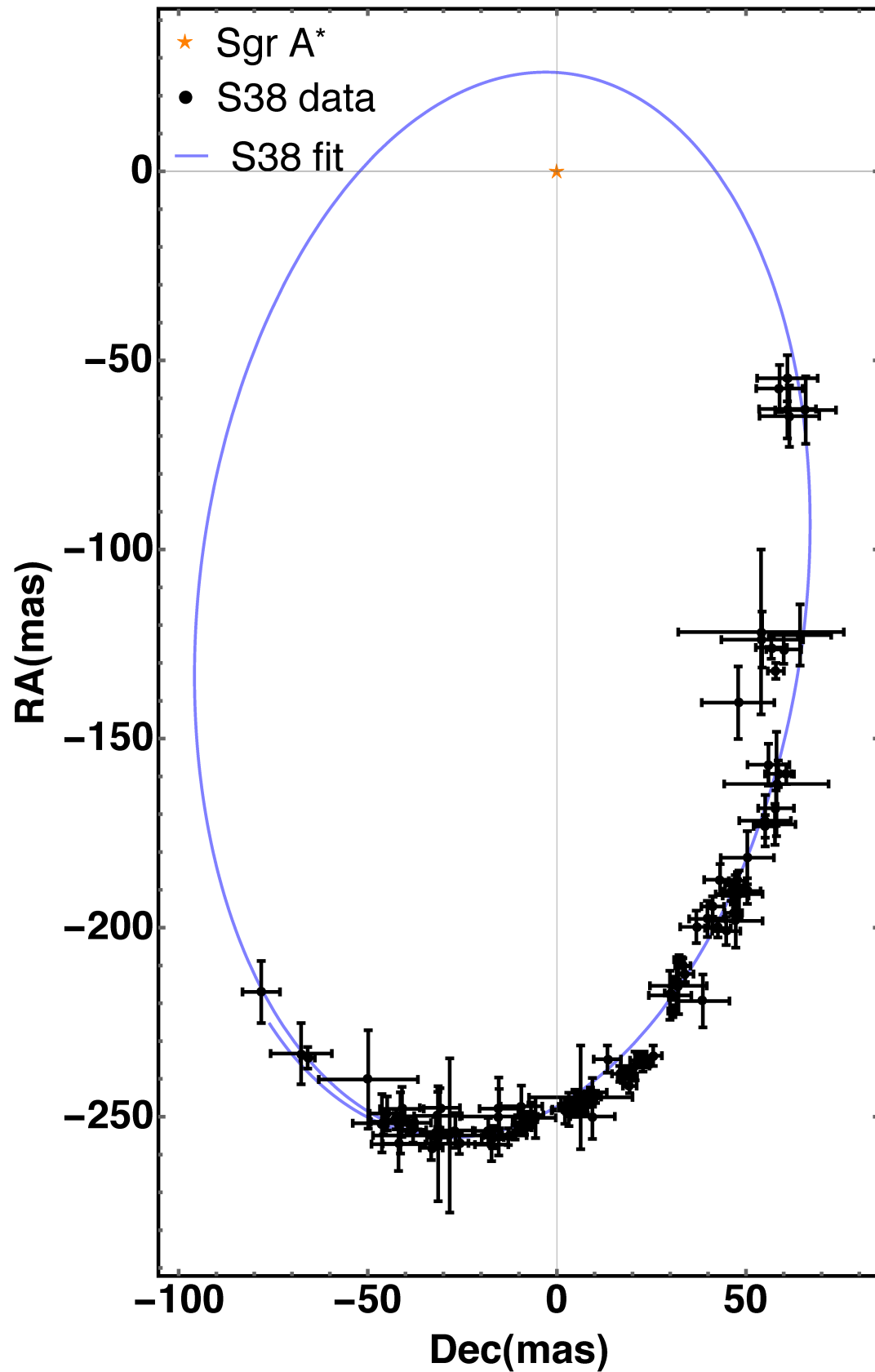


Figure 5.11: Comparison between the NTT/VLT astrometric observations (black circles) and the orbit of *S38* predicted in Bootstrapped gravity using the best fit parameter reported in Table 5.4.

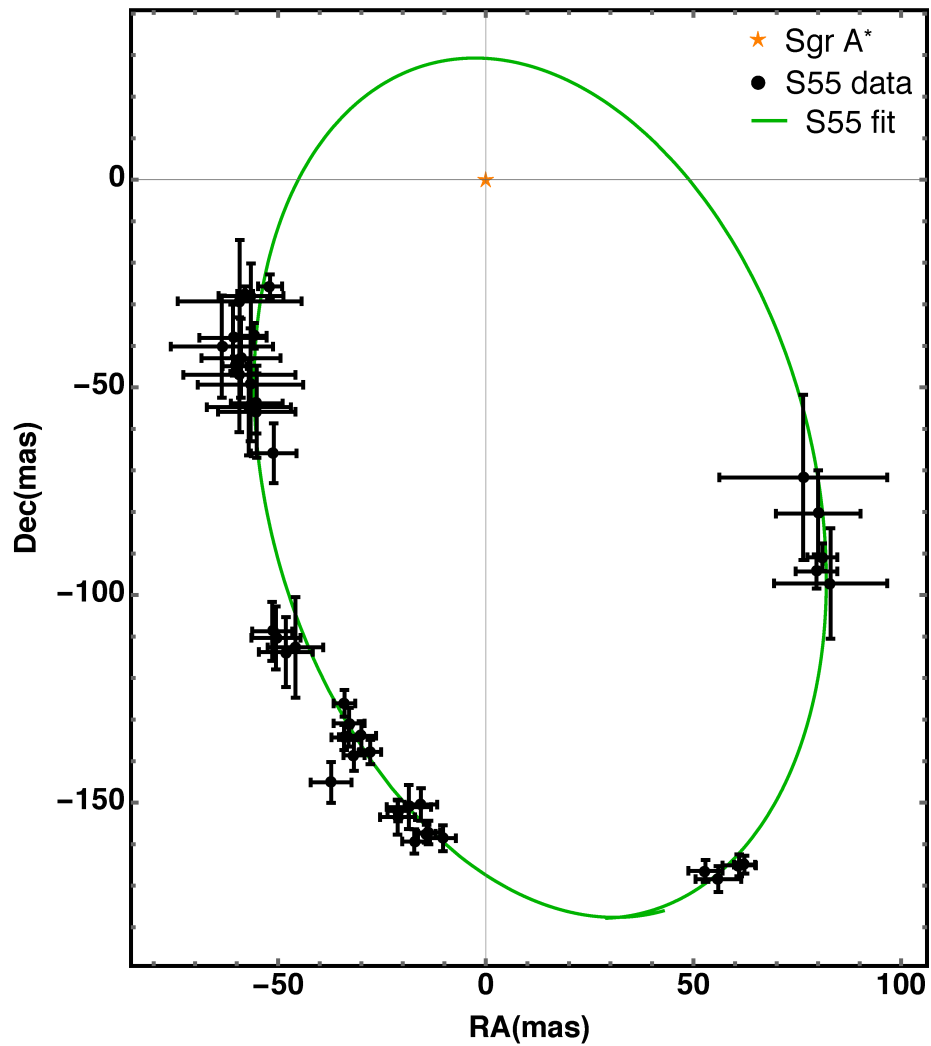


Figure 5.12: Comparison between the NTT/VLT astrometric observations (black circles) and the orbit of *S55* predicted in Bootstrapped gravity using the best fit parameter reported in Table 5.4.

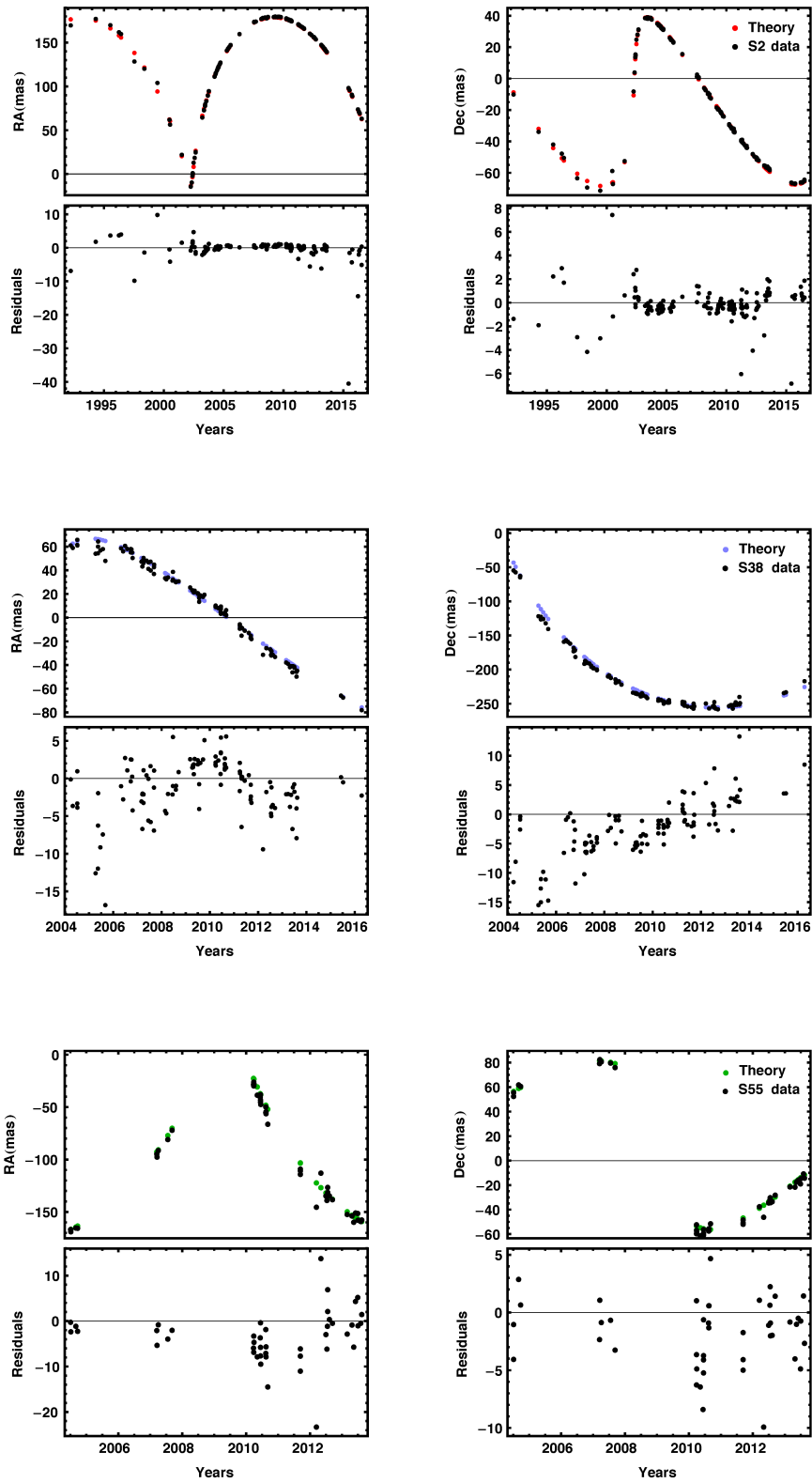


Figure 5.13: Top panels show the comparison between the observed and fitted coordinates, and bottom panels the corresponding residuals for *S2*, *S38* and *S55* for the Bootstrapped gravity.

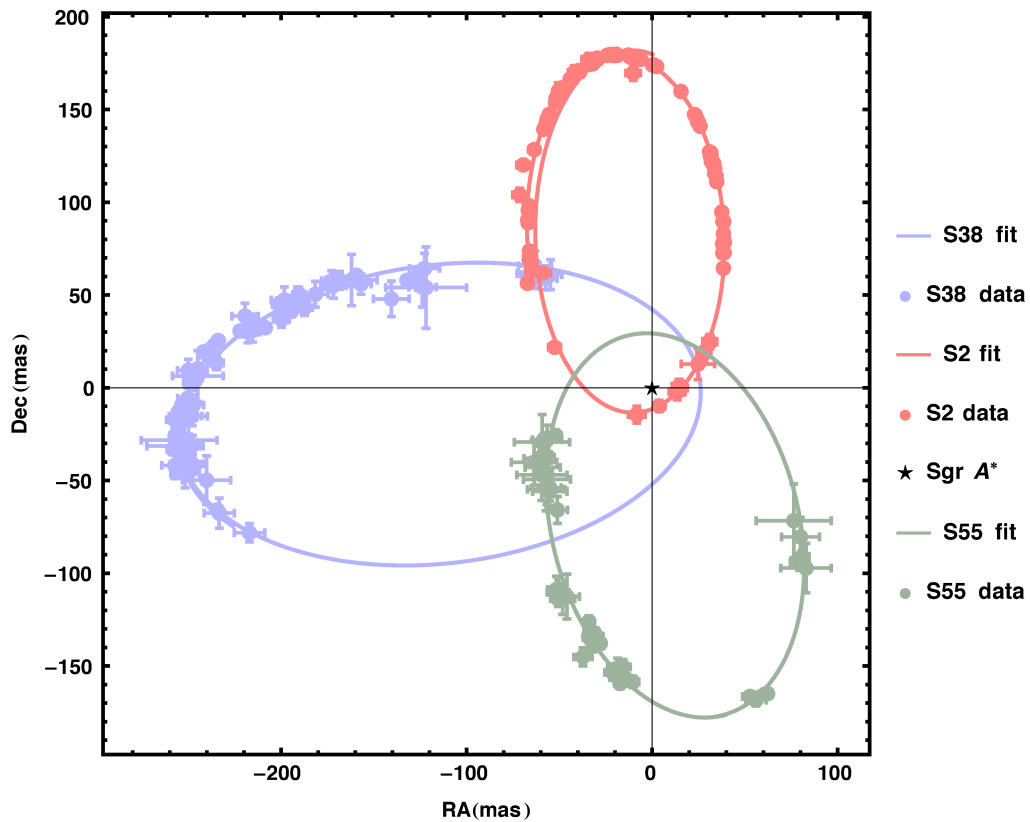


Figure 5.14: Best relativistic multi-star orbit fit of $S2$, $S38$ and $S55$ for the Bootstrapped gravity.

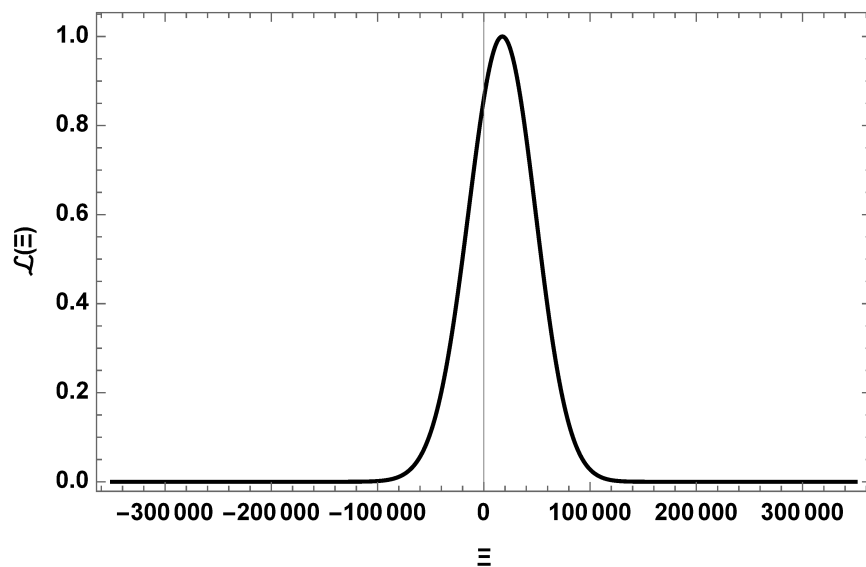


Figure 5.15: Likelihood function $\mathcal{L}(\Xi)$.

TEST II: PRECESSION OF THE PERIHELIA

Adeo ut coelestis hic Mercurius non minùs Astronomos torserit, quàm terrestris Alchimistas eludat.

– G. B. Riccioli

6.1	Precession	112
6.1.1	Bootstrapped Newtonian gravity	112
6.1.2	$f(R)$ -gravity	112
6.2	Astronomical tests	113
6.2.1	Test II.a: Bootstrapped Newtonian gravity	113
6.2.2	Test II.b: $f(R)$ -gravity	116
6.3	Concluding remarks	117

In the previous chapter, we presented a relativistic approach to test theories of gravity using stellar orbits observations at the GC. In this chapter, based on the article [56], we want to check the validity of our results by performing further analysis. To this end, we present a phenomenological investigation aiming at placing bounds on the parameters of interest from observations of the precession of the perihelia of planets in the Solar System. We will report the results for the $f(R)$ -gravity theory (inspired by De Laurentis and De Martino [59]), and those for the Bootstrapped Newtonian gravity theory.

6.1 Precession

It's useful to recall theoretical expressions for the periastron advance. The following results will be applied to an astronomical system to constrain the characteristic parameters, as we will see in Sec. 6.2.

6.1.1 Bootstrapped Newtonian gravity

The expression at the leading order of the perihelion precession in terms of the PPN parameters (Eq. 2.167) is:

$$\Delta\phi^{(1)} = \pi (2 - \beta + 2\gamma) \frac{R_S}{\ell}. \quad (6.1)$$

As we saw in Sec. 3.4.4, the second-order correction depends on both ξ and ζ and, for $\beta = \gamma = 1$, is given by Eq. (3.151):

$$\begin{aligned} \Delta\phi^{(2)} &= \pi \left[(41 + 10\xi - 24\zeta) + (16\xi - 13) \frac{e^2}{2} \right] \frac{R_S^2}{4\ell^2} \\ &\simeq \pi \left[(37 + 22\Xi) + (3 + 16\Xi) \frac{e^2}{2} \right] \frac{R_S^2}{4\ell^2} \\ &\simeq \Delta\phi_S^{(2)} + 2\pi \left[11\xi - 7 + 4(\xi - 1)e^2 \right] \frac{R_S^2}{4\ell^2}. \end{aligned} \quad (6.2)$$

From Eq. (3.142), it follows that we cannot have $\xi = \zeta = 1$ for any value of Ξ . A deviation from GR, quantified by Ξ , remains.

In order to constrain the parameter Ξ by observed values of celestial bodies precession, we can identify its confidence region as the set of values such that the precession

$$\Delta\phi = \Delta\phi^{(1)} + \Delta\phi^{(2)} \quad (6.3)$$

is compatible with data.

6.1.2 $f(R)$ -gravity

As demonstrated in Ref. [59], the equation for the periastron advance in $f(R)$ -gravity is given by

$$\Delta\phi = \frac{3\pi R_S}{a(1-e^2)} \left(1 + \frac{\delta R_S^2}{6a^2(1-e^2)^2} - \frac{\pi\delta R_S^2}{2a(1-e^2)\lambda} - \frac{3\delta R_S}{2a(1-e^2)} - \frac{\delta R_S^2}{24(\delta+1)\lambda^2} + \frac{\delta R_S}{6\lambda} \right). \quad (6.4)$$

It is immediate to notice that Eq. 6.4 reduces to the GR expression $\Delta\phi_{\text{GR}}$ if $\delta = 0$:

$$\Delta\phi_{\text{GR}} = \frac{3\pi R_S}{a(1-e^2)}. \quad (6.5)$$

Planet	$a(10^6 \text{ km})$	$P(\text{years})$	$i(^{\circ})$	e	$\Delta\phi_{\text{obs}}(''/\text{cy})$	$\Delta\phi_{\text{S}}(''/\text{cy})$	$[\Xi_{\text{min}}; \Xi_{\text{max}}]$
Mercury ☿	57.909	0.24	7.005	0.2056	43.1000 ± 0.5000	42.9822	$[-89708.7; 144995]$
Venus ♀	108.209	0.61	3.395	0.0067	8.6247 ± 0.0005	8.6247	$[-1149.67; 1167.47]$
Earth ♂	149.596	1.00	0.000	0.0167	3.8387 ± 0.0004	3.83881	$[-3660.86; 2094.96]$
Mars ♂	227.923	1.88	1.851	0.0935	1.3565 ± 0.0004	1.35106	$[155248.; 179879.]$
Jupiter ♃	778.570	11.86	1.305	0.0489	0.6000 ± 0.3000	0.0623142	$[5.46709 \cdot 10^8; 1.92679 \cdot 10^9]$
Saturn ♄	1433.529	29.45	2.485	0.0565	0.0105 ± 0.0050	0.0136394	$[-1.57315 \cdot 10^8; 3.59618 \cdot 10^7]$

Table 6.1: Values of semi-major axis (a), orbital period (P), tilt angle (i), eccentricity (e), observed orbital precession ($\Delta\phi_{\text{obs}}$), orbital precession as predicted by GR ($\Delta\phi_{\text{S}}$) and constraints on Ξ for Solar System’s planets.

6.2 Astronomical tests

To constrain the free parameters of the theories under consideration, we confronted the theoretical results exposed in Sec. 6.1 with the astronomical data. To infer a range of validity for a given parameter, we compared the analytical expression of the precession with the observed values of the perihelion advance of the Solar System’s planets.

6.2.1 Test II.a: Bootstrapped Newtonian gravity

Precession in the Solar System

We can put constraints on Ξ starting from the Solar System planets whose orbital precession has been measured: Mercury, Venus, Earth, Mars, Jupiter, and Saturn [178]. Let us describe Table 6.1. Column (1) gives the name of the planet and its corresponding symbol. From column (2) to column (5) values of the planetary parameters¹ are quoted: semi-major axis (a), orbital period (P), tilt angle (i), and eccentricity (e). Column (6) gives the observed values of the precession [178] while the GR values as obtained by Eq. (2.167) are reported in column (7). For each planet, we can define an allowed region of the parameter Ξ as the interval of values such that its extremes solve the equation

$$\Delta\phi(\Xi) = \Delta\phi_{\text{obs}}, \quad (6.6)$$

where $\Delta\phi_{\text{obs}}$ include the observative uncertainties. The inferred lower and upper limits for Ξ , which then outline the range of values compatible with data, are reported in column (8) of Table 6.1 while a graphical representation is given by Figure 6.1. Grey shades represent the allowed regions for Ξ , that is the region under the curve $\Delta\phi(\Xi)$ delimited by the values $[\Delta\phi(\Xi_{\text{min}}); \Delta\phi(\Xi_{\text{max}})]$. Graphically, the values $\Delta\phi(\Xi_{\text{min}})$ and $\Delta\phi(\Xi_{\text{max}})$ are obtained intercepting the theoretical black line with the blue dashed lines, that is the measured values taken from [178]. Finally, red lines mark the GR values

¹The reported values are taken from NASA fact sheet at <https://nssdc.gsfc.nasa.gov/planetary/factsheet/>

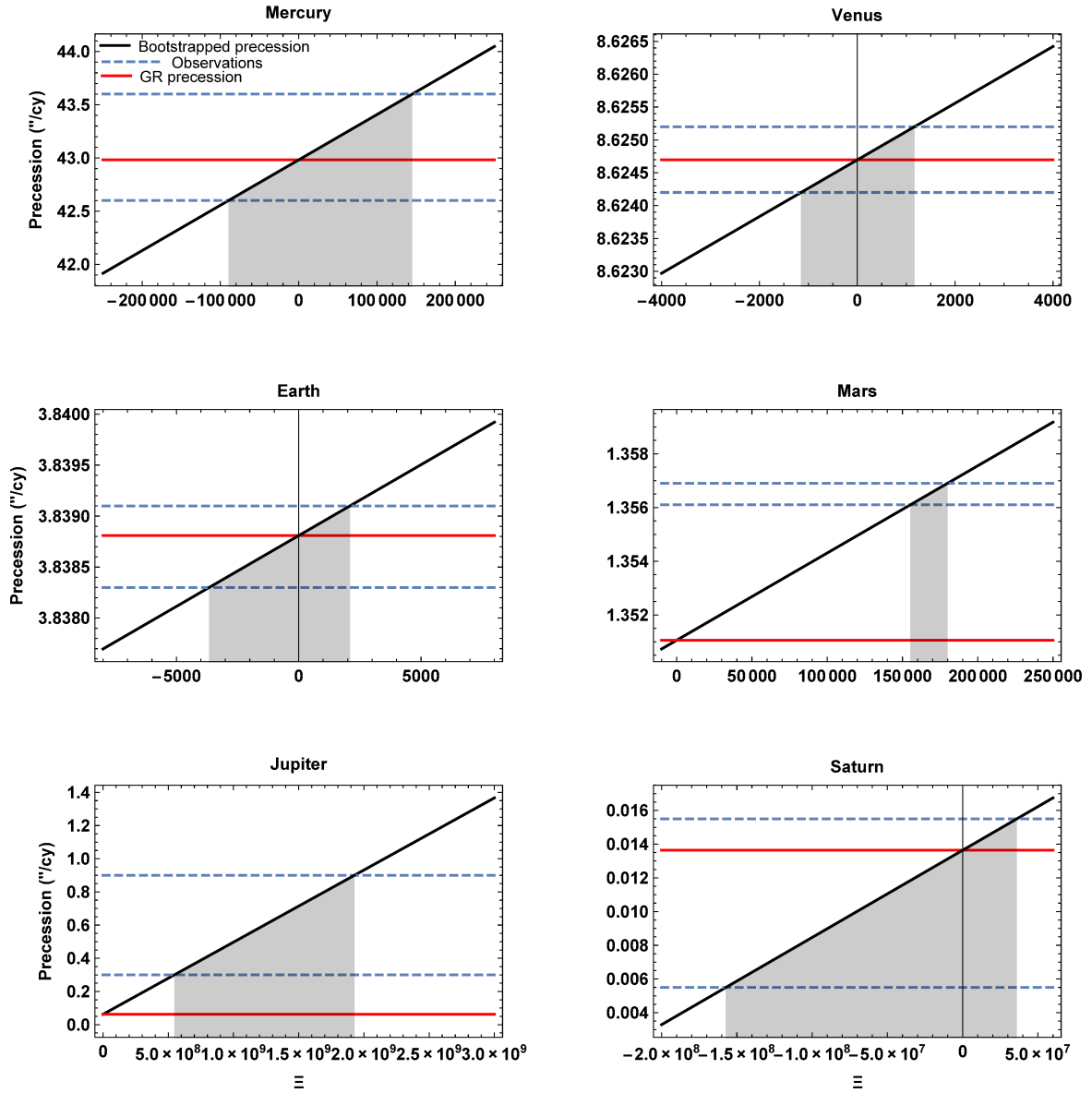


Figure 6.1: Bootstrapped orbital precession as a function of the parameter Ξ . Black lines give the theoretical prediction from Eq. (6.3), blue dashed lines represent the measurements adapted from [178] and red lines depict the GR values as in Eq. (2.167). Confidence regions for Ξ are shaded in grey.

derived by Eq. (2.171). It is worth noticing the discrepancy between the GR value (the red line) and the observed precession (blue dashed lines) for Mars and Jupiter; it could be attributed to the incomplete subtraction of non-relativistic effects from observed value, complicated by the presence of the asteroid belt between Mars and Jupiter, and the appearance of an anomalous residual precession [178, 190].

We deduced the tightest interval on parameter Ξ with Venus, which is $\Xi \in [1149.67;$

Planet	$a(10^6 \text{ km})$	$P(\text{years})$	$i(^{\circ})$	e	$\Delta\phi_S(\text{''/cy})$	$[\Delta\phi_{\min}; \Delta\phi_{\max}]$
Uranus ♅	2872.463	84.01	0.772	0.0457	0.00238404	[0.00238404; 0.00238405]
Neptune ♆	4495.060	164.786	1.769	0.0113	0.000775374	[0.000775373; 0.000775375]
Pluto ♇	5869.656	247.936	17.16	0.2444	0.000419669	[0.000419669; 0.00041967]

Table 6.2: Orbital parameters from the Nasa Fact Sheet, the GR prediction for the precession in the sixth column and the values predicted by the bounds on the parameter Ξ of the Bootstrapped theory deduced for Venus (see Table 6.1).

Object	$\Delta\phi_{\text{GR}}(\text{''/cy})$	$\Delta\phi(\Xi_{\text{v}})$	$\Delta\phi(\Xi_{\text{e}})$	$\Delta\phi(\Xi_{\text{s}})$	$\Delta\phi(\Xi_{\text{m}})$
Mars	1.35106	[1.34814; 1.35577]	[1.35102; 1.3511]	[1.35094; 1.35113]	[-3.75855; 2.5191]
Jupiter	0.0623142	[0.0622752; 0.0623773]	[0.0623137; 0.0623147]	[0.0623126; 0.0623151]	[-0.00607962; 0.0779489]

Table 6.3: Precession for Mars and Jupiter as predicted by confidence values for Ξ inferred from Mercury, Venus, Earth, and Saturn.

1167.47]. We can use the values defining such an interval to predict the precession for Uranus, Neptune and Pluto, for which no observation is available. The results, summarized in Table 2, show that the Bootstrapped Gravity theory predictions perfectly agree with GR.

We can next calculate the precession for Mars and Jupiter with the values of Ξ as obtained by Mercury, Venus, Earth, and Saturn to check agreement with the corresponding Schwarzschild value (Table 6.3).

Precession of $S2$ -star

When in 2002 the star $S2$ passed the pericentre at 120 AU ($\sim 1400 R_{\text{S}}$) with an orbital speed of 7700 km/s ($\beta = v/c = 2.56 \times 10^{-2}$), the first-order GR-effects, as the gravitational redshift and the Schwarzschild precession, were in reach of accurate observations thanks to GRAVITY [116]. The results, summed up in Table 6.4 and depicted in Fig. 6.2, confirm the compatibility of our predictions with GR. In Table 6.5 we report values of the precession as obtained by the extremes of the confidence regions for Ξ inferred from Mercury, Venus, Earth and Saturn: GR value always lies in such intervals.

The mean value of the parameter Ξ such that

$$\Delta\phi(\Xi) = \Delta\phi_{\text{S}} \quad (6.7)$$

is given by

$$\Xi = -1.64236 \pm 0.10305 . \quad (6.8)$$

Star	$a(\text{AU})$	$P(\text{years})$	$i(^{\circ})$	e	$\Delta\phi_{\text{obs}}(\text{''/orbit})$	$\Delta\phi_{\text{S}}(\text{''/orbit})$	$[\Xi_{\text{min}}; \Xi_{\text{max}}]$
S2	1031.32	16.0455	134.567	0.884649	$730.382 \cdot (1.10 \pm 0.19)$	730.382	$[-103.066; 326.398]$

Table 6.4: For the star $S2$, orbital parameters [116], observed orbital precession ($\Delta\phi_{\text{obs}}$), orbital precession as predicted by GR ($\Delta\phi_{\text{S}}$) and constraints on Ξ .

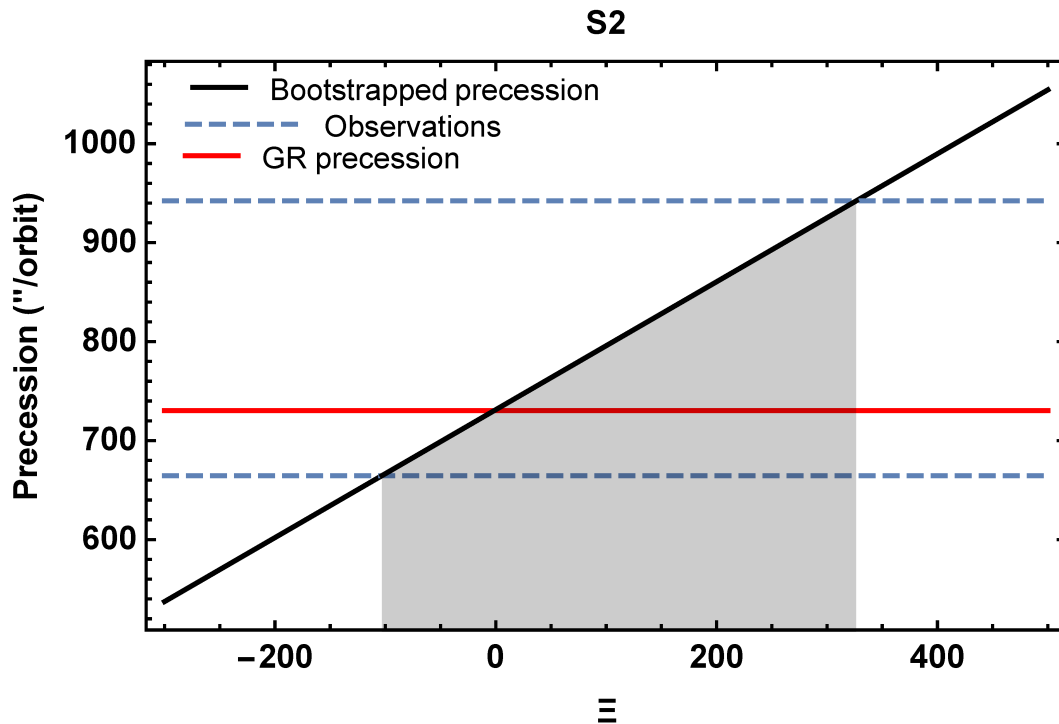


Figure 6.2: Bootstrapped orbital precession as a function of the parameter Ξ for the star $S2$.

6.2.2 Test II.b: $f(R)$ -gravity

We repeated the same analysis for the $f(R)$ -theory. Analysis of the Solar System's planets was already performed in Ref. [63] with a semiclassical approach. For completeness of the discussion, we compared the relativistic result derived in Ref. [59] to the observed precession of planets and $S2$.

Precession in the Solar System

In this case, the parameter space is larger due to the presence of two parameters: δ and λ . Anyway, to infer a lower and upper limit on δ we can fix the scale length to the lower limit $\lambda = 6336.23$ AU. The inferred confidence regions for δ are reported in column (8) of Table 6.6 (the meaning of the symbols is the same as in the previous section) and are graphically depicted in Figure 6.3. We get the tightest interval on δ by Venus, which is $\delta \in [-0.0000584993; 0.0000574467]$. We can use these latter values

Object	$\Delta\phi_{\text{GR}}(^{\prime\prime}/\text{orbit})$	$\Delta\phi(\Xi_{\text{Mercury}})$	$\Delta\phi(\Xi_{\text{Venus}})$	$\Delta\phi(\Xi_{\text{Earth}})$	$\Delta\phi(\Xi_{\text{Saturn}})$
S2	730.382	$[-57243.9; 94435.7]$	$[-11.7295; 1485.75]$	$[-1634.61; 2085.15]$	$[-1.01666 \cdot 10^8; 2.32414 \cdot 10^7]$

Table 6.5: Precession for *S2* as predicted by confidence regions for Ξ inferred from Mercury, Venus, Earth and Saturn.

Planet	$a(10^6 \text{ km})$	$P(\text{years})$	$i(^{\circ})$	e	$\Delta\phi_{\text{obs}}(^{\prime\prime}/\text{cy})$	$\Delta\phi_{\text{S}}(^{\prime\prime}/\text{cy})$	$[\delta_{\text{min}}; \delta_{\text{max}}]$
Mercury ☿	57.909	0.24	7.005	0.2056	43.1000 ± 0.5000	42.9822	$[-0.0141694; 0.00897216]$
Venus ♀	108.209	0.61	3.395	0.0067	8.6247 ± 0.0005	8.6247	$[-0.0000584993; 0.0000574467]$
Earth ♂	149.596	1.00	0.000	0.0167	3.8387 ± 0.0004	3.83881	$[-0.0000759063; 0.000132503]$
Mars ♂	227.923	1.88	1.851	0.0935	1.3565 ± 0.0004	1.35106	$[-0.0043058; -0.00371842]$
Jupiter ♃	778.570	11.86	1.305	0.0489	0.6000 ± 0.3000	0.0623142	$[-0.930762; -0.792286]$
Saturn ♄	1433.529	29.45	2.485	0.0565	0.0105 ± 0.0050	0.0136394	$[-0.120041; 1.47988]$

Table 6.6: Values of semi-major axis (a), orbital period (P), tilt angle (i), eccentricity (e), observed orbital precession ($\Delta\phi_{\text{obs}}$), orbital precession as predicted by GR ($\Delta\phi_{\text{S}}$) and constraints on δ for Solar System’s planets.

to predict the precession for Uranus, Neptune, and Pluto. We report the results in Table 6.7 and we can easily ascertain that GR value lies in the interval predicted by the $f(R)$ -gravity. As a final check, we can calculate the precession for Mars and Jupiter with the values of δ as obtained by the remaining four planets (Table 6.8). The latter Table shows full compatibility between the standard value and those predicted by the extended theory.

Precession of *S2*-star

We performed the same analysis with *S2*. We report the results in Table 6.9 and we portray them in Figure 6.4. Finally, in Table 6.10 we put the values of the precession as obtained by confidence values of δ deduced from Mercury, Venus, Earth, and Saturn.

6.3 Concluding remarks

In this chapter, we performed a further astronomical test to cross-check constraints obtained using stellar orbit at the GC. Bounds on Ξ and δ can be deduced from the comparison between the measurements of the orbital precession of Solar System bodies and the theoretical predictions arising from bootstrapped Newtonian metric (computed in Ref. [47]) and the $f(R)$ -gravity metric (computed in Ref. [59]). The inferred confidence regions for Ξ and δ for each planet are reported, respectively, in Tables 6.1 and 6.6. Their graphical representation can be found in Figures 6.1 and 6.1. We obtained

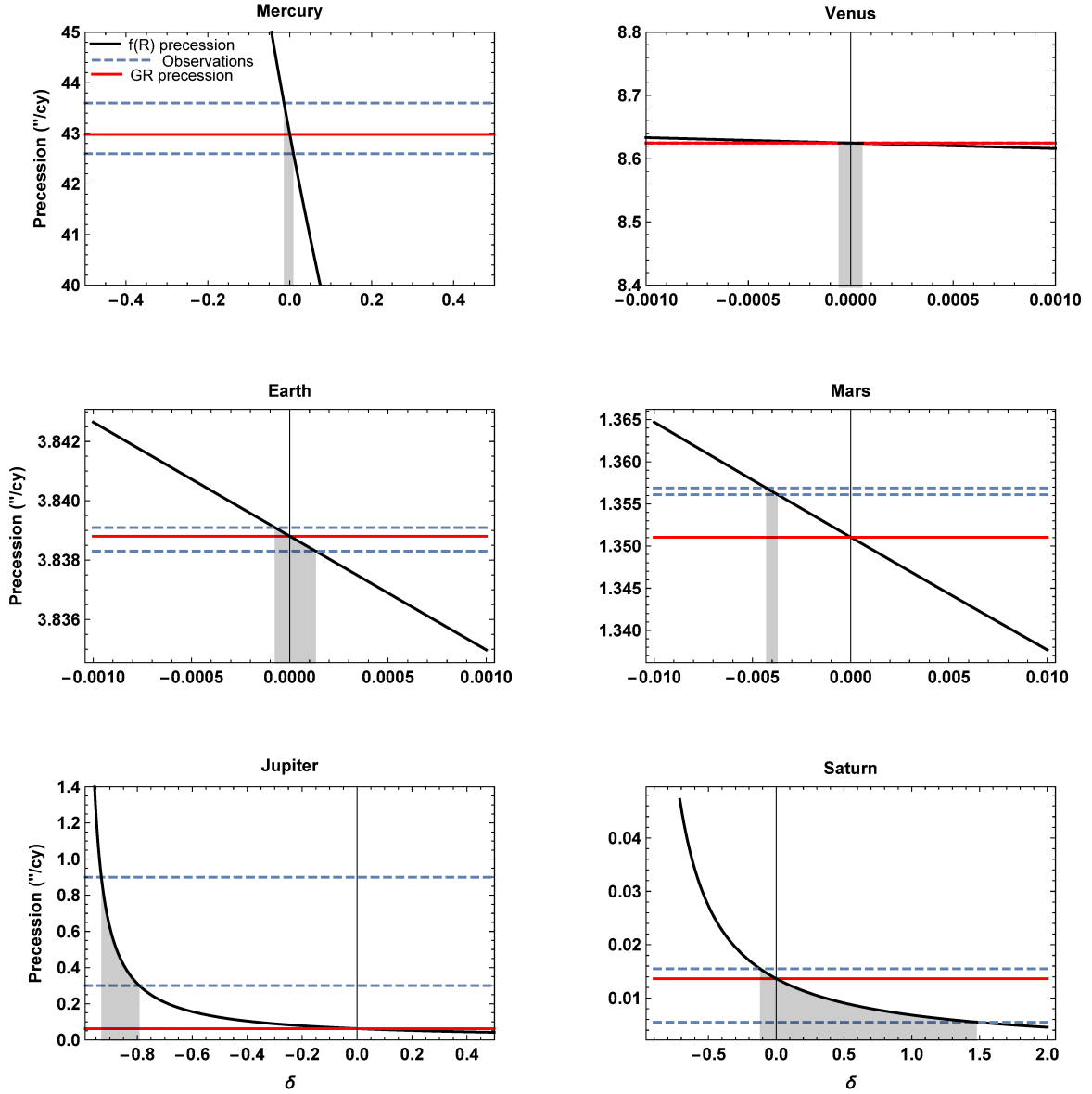


Figure 6.3: $f(R)$ -gravity orbital precession as a function of the parameter δ . Black lines give the theoretical prediction, blue dashed lines represent the measurements adapted from [178] and red lines depict the GR values. Confidence regions for δ are shaded in grey.

the tightest intervals with Venus, which are

$$\Xi \in [-1149.67; +1167.47], \quad (6.9)$$

$$\delta \in [-0.0000584993; 0.0000574467]. \quad (6.10)$$

With these values of the parameters Ξ and δ we predicted the orbital precession for Uranus, Neptune, and Pluto; we found a theoretical precession in great agreement with the GR value. Such compatibility was confirmed by turning our attention to

Planet	$a(10^6 \text{ km})$	$P(\text{years})$	$i(^{\circ})$	e	$\Delta\phi_S(\text{''/cy})$	$[\Delta\phi_{\min}; \Delta\phi_{\max}]$
Uranus ♅	2872.463	84.01	0.772	0.0457	0.00238404	[0.00238391; 0.00238418]
Neptune ♆	4495.060	164.786	1.769	0.0113	0.000775374	[0.000775329; 0.000775419]
Pluto ♇	5869.656	247.936	17.16	0.2444	0.000419669	[0.000419645; 0.000419669]

Table 6.7: Orbital parameters from Nasa Fact Sheet, the GR prediction for the precession in the sixth column and the values predicted by the bounds on the parameter δ of the $f(R)$ -gravity theory deduced for Venus (see Table 6.6).

Object	$\Delta\phi_S(\text{''/cy})$	$\Delta\phi(\delta_{\S})$	$\Delta\phi(\delta_{\Psi})$	$\Delta\phi(\delta_{\oplus})$	$\Delta\phi(\delta_{\Sat})$
Mars	1.35106	[1.33904; 1.37048]	[1.35098; 1.35114]	[1.35088; 1.35116]	[0.544807; 1.53536]
Jupiter	0.0623142	[0.0617601; 0.0632099]	[0.0623107; 0.0623179]	[0.062306; 0.062319]	[0.0251279; 0.0708149]

Table 6.8: Precession for Mars and Jupiter as predicted by confidence values for δ inferred from Mercury, Venus, Earth, and Saturn.

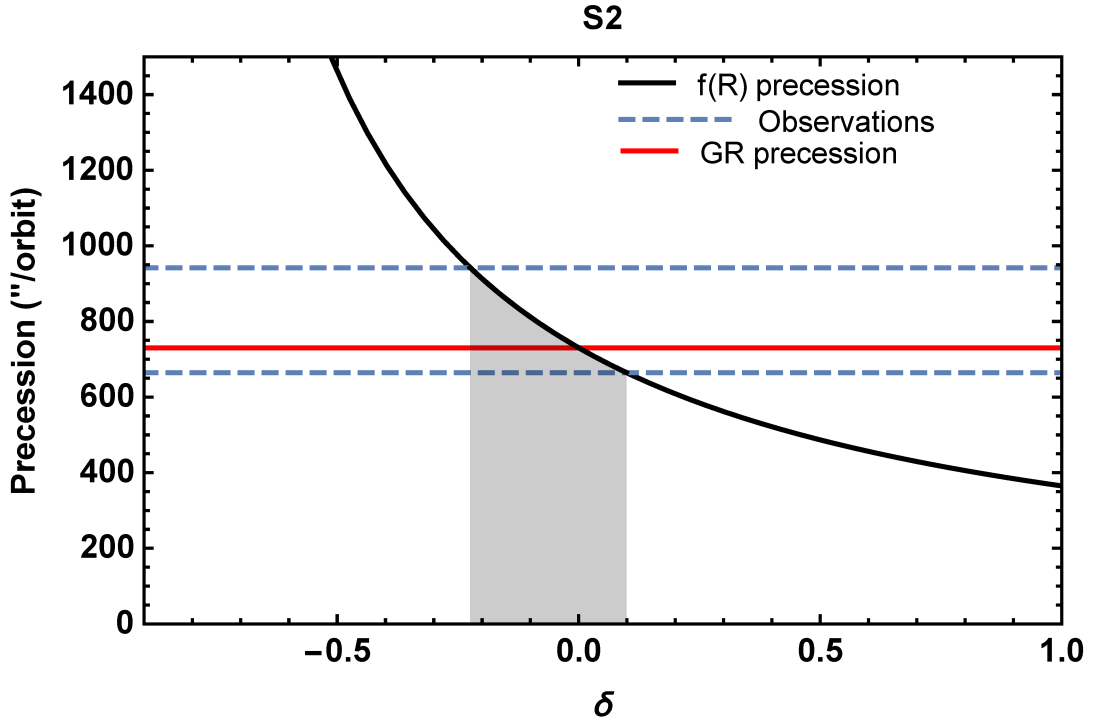


Figure 6.4: $f(R)$ -gravity theory precession as a function of the parameter δ for the star $S2$.

Star	$a(\text{AU})$	$P(\text{years})$	$i(^{\circ})$	e	$\Delta\phi_{\text{obs}}(\text{''/orbit})$	$\Delta\phi_S(\text{''/orbit})$	$[\delta_{\min}; \delta_{\max}]$
S2	1031.32	16.0455	134.567	0.884649	$730.382 \cdot (1.10 \pm 0.19)$	730.382	$[-0.224708; 0.0988401]$

Table 6.9: For the star $S2$, orbital parameters [116], observed orbital precession ($\Delta\phi_{\text{obs}}$), orbital precession as predicted by GR ($\Delta\phi_S$), and constraints on δ .

Object	$\Delta\phi_S$ ("/orbit)	$\Delta\phi(\delta_{\text{Mercury}})$	$\Delta\phi(\delta_{\text{Venus}})$	$\Delta\phi(\delta_{\text{Earth}})$	$\Delta\phi(\delta_{\text{Saturn}})$
S2	730.382	[723.883; 740.885]	[730.34; 730.424]	[730.285; 730.437]	[294.278; 830.074]

Table 6.10: Precession for Mars, Jupiter, and *S2* as predicted by confidence regions for δ inferred from Mercury, Venus, Earth, and Saturn.

the Galactic Center and repeating the same analysis for the star S2 [116]. The mean value of the parameter Ξ such that the Bootstrapped Newtonian precession equals the Schwarzschild value is

$$\Xi = 1.64236 \pm 0.10305. \quad (6.11)$$

Finally, the value of δ which recovers the Schwarzschild precession is $\delta = 0$. As we expected, the confidence regions inferred by precession measurements slightly extend around zero.

CONCLUSIONS

Nature uses only the longest threads to weave her patterns, so that each small piece of her fabric reveals the organization of the entire tapestry.

– R. Feynman

7.1	Summary	121
7.2	Future prospects	122

7.1 Summary

When we are in the presence of a new mathematically consistent theory, that is, one that respects a series of specific theoretical principles, we must understand if its predictions are consistent with the data provided by the reality or, if not, relegate it to the abstract realm of mathematics. In this thesis, we address this need to the plethora of theories of gravity and we pursue the goal of building an applicative counterpart to the extensive theoretical work aimed at developing suitable models. We have divided this thesis into two parts: in the first part we presented the foundations of General Relativity and its extensions; in the second part we wondered if these extensions could describe reality. In particular, we focused on two theories that could help to solve the flaws that undermine the General Relativity on two sides: the $f(R)$ -gravity theory on the infrared side and the Bootstrapped Newtonian gravity on the ultraviolet side.

First, we investigated the orbital motion of S -stars around Sgr A* to constrain the free parameters emerging from the aforementioned theories: $\{\delta, \lambda\}$ from the $f(R)$ -gravity and Ξ from the Bootstrapped gravity. To bound such parameters, we adopted a completely agnostic method without imposing a priori any fiducial value, that is, we

varied them freely in an appropriate range. For each point in the parameters space, we solved the relativistic geodesic equations numerically by the Runge-Kutta method by setting initial conditions at the apocenter. To tackle the problem of stellar motion we chose to integrate the exact geodesics equations instead of solving the classical Newtonian equations of motion as previously was done. This is the correct way to proceed if we want to take into account accurately the relativistic effects induced by the central compact object. Then, we applied the Thiele-Innes formulas to project the theoretical positions to the reference frame of a distant observer. The numerical integration was carried out neglecting perturbations due to other members of the S -stars cluster and other possible existing extended structures of matter. Finally, we performed χ^2 -statistics to compute the best fit values of the parameters, and their uncertainties [55, 55]. We did not find any significant deviation from GR, even using more stars simultaneously. Indeed, we got $\delta = 0.00_{-0.52}^{+1.69}$, where $\delta = 0$ reduces our geodesics to the GR ones. Additionally, we set a lower bound on λ that excludes regions of the parameter space where $\lambda < 6336.23$ AU, in agreement with the results obtained by Borika et al. [22] and Hees et al. [126]. Finally, we found $\Xi = 17400_{-32244.3}^{+30555.6}$. We expected this result because S -stars are, on average, at a distance $r > 1000 R_S$ from the source and strong-field effects are negligible.

Next, we exploited the measurements of perihelion precession of Solar System planets to investigate phenomenologically the considered theories. In particular, we checked for which values of the parameters there is no contradiction between observations and theoretical expressions for the precession. Among the planets whose precession has been observed (that is Mercury, Venus, Earth, Mars, Jupiter, and Saturn) the tightest allowed interval for Ξ and δ was obtained with Venus:

$$\Xi \in [-1149.67; +1167.47], \quad (7.1)$$

$$\delta \in [-0.0000584993; 0.0000574467]. \quad (7.2)$$

Predicting the orbital precession for the remaining planets (Uranus, Neptune and Pluto) with such values, we found a great agreement between the theoretical precession and the GR value. Such compatibility was confirmed by repeating the same analysis for the star $S2$, whose precession has been robustly detected by the GRAVITY collaboration [116].

The proposed approach is completely general and puts this work into a broader program that aims at constraining other theories still untested at the Galactic scale.

7.2 Future prospects

Gravitational research is at a crucial, exciting point. The possibility of a critical test of GR is in reach of the second generation facilities, which are probing space-time deeper and deeper towards the event horizon. Efforts to achieve this goal are mainly on two

fronts.

From one side, at NIR wavelengths, constraints on the parameters of a particular gravitational theory could be improved with increasing high accuracy observations of stars near the GC by advanced facilities such as GRAVITY [18]. Following the recent detection of the three stars *S62*, *S4711*, and *S4714* [185, 186], moving on highly eccentric orbits with a short semi-major axis, new stars are likely to be found within the orbit of *S2* [114]. Looking for stars at smaller radii is fundamental to find possible deviations from GR since strong field effects, such as the Lense-Thirring precession, are no longer negligible for distances of the pericenter close to R_s . Good candidates for this measurement are *S62* and *S4714* [186], which can reliably provide an estimate of the central object spin thus helping to test the gravitational theory at the basis. In this context, the most stringent test would be offered by a pulsar-black hole binary system, with a pulsar spinning hundred times per second. In that case, we would observe the largest deviations from GR. Prospects of finding such a system at the center of the Milky Way are increasing immensely thanks to the explorations currently conducted by BlackHoleCam and EHT.

From the other side, the incontrovertible proof that Sgr A* is a supermassive black hole requires an angular resolution close to the object's event horizon. Shadow observations conducted by EHT Collaboration, with a high angular resolution of better than 60 μas , will concretize this delicate purpose. They will use VLBI images to determine if they correspond to a black hole described by GR or a black hole in ETG.

There will be further progress thanks to the high point-source sensitivity of the new instrumentation like James Webb Space Telescope (JWST)¹. New investigations of faint flares will explain better the energetics near Sgr A*.

We do not know where we are on the long and compelling history of gravitational theories. However, looking for a way to orient ourselves among the extended family of theoretical models on the basis of astronomical observations, we hope to have indicated the direction to take to catch a glimpse of the truth.

¹<http://www.jwst.nasa.gov/>

BIBLIOGRAPHY

- [1] B. P. Abbott et al. “Observation of Gravitational Waves from a Binary Black Hole Merger”. In: *Physical Review Letters* 116.6, 061102 (Feb. 2016), p. 061102. DOI: [10.1103/PhysRevLett.116.061102](https://doi.org/10.1103/PhysRevLett.116.061102). arXiv: [1602.03837 \[gr-qc\]](https://arxiv.org/abs/1602.03837).
- [2] R. G. Aitken. *The Binary Stars*. Dover Publications, 1964.
- [3] D. A. Allen and R. H. Sanders. “Is the galactic centre black hole a dwarf?” In: *Nature* 319.6050 (Jan. 1986), pp. 191–194. DOI: [10.1038/319191a0](https://doi.org/10.1038/319191a0).
- [4] M. Bañados and P. G. Ferreira. “Eddington’s Theory of Gravity and Its Progeny”. In: *Physical Review Letters* 105.1, 011101 (July 2010), p. 011101. DOI: [10.1103/PhysRevLett.105.011101](https://doi.org/10.1103/PhysRevLett.105.011101). arXiv: [1006.1769 \[astro-ph.CO\]](https://arxiv.org/abs/1006.1769).
- [5] D. C. Backer et al. “Upper Limit of 3.3 Astronomical Units to the Diameter of the Galactic Center Radio Source Sgr A^{*}”. In: *Science* 262.5138 (Nov. 1993), pp. 1414–1416. DOI: [10.1126/science.262.5138.1414](https://doi.org/10.1126/science.262.5138.1414).
- [6] F. K. Baganoff et al. “Chandra X-Ray Spectroscopic Imaging of Sagittarius A^{*} and the Central Parsec of the Galaxy”. In: *The Astrophysical Journal* 591.2 (July 2003), pp. 891–915. DOI: [10.1086/375145](https://doi.org/10.1086/375145). arXiv: [astro-ph/0102151 \[astro-ph\]](https://arxiv.org/abs/astro-ph/0102151).
- [7] F. K. Baganoff et al. “Rapid X-ray flaring from the direction of the supermassive black hole at the Galactic Centre”. In: *Nature* 413.6851 (Sept. 2001), pp. 45–48. DOI: [10.1038/35092510](https://doi.org/10.1038/35092510). arXiv: [astro-ph/0109367 \[astro-ph\]](https://arxiv.org/abs/astro-ph/0109367).
- [8] T. Baker, D. Psaltis, and C. Skordis. “Linking Tests of Gravity on All Scales: from the Strong-field Regime to Cosmology”. In: *The Astrophysical Journal* 802.1, 63 (Mar. 2015), p. 63. DOI: [10.1088/0004-637X/802/1/63](https://doi.org/10.1088/0004-637X/802/1/63). arXiv: [1412.3455 \[astro-ph.CO\]](https://arxiv.org/abs/1412.3455).
- [9] H. Balasin and H. Nachbagauer. “The energy-momentum tensor of a black hole, or what curves the Schwarzschild geometry?” In: *Classical and Quantum Gravity* 10.11 (Nov. 1993), pp. 2271–2278. DOI: [10.1088/0264-9381/10/11/010](https://doi.org/10.1088/0264-9381/10/11/010). arXiv: [gr-qc/9305009 \[gr-qc\]](https://arxiv.org/abs/gr-qc/9305009).
- [10] B. Balick and R. L. Brown. “Intense sub-arcsecond structure in the galactic center.” In: *The Astrophysical Journal* 194 (Dec. 1974), pp. 265–270. DOI: [10.1086/153242](https://doi.org/10.1086/153242).
- [11] R. Barlow. “A note on $\Delta \ln L = -1/2$ Errors”. In: *arXiv e-prints*, physics/0403046 (Mar. 2004), physics/0403046. arXiv: [physics/0403046 \[physics.data-an\]](https://arxiv.org/abs/physics/0403046).
- [12] N. M. Barrière et al. “NuSTAR Detection of High-energy X-Ray Emission and Rapid Variability from Sagittarius A^{*} Flares”. In: *The Astrophysical Journal* 786.1, 46 (May 2014), p. 46. DOI: [10.1088/0004-637X/786/1/46](https://doi.org/10.1088/0004-637X/786/1/46). arXiv: [1403.0900 \[astro-ph.HE\]](https://arxiv.org/abs/1403.0900).

- [13] E. E. Becklin, I. Gatley, and M. W. Werner. “Far-infrared observations of Sagittarius A - The luminosity and dust density in the central parsec of the Galaxy”. In: *The Astrophysical Journal* 258 (July 1982), pp. 135–142. DOI: [10.1086/160060](https://doi.org/10.1086/160060).
- [14] E. E. Becklin and G. Neugebauer. “Infrared Observations of the Galactic Center”. In: *The Astrophysical Journal* 151 (Jan. 1968), p. 145. DOI: [10.1086/149425](https://doi.org/10.1086/149425).
- [15] E. Berti et al. “Testing general relativity with present and future astrophysical observations”. In: *Classical and Quantum Gravity* 32.24, 243001 (Dec. 2015), p. 243001. DOI: [10.1088/0264-9381/32/24/243001](https://doi.org/10.1088/0264-9381/32/24/243001). arXiv: [1501.07274 \[gr-qc\]](https://arxiv.org/abs/1501.07274).
- [16] O. Bertolami et al. “Extra force in f(R) modified theories of gravity”. In: *Physical Review D* 75 (2007), p. 104016.
- [17] N. Bilic, G. B. Tupper, and R. D. Viollier. “Supermassive fermion balls and constraints from stellar dynamics near Sgr A*”. In: *arXiv e-prints*, astro-ph/0310172 (Oct. 2003), astro-ph/0310172. arXiv: [astro-ph/0310172 \[astro-ph\]](https://arxiv.org/abs/astro-ph/0310172).
- [18] N. Blind et al. “GRAVITY: the VLTI 4-beam combiner for narrow-angle astrometry and interferometric imaging”. In: *arXiv e-prints*, arXiv:1503.07303 (Mar. 2015), arXiv:1503.07303. arXiv: [1503.07303 \[astro-ph.IM\]](https://arxiv.org/abs/1503.07303).
- [19] R. Blum et al. “Really Cool Stars and the Star Formation History at the Galactic Center”. In: *The Astrophysical Journal* 597 (July 2003). DOI: [10.1086/378380](https://doi.org/10.1086/378380).
- [20] R. D. Blum, D. L. Depoy, and K. Sellgren. “A Comparison of Near-Infrared Spectra of the Galactic Center Compact He I Emission-Line Sources and Early-Type Mass-losing Stars”. In: *The Astrophysical Journal* 441 (Mar. 1995), p. 603. DOI: [10.1086/175386](https://doi.org/10.1086/175386).
- [21] C. T. Bolton. “Identification of Cygnus X-1 with HDE 226868”. In: *Nature* 235.5336 (Feb. 1972), pp. 271–273. DOI: [10.1038/235271b0](https://doi.org/10.1038/235271b0).
- [22] D. Borika et al. “Constraining the range of Yukawa gravity interaction from S2 star orbits”. In: 2013.11, 050 (Nov. 2013), p. 050. DOI: [10.1088/1475-7516/2013/11/050](https://doi.org/10.1088/1475-7516/2013/11/050). arXiv: [1311.1404 \[astro-ph.GA\]](https://arxiv.org/abs/1311.1404).
- [23] G. C. Bower et al. “Detection of the Intrinsic Size of Sagittarius A* Through Closure Amplitude Imaging”. In: *Science* 304.5671 (Apr. 2004), pp. 704–708. DOI: [10.1126/science.1094023](https://doi.org/10.1126/science.1094023). arXiv: [astro-ph/0404001 \[astro-ph\]](https://arxiv.org/abs/astro-ph/0404001).
- [24] V. Bozza and L. Mancini. “Gravitational Lensing by Black Holes: A Comprehensive Treatment and the Case of the Star S2”. In: *The Astrophysical Journal* 611.2 (Aug. 2004), pp. 1045–1053. DOI: [10.1086/422309](https://doi.org/10.1086/422309). arXiv: [astro-ph/0404526 \[astro-ph\]](https://arxiv.org/abs/astro-ph/0404526).

- [25] V. Bozza and L. Mancini. “Gravitational Lensing of Stars in the Central Arcsecond of Our Galaxy”. In: *The Astrophysical Journal* 627.2 (July 2005), pp. 790–802. DOI: [10.1086/430664](https://doi.org/10.1086/430664). arXiv: [astro-ph/0503664](https://arxiv.org/abs/astro-ph/0503664) [[astro-ph](#)].
- [26] V. Bozza and L. Mancini. “Gravitational Lensing of Stars Orbiting the Massive Black Hole in the Galactic Center”. In: *The Astrophysical Journal* 696.1 (May 2009), pp. 701–705. DOI: [10.1088/0004-637X/696/1/701](https://doi.org/10.1088/0004-637X/696/1/701). arXiv: [0812.3853](https://arxiv.org/abs/0812.3853) [[astro-ph](#)].
- [27] C. H. Brans. “Mach’s Principle and a Relativistic Theory of Gravitation. II”. In: *Physical Review* 125 (1962), pp. 2194–2201.
- [28] D. R. Brill and R. H. Gowdy. “Quantization of general relativity”. In: *Reports on Progress in Physics* 33 (1970), p. 413.
- [29] R. L. Brown, K. J. Johnston, and K. Y. Lo. “High resolution VLA observations of the Galactic Center.” In: *The Astrophysical Journal* 250 (Nov. 1981), pp. 155–159. DOI: [10.1086/159356](https://doi.org/10.1086/159356).
- [30] R. L. Brown and K. Y. Lo. “Variability of the compact radio source at the Galactic Center.” In: *The Astrophysical Journal* 253 (Feb. 1982), pp. 108–114. DOI: [10.1086/159615](https://doi.org/10.1086/159615).
- [31] S. Capozziello, E. de Filippis, and V. Salzano. “Modelling clusters of galaxies by f(R) gravity”. In: *Monthly Notices of the Royal Astronomical Society* 394.2 (Apr. 2009), pp. 947–959. DOI: [10.1111/j.1365-2966.2008.14382.x](https://doi.org/10.1111/j.1365-2966.2008.14382.x). arXiv: [0809.1882](https://arxiv.org/abs/0809.1882) [[astro-ph](#)].
- [32] S. Capozziello and M. de Laurentis. “Extended Theories of Gravity”. In: *Physics Report* 509.4 (Dec. 2011), pp. 167–321. DOI: [10.1016/j.physrep.2011.09.003](https://doi.org/10.1016/j.physrep.2011.09.003). arXiv: [1108.6266](https://arxiv.org/abs/1108.6266) [[gr-qc](#)].
- [33] S. Capozziello and M. De Laurentis. “Noether symmetries in extended gravity quantum cosmology”. In: *arXiv e-prints*, arXiv:1308.1208 (Aug. 2013), p. 1460004. arXiv: [1308.1208](https://arxiv.org/abs/1308.1208) [[gr-qc](#)].
- [34] S. Capozziello and M. De Laurentis. “The dark matter problem from f(R) gravity viewpoint”. In: *Annalen der Physik* 524.9-10 (Oct. 2012), pp. 545–578. DOI: [10.1002/andp.201200109](https://doi.org/10.1002/andp.201200109).
- [35] S. Capozziello and V. Faraoni. “The landscape beyond Einstein gravity”. In: *Beyond Einstein Gravity*. Ed. by Valerio Faraoni and Salvatore Capozziello. Vol. 170. 2011, p. 59. DOI: [10.1007/978-94-007-0165-6_3](https://doi.org/10.1007/978-94-007-0165-6_3).
- [36] S. Capozziello and M. Funaro. *Introduzione alla relatività generale: con applicazioni all’astrofisica relativistica e alla cosmologia*. Liguori, 2006.
- [37] S. Capozziello, A. Stabile, and A. Troisi. “Spherical symmetry in f(R)-gravity”. In: *Classical and Quantum Gravity* 25.8 (2008), p. 085004.

- [38] S. Capozziello, A. Stabile, and A. Troisi. “Spherically symmetric solutions in $f(R)$ gravity via the Noether symmetry approach”. In: *Classical and Quantum Gravity* 24.8 (Apr. 2007), pp. 2153–2166. DOI: [10.1088/0264-9381/24/8/013](https://doi.org/10.1088/0264-9381/24/8/013). arXiv: [gr-qc/0703067](https://arxiv.org/abs/gr-qc/0703067) [gr-qc].
- [39] S. Capozziello et al. “From Dark Energy & Dark Matter to Dark Metric”. In: *Foundations of Physics* 39.10 (Oct. 2009), pp. 1161–1176. DOI: [10.1007/s10701-009-9332-7](https://doi.org/10.1007/s10701-009-9332-7). arXiv: [0805.3642](https://arxiv.org/abs/0805.3642) [gr-qc].
- [40] B. Carter. “Global Structure of the Kerr Family of Gravitational Fields”. In: *Physical Review* 174.5 (Oct. 1968), pp. 1559–1571. DOI: [10.1103/PhysRev.174.1559](https://doi.org/10.1103/PhysRev.174.1559).
- [41] R. Casadio, A. Giugno, and A. Giusti. “Matter and gravitons in the gravitational collapse”. In: *Physics Letters B* 763 (Dec. 2016), pp. 337–340. DOI: [10.1016/j.physletb.2016.10.058](https://doi.org/10.1016/j.physletb.2016.10.058). arXiv: [1606.04744](https://arxiv.org/abs/1606.04744) [hep-th].
- [42] R. Casadio and I. Kuntz. “Bootstrapped Newtonian quantum gravity”. In: *European Physical Journal C* 80.6, 581 (June 2020), p. 581. DOI: [10.1140/epjc/s10052-020-8146-9](https://doi.org/10.1140/epjc/s10052-020-8146-9). arXiv: [2003.03579](https://arxiv.org/abs/2003.03579) [gr-qc].
- [43] R. Casadio, M. Lenzi, and O. Micu. “Bootstrapped Newtonian stars and black holes”. In: *European Physical Journal C* 79.11, 894 (Nov. 2019), p. 894. DOI: [10.1140/epjc/s10052-019-7410-3](https://doi.org/10.1140/epjc/s10052-019-7410-3). arXiv: [1904.06752](https://arxiv.org/abs/1904.06752) [gr-qc].
- [44] R. Casadio, M. Lenzi, and O. Micu. “Bootstrapping Newtonian gravity”. In: *Physical Review D* 98.10, 104016 (Nov. 2018), p. 104016. DOI: [10.1103/PhysRevD.98.104016](https://doi.org/10.1103/PhysRevD.98.104016). arXiv: [1806.07639](https://arxiv.org/abs/1806.07639) [gr-qc].
- [45] R. Casadio and O. Micu. “Polytropic stars in bootstrapped Newtonian gravity”. In: *Physical Review D* 102.10, 104058 (Nov. 2020), p. 104058. DOI: [10.1103/PhysRevD.102.104058](https://doi.org/10.1103/PhysRevD.102.104058). arXiv: [2005.09378](https://arxiv.org/abs/2005.09378) [gr-qc].
- [46] R. Casadio, O. Micu, and J. Mureika. “On the mass of bootstrapped Newtonian sources”. In: *Modern Physics Letters A* 35.21, 2050172 (July 2020), p. 2050172. DOI: [10.1142/S0217732320501722](https://doi.org/10.1142/S0217732320501722). arXiv: [1910.03243](https://arxiv.org/abs/1910.03243) [gr-qc].
- [47] R. Casadio et al. “Effective metric outside bootstrapped Newtonian sources”. In: *Physical Review D* 103.6, 064001 (Mar. 2021), p. 064001. DOI: [10.1103/PhysRevD.103.064001](https://doi.org/10.1103/PhysRevD.103.064001). arXiv: [2101.12471](https://arxiv.org/abs/2101.12471) [gr-qc].
- [48] R. Casadio et al. “Quantum corpuscular corrections to the Newtonian potential”. In: *Physical Review D* 96.4, 044010 (Aug. 2017), p. 044010. DOI: [10.1103/PhysRevD.96.044010](https://doi.org/10.1103/PhysRevD.96.044010). arXiv: [1702.05918](https://arxiv.org/abs/1702.05918) [gr-qc].
- [49] S. Chandrasekhar. *The mathematical theory of black holes*. Oxford University Press, 1983.
- [50] S. Chandrasekhar. “The Maximum Mass of Ideal White Dwarfs”. In: *Astrophysical Journal* 74 (July 1931), p. 81. DOI: [10.1086/143324](https://doi.org/10.1086/143324).

- [51] T. L. Chow. *Gravity, black holes, and the very early universe: an introduction to general relativity and cosmology*. Springer Science & Business Media, 2007.
- [52] M. Colpi, S. L. Shapiro, and I. Wasserman. “Boson stars: Gravitational equilibria of self-interacting scalar fields”. In: *Physical Review Letters* 57.20 (Nov. 1986), pp. 2485–2488. DOI: [10.1103/PhysRevLett.57.2485](https://doi.org/10.1103/PhysRevLett.57.2485).
- [53] E. J. Copeland, M. Sami, and S. Tsujikawa. “Dynamics of Dark Energy”. In: *International Journal of Modern Physics D* 15.11 (Jan. 2006), pp. 1753–1935. DOI: [10.1142/S021827180600942X](https://doi.org/10.1142/S021827180600942X). arXiv: [hep-th/0603057](https://arxiv.org/abs/hep-th/0603057) [hep-th].
- [54] J. M. Cordes et al. “Pulsars as tools for fundamental physics & astrophysics”. In: 48.11-12 (Dec. 2004), pp. 1413–1438. DOI: [10.1016/j.newar.2004.09.040](https://doi.org/10.1016/j.newar.2004.09.040). arXiv: [astro-ph/0505555](https://arxiv.org/abs/astro-ph/0505555) [astro-ph].
- [55] A. D’Addio. “S-star dynamics through a Yukawa-like gravitational potential”. In: *Physics of the Dark Universe* 33, 100871 (Sept. 2021), p. 100871. DOI: [10.1016/j.dark.2021.100871](https://doi.org/10.1016/j.dark.2021.100871).
- [56] A. D’Addio et al. “Orbits in bootstrapped Newtonian gravity”. In: *arXiv preprint arXiv:2110.08379* (2021).
- [57] J. A. Davidson et al. “The Luminosity of the Galactic Center”. In: *The Astrophysical Journal* 387 (Mar. 1992), p. 189. DOI: [10.1086/171071](https://doi.org/10.1086/171071).
- [58] P. de Bernardis et al. “A flat Universe from high-resolution maps of the cosmic microwave background radiation”. In: *Nature* 404.6781 (Apr. 2000), pp. 955–959. DOI: [10.1038/35010035](https://doi.org/10.1038/35010035). arXiv: [astro-ph/0004404](https://arxiv.org/abs/astro-ph/0004404) [astro-ph].
- [59] M. De Laurentis, I. De Martino, and R. Lazkoz. “Analysis of the Yukawa gravitational potential in $f(R)$ gravity. II. Relativistic periastron advance”. In: *Physical Review D* 97.10, 104068 (May 2018), p. 104068. DOI: [10.1103/PhysRevD.97.104068](https://doi.org/10.1103/PhysRevD.97.104068). arXiv: [1801.08136](https://arxiv.org/abs/1801.08136) [gr-qc].
- [60] M. De Laurentis, I. De Martino, and R. Lazkoz. “Modified gravity revealed along geodesic tracks”. In: *European Physical Journal C* 78.11, 916 (Nov. 2018), p. 916. DOI: [10.1140/epjc/s10052-018-6401-0](https://doi.org/10.1140/epjc/s10052-018-6401-0). arXiv: [1811.00046](https://arxiv.org/abs/1811.00046) [gr-qc].
- [61] I. De Martino. “ $f(R)$ -gravity model of the Sunyaev-Zeldovich profile of the Coma cluster compatible with Planck data”. In: *Physical Review D* 93.12, 124043 (June 2016), p. 124043. DOI: [10.1103/PhysRevD.93.124043](https://doi.org/10.1103/PhysRevD.93.124043). arXiv: [1605.08223](https://arxiv.org/abs/1605.08223) [astro-ph.CO].
- [62] I. de Martino, M. De Laurentis, and S. Capozziello. “Constraining $f(R)$ gravity by the Large Scale Structure”. In: *Universe* 1 (July 2015), pp. 123–157. DOI: [10.3390/universe1020123](https://doi.org/10.3390/universe1020123). arXiv: [1507.06123](https://arxiv.org/abs/1507.06123) [gr-qc].
- [63] I. De Martino, R. Lazkoz, and M. De Laurentis. “Analysis of the Yukawa gravitational potential in $f(R)$ gravity. I. Semiclassical periastron advance”. In: *Physical Review D* 97.10, 104067 (May 2018), p. 104067. DOI: [10.1103/PhysRevD.97.104067](https://doi.org/10.1103/PhysRevD.97.104067). arXiv: [1801.08135](https://arxiv.org/abs/1801.08135) [gr-qc].

- [64] F. De Paolis et al. “Astrophysical constraints on a possible neutrino ball at the Galactic Center”. In: *Astronomy Astrophysics* 376 (Sept. 2001), pp. 853–860. DOI: [10.1051/0004-6361:20010929](https://doi.org/10.1051/0004-6361:20010929). arXiv: [astro-ph/0107497](https://arxiv.org/abs/astro-ph/0107497) [[astro-ph](#)].
- [65] F. De Paolis et al. “The black hole at the galactic center as a possible retro-lens for the S2 orbiting star”. In: *Astronomy Astrophysics* 409 (Oct. 2003), pp. 809–812. DOI: [10.1051/0004-6361:20031137](https://doi.org/10.1051/0004-6361:20031137). arXiv: [astro-ph/0307493](https://arxiv.org/abs/astro-ph/0307493) [[astro-ph](#)].
- [66] C. de Rham. “Massive Gravity”. In: *Living Reviews in Relativity* 17.1, 7 (Dec. 2014), p. 7. DOI: [10.12942/lrr-2014-7](https://doi.org/10.12942/lrr-2014-7). arXiv: [1401.4173](https://arxiv.org/abs/1401.4173) [[hep-th](#)].
- [67] S. Deser. “Gravity from self-interaction redux”. In: *General Relativity and Gravitation* 42.3 (Mar. 2010), pp. 641–646. DOI: [10.1007/s10714-009-0912-9](https://doi.org/10.1007/s10714-009-0912-9). arXiv: [0910.2975](https://arxiv.org/abs/0910.2975) [[gr-qc](#)].
- [68] R. H. Dicke. “Dirac’s Cosmology and Mach’s Principle”. In: *Nature* 192.4801 (Nov. 1961), pp. 440–441. DOI: [10.1038/192440a0](https://doi.org/10.1038/192440a0).
- [69] R. H. Dicke. “Eötvös Experiment and the Gravitational Red Shift”. In: *American Journal of Physics* 28.4 (Apr. 1960), pp. 344–347. DOI: [10.1119/1.1935801](https://doi.org/10.1119/1.1935801).
- [70] S. S. Doeleman et al. “Event-horizon-scale structure in the supermassive black hole candidate at the Galactic Centre”. In: *Nature* 455.7209 (Sept. 2008), pp. 78–80. DOI: [10.1038/nature07245](https://doi.org/10.1038/nature07245). arXiv: [0809.2442](https://arxiv.org/abs/0809.2442) [[astro-ph](#)].
- [71] S. S. Doeleman et al. “Structure of Sagittarius A* at 86 GHz using VLBI Closure Quantities”. In: 121.5 (May 2001), pp. 2610–2617. DOI: [10.1086/320376](https://doi.org/10.1086/320376). arXiv: [astro-ph/0102232](https://arxiv.org/abs/astro-ph/0102232) [[astro-ph](#)].
- [72] A. Eckart and R. Genzel. “Observations of stellar proper motions near the Galactic Centre”. In: *Nature* 383.6599 (Oct. 1996), pp. 415–417. DOI: [10.1038/383415a0](https://doi.org/10.1038/383415a0).
- [73] A. Eckart and R. Genzel. “Stellar proper motions in the central 0.1 PC of the Galaxy”. In: *Monthly Notices of the Royal Astronomical Society* 284.3 (Jan. 1997), pp. 576–598. DOI: [10.1093/mnras/284.3.576](https://doi.org/10.1093/mnras/284.3.576).
- [74] A. Eckart, R. Schödel, and C. Straubmeier. *The black hole at the center of the Milky Way*. World Scientific, 2005.
- [75] A. Eckart et al. “Diffraction Limited Near-Infrared Imaging of the Galactic Center”. In: *The Nuclei of Normal Galaxies: Lessons from the Galactic Center*. Ed. by Reinhard Genzel and Andrew I. Harris. Vol. 445. NATO Advanced Study Institute (ASI) Series C. Jan. 1994, p. 305.
- [76] A. Eckart et al. “Millimeter to X-ray flares from Sagittarius A*”. In: *Astronomy Astrophysics* 537, A52 (Jan. 2012), A52. DOI: [10.1051/0004-6361/201117779](https://doi.org/10.1051/0004-6361/201117779).
- [77] A. Eckart et al. “Monitoring Sagittarius A* in the MIR with the VLT”. In: *Astronomische Nachrichten Supplement* 324.1 (Sept. 2003), pp. 557–561. DOI: [10.1002/asna.200385058](https://doi.org/10.1002/asna.200385058).

- [78] A. Eckart et al. “Stellar Orbits Near Sagittarius A*”. In: *Astronomische Gesellschaft Meeting Abstracts*. Vol. 18. Astronomische Gesellschaft Meeting Abstracts. Jan. 2001, MS 05 08.
- [79] A. Eckart et al. “The flare activity of Sagittarius A*. New coordinated mm to X-ray observations”. In: *Astronomy Astrophysics* 450.2 (May 2006), pp. 535–555. DOI: [10.1051/0004-6361:20054418](https://doi.org/10.1051/0004-6361:20054418). arXiv: [astro-ph/0512440](https://arxiv.org/abs/astro-ph/0512440) [astro-ph].
- [80] A. Eckart et al. “The Milky Way’s Supermassive Black Hole: How Good a Case Is It?” In: *Foundations of Physics* 47.5 (May 2017), pp. 553–624. DOI: [10.1007/s10701-017-0079-2](https://doi.org/10.1007/s10701-017-0079-2). arXiv: [1703.09118](https://arxiv.org/abs/1703.09118) [astro-ph.HE].
- [81] A. Einstein. “Die Grundlage der allgemeinen Relativitätstheorie”. In: *Annalen der Physik* 354.7 (Jan. 1916), pp. 769–822. DOI: [10.1002/andp.19163540702](https://doi.org/10.1002/andp.19163540702).
- [82] A. Einstein. *The meaning of relativity*. Routledge, 2003.
- [83] L. P. Eisenhart. *Riemannian geometry*. Princeton University Press, 2016.
- [84] R. D. Ekers et al. “A full synthesis map of Sgr A at 5 GHz.” In: *Astronomy Astrophysics* 43 (Oct. 1975), pp. 159–166.
- [85] R. D. Ekers et al. “The radio structure of Sgr A.” In: *Astronomy Astrophysics* 122 (June 1983), pp. 143–150.
- [86] Event Horizon Telescope Collaboration et al. “First M87 Event Horizon Telescope Results. I. The Shadow of the Supermassive Black Hole”. In: *The Astrophysical Journal Letters* 875.1, L1 (Apr. 2019), p. L1. DOI: [10.3847/2041-8213/ab0ec7](https://doi.org/10.3847/2041-8213/ab0ec7). arXiv: [1906.11238](https://arxiv.org/abs/1906.11238) [astro-ph.GA].
- [87] Event Horizon Telescope Collaboration et al. “First M87 Event Horizon Telescope Results. III. Data Processing and Calibration”. In: *The Astrophysical Journal Letters* 875.1, L3 (Apr. 2019), p. L3. DOI: [10.3847/2041-8213/ab0c57](https://doi.org/10.3847/2041-8213/ab0c57). arXiv: [1906.11240](https://arxiv.org/abs/1906.11240) [astro-ph.GA].
- [88] Event Horizon Telescope Collaboration et al. “First M87 Event Horizon Telescope Results. IV. Imaging the Central Supermassive Black Hole”. In: *The Astrophysical Journal Letters* 875.1, L4 (Apr. 2019), p. L4. DOI: [10.3847/2041-8213/ab0e85](https://doi.org/10.3847/2041-8213/ab0e85). arXiv: [1906.11241](https://arxiv.org/abs/1906.11241) [astro-ph.GA].
- [89] V. Faraoni and S. Capozziello. *Beyond Einstein gravity: A Survey of gravitational theories for cosmology and astrophysics*. Springer, 2011.
- [90] A. V. Filippenko and A. G. Riess. “Results from the High-z Supernova Search Team.” In: *Physics Report* 307 (Dec. 1998), pp. 31–44. DOI: [10.1016/S0370-1573\(98\)00052-0](https://doi.org/10.1016/S0370-1573(98)00052-0). arXiv: [astro-ph/9807008](https://arxiv.org/abs/astro-ph/9807008) [astro-ph].
- [91] D. Finkelstein. “Past-Future Asymmetry of the Gravitational Field of a Point Particle”. In: *Physical Review* 110.4 (May 1958), pp. 965–967. DOI: [10.1103/PhysRev.110.965](https://doi.org/10.1103/PhysRev.110.965).

- [92] V. Fish et al. “High-Angular-Resolution and High-Sensitivity Science Enabled by Beamformed ALMA”. In: *arXiv e-prints*, arXiv:1309.3519 (Sept. 2013).
- [93] W. J. Forrest et al. “Brackett alpha images of the Galactic center”. In: *The Galactic Center*. Ed. by Donald C. Backer. Vol. 155. American Institute of Physics Conference Series. Apr. 1987, pp. 153–156. DOI: [10.1063/1.36414](https://doi.org/10.1063/1.36414).
- [94] V. Frolov and A. Zelnikov. *Introduction to Black Hole Physics*. Oxford University Press, 2012.
- [95] V. P. Frolov and I. D. Novikov. *Black hole physics : basic concepts and new developments*. Kluwer Academic Publishers, 1998.
- [96] R. Genzel and A. Eckart. “The Galactic Center Black Hole”. In: *The Central Parsecs of the Galaxy*. Ed. by Heino Falcke et al. Vol. 186. Astronomical Society of the Pacific Conference Series. June 1999, p. 3.
- [97] R. Genzel, F. Eisenhauer, and S. Gillessen. “The Galactic Center massive black hole and nuclear star cluster”. In: *Reviews of Modern Physics* 82.4 (Oct. 2010), pp. 3121–3195. DOI: [10.1103/RevModPhys.82.3121](https://doi.org/10.1103/RevModPhys.82.3121). arXiv: [1006.0064](https://arxiv.org/abs/1006.0064) [astro-ph.GA].
- [98] R. Genzel, F. Eisenhauer, and S. Gillessen. “The Galactic Center massive black hole and nuclear star cluster”. In: *Reviews of Modern Physics* 82.4 (Oct. 2010), pp. 3121–3195. DOI: [10.1103/RevModPhys.82.3121](https://doi.org/10.1103/RevModPhys.82.3121). arXiv: [1006.0064](https://arxiv.org/abs/1006.0064) [astro-ph.GA].
- [99] R. Genzel, D. Hollenbach, and C. H. Townes. “The nucleus of our Galaxy”. In: *Reports on Progress in Physics* 57.5 (May 1994), pp. 417–479. DOI: [10.1088/0034-4885/57/5/001](https://doi.org/10.1088/0034-4885/57/5/001).
- [100] R. Genzel and C. H. Townes. “Physical conditions, dynamics, and mass distribution in the center of the galaxy.” In: *Annual Review of Astronomy and Astrophysics* 25 (Jan. 1987), pp. 377–423. DOI: [10.1146/annurev.aa.25.090187.002113](https://doi.org/10.1146/annurev.aa.25.090187.002113).
- [101] R. Genzel et al. “Near-infrared flares from accreting gas around the supermassive black hole at the Galactic Centre”. In: *Nature* 425.6961 (Oct. 2003), pp. 934–937. DOI: [10.1038/nature02065](https://doi.org/10.1038/nature02065). arXiv: [astro-ph/0310821](https://arxiv.org/abs/astro-ph/0310821) [astro-ph].
- [102] R. Genzel et al. “On the nature of the dark mass in the centre of the Milky Way”. In: *Monthly Notices of the Royal Astronomical Society* 291.1 (Oct. 1997), pp. 219–234. DOI: [10.1093/mnras/291.1.219](https://doi.org/10.1093/mnras/291.1.219).
- [103] R. Genzel et al. “Stellar dynamics in the Galactic Centre: proper motions and anisotropy”. In: *Monthly Notices of the Royal Astronomical Society* 317.2 (Sept. 2000), pp. 348–374. DOI: [10.1046/j.1365-8711.2000.03582.x](https://doi.org/10.1046/j.1365-8711.2000.03582.x). arXiv: [astro-ph/0001428](https://arxiv.org/abs/astro-ph/0001428) [astro-ph].
- [104] R. Genzel et al. “The Dark Mass Concentration in the Central Parsec of the Milky Way”. In: *The Astrophysical Journal* 472 (Nov. 1996), p. 153. DOI: [10.1086/178051](https://doi.org/10.1086/178051).

-
- [105] A. M. Ghez et al. “High Proper-Motion Stars in the Vicinity of Sagittarius A*: Evidence for a Supermassive Black Hole at the Center of Our Galaxy”. In: *The Astrophysical Journal* 509.2 (Dec. 1998), pp. 678–686. DOI: [10.1086/306528](https://doi.org/10.1086/306528). arXiv: [astro-ph/9807210](https://arxiv.org/abs/astro-ph/9807210) [[astro-ph](#)].
- [106] A. M. Ghez et al. “Measuring Distance and Properties of the Milky Way’s Central Supermassive Black Hole with Stellar Orbits”. In: *The Astrophysical Journal* 689.2 (Dec. 2008), pp. 1044–1062. DOI: [10.1086/592738](https://doi.org/10.1086/592738). arXiv: [0808.2870](https://arxiv.org/abs/0808.2870) [[astro-ph](#)].
- [107] A. M. Ghez et al. “The accelerations of stars orbiting the Milky Way’s central black hole”. In: *Nature* 407.6802 (Sept. 2000), pp. 349–351. DOI: [10.1038/35030032](https://doi.org/10.1038/35030032). arXiv: [astro-ph/0009339](https://arxiv.org/abs/astro-ph/0009339) [[astro-ph](#)].
- [108] A. M. Ghez et al. “The First Measurement of Spectral Lines in a Short-Period Star Bound to the Galaxy’s Central Black Hole: A Paradox of Youth”. In: *The Astrophysical Journal Letters* 586.2 (Apr. 2003), pp. L127–L131. DOI: [10.1086/374804](https://doi.org/10.1086/374804). arXiv: [astro-ph/0302299](https://arxiv.org/abs/astro-ph/0302299) [[astro-ph](#)].
- [109] A. M. Ghez et al. “Variable Infrared Emission from the Supermassive Black Hole at the Center of the Milky Way”. In: *The Astrophysical Journal Letters* 601.2 (Feb. 2004), pp. L159–L162. DOI: [10.1086/382024](https://doi.org/10.1086/382024). arXiv: [astro-ph/0309076](https://arxiv.org/abs/astro-ph/0309076) [[astro-ph](#)].
- [110] S. Gillessen et al. “An Update on Monitoring Stellar Orbits in the Galactic Center”. In: *The Astrophysical Journal* 837.1, 30 (Mar. 2017), p. 30. DOI: [10.3847/1538-4357/aa5c41](https://doi.org/10.3847/1538-4357/aa5c41). arXiv: [1611.09144](https://arxiv.org/abs/1611.09144) [[astro-ph.GA](#)].
- [111] S. Gillessen et al. “Monitoring Stellar Orbits Around the Massive Black Hole in the Galactic Center”. In: *The Astrophysical Journal* 692.2 (Feb. 2009), pp. 1075–1109. DOI: [10.1088/0004-637X/692/2/1075](https://doi.org/10.1088/0004-637X/692/2/1075). arXiv: [0810.4674](https://arxiv.org/abs/0810.4674) [[astro-ph](#)].
- [112] S. Gillessen et al. “The Orbit of the Star S2 Around Sgr A* from Very Large Telescope and Keck Data”. In: *The Astrophysical Journal Letters* 707.2 (Dec. 2009), pp. L114–L117. DOI: [10.1088/0004-637X/707/2/L114](https://doi.org/10.1088/0004-637X/707/2/L114). arXiv: [0910.3069](https://arxiv.org/abs/0910.3069) [[astro-ph.GA](#)].
- [113] S. Gillessen et al. “The Orbit of the Star S2 Around Sgr A* from Very Large Telescope and Keck Data”. In: *The Astrophysical Journal Letters* 707.2 (Dec. 2009), pp. L114–L117. DOI: [10.1088/0004-637X/707/2/L114](https://doi.org/10.1088/0004-637X/707/2/L114). arXiv: [0910.3069](https://arxiv.org/abs/0910.3069) [[astro-ph.GA](#)].
- [114] Gravity Collaboration et al. “Detection of faint stars near Sagittarius A* with GRAVITY”. In: *Astronomy Astrophysics* 645, A127 (Jan. 2021), A127. DOI: [10.1051/0004-6361/202039544](https://doi.org/10.1051/0004-6361/202039544). arXiv: [2011.03058](https://arxiv.org/abs/2011.03058) [[astro-ph.GA](#)].
- [115] Gravity Collaboration et al. “Detection of the gravitational redshift in the orbit of the star S2 near the Galactic centre massive black hole”. In: *Astronomy Astrophysics* 615, L15 (July 2018), p. L15. DOI: [10.1051/0004-6361/201833718](https://doi.org/10.1051/0004-6361/201833718). arXiv: [1807.09409](https://arxiv.org/abs/1807.09409) [[astro-ph.GA](#)].

- [116] Gravity Collaboration et al. “Detection of the Schwarzschild precession in the orbit of the star S2 near the Galactic centre massive black hole”. In: *Astronomy Astrophysics* 636, L5 (Apr. 2020), p. L5. DOI: [10.1051/0004-6361/202037813](https://doi.org/10.1051/0004-6361/202037813). arXiv: [2004.07187](https://arxiv.org/abs/2004.07187) [[astro-ph.GA](#)].
- [117] Gravity Collaboration et al. “Detection of the Schwarzschild precession in the orbit of the star S2 near the Galactic centre massive black hole”. In: *Astronomy Astrophysics* 636, L5 (Apr. 2020), p. L5. DOI: [10.1051/0004-6361/202037813](https://doi.org/10.1051/0004-6361/202037813). arXiv: [2004.07187](https://arxiv.org/abs/2004.07187) [[astro-ph.GA](#)].
- [118] Gravity Collaboration et al. “First light for GRAVITY: Phase referencing optical interferometry for the Very Large Telescope Interferometer”. In: *Astronomy Astrophysics* 602, A94 (June 2017), A94. DOI: [10.1051/0004-6361/201730838](https://doi.org/10.1051/0004-6361/201730838). arXiv: [1705.02345](https://arxiv.org/abs/1705.02345) [[astro-ph.IM](#)].
- [119] K. Gültekin et al. “The Fundamental Plane of Accretion onto Black Holes with Dynamical Masses”. In: *The Astrophysical Journal* 706.1 (Nov. 2009), pp. 404–416. DOI: [10.1088/0004-637X/706/1/404](https://doi.org/10.1088/0004-637X/706/1/404). arXiv: [0906.3285](https://arxiv.org/abs/0906.3285) [[astro-ph.HE](#)].
- [120] K. Gültekin et al. “The M- σ and M-L Relations in Galactic Bulges, and Determinations of Their Intrinsic Scatter”. In: *The Astrophysical Journal* 698.1 (June 2009), pp. 198–221. DOI: [10.1088/0004-637X/698/1/198](https://doi.org/10.1088/0004-637X/698/1/198). arXiv: [0903.4897](https://arxiv.org/abs/0903.4897) [[astro-ph.GA](#)].
- [121] O. K. Guseinov and Y. B. Zel’dovich. “Collapsed Stars in Binary Systems”. In: *Astronomiceskij Zhurnal* 43 (Jan. 1966), p. 313.
- [122] A. H. Guth. “Inflationary universe: A possible solution to the horizon and flatness problems”. In: *Physical Review D* 23.2 (Jan. 1981), pp. 347–356. DOI: [10.1103/PhysRevD.23.347](https://doi.org/10.1103/PhysRevD.23.347).
- [123] M. Habibi et al. “Twelve Years of Spectroscopic Monitoring in the Galactic Center: The Closest Look at S-stars near the Black Hole”. In: *The Astrophysical Journal* 847.2, 120 (Oct. 2017), p. 120. DOI: [10.3847/1538-4357/aa876f](https://doi.org/10.3847/1538-4357/aa876f). arXiv: [1708.06353](https://arxiv.org/abs/1708.06353) [[astro-ph.SR](#)].
- [124] J. W. Haller et al. “Stellar Kinematics and the Black Hole in the Galactic Center”. In: *The Astrophysical Journal* 456 (Jan. 1996), p. 194. DOI: [10.1086/176640](https://doi.org/10.1086/176640).
- [125] S. W. Hawking and G. F. R. Ellis. *The large-scale structure of space-time*. Cambridge University Press, 1973.
- [126] A. Hees et al. “Testing General Relativity with Stellar Orbits around the Supermassive Black Hole in Our Galactic Center”. In: *Physical Review Letters* 118.21, 211101 (May 2017), p. 211101. DOI: [10.1103/PhysRevLett.118.211101](https://doi.org/10.1103/PhysRevLett.118.211101). arXiv: [1705.07902](https://arxiv.org/abs/1705.07902) [[astro-ph.GA](#)].

- [127] T. M. Herbst et al. “Infrared Imaging Spectroscopy of the Galactic Center: Distribution and Motion of the Ionized Gas”. In: 105 (Mar. 1993), p. 956. DOI: [10.1086/116484](https://doi.org/10.1086/116484).
- [128] G. Hinshaw et al. “First-Year Wilkinson Microwave Anisotropy Probe (WMAP) Observations: The Angular Power Spectrum”. In: 148.1 (Sept. 2003), pp. 135–159. DOI: [10.1086/377225](https://doi.org/10.1086/377225). arXiv: [astro-ph/0302217](https://arxiv.org/abs/astro-ph/0302217) [astro-ph].
- [129] P. Hořava. “Quantum gravity at a Lifshitz point”. In: *Physical Review D* 79.8, 084008 (Apr. 2009), p. 084008. DOI: [10.1103/PhysRevD.79.084008](https://doi.org/10.1103/PhysRevD.79.084008). arXiv: [0901.3775](https://arxiv.org/abs/0901.3775) [hep-th].
- [130] L. Iorio. “Constraints on the range λ of Yukawa-like modifications to the Newtonian inverse-square law of gravitation from Solar System planetary motions”. In: *Journal of High Energy Physics* 2007.10, 041 (Oct. 2007), p. 041. DOI: [10.1088/1126-6708/2007/10/041](https://doi.org/10.1088/1126-6708/2007/10/041). arXiv: [0708.1080](https://arxiv.org/abs/0708.1080) [gr-qc].
- [131] C. J. Isham, R. Penrose, and D. W. Sciama. *Quantum gravity 2: a second Oxford symposium*. Oxford University Press, USA, 1981.
- [132] T. Johannsen et al. “Masses of nearby Supermassive Black Holes with Very Long Baseline Interferometry”. In: *The Astrophysical Journal* 758.1, 30 (Oct. 2012), p. 30. DOI: [10.1088/0004-637X/758/1/30](https://doi.org/10.1088/0004-637X/758/1/30). arXiv: [1201.0758](https://arxiv.org/abs/1201.0758) [astro-ph.GA].
- [133] R. A. Knop et al. “New Constraints on Ω_M , Ω_Λ , and w from an Independent Set of 11 High-Redshift Supernovae Observed with the Hubble Space Telescope”. In: *The Astrophysical Journal* 598.1 (Nov. 2003), pp. 102–137. DOI: [10.1086/378560](https://doi.org/10.1086/378560). arXiv: [astro-ph/0309368](https://arxiv.org/abs/astro-ph/0309368) [astro-ph].
- [134] J. Kormendy. “The Stellar-Dynamical Search for Supermassive Black Holes in Galactic Nuclei”. In: *Coevolution of Black Holes and Galaxies*. Ed. by Luis C. Ho. Jan. 2004, p. 1. arXiv: [astro-ph/0306353](https://arxiv.org/abs/astro-ph/0306353) [astro-ph].
- [135] J. Kormendy and L. C. Ho. “Coevolution (Or Not) of Supermassive Black Holes and Host Galaxies”. In: *Annual Review of Astronomy and Astrophysics* 51.1 (Aug. 2013), pp. 511–653. DOI: [10.1146/annurev-astro-082708-101811](https://doi.org/10.1146/annurev-astro-082708-101811). arXiv: [1304.7762](https://arxiv.org/abs/1304.7762) [astro-ph.CO].
- [136] J. Kormendy and D. Richstone. “Inward Bound—The Search For Supermassive Black Holes In Galactic Nuclei”. In: *Annual Review of Astronomy and Astrophysics* 33 (Jan. 1995), p. 581. DOI: [10.1146/annurev.aa.33.090195.003053](https://doi.org/10.1146/annurev.aa.33.090195.003053).
- [137] K Koyama et al. “ASCA View of Our Galactic Center: Remains of Past Activities in X-Rays?” In: 48 (Apr. 1996), pp. 249–255. DOI: [10.1093/pasj/48.2.249](https://doi.org/10.1093/pasj/48.2.249).
- [138] A. Krabbe et al. “A Cluster of He i Emission-Line Stars in the Galactic Center”. In: *The Astrophysical Journal Letters* 382 (Nov. 1991), p. L19. DOI: [10.1086/186204](https://doi.org/10.1086/186204).

- [139] M. Kramer et al. “Strong-field tests of gravity using pulsars and black holes”. In: 48.11-12 (Dec. 2004), pp. 993–1002. DOI: [10.1016/j.newar.2004.09.020](https://doi.org/10.1016/j.newar.2004.09.020). arXiv: [astro-ph/0409379](https://arxiv.org/abs/astro-ph/0409379) [[astro-ph](#)].
- [140] T. P. Krichbaum et al. “First 43 GHz VLBI detection of the compact source Sgr A in the Galactic Center.” In: *Astronomy Astrophysics* 274 (July 1993), pp. L37–L40.
- [141] T. P. Krichbaum et al. “VLBI observations of the galactic center source Sgr A* at 86 GHz and 215 GHz”. In: *Astronomy Astrophysics* 335 (July 1998), pp. L106–L110.
- [142] J. H. Lacy, C. H. Townes, and D. J. Hollenbach. “The nature of the central parsec of the Galaxy”. In: *The Astrophysical Journal* 262 (Nov. 1982), pp. 120–134. DOI: [10.1086/160402](https://doi.org/10.1086/160402).
- [143] J. H. Lacy et al. “Observations of the motion and distribution of the ionized gas in the central parsec of the Galaxy. II.” In: *The Astrophysical Journal* 241 (Oct. 1980), pp. 132–146. DOI: [10.1086/158324](https://doi.org/10.1086/158324).
- [144] H. M. Latvakoski et al. “Kuiper Widefield Infrared Camera Far-Infrared Imaging of the Galactic Center: The Circumnuclear Disk Revealed”. In: *The Astrophysical Journal* 511.2 (Feb. 1999), pp. 761–773. DOI: [10.1086/306689](https://doi.org/10.1086/306689).
- [145] U. J. Le Verrier. “Theorie du mouvement de Mercure”. In: *Annales de l’Observatoire de Paris* 5 (Jan. 1859), p. 1.
- [146] R. Lenzen et al. “CONICA: the high-resolution near-infrared camera for the ESO VLT”. In: *Infrared Astronomical Instrumentation*. Ed. by Albert M. Fowler. Vol. 3354. Society of Photo-Optical Instrumentation Engineers (SPIE) Conference Series. Aug. 1998, pp. 606–614. DOI: [10.1117/12.317287](https://doi.org/10.1117/12.317287).
- [147] T. Levi-Civita. *The absolute differential calculus (calculus of tensors)*. Courier Corporation, 1977.
- [148] S. Libonate et al. “Near-Infrared Spectra of Compact Stellar Wind Sources at the Galactic Center”. In: *The Astrophysical Journal* 439 (Jan. 1995), p. 202. DOI: [10.1086/175165](https://doi.org/10.1086/175165).
- [149] K. Liu et al. “Prospects for Probing the Spacetime of Sgr A* with Pulsars”. In: *The Astrophysical Journal* 747.1, 1 (Mar. 2012), p. 1. DOI: [10.1088/0004-637X/747/1/1](https://doi.org/10.1088/0004-637X/747/1/1). arXiv: [1112.2151](https://arxiv.org/abs/1112.2151) [[astro-ph.HE](#)].
- [150] K. Lo et al. “High-resolution VLBA imaging of the radio source Sgr A* at the Galactic Centre”. In: *Nature* 362 (Apr. 1993). DOI: [10.1038/362038a0](https://doi.org/10.1038/362038a0).
- [151] K. Y. Lo and M. J. Claussen. “High-resolution observations of ionized gas in central 3 parsecs of the Galaxy: possible evidence for infall”. In: *Nature* 306.5944 (Dec. 1983), pp. 647–651. DOI: [10.1038/306647a0](https://doi.org/10.1038/306647a0).

- [152] K. Y. Lo et al. “Intrinsic Size of Sagittarius A*: 72 Schwarzschild Radii”. In: *The Astrophysical Journal Letters* 508.1 (Nov. 1998), pp. L61–L64. DOI: [10.1086/311726](https://doi.org/10.1086/311726). arXiv: [astro-ph/9809222](https://arxiv.org/abs/astro-ph/9809222) [[astro-ph](#)].
- [153] K. Y. Lo et al. “On the size of the galactic centre compact radio source: diameter <20 AU”. In: *Nature* 315.6015 (May 1985), pp. 124–126. DOI: [10.1038/315124a0](https://doi.org/10.1038/315124a0).
- [154] K. Y. Lo et al. “VLBI observations of the compact radio source in the center of the Galaxy.” In: *The Astrophysical Journal Letters* 202 (Dec. 1975), pp. L63–L65. DOI: [10.1086/181982](https://doi.org/10.1086/181982).
- [155] D. Lovelock. “The Einstein Tensor and Its Generalizations”. In: *Journal of Mathematical Physics* 12.3 (Mar. 1971), pp. 498–501. DOI: [10.1063/1.1665613](https://doi.org/10.1063/1.1665613).
- [156] D. Lovelock. “The Four-Dimensionality of Space and the Einstein Tensor”. In: *Journal of Mathematical Physics* 13.6 (June 1972), pp. 874–876. DOI: [10.1063/1.1666069](https://doi.org/10.1063/1.1666069).
- [157] D. Lynden-Bell. “Galactic Nuclei as Collapsed Old Quasars”. In: *Nature* 223.5207 (Aug. 1969), pp. 690–694. DOI: [10.1038/223690a0](https://doi.org/10.1038/223690a0).
- [158] E. Maoz. “Dynamical constraints on alternatives to massive black holes in galactic nuclei”. In: *The Central Regions of the Galaxy and Galaxies*. Ed. by Yoshiaki Sofue. Vol. 184. Jan. 1998, p. 447.
- [159] F. Martins et al. “On the Nature of the Fast-Moving Star S2 in the Galactic Center”. In: *The Astrophysical Journal Letters* 672.2 (Jan. 2008), p. L119. DOI: [10.1086/526768](https://doi.org/10.1086/526768). arXiv: [0711.3344](https://arxiv.org/abs/0711.3344) [[astro-ph](#)].
- [160] F. Martins et al. “Stellar and wind properties of massive stars in the central parsec of the Galaxy”. In: *Astronomy Astrophysics* 468.1 (June 2007), pp. 233–254. DOI: [10.1051/0004-6361:20066688](https://doi.org/10.1051/0004-6361:20066688). arXiv: [astro-ph/0703211](https://arxiv.org/abs/astro-ph/0703211) [[astro-ph](#)].
- [161] M. T. McGinn et al. “Stellar Kinematics in the Galactic Center”. In: *The Astrophysical Journal* 338 (Mar. 1989), p. 824. DOI: [10.1086/167239](https://doi.org/10.1086/167239).
- [162] F. Melia and H. Falcke. “The Supermassive Black Hole at the Galactic Center”. In: *Annual Review of Astronomy and Astrophysics* 39 (Jan. 2001), pp. 309–352. DOI: [10.1146/annurev.astro.39.1.309](https://doi.org/10.1146/annurev.astro.39.1.309). arXiv: [astro-ph/0106162](https://arxiv.org/abs/astro-ph/0106162) [[astro-ph](#)].
- [163] L. Meyer et al. “The Shortest-Known-Period Star Orbiting Our Galaxy’s Supermassive Black Hole”. In: *Science* 338.6103 (Oct. 2012), p. 84. DOI: [10.1126/science.1225506](https://doi.org/10.1126/science.1225506). arXiv: [1210.1294](https://arxiv.org/abs/1210.1294) [[astro-ph.GA](#)].
- [164] P. G. Mezger, W. J. Duschl, and R. Zylka. “The Galactic Center: a laboratory for AGN?” In: *Astronomy and Astrophysics Reviews* 7.4 (Jan. 1996), pp. 289–388. DOI: [10.1007/s001590050007](https://doi.org/10.1007/s001590050007).

- [165] E. W. Mielke and F. E. Schunck. “Boson and Axion Stars”. In: *The Ninth Marcel Grossmann Meeting*. Ed. by Vahe G. Gurzadyan, Robert T. Jantzen, and Remo Ruffini. Dec. 2002, pp. 581–591. DOI: [10.1142/9789812777386_0041](https://doi.org/10.1142/9789812777386_0041).
- [166] E. W. Mielke and F. E. Schunck. “Boson stars: alternatives to primordial black holes?” In: *Nuclear Physics B* 1 (Jan. 2000), pp. 185–203. DOI: [10.1016/S0550-3213\(99\)00492-7](https://doi.org/10.1016/S0550-3213(99)00492-7). arXiv: [gr-qc/0001061](https://arxiv.org/abs/gr-qc/0001061) [[gr-qc](#)].
- [167] C. W. Misner, K. S. Thorne, and J. A. Wheeler. *Gravitation*. Princeton University Press, 1973.
- [168] Y. Mizuno et al. “Testing Theories of Gravity via Black Hole Shadows in Sgr A*”. In: *New Horizons in Galactic Center Astronomy and Beyond*. Ed. by M. Tsuboi and T. Oka. Vol. 528. Astronomical Society of the Pacific Conference Series. July 2021, p. 255.
- [169] J. W. Moffat. “A Modified Gravity and its Consequences for the Solar System, Astrophysics and Cosmology”. In: *International Journal Modern Physics D* 16 (2008), pp. 2075–2090. DOI: [10.1142/S0218271807011577](https://doi.org/10.1142/S0218271807011577). arXiv: [0608074](https://arxiv.org/abs/0608074) [[gr-qc](#)].
- [170] C. Møller. *The theory of relativity*. Oxford, Clarendon Press, 1972.
- [171] E. Mossoux et al. “Study of the X-ray activity of Sagittarius A* during the 2011 XMM-Newton campaign”. In: *Astronomy Astrophysics* 573, A46 (Jan. 2015), A46. DOI: [10.1051/0004-6361/201424682](https://doi.org/10.1051/0004-6361/201424682). arXiv: [1409.6452](https://arxiv.org/abs/1409.6452) [[astro-ph.HE](#)].
- [172] F. Najarro et al. “The nature of the brightest galactic center HeI emission line star”. In: *Astronomy Astrophysics* 285 (May 1994), pp. 573–584.
- [173] N. R. Napolitano et al. “Testing Yukawa-like Potentials from f(R)-gravity in Elliptical Galaxies”. In: *The Astrophysical Journal* 748.2, 87 (Apr. 2012), p. 87. DOI: [10.1088/0004-637X/748/2/87](https://doi.org/10.1088/0004-637X/748/2/87). arXiv: [1201.3363](https://arxiv.org/abs/1201.3363) [[astro-ph.CO](#)].
- [174] J. Neilsen et al. “The X-Ray Flux Distribution of Sagittarius A* as Seen by Chandra”. In: *The Astrophysical Journal* 799.2, 199 (Feb. 2015), p. 199. DOI: [10.1088/0004-637X/799/2/199](https://doi.org/10.1088/0004-637X/799/2/199). arXiv: [1412.3106](https://arxiv.org/abs/1412.3106) [[astro-ph.HE](#)].
- [175] I. Newton. *Philosophiae Naturalis Principia Mathematica. Auctore Js. Newton*. 1687. DOI: [10.3931/e-rara-440](https://doi.org/10.3931/e-rara-440).
- [176] S. Nojiri, S. D. Odintsov, and S. Tsujikawa. “Properties of singularities in the (phantom) dark energy universe”. In: *Physical Review D* 71.6, 063004 (Mar. 2005), p. 063004. DOI: [10.1103/PhysRevD.71.063004](https://doi.org/10.1103/PhysRevD.71.063004). arXiv: [hep-th/0501025](https://arxiv.org/abs/hep-th/0501025) [[hep-th](#)].
- [177] G. Nordström. “On the Energy of the Gravitation field in Einstein’s Theory”. In: *Koninklijke Nederlandse Akademie van Wetenschappen Proceedings Series B Physical Sciences* 20 (Jan. 1918), pp. 1238–1245.

- [178] G. G. Nyambuya. “Azimuthally symmetric theory of gravitation - II. On the perihelion precession of solar planetary orbits”. In: *Monthly Notices of the Royal Astronomical Society* 451.3 (Aug. 2015), pp. 3034–3043. DOI: [10.1093/mnras/stv1100](https://doi.org/10.1093/mnras/stv1100).
- [179] J. H. Oort. “The force exerted by the stellar system in the direction perpendicular to the galactic plane and some related problems”. In: 6 (Aug. 1932), p. 249.
- [180] J. R. Oppenheimer and H. Snyder. “On Continued Gravitational Contraction”. In: *Physical Review* 56.5 (Sept. 1939), pp. 455–459. DOI: [10.1103/PhysRev.56.455](https://doi.org/10.1103/PhysRev.56.455).
- [181] J. R. Oppenheimer and G. M. Volkoff. “On Massive Neutron Cores”. In: *Physical Review* 55.4 (Feb. 1939), pp. 374–381. DOI: [10.1103/PhysRev.55.374](https://doi.org/10.1103/PhysRev.55.374).
- [182] T. Padmanabhan. “Cosmological constant—the weight of the vacuum”. In: *Physics Report* 380.5-6 (July 2003), pp. 235–320. DOI: [10.1016/S0370-1573\(03\)00120-0](https://doi.org/10.1016/S0370-1573(03)00120-0). arXiv: [hep-th/0212290](https://arxiv.org/abs/hep-th/0212290) [hep-th].
- [183] P. Pani, T. P. Sotiriou, and D. Vernieri. “Gravity with auxiliary fields”. In: *Physical Review D* 88.12 (2013), p. 121502.
- [184] T. Paumard, J. P. Maillard, and S. Stolovy. “New results on the Galactic Center Helium stars”. In: *Astronomische Nachrichten Supplement* 324.1 (Sept. 2003), pp. 303–307. DOI: [10.1002/asna.200385038](https://doi.org/10.1002/asna.200385038).
- [185] F. Peissker, A. Eckart, and M. Parsa. “S62 on a 9.9 yr Orbit around SgrA*”. In: *The Astrophysical Journal* 889.1, 61 (Jan. 2020), p. 61. DOI: [10.3847/1538-4357/ab5afd](https://doi.org/10.3847/1538-4357/ab5afd). arXiv: [2002.02341](https://arxiv.org/abs/2002.02341) [astro-ph.GA].
- [186] F. Peissker et al. “S62 and S4711: Indications of a Population of Faint Fast-moving Stars inside the S2 Orbit—S4711 on a 7.6 yr Orbit around Sgr A*”. In: *The Astrophysical Journal* 899.1, 50 (Aug. 2020), p. 50. DOI: [10.3847/1538-4357/ab9c1c](https://doi.org/10.3847/1538-4357/ab9c1c). arXiv: [2008.04764](https://arxiv.org/abs/2008.04764) [astro-ph.GA].
- [187] R. Penrose. “Gravitational Collapse and Space-Time Singularities”. In: *Physical Review Letters* 14.3 (Jan. 1965), pp. 57–59. DOI: [10.1103/PhysRevLett.14.57](https://doi.org/10.1103/PhysRevLett.14.57).
- [188] S. Perlmutter et al. “Measurements of Ω and Λ from 42 High-Redshift Supernovae”. In: *The Astrophysical Journal* 517.2 (June 1999), pp. 565–586. DOI: [10.1086/307221](https://doi.org/10.1086/307221). arXiv: [astro-ph/9812133](https://arxiv.org/abs/astro-ph/9812133) [astro-ph].
- [189] E. Pfahl and A. Loeb. “Probing the Spacetime around Sagittarius A* with Radio Pulsars”. In: *The Astrophysical Journal* 615.1 (Nov. 2004), pp. 253–258. DOI: [10.1086/423975](https://doi.org/10.1086/423975). arXiv: [astro-ph/0309744](https://arxiv.org/abs/astro-ph/0309744) [astro-ph].
- [190] E. V. Pitjeva and N. P. Pitjev. “Relativistic effects and dark matter in the Solar system from observations of planets and spacecraft”. In: *Monthly Notices of the Royal Astronomical Society* 432.4 (July 2013), pp. 3431–3437. DOI: [10.1093/mnras/stt695](https://doi.org/10.1093/mnras/stt695). arXiv: [1306.3043](https://arxiv.org/abs/1306.3043) [astro-ph.EP].

- [191] P. M. Plewa et al. “Pinpointing the near-infrared location of Sgr A* by correcting optical distortion in the NACO imager”. In: *Monthly Notices of the Royal Astronomical Society* 453.3 (Nov. 2015), pp. 3234–3244. DOI: [10.1093/mnras/stv1910](https://doi.org/10.1093/mnras/stv1910). arXiv: [1509.01941](https://arxiv.org/abs/1509.01941) [astro-ph.GA].
- [192] D. Porquet et al. “X-ray hiccups from Sagittarius A* observed by XMM-Newton. The second brightest flare and three moderate flares caught in half a day”. In: *Astronomy Astrophysics* 488.2 (Sept. 2008), pp. 549–557. DOI: [10.1051/0004-6361:200809986](https://doi.org/10.1051/0004-6361:200809986). arXiv: [0806.4088](https://arxiv.org/abs/0806.4088) [astro-ph].
- [193] P. Predehl and J. Truemper. “ROSAT observation of the Sgr A region”. In: *Astronomy Astrophysics* 290 (Oct. 1994), pp. L29–L32.
- [194] D. Psaltis. “Probes and Tests of Strong-Field Gravity with Observations in the Electromagnetic Spectrum”. In: *Living Reviews in Relativity* 11.1, 9 (Nov. 2008), p. 9. DOI: [10.12942/lrr-2008-9](https://doi.org/10.12942/lrr-2008-9). arXiv: [0806.1531](https://arxiv.org/abs/0806.1531) [astro-ph].
- [195] D. Psaltis. “Two approaches to testing general relativity in the strong-field regime”. In: *Journal of Physics Conference Series*. Vol. 189. Journal of Physics Conference Series. Oct. 2009, p. 012033. DOI: [10.1088/1742-6596/189/1/012033](https://doi.org/10.1088/1742-6596/189/1/012033). arXiv: [0907.2746](https://arxiv.org/abs/0907.2746) [astro-ph.HE].
- [196] D. Psaltis, N. Wex, and M. Kramer. “A Quantitative Test of the No-hair Theorem with Sgr A* Using Stars, Pulsars, and the Event Horizon Telescope”. In: *The Astrophysical Journal* 818.2, 121 (Feb. 2016), p. 121. DOI: [10.3847/0004-637X/818/2/121](https://doi.org/10.3847/0004-637X/818/2/121). arXiv: [1510.00394](https://arxiv.org/abs/1510.00394) [astro-ph.HE].
- [197] M. J. Rees. “The Compact source at the Galactic Center”. In: *The Galactic Center*. Ed. by G. R. Riegler and R. D. Blandford. Vol. 83. American Institute of Physics Conference Series. Jan. 1982, pp. 166–176. DOI: [10.1063/1.33482](https://doi.org/10.1063/1.33482).
- [198] G. H. Rieke and M. J. Rieke. “Stellar Velocities and the Mass Distribution in the Galactic Center”. In: *The Astrophysical Journal Letters* 330 (July 1988), p. L33. DOI: [10.1086/185199](https://doi.org/10.1086/185199).
- [199] D. A. Roberts, F. Yusef-Zadeh, and W. M. Goss. “Kinematics of the Ionized Gas in Sagittarius A West: Mass Estimates of the Inner 0.13 Parsecs of the Galaxy”. In: *The Astrophysical Journal* 459 (Mar. 1996), p. 627. DOI: [10.1086/176927](https://doi.org/10.1086/176927).
- [200] A. E. E. Rogers et al. “Small-Scale Structure and Position of Sagittarius A* from VLBI at 3 Millimeter Wavelength”. In: *The Astrophysical Journal Letters* 434 (Oct. 1994), p. L59. DOI: [10.1086/187574](https://doi.org/10.1086/187574).
- [201] G. Rousset et al. “Design of the Nasmyth adaptive optics system (NAOS) of the VLT”. In: *Adaptive Optical System Technologies*. Ed. by Domenico Bonaccini and Robert K. Tyson. Vol. 3353. Society of Photo-Optical Instrumentation Engineers (SPIE) Conference Series. Sept. 1998, pp. 508–516. DOI: [10.1117/12.321686](https://doi.org/10.1117/12.321686).

- [202] C. Rubano and P. Scudellaro. “Variable G and Λ : Scalar-tensor versus RG-improved cosmology”. In: *General Relativity and Gravitation* 37 (2005), pp. 521–539. DOI: [10.1007/s10714-005-0040-0](https://doi.org/10.1007/s10714-005-0040-0). arXiv: [0410260](https://arxiv.org/abs/0410260) [[astro-ph](#)].
- [203] G. F. Rubilar and A. Eckart. “Periastron shifts of stellar orbits near the Galactic Center”. In: *Astronomy Astrophysics* 374 (July 2001), pp. 95–104. DOI: [10.1051/0004-6361:20010640](https://doi.org/10.1051/0004-6361:20010640).
- [204] T. D. Saini et al. “Reconstructing the Cosmic Equation of State from Supernova Distances”. In: *Physical Review Letters* 85.6 (Aug. 2000), pp. 1162–1165. DOI: [10.1103/PhysRevLett.85.1162](https://doi.org/10.1103/PhysRevLett.85.1162). arXiv: [astro-ph/9910231](https://arxiv.org/abs/astro-ph/9910231) [[astro-ph](#)].
- [205] E. E. Salpeter. “Accretion of Interstellar Matter by Massive Objects.” In: *The Astrophysical Journal* 140 (Aug. 1964), pp. 796–800. DOI: [10.1086/147973](https://doi.org/10.1086/147973).
- [206] L. I. Schiff. “On Experimental Tests of the General Theory of Relativity”. In: *American Journal of Physics* 28.4 (Apr. 1960), pp. 340–343. DOI: [10.1119/1.1935800](https://doi.org/10.1119/1.1935800).
- [207] M. Schmidt. “3C 273 : A Star-Like Object with Large Red-Shift”. In: *Nature* 197.4872 (Mar. 1963), p. 1040. DOI: [10.1038/1971040a0](https://doi.org/10.1038/1971040a0).
- [208] R. Schödel, D. Merritt, and A. Eckart. “The nuclear star cluster of the Milky Way: proper motions and mass”. In: *Astronomy Astrophysics* 502.1 (July 2009), pp. 91–111. DOI: [10.1051/0004-6361/200810922](https://doi.org/10.1051/0004-6361/200810922). arXiv: [0902.3892](https://arxiv.org/abs/0902.3892) [[astro-ph.GA](#)].
- [209] R. Schödel et al. “A star in a 15.2-year orbit around the supermassive black hole at the centre of the Milky Way”. In: *Nature* 419.6908 (Oct. 2002), pp. 694–696. DOI: [10.1038/nature01121](https://doi.org/10.1038/nature01121). arXiv: [astro-ph/0210426](https://arxiv.org/abs/astro-ph/0210426) [[astro-ph](#)].
- [210] R. Schödel et al. “Stellar Dynamics in the Central Arcsecond of Our Galaxy”. In: *The Astrophysical Journal* 596.2 (Oct. 2003), pp. 1015–1034. DOI: [10.1086/378122](https://doi.org/10.1086/378122). arXiv: [astro-ph/0306214](https://arxiv.org/abs/astro-ph/0306214) [[astro-ph](#)].
- [211] K. Schwarzschild. “On the Gravitational Field of a Mass Point According to Einstein’s Theory”. In: *Abh. Konigl. Preuss. Akad. Wissenschaften Jahre 1906,92, Berlin,1907* 1916 (Jan.1916), pp. 189–196.
- [212] K. Sellgren et al. “Velocity Dispersion and the Stellar Population in the Central 1.2 Parsecs of the Galaxy”. In: *The Astrophysical Journal* 359 (Aug. 1990), p. 112. DOI: [10.1086/169039](https://doi.org/10.1086/169039).
- [213] E. Serabyn et al. “High-Resolution [Ne II] Observations of the Ionized Filaments in the Galactic Center”. In: *The Astrophysical Journal* 326 (Mar. 1988), p. 171. DOI: [10.1086/166078](https://doi.org/10.1086/166078).
- [214] Z. Q. Shen et al. “A size of ~ 1 AU for the radio source Sgr A* at the centre of the Milky Way”. In: *Nature* 438.7064 (Nov. 2005), pp. 62–64. DOI: [10.1038/nature04205](https://doi.org/10.1038/nature04205). arXiv: [astro-ph/0512515](https://arxiv.org/abs/astro-ph/0512515) [[astro-ph](#)].

- [215] L. Sidoli and S. Mereghetti. “The X-ray diffuse emission from the Galactic Center”. In: *Astronomy Astrophysics* 349 (Sept. 1999), pp. L49–L52. arXiv: [astro-ph/9908164](#) [[astro-ph](#)].
- [216] W. M. Smart. “On the derivation of the elements of a visual binary orbit by Kowalsky’s method”. In: *Monthly Notices of the Royal Astronomical Society* 90 (Mar. 1930), pp. 534–538. DOI: [10.1093/mnras/90.5.534](#).
- [217] D. N. Spergel et al. “First-Year Wilkinson Microwave Anisotropy Probe (WMAP) Observations: Determination of Cosmological Parameters”. In: 148.1 (Sept. 2003), pp. 175–194. DOI: [10.1086/377226](#). arXiv: [astro-ph/0302209](#) [[astro-ph](#)].
- [218] D. N. Spergel et al. “Three-Year Wilkinson Microwave Anisotropy Probe (WMAP) Observations: Implications for Cosmology”. In: 170.2 (June 2007), pp. 377–408. DOI: [10.1086/513700](#). arXiv: [astro-ph/0603449](#) [[astro-ph](#)].
- [219] L. Staveley-Smith and T. Oosterloo. “HI Science with the Square Kilometre Array”. In: *Advancing Astrophysics with the Square Kilometre Array (AASKA14)*. Apr. 2015, p. 167. arXiv: [1506.04473](#) [[astro-ph.GA](#)].
- [220] R. Stompor et al. “Cosmological Implications of the MAXIMA-1 High-Resolution Cosmic Microwave Background Anisotropy Measurement”. In: *The Astrophysical Journal Letters* 561.1 (Nov. 2001), pp. L7–L10. DOI: [10.1086/324438](#). arXiv: [astro-ph/0105062](#) [[astro-ph](#)].
- [221] P. Tambllyn and G. H. Rieke. “IRS 16: The Galaxy’s Central Wimp?” In: *The Astrophysical Journal* 414 (Sept. 1993), p. 573. DOI: [10.1086/173104](#).
- [222] P. Tambllyn et al. “The Peculiar Population of Hot Stars at the Galactic Center”. In: *The Astrophysical Journal* 456 (Jan. 1996), p. 206. DOI: [10.1086/176641](#).
- [223] K. S. Thorne, R. H. Price, and D. A. MacDonald. *Black holes: The membrane paradigm*. Yale University Press, 1986.
- [224] J. L. Tonry et al. “Cosmological Results from High-z Supernovae”. In: *The Astrophysical Journal* 594.1 (Sept. 2003), pp. 1–24. DOI: [10.1086/376865](#). arXiv: [astro-ph/0305008](#) [[astro-ph](#)].
- [225] D. F. Torres, S. Capozziello, and G. Lambiase. “Supermassive boson star at the galactic center?” In: *Physical Review D* 62.10, 104012 (Nov. 2000), p. 104012. DOI: [10.1103/PhysRevD.62.104012](#). arXiv: [astro-ph/0004064](#) [[astro-ph](#)].
- [226] D. F. Torres, S. Capozziello, and G. Lambiase. “Supermassive boson stars: Prospects for observational detection”. In: *9th Marcel Grossmann Meeting on Recent Developments in Theoretical and Experimental General Relativity, Gravitation and Relativistic Field Theories (MG 9)*. July 2000. arXiv: [gr-qc/0012031](#).

- [227] S. Trippe et al. “Kinematics of the Old Stellar Population at the Galactic Centre”. In: *The Galactic Center: a Window to the Nuclear Environment of Disk Galaxies*. Ed. by M. R. Morris, Q. D. Wang, and F. Yuan. Vol. 439. Astronomical Society of the Pacific Conference Series. May 2011, p. 232.
- [228] R. D. Viollier, F. R. Leimgruber, and D. Trautmann. “Halos of heavy neutrinos around baryonic stars”. In: *Physics Letters B* 297.1-2 (Dec. 1992), pp. 132–137. DOI: [10.1016/0370-2693\(92\)91081-J](https://doi.org/10.1016/0370-2693(92)91081-J).
- [229] K. S. Virbhadra and G. F. R. Ellis. “Schwarzschild black hole lensing”. In: *Physical Review D* 62.8, 084003 (Oct. 2000), p. 084003. DOI: [10.1103/PhysRevD.62.084003](https://doi.org/10.1103/PhysRevD.62.084003). arXiv: [astro-ph/9904193](https://arxiv.org/abs/astro-ph/9904193) [astro-ph].
- [230] R. M. Wald. *General relativity*. University of Chicago Press, 1984.
- [231] J. L. Walsh et al. “The M87 Black Hole Mass from Gas-dynamical Models of Space Telescope Imaging Spectrograph Observations”. In: *The Astrophysical Journal* 770.2, 86 (June 2013), p. 86. DOI: [10.1088/0004-637X/770/2/86](https://doi.org/10.1088/0004-637X/770/2/86). arXiv: [1304.7273](https://arxiv.org/abs/1304.7273) [astro-ph.CO].
- [232] B. L. Webster and P. Murdin. “Cygnus X-1-a Spectroscopic Binary with a Heavy Companion ?” In: *Nature* 235.5332 (Jan. 1972), pp. 37–38. DOI: [10.1038/235037a0](https://doi.org/10.1038/235037a0).
- [233] S. Weinberg. *Gravitation and Cosmology: Principles and Applications of the General Theory of Relativity*. Wiley, 1972.
- [234] J. A. Wheeler and K. Ford. *Geons, black holes and quantum foam : a life in physics*. W.W. Norton Co Inc, 1998.
- [235] C. M. Will. “The Confrontation between General Relativity and Experiment”. In: *Living Reviews in Relativity* 17.1, 4 (Dec. 2014), p. 4. DOI: [10.12942/lrr-2014-4](https://doi.org/10.12942/lrr-2014-4). arXiv: [1403.7377](https://arxiv.org/abs/1403.7377) [gr-qc].
- [236] C. M. Will. *Theory and Experiment in Gravitational Physics*. Cambridge University Press, 1993.
- [237] L. Witten. *Gravitation: an Introduction to current research*. Wiley, 1962.
- [238] E. R. Wollman et al. “Ne II 12.8 micron emission from the galactic center. II.” In: *The Astrophysical Journal Letters* 218 (Dec. 1977), pp. L103–L107. DOI: [10.1086/182585](https://doi.org/10.1086/182585).
- [239] F. Yusef-Zadeh et al. “Nonthermal Radio Emission from the Galactic Center Arc”. In: *The Astrophysical Journal* 310 (Nov. 1986), p. 689. DOI: [10.1086/164719](https://doi.org/10.1086/164719).
- [240] Y. B. Zel’dovich. “The Fate of a Star and the Evolution of Gravitational Energy Upon Accretion”. In: *Soviet Physics Doklady* 9 (Sept. 1964), p. 195.
- [241] Y. B. Zeldovich and I. D. Novikov. *Relativistic astrophysics. Vol.1: Stars and relativity*. University of Chicago Press, 1971.

- [242] F. Zwicky. “Republication of: The redshift of extragalactic nebulae”. In: *General Relativity and Gravitation* 41.1 (Jan. 2009), pp. 207–224. DOI: [10.1007/s10714-008-0707-4](https://doi.org/10.1007/s10714-008-0707-4).